Towards a unified approach for the control of aerial vehicles

Daniele Pucci

UNIVERSITÉ DE NICE-SOPHIA ANTIPOLIS

ÉCOLE DOCTORALE STIC

Sciences et Technologies de l'Information et de la Communication

SAPIENZA UNIVERSITÀ DI ROMA

Dipartimento di Ingegneria Informatica Automatica e Gestionale

Ingegneria dei Sistemi

Towards a unified approach for the control of aerial vehicles

Thèse pour obtenir les titres de:

Docteur en Automatique Traitement du Signal et des Images

de l'Université de Nice-Sophia Antipolis

et

Dottore in Ingegneria dei Sistemi

Sapienza Università di Roma

Présentée par

Daniele PUCCI

Dirigée par

Tarek Hamel, Professeur, UNSA and I3S-CNRS

Salvatore Monaco, Professore, Sapienza Università di Roma

Claude Samson, Directeur de Recherche, INRIA

Soutenue publiquement le 11 Avril 2013 devant le jury composé de :

Président :	Dorothée Normand-Cyrot, Directeur de Recherche, CNRS – Supélec
Rapporteurs :	Lorenzo Marconi, Professore, D.E.I.S. – University of Bologna
	Nicolas Petit, Professeur, head of C.A.S. – MINES ParisTech
Examinateurs :	Brigitte D'Andrea-Novel, Professeur, C.A.O.R. – MINES ParisTech
	Pascal Morin, Professeur Contractuel, ISIR – UPMC

Daniele PUCCI

TOWARDS A UNIFIED APPROACH FOR THE CONTROL OF AERIAL VEHICLES

Abstract

Over the last century, the scientific community has dealt with the control of flying machines by mainly developing different strategies in relation to different classes of aircraft, and no unified control approach has been developed so far. The present thesis contributes towards the development of a unified control approach for aerial vehicles by maintaining aerodynamic forces in the control design. It is assumed, however, that the aerodynamic effects of rotational and unsteady motions are negligible, and that the means of actuation for an aerial vehicle consist of a body-fixed thrust force for translational motion and a control torque for attitude monitoring. This thesis then focuses on the guidance loop of the control problem. One of the main objectives has been to determine how to regulate the thrust intensity and the vehicle orientation to compensate for the orientation-dependent external forces. In particular, the modelling, analysis, and control of the longitudinal aircraft dynamics is first addressed. Then, some of these studies are extended to three-dimensional motions of symmetric aircraft, such as missile-like bodies. An original outcome of this thesis is to state conditions on the aerodynamic force that allow the control problem to be recasted into that of controlling a spherical body. In this case, strong stability results can be shown. The proposed control laws incorporate integral and anti-wind up terms and do not rely on a switching policy between several control laws.

Résumé

Au cours du siècle dernier, la communauté scientifique a traité le contrôle des véhicules aériens principalement par l'élaboration de stratégies ad hoc, mais aucune approche unifiée n'a été développé jusqu'à présent. Cette thèse participe à l'élaboration d'une approche unifiée pour le contrôle des véhicules aériens en prenant en compte les forces aérodynamiques dans la conception de la commande. Nous supposons les effets aérodynamiques de rotation et les effets non stationnaires négligeables. Les actionneurs du véhicule sont supposés être composés d'une force de poussé fixée au corps pour le mouvement en translation, et d'un couple de contrôle pour la régulation d'attitude. Cette thèse se concentre ensuite sur la boucle de guidage, traitant du contrôle de la vitesse linéaire. L'un des principaux objectifs a été de déterminer la façon de réguler la force de poussée et l'orientation du véhicule pour compenser les forces extérieures. Tout d'abord nous abordons la modélisation, l'analyse et le contrôle de la dynamique longitudinale de l'avion. Ensuite nous étendons certaines de ces études aux mouvements tridimensionnels d'avions au corps symétrique, tels que les missiles. Un résultat original de cette thèse est de préciser les conditions sur la force aérodynamique permettant de reformuler le problème du contrôle dans celui de la commande d'un corps sphérique, pour lequel des résultats de stabilité peuvent être démontrés. Les lois de commande proposées intègrent des termes intégraux et anti-wind up sans reposer sur une politique de commutation entre plusieurs lois de commande.

"I am and will always be a student."

Contents

Prologue in English

Feedback control of aerial vehicles in order to achieve some degree of autonomy remains an active research domain after decades of studies in the subject. The complexity of aerodynamic effects and the diversity of flying vehicles partly account for this continued interest. Over the last decades, the scientific community has dealt with the control of flying machines by mainly developing different strategies in relation to different classes of aerial vehicles – as exemplified by airliners and helicopters – but no unified approach has been developed so far. The present thesis contributes towards the development of such an approach by taking into account aerodynamic effects in the control design.

Most aerial vehicles developed in the 20th century belong either to the class of fixed-wing vehicles, or to that of Vertical Take Off and Landing (VTOLs) vehicles. The first class is mainly comprised of airplanes, while the second class concerns several types of systems, like helicopters, ducted fans, quad-rotors, etc. Control design techniques for fixed-wing and VTOL vehicles have developed in different directions and suffer from specific limitations. Classically, feedback control of fixed-wing aircraft explicitly takes into account aerodynamic forces via linearized models, and stabilization is usually achieved by applying linear control techniques. Linear techniques are used for hovering VTOL vehicles too, but several nonlinear feedback methods have also been proposed in the last decade to enlarge the provable domain of stability. These methods, however, are based on simplified dynamic models that neglect aerodynamic forces, so they are not best suited to the control of aircraft moving fast or subjected to strong wind variations.

A drawback of the independent development of control methods for fixed-wing and VTOL aircraft is the lack of tools for flying vehicles that belong to both classes. One can mention the example of *convertible aircraft*, which can perform stationary flight and also benefit from lift properties at high airspeed via optimized aerodynamic profiles. The renewed interest in convertible vehicles and their control is reflected in the growing number of studies devoted to them in recent years, even though the literature in this domain is not extensive. One of the motivations for elaborating more versatile control solutions is that the automatic monitoring of the delicate transitions between stationary flight and cruising modes, in relation to the strong variations of aerodynamic forces during these transitions, remains a challenge even now.

Lately, advances in technology have given impetus to the development of small aerial vehicles: lighter and more powerful engines, more efficient batteries, lighter materials, and more reliable miniature electronics and sensors make it possible to embark all elements necessary for autonomous navigation in small aircraft, which are thus versatile to numerous applications such as inspection, surveillance, cartography, cinematography, etc. Among these emerging aerial vehicles, one can mention the HoverEye (Pfimlin, 2006), the iSTAR (Lipera et al., 2001), the GTSpy (Johnson and Turbe, 2005), the University of Bologna's ducted fan tailsitter (Naldi, 2008a), the SLADe (Peddle et al., 2009), the X4-flyer (Hamel et al., 2002a), the vigilant (Fabiani et al., 2007), the Goliath (Vissiere et al., 2008), the GTMax (Johnson and Kannan, 2005), and the AVATAR (Saripalli et al., 2002). Although nowadays navigation systems are reliable for autonomous flights, the control of

small aerial vehicles is still an open avenue. One of the major difficulties in developing these strategies is that a small aircraft can (usually) fly within a large *flight envelope*, which impairs most of the control solutions proposed in the existing literature.

In view of these observations, we believe that there is a strong potential benefit in bringing control techniques for fixed-wing and VTOL vehicles closer. The present thesis takes a step in this direction by proposing a unified strategy that takes into account aerodynamic forces in the control design. By neglecting so-called *unsteady-aerodynamic effects*, an original outcome of the present thesis is to point out conditions upon the aerodynamic forces that allow one to recast the control problem into the one of controlling an equivalent body with a spherical shape subjected to an orientation-independent drag force only. Once this transformation – referred to as *spherical equivalency* – is done, strong stability and convergence results for reference trajectories can be demonstrated.

This work has been carried out during my Ph.D. within AROBAS – a robotics research team of INRIA[1] – and I3S UNSA/CNRS. The Ph.D. program has been under a co-tutorship between the university of "Nice Sophia Antipolis" and "Sapienza" university of Rome in order to obtain a PhD title from each of these universities according to the "convention internationale de cotutelle de these" stated by the "Université Franco Intalienne". My research was funded by the *I3S-CNRS/UNS University of Nice Sophia Antipolis*. The present document is organized into two parts:

Part 1: Principles of flight and thesis context. This part of the thesis recalls the principles of flight, thus providing the reader with basic aerodynamic and flight dynamics knowledge. Also, some of the control techniques for aerial vehicles are reviewed in order to clarify the thesis context with respect to the existing literature. This part of the thesis consists of five chapters:

- **Chapter 1 The origin of the science of flight**: this chapter presents historical notes on the origin of the science of flight.
- **Chapter 2 Aerial vehicles**: this chapter describes the main components and flight characteristics of three classes of aerial vehicles: Fixed-wing aircraft, Vertical Take Off and Landing aircraft, and Convertible vehicles.
- **Chapter 3 Basics of aerodynamics**: this chapter introduces basic aerodynamic background by focusing on the aerodynamic forces acting on common *flat* wings.
- **Chapter 4 Basics of flight dynamics**: this chapter introduces basic flight dynamics background by discussing classical modeling and control strategies for aerial vehicles.
- **Chapter 5: Motivations and thesis context**: this short chapter presents the main thesis assumptions and motivations.

[1]The French *National Institute for Research in Computer Science and Control*- http://www.inria.fr.

Part 2: Modeling Analysis and Control of Aerial Vehicles. This part of the thesis is dedicated to the modeling, analysis and control of two-dimensional and three-dimensional body motions. However, three of the four chapters composing this part concern two-dimensional motions, also referred to as *aircraft longitudinal dynamics*.
In particular:

- **Chapter 6 System modeling**: this chapter recalls the equations of motions for two-dimensional bodies subjected to aerodynamic reaction forces. Models representative of the *aerodynamic coefficients* of NACA airfoils in sub-sonic flows are also presented. *Stall phenomena* are taken into account in this modeling process.

- **Chapter 7 Equilibria analysis**: this chapter presents an equilibrium analysis for the vehicle's longitudinal dynamics, and focuses on basic but important control issues. First, the *feasibility* of a reference trajectory is shown to require the existence of a vehicle's (equilibrium) orientation along the reference. Then, the existence of this orientation is shown to follow from the *symmetries* of the body's shape independently from fluid regimes and specific classes of reference trajectories. Once the existence of the vehicle's equilibrium orientation is studied, this chapter discusses the uniqueness and multiplicity of this equilibrium orientation. In doing so, the aforementioned *spherical equivalency* is presented: it is shown that for the aerodynamic forces allowing for this equivalency the vehicle's equilibrium orientation is unique over large domains of the reference trajectory. For other classes of aerodynamic forces, this chapter shows that a reference velocity may be associated with several vehicle's equilibrium orientations, the occurrence of which is related to the *stall phenomena*. As a consequence of the existence of several equilibria, this chapter shows that some reference trajectories require a discontinuous vehicle's orientation profile to be stabilized; in this case, the reference trajectory is not feasible. With this equilibria picture in mind, a study of the local uniqueness of the vehicle's equilibrium orientation is presented, thus laying down the basis for the control design method presented in chapter 8. Another original outcome of this chapter is to show that at a fixed vehicle's thrust intensity and orientation there may exist several stable equilibrium velocities associates with large angles of attack and loss-of-altitude; this result is reminiscent of the *deep stall* situation.

- **Chapter 8 Control design**: relying on the equilibria analysis developed in Chapter 7, this chapter presents local controllers for reference trajectories and velocities. When the aerodynamic coefficients allow for the aforementioned *spherical equivalency*, the basin of attraction of these controllers becomes semi-global under conditions that are satisfied in most practical cases. Simulations results verify the effectiveness and robustness of the proposed control approach for aerial vehicles flying in the vertical plane.

- **Chapter 9 Extension to 3-D symmetric aircraft**: assuming a rotational symmetry of the vehicle's shape about the thrust force axis, this chapter extends some of the results found for the two-dimensional motions to aircraft flying in three-dimensional space. Original results concern the modeling of aerodynamic forces acting on symmetric bodies and the characterization of a family of models that allow one to apply the aforementioned *spherical-equivalency*. Members of this family are representative of the aerodynamic force acting on elliptic-shaped and missile-like bodies in subsonic and hypersonic flows. To illustrate the usefulness of these

results at the control design level, prior control controllers are applied to provide the reader with laws that stabilize either a reference velocity or a reference trajectory. Simulations results verify the effectiveness and robustness of the proposed control approach for symmetric aerial vehicles.

Some of the results reported in this thesis have been published (or are about to) in research papers (Pucci et al., 2011) (Pucci, 2012) (Pucci et al., 2012) (Pucci et al., 2013). According to the "convention internationale de cotutelle de these" stated by the "Université Franco Italienne", I spent a period of time of my Ph.D. program in Italy at "Sapienza" university of Rome under the supervision of Professor Salvatore Monaco. The results to which I collaborated are not reported in this manuscript, but they are reported in (Boncagni et al., 2011) (Boncagni et al., 2012c) (Boncagni et al., 2012a) (Boncagni et al., 2012b).

Prologue in French

La commande de véhicules aériens dans le but d'atteindre un certain degré d'autonomie reste un domaine de recherche actif après des décennies de recherche. La complexité des effets aérodynamiques et la diversité des véhicules volants expliquent partiellement cet intérêt continu. Durant les dernières décennies, la communauté scientifique a relevé le défis de contrôler des machines volantes principalement en développant différentes stratégies en relation avec les différentes classes de véhicules, comme le montre les avions et les hélicoptères, mais aucune approche unifiée n'a été développée jusqu'ici. La présente thèse contribue au développement de cette approche en prenant en compte les effets aérodynamiques complexes dans la conception des commandes.

La plupart des véhicules aériens développés au 20ieme siècle appartiennent soit à la classe des véhicules à voilure fixe soit a celle des véhicules à décollage verticale (VTOLs). La première classe de véhicule comprend principalement les avions alors que la seconde concernent plusieurs types d'appareil comme les hélicoptères, les quadrirotors etc. Les techniques de conception des commandes pour les véhicules à voilure fixe ou VTOL ont été développées dans différentes directions et souffrent de limitations spécifiques. Classiquement, la commande en boucle fermée de véhicules à voilure fixe prend en compte explicitement les forces aérodynamiques via des modèles linéarisés et la stabilisation est traditionnellement réalisée en appliquant des méthodes de commande linéaire. Des méthodes linéaires sont utilisées pour la phase ascensionnelle du vol des VTOL aussi, mais plusieurs méthodes de contrôle non linéaire ont aussi été proposées durant la dernière décennie pour augmenter le domaine de stabilité. Cependant ces méthodes sont basées sur des modèles dynamiques simplifiés qui négligent les forces aérodynamiques, ce qui fait qu'elles ne sont pas adaptées au contrôle d'un appareil se déplaçant à grande vitesse ou sujet à de fortes variations du vent.

Un inconvénient du développement indépendant des méthodes de contrôle pour appareils à voilure fixe et VTOL est le manque d'outils pour les véhicules appartenant aux deux classes. On peut mentionner les véhicules convertibles qui réalisent un vol stationnaire et bénéficient aussi de propriétés de portance pour de haute vitesse du flux d'air autour de l'appareil via des profiles aérodynamiques optimisés. Le renouvellement de l'intérêt pour les véhicules convertibles et leur commande est reflété par le nombre de plus en plus important d'études liées au sujet ces dernières années bien que la littérature dans le domaine n'est pas très étendu. Une des raisons d'élaborer des commandes plus souples est que la surveillance automatique des délicates transitions entre le vol stationnaire et le vol de croisière, en relation avec les grandes variations des forces aérodynamiques pendant ces transitions, reste un challenge aujourd'hui.

Récemment, les avancées technologiques ont donné une impulsion au développement de petits véhicules aériens : des moteurs plus petits et plus puissants, des batteries plus efficaces, des matériaux plus légers et des capteurs et de l'électronique plus fiable rendent possible l'intégration de tout ce qui est nécessaire pour la navigation autonome de petits appareils qui sont adaptés à de nombreux type d'application comme l'inspection, la surveillance,la cartographie, la cinématographie etc. Parmi ces nouveaux appareils, on

peut citer l'HoverEye (Pfimlin, 2006), l'iSTAR (Lipera et al., 2001), le GTSpy (Johnson and Turbe, 2005), le ducted fan tailsitter (Naldi, 2008a) de l'universitè de Bologne, le SLADe (Peddle et al., 2009), le X4-flyer (Hamel et al., 2002a), le vigilant (Fabiani et al., 2007), le Goliath (Vissiere et al., 2008), le GTMax (Johnson and Kannan, 2005), et le AVATAR (Saripalli et al., 2002). Bien qu'aujourd'hui les systèmes de navigation sont fiables pour un vol autonome, la commande des petits véhicules reste un problème ouvert. L'une des principales difficultés pour le développement de ces stratégies est que ces petits appareils peuvent typiquement voler dans de large enveloppes de vol qui rendent caduque la plupart des solutions pour la commande proposées dans la littérature existante.

Ayant fait ces observations, nous pensons qu'il existe un fort bénéfice potentiel à rapprocher les techniques de contrôle des véhicules à voilure fixe et VTOL. La présente thèse fait un pas dans cette direction en proposant une stratégie unifiée qui prend en compte les forces aéronautiques dans la conception des commandes. Un résultat original de cette thèse est de souligner les conditions sur la force aérodynamique qui permettent de reformuler le problème sous la forme du contrôle d'un corps sphérique sujet uniquement à une traînée indépendante de l'orientation. Une fois réalisée cette transformation, appelée équivalence sphérique, des propriétés de stabilité et de convergence fortes pour des trajectoires de référence peuvent être démontrées.

Ce travail a été effectué durant ma thèse dans l'équipe AROBAS de l'INRIA Sophia Antipolis et dans le laboratoire I3S UNSA/CNRS en cotutelle avec Sapienza-Università di Roma selon la "convention internationale de cotutelle de thèse" établie par "l'Université Franco Intalienne".

Ces travaux de recherche ont été financés par l'I3S-CNRS Université de Nice Sophia Antipolis. Le manuscrit de thèse est divisé en deux parties:

Part1 : principe de vol et contexte de la thèse. Cette partie de la thèse rappelle les principes du vol en donnant au lecteur les bases de l'aérodynamique et de la mécanique du vol. Plusieurs techniques de contrôle des véhicules aériens sont revus dans le but de clarifier le contexte de la thèse par rapport à la littérature existante. Cette partie de la thèse consiste en 5 chapitres.

- **Chapitre 1 : les origines de la science du vol**: ce chapitre présente des notes historiques sur l'origine de la science du vol.
- **Chapitre 2 : Véhicules aériens** : ce chapitre décrit les composants principaux et les caractéristiques de vol de trois classes de véhicules : voilure fixe, VTOL et convertibles.
- **Chapitre 3 : Bases de l'aérodynamique** : ce chapitre introduit les bases de l'aérodynamique en se focalisant sur les forces agissant sur des profiles plats.
- **Chapitre 4 : Bases de la dynamique du vol**: ce chapitre introduit les bases de la dynamique du vol en discutant des méthodes classiques de modélisation et de conception des commandes des véhicules aériens.
- **Chapitre 5: Motivations et contexte de la thèse**: ce court chapitre présente les hypothèses principales et les motivations de la thèse.

Part 2: Modélisation et Commande des véhicules aériens. Cette partie de la thèse est dédiée à la modélisation a l'analyse et à la commande du mouvement des corps en 2-D et en 3-D. Cependant trois des ' chapitres composant cette partie concerne le mouvement bidimensionnel, aussi appelé dynamique longitudinale de l'avion. En particulier :

- **Chapitre 6 Modélisation du système**: ce chapitre rappelle les équations du mouvement pour des objets en deux dimensions sujets à des forces aérodynamiques. Des modèles représentatifs des coefficients aérodynamiques des profiles NACA dans des flux d'air subsoniques sont aussi présentés. Le "stall phenomena" est pris en compte dans cette modélisation.
- **Chapitre 7 : Analyse des équilibres**: Ce chapitre présente une analyse des équilibres de la dynamique longitudinale du véhicule et se focalise sur des problèmes de commande basiques mais importants. Premièrement on montre que la faisabilité de la trajectoire de référence nécessite l'existence d'une orientation d'équilibre pour le véhicule le long de la référence. Ensuite on montre que l'existence de cette orientation vient des symétries du véhicule, indépendamment du régime d'écoulement fluide et des classes de trajectoires de référence spécifique. Une fois l'existence d'une orientation d'équilibre étudiée, ce chapitre discute de l'unicité et de la multiplicité de cette orientation. Ensuite, l'équivalence sphérique précitée est introduite : on montre que pour des forces permettant cette équivalence, l'orientation d'équilibre du véhicule est unique dans un large domaine de trajectoires de références. Pour d'autres classes de forces aérodynamiques, ce chapitre montre qu'une vitesse de référence peut être associée a plusieurs orientations d'équilibre du véhicule, l'occurrence desquelles est liée au stall phenomena. En conséquence de l'existence de plusieurs équilibres, ce chapitre montre que certaines trajectoires de référence requièrent que le profile d'orientation du véhicule discontinu soit stabilisé, dans ce cas, la trajectoire de référence n'est pas faisable. Avec cette image en tête, une étude de l'unicité locale de l'orientation d'équilibre est présentée, posant les bases de la méthode de commande présentée au chapitre 8. Un autre résultat original de ce chapitre est de montrer qu'à une poussée et une orientation fixées, il peut exister plusieurs vitesses d'équilibre stable associées avec de grands angles d'attaque et des pertes d'altitude ; ce résultat est réminiscent de la situation de "deep stall".
- **Chapitre 8 : conception de la commande**: en s'appuyant sur l'analyse de l'équilibre développée précédemment, ce chapitre présente des contrôleurs locaux pour des trajectoires et vitesses de référence. Lorsque les coefficients aérodynamiques permettent l'équivalence sphérique, le bassin d'attraction de ces contrôleurs devient semi-global sous des conditions remplies dans la plupart des cas. Les résultats des simulations vérifient l'efficacité et la robustesse des commandes proposées pour des véhiculent volant dans le plan vertical.
- **Chapitre 9 : extension en 3D pour des véhicules symétriques**: En supposant une symétrie de rotation autour de l'axe de la poussée du véhicule, ce chapitre étend certains des résultats trouvés pour le cas d'un mouvement bidimensionnel au cas d'un avion se déplaçant en 3D. Des résultats originaux concernent la modélisation des forces aérodynamiques agissant sur des corps symétriques et la caractérisation d'une famille de modèles qui permettent d'appliquer le principe d'équivalence sphérique précité. Les membres de cette famille sont les représentants de la force aérodynamique agissant sur des corps ellipsoïde ou en forme de missile dans des flux d'air subsoniques et hypersoniques. Pour illustrer l'utilité des

résultats de cette thèse au niveau de la conception de la commande, des contrôleurs développés pour le cas sphérique sont appliqués pour donner au lecteur les lois qui stabilisent la vitesse de référence ou la trajectoire de référence. Les résultats des simulations vérifient l'efficacité et la robustesse des approches proposées pour la commande des véhicules symétriques.

Certains des résultats présentés dans cette thèse ont été publiés dans les articles de recherche (Pucci et al., 2011) (Pucci, 2012) (Pucci et al., 2012) (Pucci et al., 2013). Selon la "convention internationale de cotutelle de these" établie par l'"Université Franco Italienne", j'ai passé une période durant mon doctorat en Italie à "Sapienza" universitè de Rome sous la supervision de Professor Salvatore Monaco. Les résultats obtenus durant cette période ne sont pas présentés dans ce manuscrit, mais ils sont présentés dans (Boncagni et al., 2011) (Boncagni et al., 2012c) (Boncagni et al., 2012a) (Boncagni et al., 2012b).

Prologue in Italian

Le strategie di comando per gli aeromobili rappresentano un attivo dominio di ricerca e attraggono una grande parte della comintà scientifica odierna. La complessità degli effetti aerodinamici e la diversità fra i sistemi capaci di volare sono fra i fattori che complicano lo sviluppo di una strategia di controllo che sia robusta e completa. Infatti, al giorno d'oggi il controllo degli aeromobili viene effettuato progettando strategie ad hoc per diverse tipologie di sistemi, come le leggi di controllo per gli aerei di linea e gli elicotteri. Questa tesi partecipa allo sviluppo di una teoria unica per il controllo degli aeromobili.

Gran parte degli aeromobili sviluppati nel ventesimo secolo appartengono o alla classe degli *aerei ad ala fissa*, o alla classe degli *aerei a decollo verticale (VTOLs)*. La prima classe è sopratutto composta da aerei di linea, mentre la seconda contiene un'ampia gamma di sistemi come elicotteri, quad-rotos, etc. Le strategie di comando per gli aerei ad ala fissa ed i VTOLs si sono sviluppate lungo direzioni diverse e soffrono di limiti specifici collegati ad ogni classe. Il controllo degli aerei ad ala fissa prende in considerazione le forze aerodinamiche attraverso dei modelli linearizzati e la stabilità del sistema è il più delle volte garantita attraverso tecniche di controllo lineari. Simili tecniche lineari sono state utilizzate anche per il controllo dei VTOLs, ma molti metodi nonlineari sono stati sviluppati nell'ultima decade per allargare il dominio di stabilità. Questi metodi nonlineari, tuttavia, son basati su modelli che spesso trascurano completamente la forza aerodinamica sul corpo del veicolo, e quindi non sono adatti al controllo di aeromobili che si muovono ad alte velocità.

Un problema dello sviluppo indipendente delle metodologie di controllo per aeromobili ad ala fissa e VTOLs è la mancanza di strategie per quei aeromobili che appartengono ad entrambe le classi. Si possono menzionare i cosidetti *aeromobili convertibili* che sono in grado sia di effettuare il decollo verticale che di beneficiare delle proprietà di portanza di ali attaccate al corpo del veicolo. Il rinnovato interesse per gli aeromobili convertibili si riflette nel crescente numero di studi devoti ad essi negli anni recenti, sebbene la letteratura sul loro controllo non è ancora molto sviluppata. Uno dei maggiori problemi è il controllo della transizione tra volo verticale e volo orizzontale, la quale genera una grande variazione delle forze aerodinamiche applicate al veicolo.

Ultimamente, gli sviluppi della tecnologia hanno dato un impulso allo sviluppo di *piccoli* aeromobili: motori elettrici più leggeri e più potenti, batterie più efficienti, materiali più leggeri, e un'elettronica di bordo più affidabile hanno reso possibile l'imbarco di tutti gli elementi necessari al volo autonomo su un piccolo aeromobile, che risulta così molto utile per numerose applicazioni come l'ispezione, la sorveglienza, la cartografia, etc. Tra questi piccoli aeromobili si può menzionare l'HoverEye (Pfimlin, 2006), l'iSTAR (Lipera et al., 2001), il GTSpy (Johnson and Turbe, 2005), il ducted fan tailsitter (Naldi, 2008a) dell'università di Bologna, il SLADe (Peddle et al., 2009), il X4-flyer (Hamel et al., 2002a), il vigilant (Fabiani et al., 2007), il Goliath (Vissiere et al., 2008), il GTMax (Johnson and Kannan, 2005), e il AVATAR (Saripalli et al., 2002). Sebbene ai giorni d'oggi i sistemi di navigazione siano affidabili per il volo autonomo di piccoli aeromobili, il controllo di tali sistemi è ancora una strada aperta. Una delle difficoltà maggiori è data dal fatto che un

piccolo aeromobile può volare in un grande inviluppo di volo, il che rende inapplicabile quasi tutte le strategie di comando per gli aerei ad ala fissa e per i VTOLs.

Alla luce di queste osservazioni, noi crediamo che si possa ottenere un beneficio notevole nell'unificare le strategie di comando per gli aerei ad ala fissa ed i VTOLs in una sola teoria per il controllo degli aeromobili. La presente tesi propone una strategia unica per il controllo dei veicoli aerei. Un risultato originale di questa tesi è la definizione di condizioni per le quali il problema del controllo può essere riscritto come se la forma del veicolo fosse una sfera. Tale riformulazione viene chiamata *equivalenza sferica*, ed una volta effettuata permette di dimostrare grandi domini di stabilità per ogni traitettoria di riferimento.

La tesi di dottorato è stata sviluppata nel team AROBAS all'INRIA Sophia Antipolis. Il programma di dottorato è stato in cotutela tra l'università di Nizza Sophia Antipolis e l'università di Roma "La Sapienza" ai fini di ottenere un titolo di dottorato da ciascuna di queste università, come definito dalla "convention internationale de cotutelle de these" dell'"Université Franco Intalienne". Il programma di dottorato fu finanziato dall'*I3S-CNRS/UNS University of Nice Sophia Antipolis*. Questo documento è diviso in due parti:

Parte 1: I principi della dinamica del volo ed il contesto della tesi. Questa parte richiama i principi della dinamica del volo. Inoltre, essa si focalizza su una parte delle tecniche di controllo per gli aeromobili in modo tale da chiarire il contesto della tesi rispetto la letteratura esistente. Questa parte della tesi è suddivisa in cinque capitoli:

- **Capitolo 1 Cenni sull'origine della *dinamica del volo***: questo capitolo presenta cenni storici sulla nascita e sviluppo della scienza che studia la modellazione ed il controllo degli aeromobili, chiamata *dinamica del volo*.
- **Capitolo 2 Aeromobili**: questo capitolo descrive i componenti principali e le caratteristiche di volo di tre classi di aeromobili: aeromobili ad ala fissa, aeromobili a decollo e atterraggio verticale, ed aeromobili convertibili.
- **Capitolo 3 Basi di aerodinamica**: questo capitolo introduce i principi dell'aerodinamica focalizzandosi sulle forze aerodinamiche che agiscono su comuni ali "piatte".
- **Capitolo 4 Basi di dinamica del volo**: questo capitolo introduce le basi della dinamica del volo e discute le metodologie classiche per il controllo degli aeromobili.
- **Capitolo 5: Motivazioni e contesto della tesi**: questo breve capitolo presenta le ipotesi e le motivazioni della tesi.

Parte 2: Modellizzazione Analisi e Controllo degli aeromobili. Questa parte della tesi è dedicata alla modellizzazione, analisi e controllo degli aeromobili. Tre dei quattro capitoli che compongono questa parte della tesi sono dedicati a moti planari, chiamati *dinamica longitudinale* dell'aeromobile.
In particolare:

- **Capitolo 6 Modellizzazione del sistema**: questo capitolo richiama le equazioni che governano il moto di corpi planari sottoposti a forze di reazioni aerodinamiche. Modelli che sono rappresentativi dei *coefficienti aerodinamici* dei profili NACA in regime sub-sonico vengono presentati. I *fenomeni di stallo* sono presi in considerazione in tale processo di modellizzazione.
- **Capitolo 7 Analisi degli equilibri**: questo capitolo presenta un'analisi degli equilibri della dinamica longitudinale, e si focalizza su basiche ma importanti questioni di controllo. Innanzitutto, si dimostra l'ovvio fatto che la *fattibilità* di una traiettoria di riferimento necessità l'esistenza di un *orientamento di equilibrio* lungo la traiettoria. Successivamente, si mostra che l'esistenza di tale orientamento è implicata dalle simmetrie della forma dell'aeromobile independentemente dal regime del fluido nel quale il veivolo vola, o classi specifiche di traiettorie di riferimento. Dopo lo studio dell'esistenza dell'orientamento di equilibrio, questo capitolo studia l'unicità e la multiplicità di tale orientamento. Durante tale analisi viene presentata la menzionata *equivalenza sferica*: si dimostra che per le classi di forze aerodinamiche che permettono tale equivalenza l'orientamento di equilibrio è unico per grandi domini di traittorie di riferimento. Per le altre classi di forze aerodinamiche, questo capitolo mostra che una velocità di riferimento può essere associata a diversi orientamenti di equilibrio: il verificarsi di tale fatto è legato ai fenomini di stallo. Come conseguenza dell'esistenza di molteplici orientamenti di equilibrio, si dimostra che la stabilizzazione asintotica di certe traiettorie di riferimento necessita di variazioni discontinue dell'orientamento dell'aeromobile; in questo caso, la traiettoria di riferimento non è fattibile. Dopo questo studio, l'unicità locale degli orientamenti di equilibrio è analizzata. Tale studio permette di gettare le basi alla strategia del controllo presentata nel capitolo 8. Un altro risultato originale di questo capitolo è mostrare che a fissata intensità di propulsione e orientamento del veivolo possono esistere diverse velocità di equilibrio associate a grandi angoli di attacco e perdite di altitudine.
- **Capitolo 8 Progettazione del controllo**: basandosi sull'analisi degli equilibri presentata nel capitolo 7, questo capitolo presenta degli stabilizzatori locali per traiettorie di riferimento. Quando i coefficienti aerodinamici permettono per l'*equivalenza sferica*, il dominio di attrazione garantito da tali controllori diventa semi-globale sotto condizioni che sono soddisfatte per la grande maggioranza dei casi pratici. Risultati di simulazione son presentati per verificare l'efficacia della strategia presentata.
- **Capitolo 9 Estensione ai corpi simmetrici 3-D**: assumendo una simmetria del corpo dell'aeromobile attorno l'asse di propulsione, questo capitolo estende una parte dei risultati trovati per il caso 2-D al caso di aeromobili che volando nello spazio tridimensionale. I risultati originali riguardano la modellizzazione delle forze aerodinamiche agenti sui corpi simmetrici e la caratterizzazione di una famiglia di modelli che permettono l'*equivalenza sferica*. Alcuni membri di tale famiglia sono rappresentativi della forza aerodinamica che agisce su missili che volano in regime sub-sonico e super-sonico. Per illustrare l'utilità di tale equivalenza sferica, dei risultati presenti nella letteratura vengono applicati al sistema equivalente per stabilizzare traittorie di riferimento. Risultati di simulazione sono presentati per verificare l'efficacia della strategia proposta.

Una parte dei risultati riportati in questa tesi sono stati pubblicati (o stanno per essere) in articoli scientifici (Pucci et al., 2011) (Pucci, 2012) (Pucci et al., 2012) (Pucci et al., 2013). Secondo la "convention internationale de cotutelle de these" definita dall'"Université Franco Italienne" ho speso un periodo di tempo in Italia presso la "Sapienza" università di Roma sotto la supervisione del Professor Salvatore Monaco. I risultati ai quali ho collaborato non sono descritti in questo manuscritto, ma sono presentati in (Boncagni et al., 2011) (Boncagni et al., 2012c) (Boncagni et al., 2012a) (Boncagni et al., 2012b).

Part I

Principles of flight and thesis context

1 The origin of the science of flight

Mankind has never ceased to envy birds' capacity for flying. The profound human curiosity about nature's flight systems and the dream of flying have prompted a long, irregular, and faltering understanding of basic aerodynamic phenomena, which culminated in 1903 with the following words:

> *"Success four flights Thursday morning all against twenty-one mile wind started from level with engine power alone average speed through air thirty-one miles longest 57 seconds inform press home Christmas."*

This is the Orville Wright telegram sent on 17 December 1903 from the lifesaving station in Kitty Hawk, North Carolina, to his father, Bishop Milton Wright, in Dayton Ohio. This document announced humankind's first successful powered flight of a heavier-than-air flying machine[1]. Since then, the history of aviation has been closely tied to advancements in technology, and mankind can now fly longer, faster, and higher than birds, but neither more efficiently nor with the same degree of maneuverability. In fact, birds have evolved since the Jurassic era – about 170 million years ago – thus developing features that man still cannot match with an aerial machine despite tremendous advancements in aviation. For instance, the supersonic aircraft SR-71 "Blackbird" attains speeds of 32 body-lengths per second – that is Mach 3 $\approx$ 3220 Km/h – while pigeons frequently cover 75 body-lengths per second (Shyy et al., 2008). And that is not all. Rotation rates and G-forces of highly aerobatic aircraft in flight are smaller than those frequently experienced by birds, which can withstand solicitations that our current technology still does not allow for. To cite (McMasters and Henderson, 1979),

> *"humans fly commercially or recreationally, but animals fly professionally."*

Such superior abilities for flying are the fruit of the aforementioned evolution that provided birds with highly effective capacities in perceiving their surrounding environment and controlling their wings. Most birds are thus capable of taking off almost vertically[2], climbing in altitude, gliding, and landing vertically. The importance of the wings' motion to birds' flight goes without saying, and this motion attracted the attention of humans as soon as humankind began dreaming of flying.

The astonishing attempt to understand the aerodynamic phenomena between birds and their surrounding air was made by Leonardo da Vinci (1452 - 1519) in his "Sul volo degli uccelli". Leonardo had the fundamental understanding that

[1] From (Hansen, 2003, p. 1).

[2] The "vertical direction" is given by the direction of the force of gravity.

> *"A bird is an instrument working according to mathematical law, an instrument which is within the capacity of man to reproduce with all its movements*[3]*."*

However, Leonardo's work unfortunately "stayed looked up and unknown in the hands of different private collectors for 300 years" (Hansen, 2003), so the question of what mankind would have achieved if this work had been rendered public before arises naturally.

In the 16th century, the naval battles between England and Spain gave impetus to the development of the so-call *fluid dynamics*, a general theory dealing with fluids and gases. In fact, the defeat of the Spanish Armada – a fleet of awe-inspiring battleships developed to invade England in 1588 – pointed out that the higher the agility and maneuverability, the higher the chances for battleships to win a naval combat.

What is considered the "first major breakthrough in the evolution of fluid dynamics" was made by Isaac Newton (1642-1727) in 1687 when he published *PhilosophiæNaturalis Principia Mathematica*: the second book of this manuscript, composed of three books, was wholly dedicated to fluids. Newton attempted to address the modeling of fluid flows by applying the young "mechanics of rigid bodies" developed by Newton himself. However, the fluid being a "geometrically undefined" matter rendered the application of his theory much involved, and several issues that did not arise when considering geometrically-well-defined (rigid) bodies remained unsolved.

> *"There is so great a difference between a fluid and a collection of solids particles that the laws of pressure and of equilibrium of fluids are very different from the laws of the pressure and equilibrium of solids*[4]*."*

Despite these difficulties, in his *Principia* Newton derived a law that describes the force exerted by a fluid on a planar surface. This law varies with the sine square of the *angle of incidence* between flow and plate (see Figure 1.1), and is widely known as *Newton's sine-squared law*. Although inaccurate, it was widely used in the design stage of boats. Amazingly, *Newton's sine-squared law* is applied nowadays in hypersonic applications. Newton, however, was not able to develop a general theory for moving fluids.

A giant leap in the development of theoretical fluid dynamics was made by the contributions of Daniel Bernoulli (1700-1782), Leonhard Euler (1707-1783) and Jean LeRond d'Alembert (1717-1783). Probably, Bernoulli's most important contributions to fluid dynamics can be found in his book *Hydrodinamica* (1738) where, for the first time in history, *calculus* was used to study the physics of a fluid (Anderson, 1997, p. 43). However, in this book Daniel Bernoulli did not present the famous *Bernoulli's equation*: he presented only an attempt at a partially-flawed relationship relating pressure and velocity of a fluid. The history of *Bernoulli's equation* involves also Johann Bernoulli[5], father of Daniel, a leading mathematician at that time who published a book entitled *Hydraulica* (1743). In contrast to his son who related the pressure to a manometer column, in *Hydraulica* Johann Bernoulli presented the pressure as a force on the fluid: clearly, Johann had a deeper understanding of the physics of fluids. Nevertheless, not even Johann presented *Bernoulli's equation* that was however attributed to Daniel for his attempt at the aforementioned relationship presented in *Hydrodinamica*.

[3]Leonardo da Vinci, from his "Sul volo degli uccelli" ("Codex on the Flight of Birds"), 1505.

[4]Jean Le Rond d'Alembert, 1768.

[5]Historians describe Johann Bernoulli as "a person of sensitivity and irritability, with an overpowering drive for recognition. He tried to undercut the impact of Daniel's *Hydrodinamica* by predating the publication date of *Hydraulica* to 1728" (Anderson, 2010, p. 303).

In contrast to its name, *Bernoulli's equation* was derived by Euler. Euler was the first to conceive of pressure as a position-dependent point property. In 1757, he derived two of the three[6] pivotal differential equations used today in modern fluid dynamics, which are for this reason called *Euler's equations*. Then, Euler integrated these differential equations and obtained, for the first time in history, the so-called *Bernoulli's equation* in the form we know today (Anderson, 2010, p. 303). It is important to remark that *Euler's equations* were extensions of previous results published by d'Alembert eight years earlier (1749) in a paper entitled *Essai d'une nouvelle thorie de la resistance des fluides*.

Although the theory developed by Euler and d'Alembert was a theoretical breakthrough, it led to a prediction of zero resistance on a closed two-dimensional body immersed in a fluid. This prediction is known as the d'Alembert's paradox.

> *"I do not see then, I admit, how one can explain the resistance of fluids by the theory in a satisfactory manner. It seems to me on the contrary that this theory, dealt with and studied with profound attention gives, at least in most cases, resistance absolutely zero: a singular paradox which I leave to geometricians to explain*[7]*."*

In reality, a body immersed in a moving fluid is always subjected to a finite force, and the prediction of zero resistance was due to the assumption of friction-less flow made by Euler and d'Alembert. Despite minds of the caliber of Euler attempted to solve d'Alembert's paradox, in the 18th century nobody noticed the importance of friction, or *viscosity*, in producing the force of resistance.

The modeling of viscosity effects received much attention from the scientific community in the 19th century. The equations taking friction effects into account were stated independently by Louis Navier (1785 - 1836) in 1822 and by George Stokes (1819-1903) in 1845 (Anderson, 1997, p. 89). More specifically, the *Navier-Stokes equations* have similar forms of *Euler's equations*, but they explicitly relate friction effects to some variables representing the state of the flow (velocity, pressure, etc.). These equations, however, consist of a set of nonlinear partial differential equations to which there do not exist closed-form solutions except for very specific cases. In fact, the existence of a smooth, *physically reasonable*[8] solution to the *Navier-Stokes equations* for three-dimensional flows is still a matter of conjecture to this day (Fefferman, 2000) (Constantin, 2001). Thus, in the 19th century the *Navier-Stokes equations* remained unsolved although the theory behind them was well understood. A breakthrough in this sense was made by Ludwing Prandtl (1875 - 1953) when he introduced the concept of a *boundary layer*: the effects of friction, though present everywhere, are usually negligible except[9] "in a thin region adjacent to the surface of a body" (Anderson, 2010, p. 965).

The resolution of d'Alembert paradox was ascribed by history to Prandtl via his "On the motion of fluids with very small viscosity" (1904) in which he presented the concept of a boundary layer. The advent of this concept allowed to find approximated, reliable solutions to the *Navier-Stokes equations* in planar problems, and completely changed the history of theoretical fluid dynamics applied to airflows, called *theoretical aerodynamics*.

[6] The third equation is the so-called *energy equation*, derived in thermodynamics in the 19th century.
[7] Jean LeRond d'Alembert from his "Opuscules mathematiques", 1768.
[8] A fluid is physically reasonable if its velocity field is bounded.
[9] Modern fluid dynamics explains that the effects of friction are non-negligible even "in the boundary region between two flows of widely different velocities" (Anderson, 2010, p. 965), called *shear layer*.

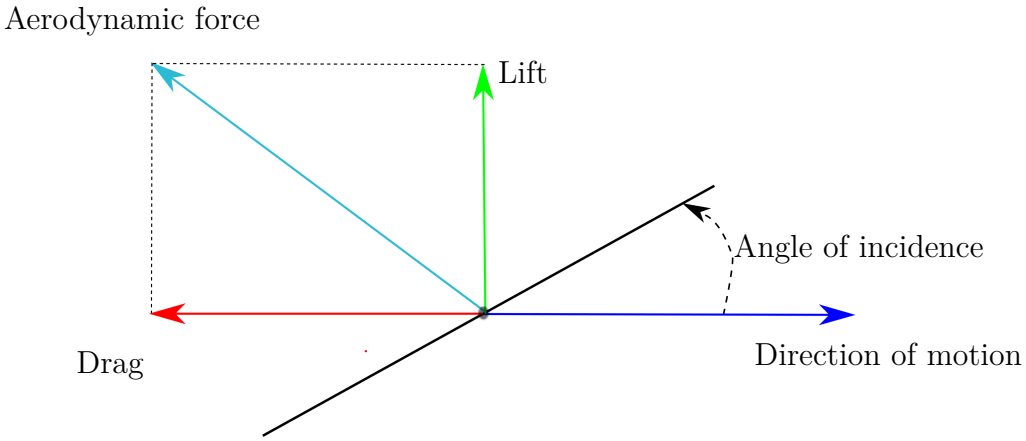

Figure 1.1: Decomposition of aerodynamic forces and angle of incidence.

Since theoretical aerodynamics did not provide relevant applicable results until the advent of a boundary layer, in the 19th century the experimental learning of the nature of flight moved, to a great extent, independently from theory. It is worth saying that Newton, with his *Principia*, unintentionally delayed the development of this experimental learning. More specifically, Newton considered a flying plate subjected to an aerodynamic force decomposed into two components (see Figure 1.1): the "upward-force", (later called *lift*), and "force-preventing-motion", (later called *drag*). Then he made calculations about these components, and concluded that a manned flight would have required very big and heavy wings. This conclusion – based on the approximate *Newton's squared-law* – was definitely overestimated: the scientific community in Newton's time erroneously deduced that "human flight by means of a supporting wing was impossible" (Hansen, 2003, p. xx). The breakthrough in this sense was made by George Cayley (1773 - 1857) who is often referred to as "the father of aerodynamics". Cayley's contributions to experimental aerodynamics were monumental: he had the fundamental understanding that

the lift force is independent from propulsion.

Then, it was only a short step for him to conceive that in horizontal flight, the weight of the vehicle must be compensated for the lift force, whereas propulsion must only counteract the drag force – see the quote in Chapter 4. In addition to these basic but fundamental principles, Cayley designed and built a few gliders equipped with *control surfaces*, thus defining the basic elements of a *fixed-wing* aircraft. Furthermore, in contrast to *Newton's sine-squared law*, Cayley showed that for many wings' shapes the lift is linear and the drag is basically constant versus *low* angles of incidence. Consequently, Newton's calculations about the possibility of a human flight by means of a supporting wing were wrong: this gave impetus to science to move "off the sharp horns of the dilemma created by Newton" (von Kármán, 1967, p. 58), thus prompting scientists to a formal study of the mechanisms of flight, and giving birth to the science of *aerodynamics* and *flight dynamics*.

2 Aerial vehicles

"Nobody will fly for a thousand years."

The above words were muttered by Wilbur Wright on the 20th August, 1901, when the performances of the glider built with his brother Orville were a far cry from those expected. However, frustration rapidly vanished, and two years later they made what for mankind was a giant leap: the first powered flight of a heavier-than-air flying machine. Since then, aviation has advanced faster than it had ever done before, and today a considerable number of classes of aerial vehicles exist[1]. This chapter presents three categories of aerial vehicles recalling some of their flight characteristics.

2.1 Fixed-wing aircraft

Fixed-wing aircraft are equipped with wings permanently fixed to the aircraft's body. The main role played by these wings, which are not necessarily rigid, is to generate *lift forces* for the aircraft to take-off and fly. Many types of fixed-wing aircraft exist including kites and gliders. What follows presents the common elements of a *powered* fixed-wing aircraft, also called *airplane* or *plane*. For additional material on the elements of an airplane see, among others, (Scott, 2002) and (Stengel, 2004, p. 1).

The basic components of an airplane include (see Figure 2.1):

- A *fuselage*: the aircraft part that contains passengers, crew, etc. Most fuselages have cylindrical or rectangular forms.
- A *main wing*: a surface whose main role is to generate the *lift* force to counteract for the vehicle's weight in flight. The main wing is usually composed of two parts attached to the fuselage. The amount of lift produced by the main wing is strongly related to its cross section, also called *airfoil*.
- A *vertical tail*: a surface whose main role is to stabilize[2] the angle about an axis (almost) perpendicular to the main wing, also called *yaw* angle. This surface provides the aircraft with "a tendency to nose into the *relative wind* resulting from forward motion" (Stengel, 2004, p. 2).
- A *horizontal tail*: a surface whose main role is to stabilize the angle about an axis (almost) parallel to the main wing, also called *pitch* angle. The tail surfaces are referred to as *empennage*.

[1] A list of significant aircraft since the first Wright flyer can be found in (Hansen, 2003, p. xxxi).

[2] For the time being, stability is meant as the tendency of a system to return to its initial state following a *small* disturbance from that state (Scott, 2002).

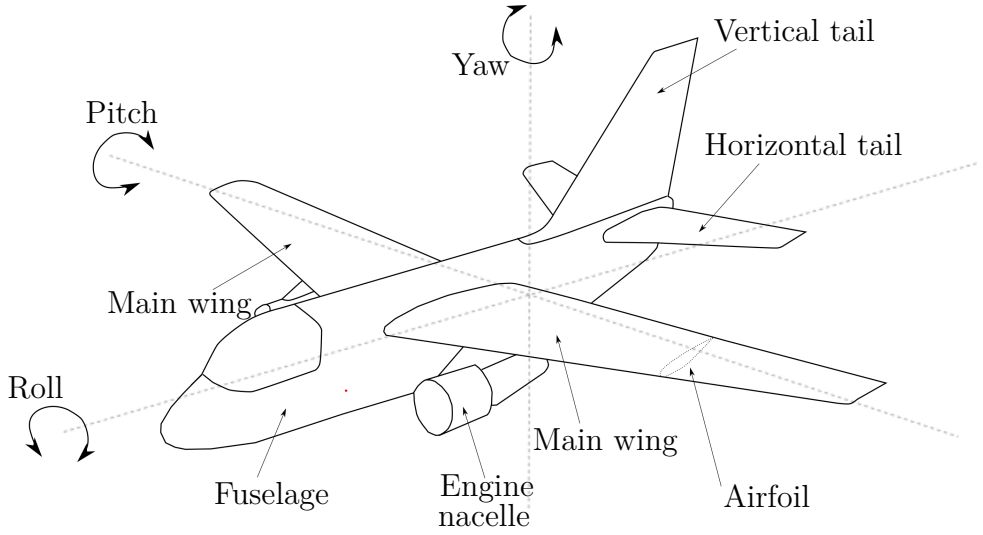

Figure 2.1: Basic components of a plane.

- *One or several engines*: propulsion devices providing the thrust for the aircraft's motion. Several kinds of engines exist, and they can be roughly classified into two main categories: *propeller-driven piston* and *jet* engines. The former were used by the early aircraft, such as the Wright Flyer and World War II aircraft, and are still common today on light planes; the latter are commonly used by modern aircraft. Engine(s) can be installed within the fuselage, although airliners usually have their engines mounted in the so-called *nacelles* (Scott, 2002).
- *Control (movable) surfaces and thrust settings* (see Figure 2.2). The control surfaces usually consist of: ailerons, elevators, rudder, and flaps. The *ailerons* are control surfaces – installed close to the wing tips – whose main role is to affect the roll angle: the two surfaces are connected by means of a mechanism ensuring opposite motions for their trailing edges (when one moves up, the other one moves down). The *elevator* and the *rudder* are control surfaces for pitch and yaw control, respectively. The *flaps* are control surfaces installed inboard of the ailerons for aerodynamic force control during take-off and landing; these surfaces work in unison (Stengel, 2004). Engine *thrust settings* provide the thrust control. In the case of airliners, thrust is only occasionally changed.

Several configurations of planes exist such as aircraft with several fuselages or with more than one horizontal or vertical stabilizer. For example, *V-tail planes* are equipped with a pair of diagonal surfaces that serve as the horizontal and vertical stabilizers. A common denominator of planes is the symmetry with respect to a plane (almost) perpendicular to the main wing.

The flight characteristics of a powered fixed-wing aircraft vary in relation to wing properties and the aircraft's means of actuations. Most airplanes, however, meet the following two properties:

1) stationary (hovering) flight is not allowed because of limitations on the thrust force and vehicle's controls (need of runways to take-off and land);

2) horizontal-constant-velocity flight can be performed with a thrust force smaller than the aircraft's weight (this property is also referred to as *efficient-steady flight*).

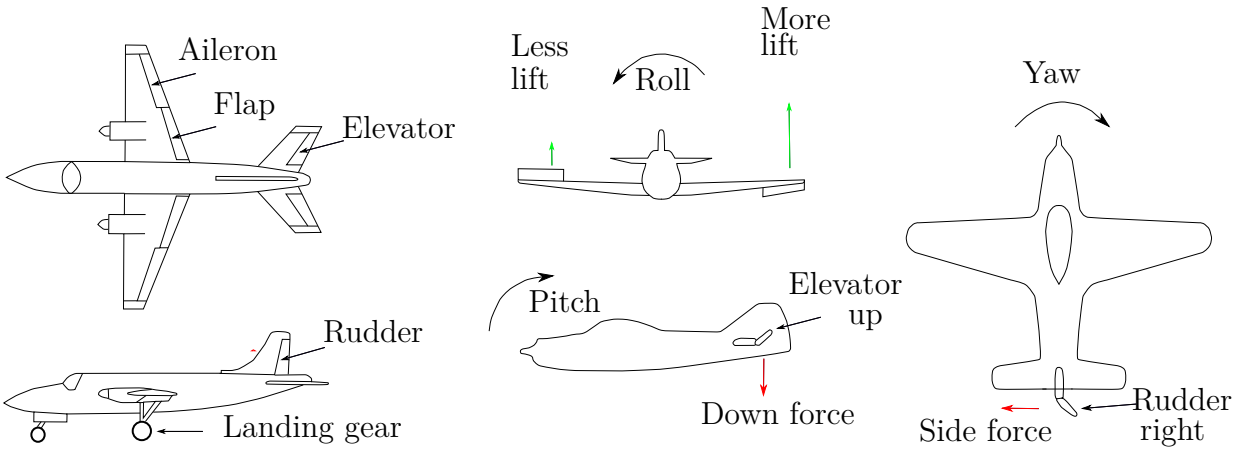

Figure 2.2: Control surfaces and their effects.

2.2 Vertical Take Off and Landing (VTOL) aircraft

As its name implies, a Vertical take-off and landing (VTOL) aircraft can perform vertical take-off and landing as well as stationary flight. Today, many families of VTOLs exist such as helicopters, tail sitters, quadrotors, etc (see Figure 2.3). The following presents the class of rotary-wing VTOL (RWVTOL) aircraft; for additional material on VTOLs see (Campbell, 1962) and (Markman and Holder, 1962).

2.2.1 Rotary-wing VTOL (RWVTOL) aircraft

RWVTOL aircraft are equipped with one (or several) main rotor(s) allowing two (or several) blades to rotate; the blades' rotation generates the *thrust force* for the aircraft to fly. This thrust depends upon the blades' orientations and the rotor's rotational velocity, also called *rounds per minute* (RPM) (Prouty, 2005). Hence, thrust control can be achieved by changing the rotor's RPM or/and the blades' orientations, depending on the vehicle's means of actuations. For example, quadrotors and tailsitters usually allow for RPM control only, while single-rotor helicopters also posses blade-orientation control.

The design of a RWVTOL aircraft must deal with the problem of counteracting parasite torques generated by the rotors. Figure 2.4 depicts three aircraft configurations that deal with this problem. Figure 2.4a shows the solution based on an auxiliary rotor

Figure 2.3: Examples of RWVTOLs (source *Wikipedia*).

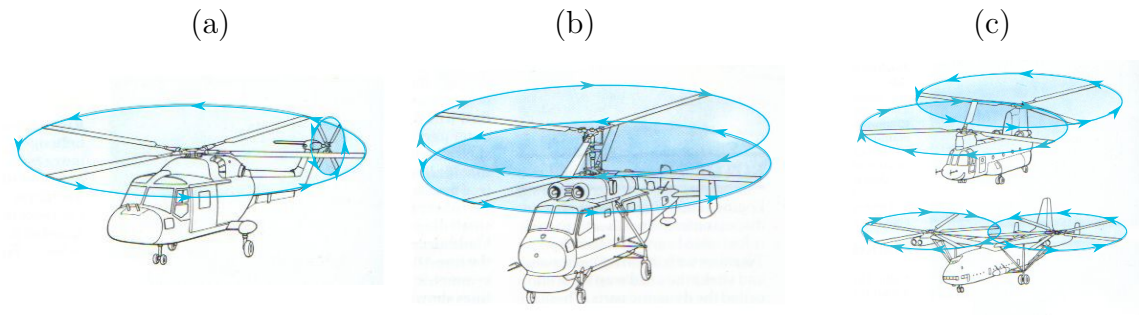

Figure 2.4: Different anti torque systems (*aerospaceweb.org*).

mounted (vertically) on the tail of the vehicle: the thrust generated by this auxiliary rotor generates the torque that compensates for the parasite torque produced by the main rotor. Figure 2.4b shows the so-called *coaxial rotor configuration*: a pair of rotors, installed one above the other, rotate in opposite directions about the same axis of rotation. Figure 2.4c shows the so-called *tandem rotor configuration*: two rotors installed on each end of the fuselage rotate in opposite directions; a transmission mechanism synchronizes the two rotors so as to avoid blades collision even during an engine failure. In the case of quadrotors, parasite torques are counteracted by rotating the four rotors in pairs and in opposite directions.

The orientation of a RWVTOL is modified mostly by unbalancing the thrust forces generated by the blades. For instance (see Figure 2.5), the yaw angle of a single-rotor helicopter can be changed via the auxiliary-rotor thrust control, while its roll and pitch angles via the main-rotor thrust control. To unbalance the thrust forces generated by the blades, helicopters use the so-called *swashplate mechanism* (Figure 2.6). The pivotal parts of this mechanism are two discs installed one above the other, and whose centers lie on the axis of the blades' rotation. The disc on the top is attached to the blades so that its vertical displacement modifies the blades' orientation; this disc rotates in unison with the blades. The disc on the bottom does not rotate with the blades, but can modify both the vertical position and orientation of the disc above it. Figure 2.6a depicts a swashplate in the resting position: the blades do not produce any thrust. By pushing the rotating disc up via the disc below it, blades bend, so a downward force is generated (Figure 2.6b). By inclining the rotating disc, the orientation of each blade varies while rotating, and force distributions such as the one shown in Figure 2.6c can be generated.

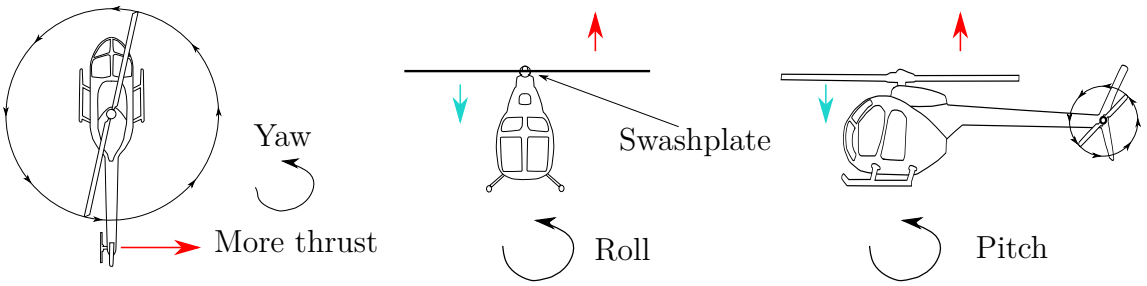

Figure 2.5: Effects of thrust regulation.

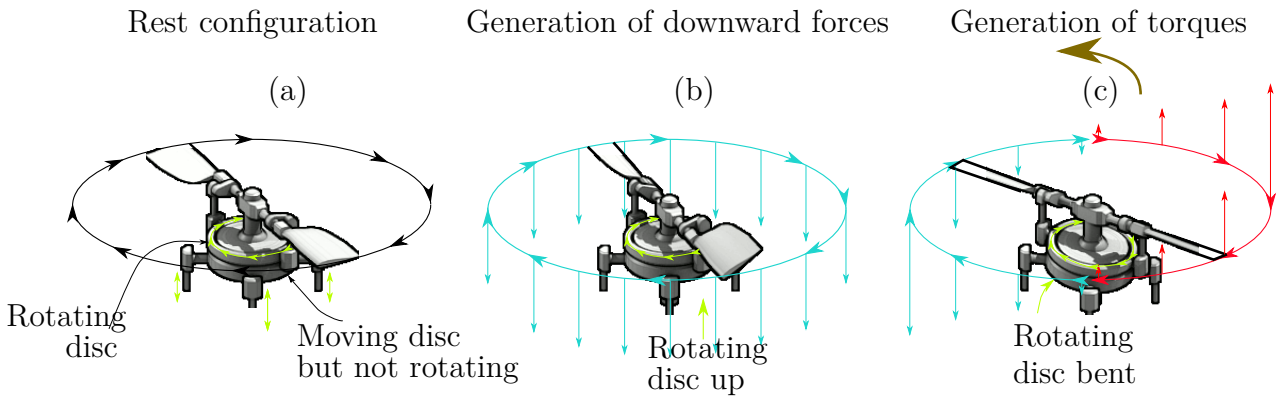

Figure 2.6: Effects of swashplate on the thrust force and torque produced by the blades.

2.3 CONVERTIBLE AIRCRAFT

Convertible aircraft – also called *hybrid aircraft* – can perform stationary flight and also benefit from lift properties via optimized fixed-wings' airfoils; therefore, they belong to both families of airplanes and VTOLs. The transitions between stationary flight and high-velocity cruise are called *transition maneuvers*, and their automatic monitoring is still a challenge these days. One of the major problems in controlling a convertible during the transition maneuvers is due to the strong variations of the aerodynamic forces, which depend upon the vehicle's velocity and orientation. However, the control of these transitions is intimately related to the nature of the convertible itself. In fact, the family of convertibles can be roughly divided in two subfamilies: tilting-thrust and fixed-thrust convertibles. The former are powered by a tilting thrust that allows one to modify the thrust's direction with respect to the vehicle; in this case, the transition maneuver can be performed by keeping approximately a constant vehicle's orientation (horizontal configuration in Figure 2.7). The latter are powered by a thrust force attached to the vehicle; in this case, important changes in the vehicle's orientation are required to perform the transition maneuver (see Figure 2.8). The control of a fixed-thrust convertible is inherently different from, and usually more involved than, the control of a tilting-thrust convertible. The present thesis deals with the control of fixed-thrust aircraft, thus encompassing the control of the transitions maneuvers of these vehicles.

Figure 2.7: A tilting-thrust convertible: AV-8B Harrier II (source *Wikipedia*).

Vertical Take-Off

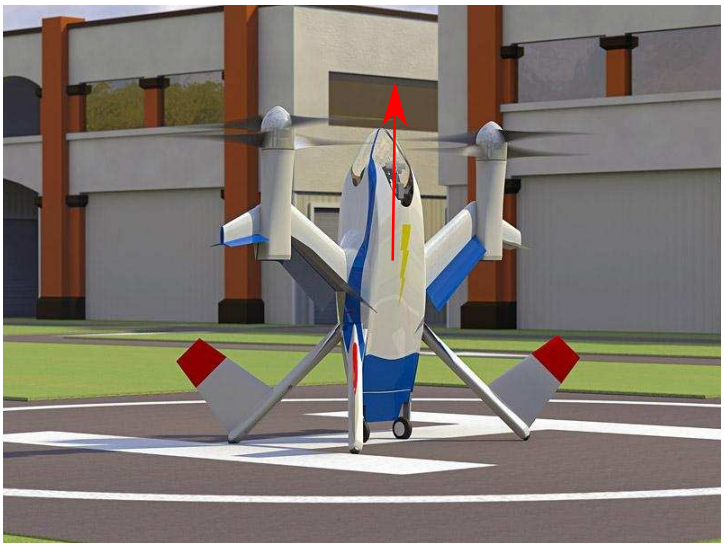

Transition maneuver

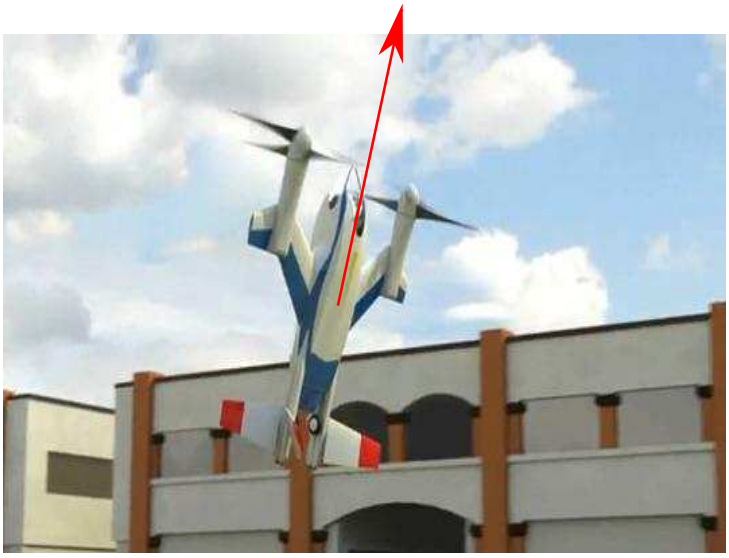

Efficient-steady flight

Figure 2.8: A fixed-thrust convertible: NASA Puffin (source *nasa.gov*).

3 Basics of aerodynamics

"The term "aerodynamics" is generally used for problems arising from flight and other topics involving the flow of air[1]*."*

The following introduces basic aerodynamic background by focusing on the aerodynamic forces and moments upon flat wings. For additional material on the fundamentals of aerodynamics see (Bertin and Smith, 2008) (Anderson, 2010).

3.1 Aerodynamic sources

The motion of a body immersed in air generates aerodynamic reaction effects that are due to only two sources (Anderson, 2010, p. 19) (Figure 3.1).

1) *Distribution of pressures.* The flow exerts pressures over the surface of the body. These pressures *act perpendicular* to the surface, and are position-dependent.

2) *Distribution of shear stresses.* Because of the friction between the flow and the body, position-dependent shear stresses *act tangentially* to the local surface.

The *sum* of pressure and shear stress distributions determine the total aerodynamic forces and moments on the body, the prediction of which is still a main concern in aerodynamics.

In practice, *wind tunnels* are the most used devices to carry out experiments for measuring aerodynamic forces and moments acting on a body since they generate constant, uniform flows of gases. An example of wind tunnel tests is shown in Figure 3.1c, where the gas used for the experiment was common smoke blown from the right of the figure to the left. The air motion over the wing is represented by several *streamlines*, which highlight some of the paths of the so-called *fluid elements* (small volumes of smoke). Figure 3.1c can be viewed as if the wing were flying into motionless air, or as if the wing were motionless and air were blown towards it; in these two cases, streamlines and aerodynamic effects would be exactly the same[2], so flight in air can be simulated in wind tunnels.

In theoretical aerodynamics, one of the main concerns is determining the distributions of pressures and shear stresses over the body's surface so that the integration of these distributions provides the aerodynamic forces and moments exerted on the body.

To date, the *Navier−Stokes equations* are the most important equations in all fluid dynamics: they describe the *local pressures and shear stresses* distributions of any flow

[1] Ludwing Prandlt, 1949.

[2] This observation was first made by Leonardo da Vinci.

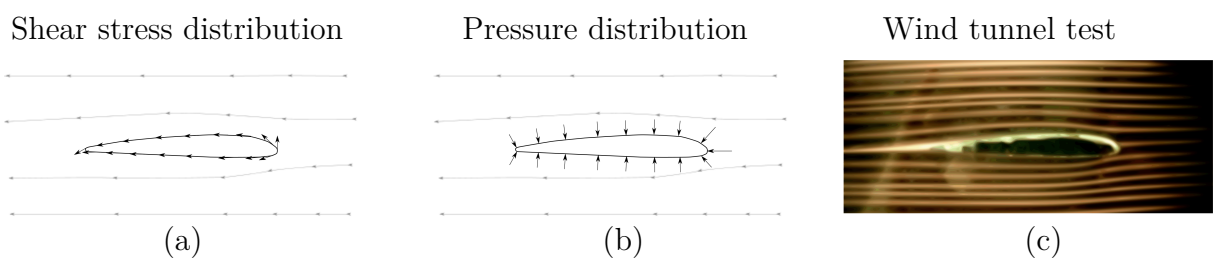

Figure 3.1: (a) and (b): forces distributions; (c): a wind tunnel test (*dept.aoe.vt.edu*).

over any body, independently from its shape. However, these equations consist of a set of nonlinear partial differential equations involving the *viscosity*, *compressibility*, *density*, and velocity of the fluid element at a given position, and their integration over the shape of the body does not typically yield closed-form expressions[3]. Thus, working out a functional model of aerodynamic forces and moments from Navier-Stokes equations is not always possible. The following presents a well-accepted general expression of aerodynamic forces and moments deduced from the application of the so-called *dimensional analysis*.

3.2 Variations of aerodynamic forces and moments: dimensional analysis

The minimum number of independent dimensionless variables that describe the variations of aerodynamic forces and moments can be found by applying the method of *dimensional analysis*. (Bridgman, 1969) writes: "the principal use of dimensional analysis is to deduce from a study of the dimensions of the variables in any physical system certain limitations on the form of any possible relationship between those variable. The method is of great generality and mathematical simplicity". The foundations of dimensional analysis were laid down by James Clerk Maxwell (1831 - 1879), Lord Rayleigh (1842-1919), Osborne Reynolds (1842-1912) and other scientists and engineers in France[4], whose theories were formalized by the Buckingham Pi theorem (Buckingham, 1914).

Theorem 3.1 (Buckingham pi theorem from (Anderson, 2010))**.** Let K equal the number of *base* dimensions required to describe the physical variables. (In mechanics, all physical variables can be expressed in terms of the dimensions of mass, length, and time; hence, $K = 3$). Let $P_1, P_2 \ldots, P_N$ represent N physical variables in the physical relation

$$f_1(P_1, P_2 \ldots, P_N) = 0. \tag{3.1}$$

Then, Eq. (3.1) may be re-expressed as a relation of $(N - K)$ dimensionless products (called Π products),

$$f_2(\Pi_1, \Pi_2 \ldots, \Pi_{N-K}) = 0,$$

where each Π product is a dimensionless product of a set of K physical variables plus one

[3]We recall that the existence of a smooth, physically reasonable solution to the *Navier-Stokes equations* for three-dimensional flows is still a conjecture to these days (Fefferman, 2000) (Constantin, 2001).
[4]For details on the history of dimensional analysis see (Macagno, 1971).

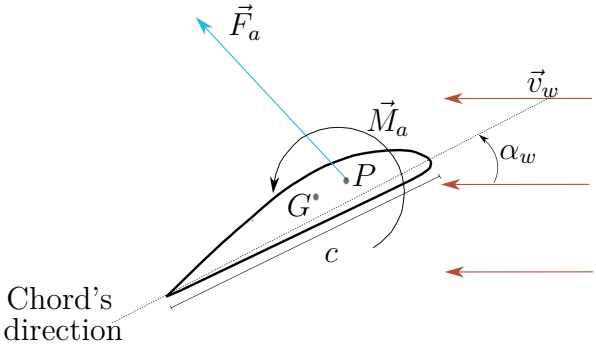

Figure 3.2: Aerodynamic forces and moments on a motionless body.

other variable. Let $P_1, P_2 \ldots, P_K$ be the selected set of K physical variables. Then

$$\begin{aligned} \Pi_1 &= f_3(P_1, P_2 \ldots, P_K, P_{K+1}) \\ \Pi_2 &= f_4(P_1, P_2 \ldots, P_K, P_{K+2}) \\ &\ldots \\ \Pi_{N-K} &= f_{N-K+2}(P_1, P_2 \ldots, P_K, P_N) \end{aligned}$$

The choice of the repeating variables $P_1, P_2 \ldots, P_K$ should be such that they include all the K dimensions used in the problem.

The underlying assumption of the above theorem is that

> *all physical quantities have dimensions which can be expressed as products of powers of the set of base dimensions*[5].

Now, focus on the motionless body shown in Figure 3.2, and assume that the wind velocity $\vec{v}_w$ is the same in the vicinity of the body. Let $\vec{F}_a$ and $\vec{M}_a$ denote the aerodynamic force and moment on the body, and P and G the application point of the aerodynamic force – also called *body's center of pressure* – and the body's center of mass, respectively. On an intuitive basis, we expect $\vec{F}_a$ to depend upon (Anderson, 2010, p. 35):

- The magnitude of the wind velocity $|\vec{v}_w|$, also called *windspeed* .
- The *freestream*[6] air density ρ.
- The effects of friction, represented by the freestream viscosity coefficient μ.
- A single reference length representing a measurement of a *dimension* of the body. In the case of wings, this reference length is usually chosen as the *chord length* c, that is the measurement of the distance between leading and trailing edge.
- The compressibility of the air, which is related to the speed of sound a.

Therefore, the above leads to write

$$\vec{F}_a = \vec{f}(|\vec{v}_w|, \rho, \mu, c, a). \tag{3.2}$$

After applying the Buckingham PI theorem, Eq. (3.2) becomes (Anderson, 2010, p. 39)

$$\vec{F}_a = \frac{\rho c^2 |\vec{v}_w|^2}{2} \vec{C}(R_e, M), \qquad R_e := \frac{\rho c |\vec{v}_w|}{\mu}, \qquad M := \frac{|\vec{v}_w|}{a}, \tag{3.3}$$

where $\vec{C}(\cdot)$ is the *dimensionless static force coefficient* that depends on the Reynolds and Mach numbers R_e and M. Now, observe that:

[5]From (Sonin, 2001), which also presents a tutorial introduction to the use of dimensional analysis.
[6]The fluid's freestream characteristics are those far from the body.

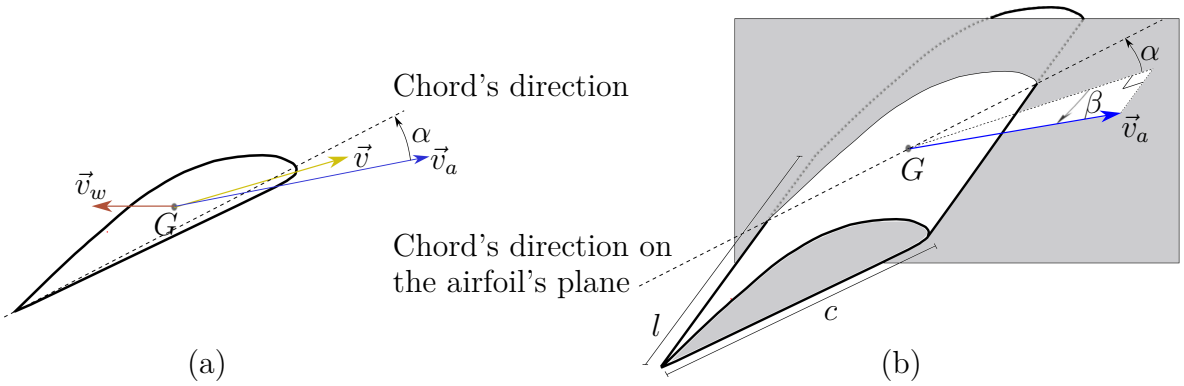

Figure 3.3: Common choices for the airflow angles in the case of flat wings.

- The term c^2 in Eq. (3.3) has the dimension of an area, so we can replace it with any reference area S (Anderson, 2010, p. 38). In the case of flat wings, the reference area is usually defined as $S := lc$, where l denotes the *wingspan* (see Figure 3.3b).
- Eq. (3.3) is derived by assuming a motionless body. If the body moves with constant velocity[7], we must replace the wind velocity $\vec{v}_w$ with the *body's relative velocity to the wind* $\vec{v}_a$, also called *airvelocity*. In particular, the airvelocity $\vec{v}_a$ is defined as the difference between the velocity of the body's center of mass, denoted by $\vec{v}$, and the wind velocity $\vec{v}_w$, that is

$$\vec{v}_a := \vec{v} - \vec{v}_w. \tag{3.4}$$

- In general, the direction of the airvelocity with respect to the body is not constant. Consequently, the force coefficient $\vec{C}(\cdot)$ in Eq. (3.3) also depends upon this direction. For planar problems (see Figure 3.3a), the airvelocity's direction with respect to the body is given by only one angle, usually defined as the *angle of attack* α between $\vec{v}_a$ and a direction attached to the body, such as the chord's direction of an airfoil. For three-dimensional problems, the airvelocity's direction with respect to the body is given by two angles, usually denoted by (α, β). In the case of "flat" wings, the common choice of (α, β) is shown in Figure 3.3b and β is called *side-slip* angle.

Therefore, Eqs. (3.3) specializes to

$$\vec{F}_a := k_a |\vec{v}_a|^2 \vec{C}(R_e, M, \alpha, \beta), \tag{3.5a}$$

$$k_a := \frac{\rho S}{2}, \quad R_e := \frac{\rho c |\vec{v}_a|}{\mu}, \quad M := \frac{|\vec{v}_a|}{a}. \tag{3.5b}$$

The expression (3.5a) implies that the static force coefficient $\vec{C}(\cdot)$ of *geometrically similar* bodies[8] at the same (R_e, M) are identical at fixed airvelocity's direction. Consequently, the force coefficient $\vec{C}(\cdot)$ of a full-size aircraft can be obtained by carrying out measurements on a small-scale model.

By applying the basic concepts of mechanics, the aerodynamic moment about the body's center of mass is given by

$$\vec{M}_a := \vec{GP} \times \vec{F}_a. \tag{3.6}$$

[7]The body's motion is supposed at low rotation rates. High body rotation rates destroy the assumption that the aerodynamic force is independent of the body's angular velocity.

[8]Two bodies are geometrically similar if the shape of either one is obtained by uniformly scaling the shape of the other one.

Let us remark that the body's center of pressure P depends on the Reynolds and Mach numbers as well as on the airvelocity's direction with respect to the body. As a consequence, taking measurements of the aerodynamic effects at the center of pressure is a difficult task, all the more so because its position is very difficult to predict over large variations of the airvelocity. The measurements of aerodynamic forces and moments are then usually taken at another fixed point, here denoted by R. Let $\vec{M}_{a_R}$ denote the aerodynamic moment measured at R. Thus , the aerodynamic moment about the center of mass is given by (Stevens and Lewis, 2003, p. 101)

$$\vec{M}_a = G\vec{R} \times \vec{F}_a + \vec{M}_{a_R}. \tag{3.7}$$

For planar problems, the (static) aerodynamic moment can be written as $\vec{M}_a = M_p \hat{n}$, where $\hat{n}$ is a unitary perpendicular to the plane and M_p the magnitude of $\vec{M}_a$, also called *pitching moment*. Dimensional analysis applied to the pitching moment yields

$$M_p := k_a c |\vec{v}_a|^2 C_M(R_e, M, \alpha), \tag{3.8}$$

where C_M is a dimensionless coefficient called *pitching moment coefficient*.

3.3 Lift and drag forces in terms of aerodynamic coefficients

The aerodynamic force is usually decomposed into two components (see Figure 3.4).

- Lift force: aerodynamic force component along a perpendicular to the airvelocity.
- Drag force: aerodynamic force component along the airvelocity's direction.

When this decomposition is applied to the static force coefficient $\vec{C}(\cdot)$ given by Eq. (3.5a), the static aerodynamic force can be expressed in terms of two dimensionless coefficients $C_L(\cdot)$ and $C_D(\cdot)$ such that

$$\vec{F}_a := k_a |\vec{v}_a| \left[C_L(R_e, M, \alpha, \beta) \vec{v}_a^{\perp} - C_D(R_e, M, \alpha, \beta) \vec{v}_a \right], \tag{3.9}$$

with $\vec{v}_a^{\perp}$ a perpendicular to the airvelocity that may depend upon (R_e, M). In the specialized literature, C_L ($\in \mathbb{R}$) and C_D ($\in \mathbb{R}^+$) are called the *aerodynamic characteristics* of the body, and also the *lift coefficient* and *drag coefficient*. Aerodynamic force coefficients were first introduced by Otto Lilienthal (1848 - 1896) in his book "Birdflight as the Basis of Aviation" (1889); however, he introduced coefficients to parametrize the aerodynamic force's components along the wing's chord direction and its perpendicular. The Wright brothers were among the first to use the coefficients C_L and C_D, but the famous form

$$\begin{aligned} \text{Lift} &= q_\infty S C_L \\ \text{Drag} &= q_\infty S C_D, \end{aligned}$$

with $q_\infty := 0.5 \rho_f |\vec{v}_a|^2$ – the *dynamic pressure* – was later introduced by Ludwig Prandtl in about 1920's[9].

As for the force coefficient $\vec{C}(\cdot)$, the lift and drag coefficients of a full-size aircraft can be obtained by performing measurements on a small-scale model.

[9]The history of the aerodynamic coefficients is detailed in (Anderson, 2010, p. 93).

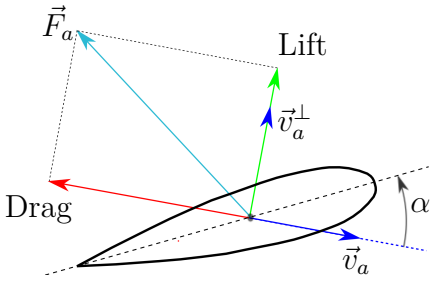

Figure 3.4: Lift and drag components when the airvelocity belongs to the *airfoil plane*.

3.3.1 EXPERIMENTAL AERODYNAMIC COEFFICIENTS OF FLAT WINGS

Figure 3.5 depicts typical experimental data – borrowed from (Davis et al., 2004) – of flat wings' aerodynamic coefficients. These data were taken for a symmetric airfoil NACA 0021 (shown in Figure 3.4) of $l = 0.91m$, $c = 0.1524m$, and at $(R_e, M) \approx (160 \cdot 10^3, 0.3)$; the angles (α, β) were defined as shown in Figure 3.3b, but β was kept equal to zero.

Figure 3.5 shows that at low angles of attack, the lift coefficient is linear while the drag coefficient is basically constant. Increasing the angle of attack produces stronger *vortex* within the flow (see Figure 3.6), but as long as the flow remains attached to the wing, the vortex effects do not basically affect the aforementioned relationships. At certain values of the angle attack, the upper-surface flow starts detaching from the surface, thus creating stronger *turbulence* both above and after the wing. For these values of α, the lift coefficient is no longer linear versus the angle of attack, and it achieves a local maximum at the so-called *stall angle* α_s. Beyond the stall angle, the upper-surface flow separates completely, and this causes rapid lift reductions and drag increases. These two variations are called *stall phenomena*, and the domain on which they occur *stall region*.

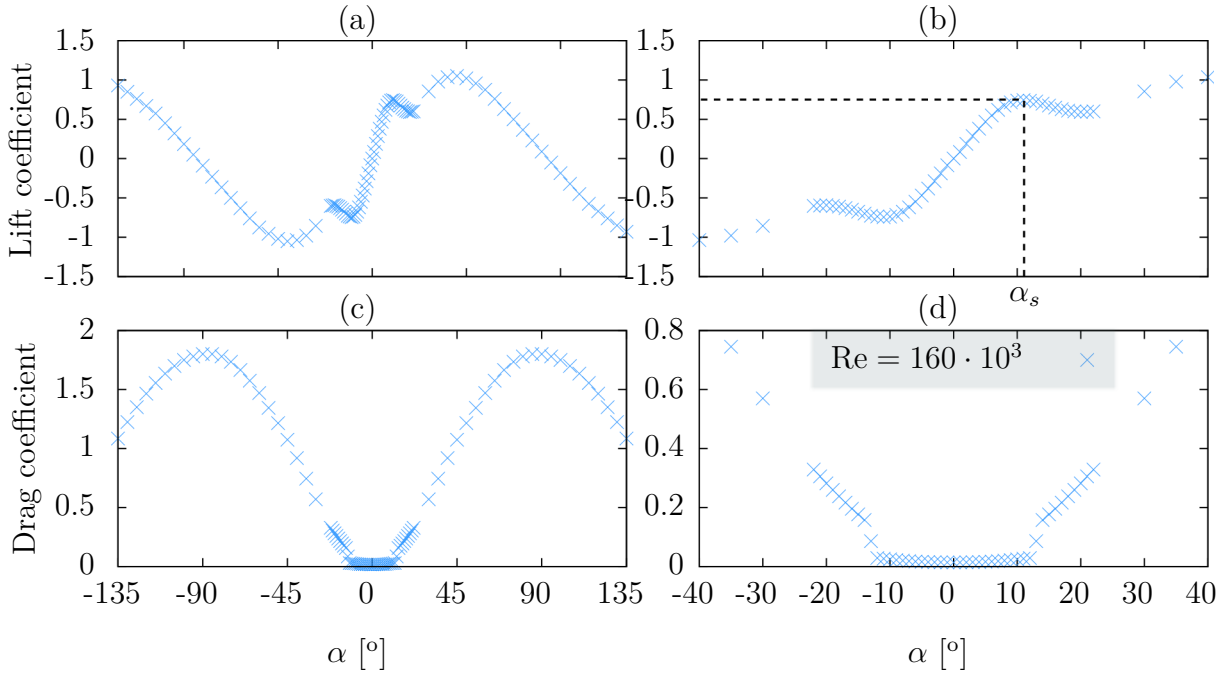

Figure 3.5: Lift and drag coefficients of NACA 0021.

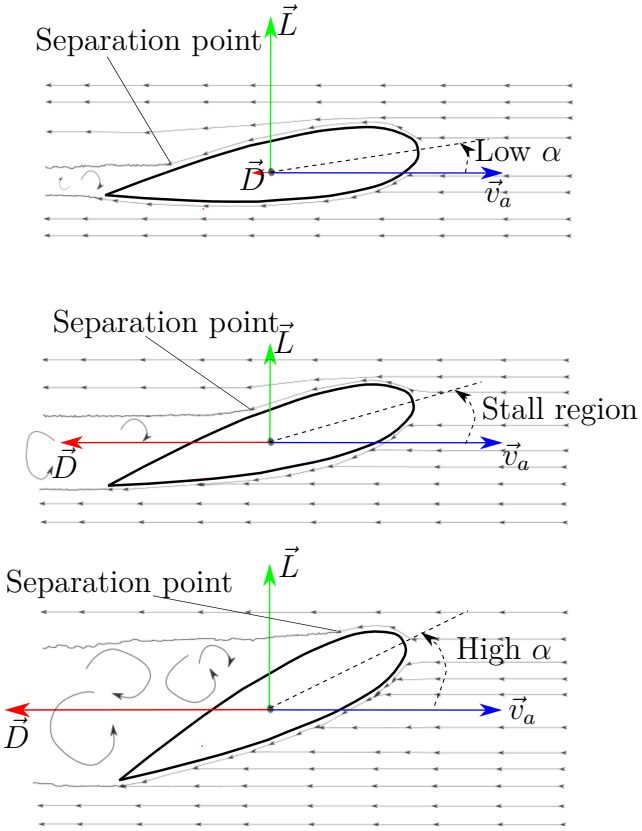

Figure 3.6: Effects of increasing the angle of attack on the airflow surrounding a wing.

Stall phenomena are highly nonlinear and predicting the behaviors of the aerodynamic characteristics on the stall region with a high degree of reliability is very challenging. As a matter of fact, the aerodynamic characteristics on the stall region depend also on the *direction of change of the angle of attack*, as shown in Figure 3.7 – data borrowed from (Critzos and Heyson, 1955, p. 17). The dependencies of the aerodynamic characteristics upon the direction of change of α are called *aerodynamic hysteresis*.

At *low-airspeeds* ($M < 0.3$), the flow can be considered incompressible, and the aerodynamic characteristics independent of the Mach number. In this regime, the aerodynamic coefficients principally vary with the angle of attack α and the Reynolds number R_e only.

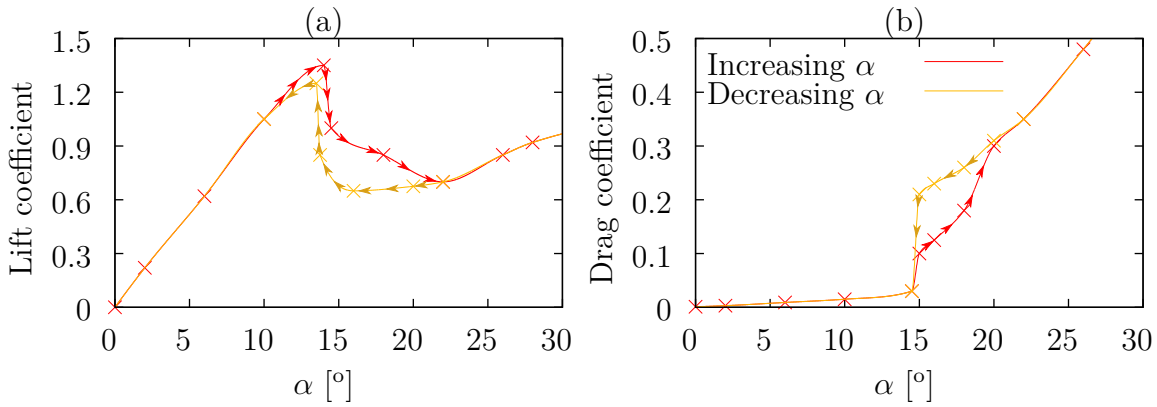

Figure 3.7: Effects of the direction of change of α on the aerodynamic coefficients.

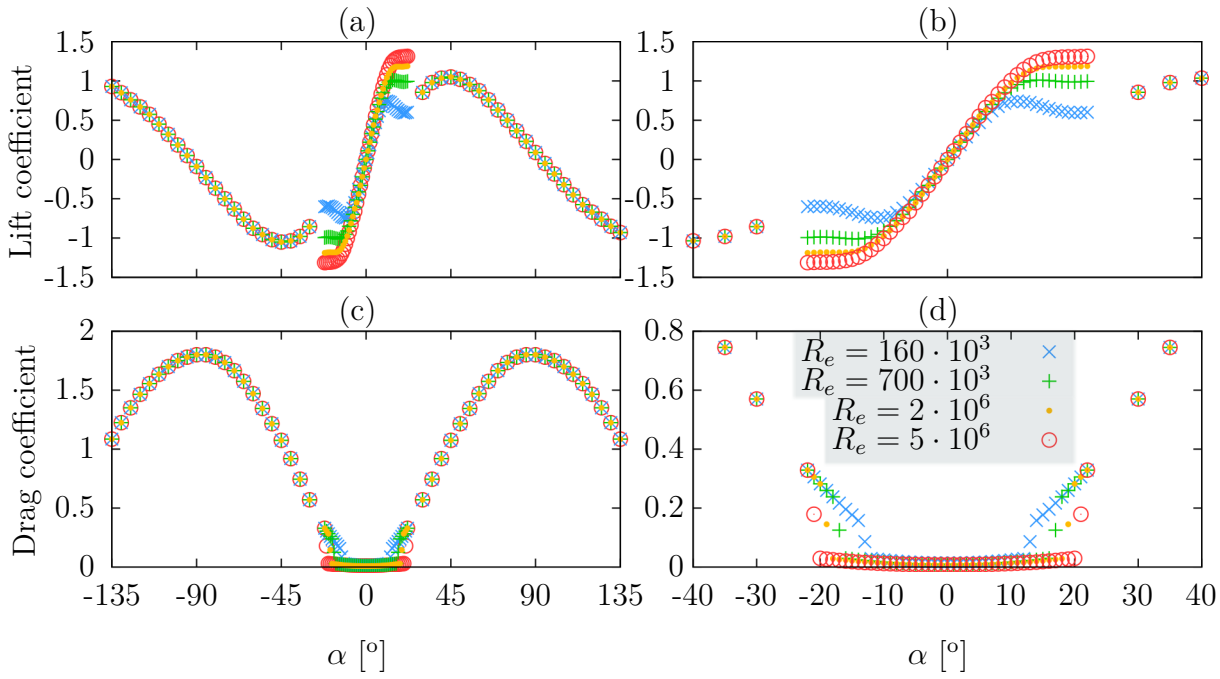

Figure 3.8: Aerodynamic characteristics of NACA 0021 at several Reynolds numbers.

Figure 3.8 shows typical (average) experimental data – still borrowed from (Davis et al., 2004) – taken at several Reynolds numbers: it is visually evident that the larger the Reynolds number, the larger the domain on which the lift is linear and the drag is (almost) constant versus small angles of attack. At high angles of attack, instead, the aerodynamic characteristics are basically independent of the Reynolds number. Observe also that stall phenomena are less pronounced at smaller Reynolds numbers. As a matter of fact, in the case of NACA airfoils (Zhou et al., 2011) shows that there exists a value for R_e, typically smaller than 10^4, under which these phenomena are basically absent.

3.3.2 EXPERIMENTAL AERODYNAMIC COEFFICIENTS OF ELLIPTIC-SHAPED BODIES

Besides flat wings, ellipsoids represent a class of shapes well-referenced in the specialized literature. Figure 3.9 depicts typical experimental data borrowed from (Keyes, 1965, p.19) taken for an ellipsoid of $h = 0.2m$, $c = 0.1m$, $t = 0.05m$ and at $(R_e, M) = (7.96 \cdot 10^6, 6)$. Although a high Reynolds number, observe that no stall phenomena occur.

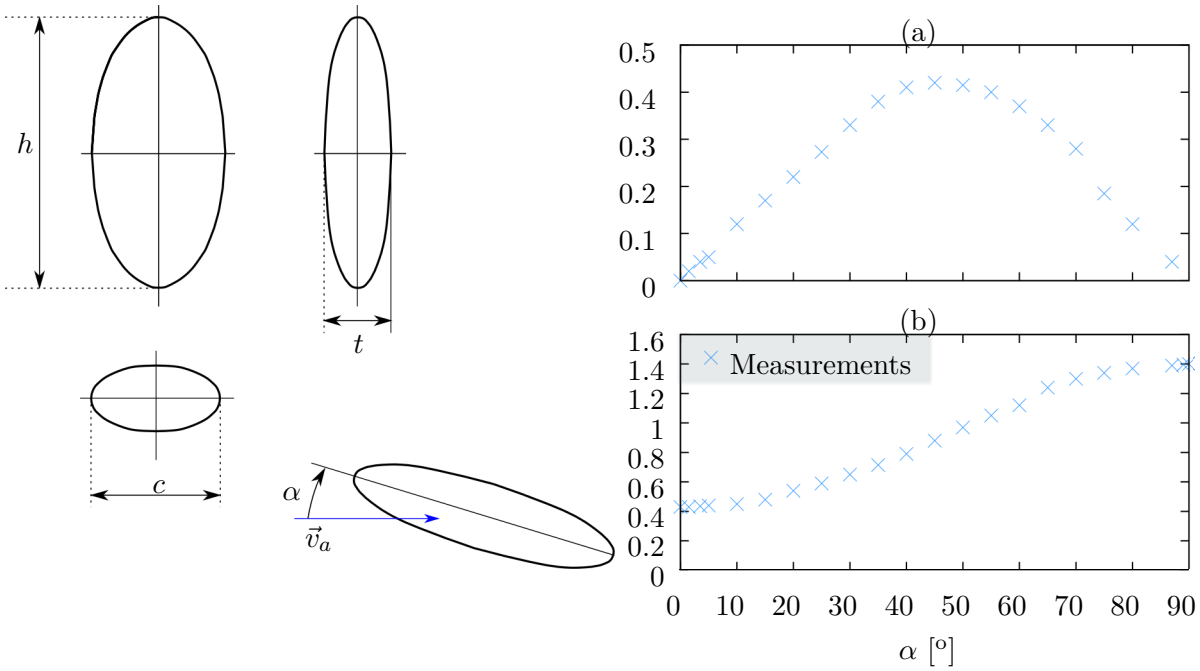

Figure 3.9: Aerodynamic coefficients of elliptic shaped bodies.

4 Basics of flight dynamics

> *"[...] the scheme of flying by artificial wings has been much ridiculed; and indeed the idea of attaching wings to the arms of a man is ridiculous enough, as the pectoral muscles of a bird occupy more than two-thirds of its whole muscular strength, whereas in man the muscles, that could operate upon wings thus attached, would probably not exceed one-tenth of his whole mass. [...]. I feel perfectly confident, however, that this noble art will soon be brought home to man's general convenience, and that we shall be able to transport ourselves and families, and their goods and chattels, more securely by air than by water, and with a velocity of from 20 to 100 miles per hour. To produce this effect, it is only necessary to have a first mover, which will generate more power in a given time, in proportion to its weight, than the animal system of muscles*[1]*."*

Flight dynamics is the study of the performance, stability, and control of aerial vehicles flying through the air or in outer space (Stengel, 2004). What follows aims at introducing the principles of aircraft dynamics in air. For additional material on this subject see, among others, (Talay, 2005), (Stevens and Lewis, 2003) and (Stengel, 2004).

4.1 Flight environment: the Earth's atmosphere

The gaseous envelope that surrounds our planet is what we commonly call the *Earth's atmosphere*, and the mixture of gases composing it is the so-called *air*. The *atmospheric circulation* maintains the ratios between the elements that compose the air approximately constant up to altitudes of approximately 90 km. Measurements and analysis of atmospheric air taken at sea level point out that air is principally composed of four elements (Talay, 2005): Nitrogen (N_2) 78.084 %, Oxygen (O_2) 20.948 %, Argon (Ar) 0.934 %, Carbon Dioxide (CO_2) 0.031 %. This normal composition can vary considerably when measured in industrialized areas, where air pollution raises the percentages of several harmful elements.

Besides air composition, one way to characterize different *atmosphere's layers* is the gradient of the air's temperature. By using the temperature gradient-based criterion (see Figure 4.1), the atmosphere is commonly subdivided into five layers (ascending order): troposphere, stratosphere, mesosphere, thermosphere, and exosphere. Airliners fly in the troposphere since it yields a good trade-off for lift versus air resistance.

[1] George Cayley, from his "On Aerial Navigation, part one", 1809.

(a) (b)

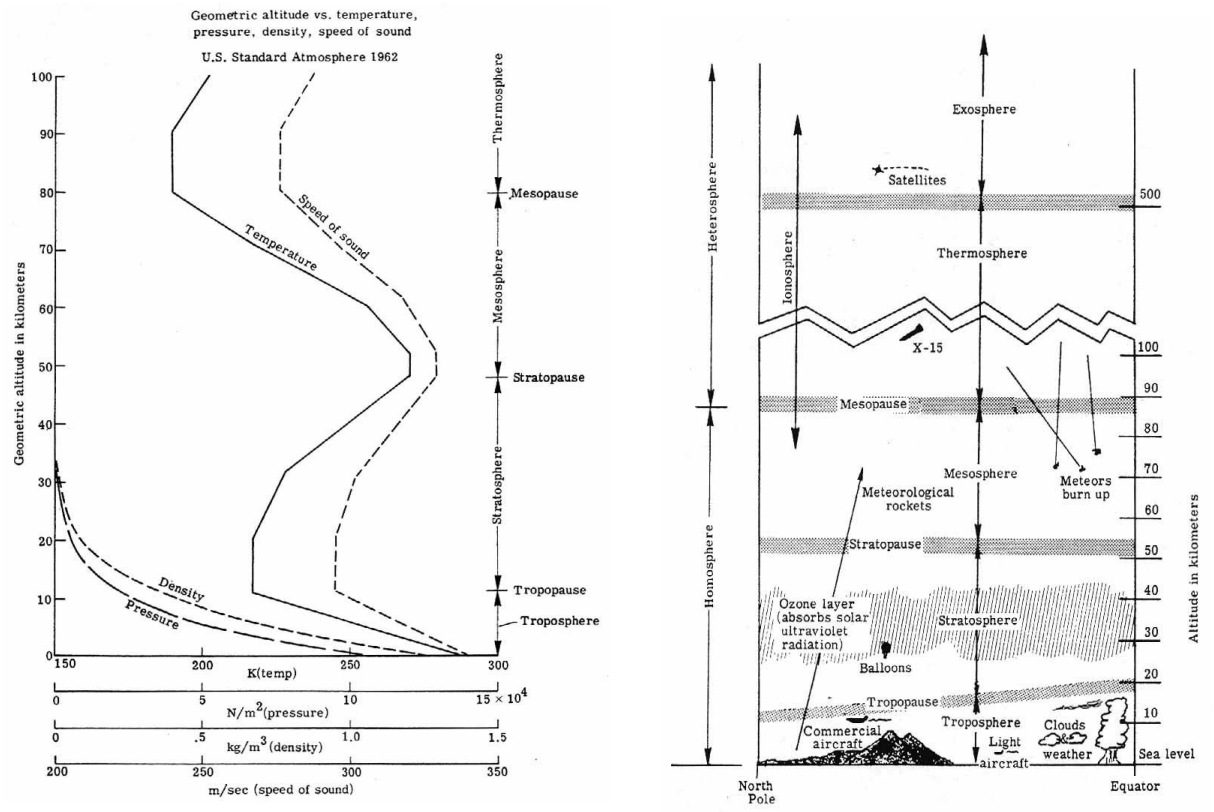

Figure 4.1: (Talay, 2005) (a): atmosphere's characteristics; (b): atmosphere's sketch.

The atmosphere's characteristics are in general dependent on time (atmospheric circulation) and on position (altitude dependence). Several models of these dependencies have been derived in the last decades, among which the so-called *standard atmosphere model*. This model assumes the air "to be devoid of dust, moisture, and water vapor, and to be at rest with respect to the Earth" (Talay, 2005). Figure 4.1 shows the variations of the speed of sound, temperature, density, and pressure given by the U.S. Standard Atmosphere model (1962). This model still plays a fundamental role in the design of an aerial vehicle.

For aircraft flying at low altitudes, the atmosphere's characteristics can be considered constant and equal to those measured at sea level. The 1962 U.S. Standard Atmosphere gives the following sea level characteristics.

Table 4.1: Sea level conditions from 1962 U.S. Standard Atmosphere

Variable	Value
Pressure	$p = 1.03\ Kg/cm^2$
Density	$\rho = 1.225\ kg/m^3$
Temperature	$T = 288.15\ K$ (15° C)
Acceleration of gravity	$g = 9.807\ m/sec^2$
Speed of sound	$a = 340.29\ m/sec$

4.2 Dynamics of aircraft motions

Aircraft dynamics are described by a set of differential equations that can characterize the *state of the aircraft* in terms of the vehicle's orientation, position, and *angular* and *linear* velocities. These variables are measured with respect to some reference frames.

4.2.1 Reference frames

Let $\mathcal{I} = \{O; \vec{\imath}_0, \vec{\jmath}_0, \vec{k}_0\}$ be a fixed inertial frame with respect to (w.r.t.) which the vehicle's absolute pose is measured. This frame is chosen as the NED frame (North-East-Down) with $\vec{\imath}_0$ pointing to the North, $\vec{\jmath}_0$ pointing to the East, and $\vec{k}_0$ pointing to the center of the earth. Let $\mathcal{B} = \{G; \vec{\imath}, \vec{\jmath}, \vec{k}\}$ be a frame attached to the body, with G the body's center of mass. The linear and angular velocities $\vec{v}$ and $\vec{\omega}$ of the body frame $\mathcal{B}$ are then defined by

$$\vec{v} := \frac{d}{dt}\vec{OG} \ , \tag{4.1a}$$

$$\frac{d}{dt}(\vec{\imath}, \vec{\jmath}, \vec{k}) := \vec{\omega} \times (\vec{\imath}, \vec{\jmath}, \vec{k}). \tag{4.1b}$$

The vehicle's orientation w.r.t. the inertial frame is represented by the rotation matrix R whose column vectors are the vectors of coordinates of $\vec{\imath}, \vec{\jmath}, \vec{k}$ expressed in the basis of $\mathcal{I}$.

4.2.2 Aircraft dynamics equations for a flat earth

Let $\vec{F}$ and $\vec{M}$ denote the resultants of the external forces and moments on a rigid body of mass m. By taking the external moments $\vec{M}$ about the body's center of mass G, Newton's and Euler's theorems of mechanics state that

$$\frac{d}{dt}\vec{p} = \vec{F} \ , \tag{4.2a}$$

$$\frac{d}{dt}\vec{h} = \vec{M} \ , \tag{4.2b}$$

with

$$\vec{p} := m\vec{v} \ , \tag{4.3a}$$

$$\vec{h} := -\int_{P' \in \text{ body}} \vec{GP'} \times (\vec{GP'} \times \vec{\omega}) \ dm. \tag{4.3b}$$

In the first approximation, aircraft can be modeled as rigid bodies immersed in air. Also, aerial vehicles are usually controlled via a thrust force $\vec{T} = -T\vec{k}$ for translational motion – with $T \in \mathbb{R}$ the thrust intensity – and a torque vector $\vec{M}_I$ for attitude monitoring. The torque actuation is typically generated in several ways (see Chapter 2), e.g. control surfaces (fixed-wing aircraft), propellers (quadrotors), etc. By neglecting round-earth effects, buoyancy forces[2], and gravity torques, the external forces and moments on an

[2]The aircraft is assumed to be much heavier than air.

aircraft are commonly modeled as follows (Fossen, 1994, Ch. 2), (Hua et al., 2009b), (Stengel, 2004), (Stevens and Lewis, 2003):

$$\vec{F} = \vec{F}_a + mg\vec{k}_0 - T\vec{k} + \vec{F}_b \ , \tag{4.4a}$$
$$\vec{M} = \vec{M}_a + T\vec{k} \times G\vec{\Theta} + \vec{M}_I \ , \tag{4.4b}$$

where $(\vec{F}_a, \vec{M}_a)$ are the aerodynamic forces and moments, Θ is the application point of the thrust force, and g is the gravity acceleration. In Eqs (4.4b) the gyroscopic torque, usually associated with rotor craft, has been neglected. The force $\vec{F}_b$ is referred to as *body force*, and is usually generated to create the torque input $\vec{M}_I$. Thus, this force represents a coupling between the torque actuation and the external force $\vec{F}$, and its importance at the control level is discussed in Section 4.3. An expression of the body force on a common helicopter is given in (Hua, 2009, Ch.1) (Olfati-Saber, 2001, Ch.5) (Koo and Sastry, 1998), and on the HoverEye tailsitter in (Pflimlin et al., 2004) (Pflimlin, 2006, Ch. 3).

Note that Eqs. (4.1)-(4.4) are "coordinate-free", and thus independent from the reference frame used to express the vectors in these equations. Now, assume that the mass m of the vehicle is constant. Then, Eqs. (4.1)-(4.4) expressed with coordinates in the body frame $\mathcal{B}$ can be written as

$$\dot{x} = Rv, \tag{4.5a}$$
$$\dot{R} = RS(\omega), \tag{4.5b}$$
$$m\dot{v} = -S(\omega)mv + \overline{F} \ , \tag{4.5c}$$
$$J\dot{\omega} = -S(\omega)J\omega + \overline{M} \ , \tag{4.5d}$$

with $\vec{v} = (\vec{\imath}_0, \vec{\jmath}_0, \vec{k}_0)\dot{x} = (\vec{\imath}, \vec{\jmath}, \vec{k})v$, $\vec{\omega} = (\vec{\imath}, \vec{\jmath}, \vec{k})\omega$, $\vec{F} = (\vec{\imath}, \vec{\jmath}, \vec{k})\overline{F}$, $\vec{M} = (\vec{\imath}, \vec{\jmath}, \vec{k})\overline{M}$,

$$J = -\int_{p_G \in \text{body}} S^2(p_G)\, dm, \tag{4.6}$$

and $G\vec{P}' = (\vec{\imath}, \vec{\jmath}, \vec{k})p_G$. The model (4.5) should be complemented by a modeling of the actuators that generate the inputs T and $\vec{M}_I$. However, by assuming that the dynamics of these actuators are (sufficiently) faster than the vehicle's dynamics, they can be neglected in the first approximation. This decoupling between vehicle' and actuators' dynamics allows us to focus on *common denominators* of the control problem associated with (4.5), independently from the specific issues related to the generation of the control inputs.

4.2.3 AERODYNAMIC FORCES AND MOMENTS ACTING ON THE AIRCRAFT

The modeling of aerodynamic forces and torques $\vec{F}_a$ and $\vec{M}_a$ acting on the vehicle remains one of the major problems in the modeling processes. Specialized aerodynamic discussions can be found in (Anderson, 2010) (Stengel, 2004, Ch. 2) (Stevens and Lewis, 2003, Ch. 2) for fixed-wing aircraft, in (Pounds et al., 2010a) (Huang et al., 2009) (Bristeau et al., 2009b) for quadrotors, in (Johnson and Turbe, 2006) (Ko et al., 2007) (Pflimlin, 2006, Ch. 3) (Pflimlin et al., 2010) for ducted-fan tail-sitters, and in (Naldi, 2008b), (Prouty, 2005), (Vilchis et al., 2003) for helicopters.

We have seen in Section 3.2 that the *static* aerodynamic forces and moments can be expressed in terms of the Reynolds and Mach numbers and the airvelocity's direction

with respect to the aircraft. However, the problem of finding the expressions of these dependencies was not addressed. One way to obtain a model of the aerodynamic forces and moments is based on the *superposition principle*, which essentially consists of:
i) decomposing the aircraft in several rigid bodies;
ii) computing or measuring the aerodynamic forces and moments acting on each body;
iii) summing up all these aerodynamic forces and moments to obtain $\vec{F}_a$ and $\vec{M}_a$.
The validity of this method requires close attention since the airflow on each part of the aircraft depends also upon the *positions* of the other bodies composing the vehicles. Furthermore, this method often provides only a static model of the aerodynamic effects.

A *static* model of the aerodynamic forces and moments is no longer valid when the effects of *rotational and unsteady motions* become preponderant. These motions are principally due to two different causes: spatial and temporal variations in the airflow pattern (Stengel, 2004, p. 199). For instance, a constant angular velocity flight, if it were feasible, would generate a different airflow pattern from that in steady flight. Then, the aerodynamic forces and moments depend also on the vehicle's angular velocity, and are in general different from those on the aircraft in steady flight. In addition, the aircraft *translational and rotational* accelerations also perturb the airflow pattern, which in turn "produces transitory forces and moments that depend not only on the instantaneous accelerations, but also on their *state history*" (Stengel, 2004, p. 200). Abrupt wind velocity variations produce similar unsteady effects even when the aircraft's velocity is constant.

Classically, the rotational and unsteady effects are modeled as linear perturbations to the static aerodynamic moments and forces (Stengel, 2004, p. 200). For instance, a common model for the pitching moment coefficient $C_M(\cdot)$ of a *symmetric aircraft in symmetric flight* is given by

$$C_M(M, \alpha, \dot{M}, \dot{\alpha}, q, \dot{q}) = C_M(M, \alpha) + \frac{\partial C_M}{\partial \dot{M}}\dot{M} + \frac{\partial C_M}{\partial \dot{\alpha}}\dot{\alpha} + \frac{\partial C_M}{\partial q}q + \frac{\partial C_M}{\partial \dot{q}}\dot{q},$$

where q is the pitch rate, and the Reynolds number is considered as constant. The models for the other dimensionless coefficients, such as the lift, drag, etc., can be derived analogously (Stevens and Lewis, 2003, p. 109).

4.2.4 SYMMETRIC AIRCRAFT LONGITUDINAL DYNAMICS: A PLANAR CASE

If the vehicle's shape is symmetric w.r.t. the *vertical* plane defined by (see Figure 4.2)

$$\Pi := \{\lambda_1 \vec{k} + \lambda_2 \vec{\jmath} \colon \lambda_1, \lambda_2 \in \mathbb{R}\},$$

it follows from Eq. (4.6) that $J_{12} = J_{21} = J_{13} = J_{31} = 0$, where J_{ij} denotes the element in the ith row and jth column of the matrix J. Now, assume that:

- The vector $\vec{k}_0$ is parallel to Π (wings-level flight).
- $\vec{F}_a$ and $\vec{M}_a$ are parallel to Π and $\vec{\imath}$, respectively. For slow-time-varying dynamics, this assumption can be considered to hold when the airvelocity $\vec{v}_a$ belongs to Π.
- The vehicle's center of mass G and the application point Θ of the thrust force $\vec{T}$ belong to the plane Π. Then $\vec{k} \times \vec{G\Theta}$ is parallel to $\vec{\imath}$.
- The body force $\vec{F}_b$ in Eq. (4.4) is negligible.
- The torque control input $\vec{M}_I$ is parallel to $\vec{\imath}$.

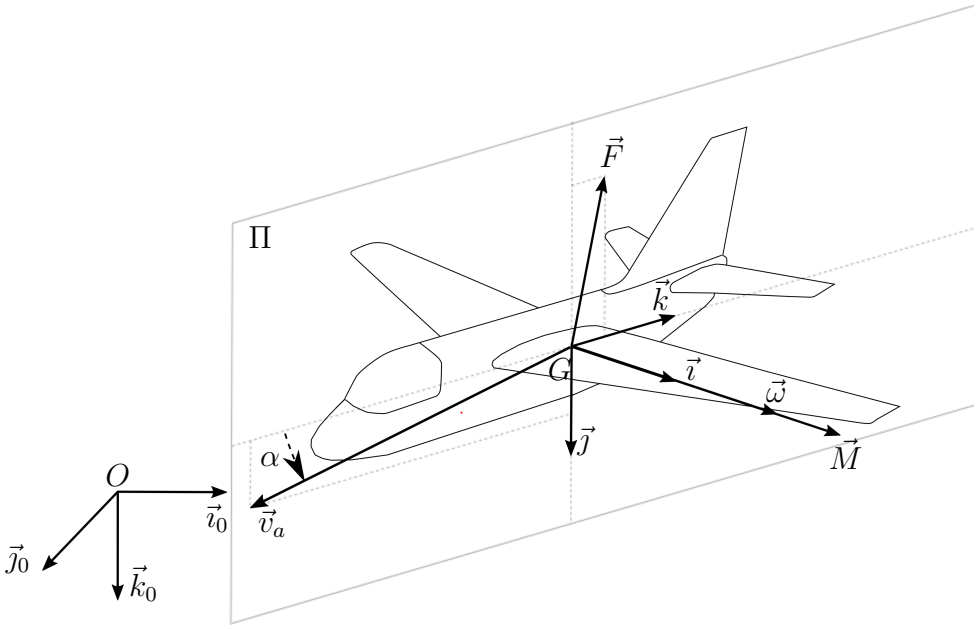

Figure 4.2: Aircraft flying it its vertical plane.

In light of the above, one has that:

- The external force $\vec{F}$ belongs to the plane Π, which implies $\overline{F}_1 \equiv 0$.
- The external moment $\vec{M}$ is parallel to $\vec{\imath}$, which implies $\overline{M}_2 \equiv \overline{M}_3 \equiv 0$.

As a consequence, the vehicle's trajectory develops in the plane Π as soon as the vehicle's linear and angular velocities are parallel and perpendicular to Π, respectively. In this case

$$v_1 \equiv \omega_2 \equiv \omega_3 \equiv 0 \quad \forall t.$$

Without loss of generality, let us further assume that $\vec{\imath}$ is parallel to $\vec{i}_0$ so that R is a rotation matrix representing a single rotation about the axis $\vec{i}_0$, that is

$$R = \begin{pmatrix} 1 & 0 & 0 \\ 0 & \cos\theta & -\sin\theta \\ 0 & \sin\theta & \cos\theta \end{pmatrix}, \quad R_\theta := \begin{pmatrix} \cos\theta & -\sin\theta \\ \sin\theta & \cos\theta \end{pmatrix},$$

and $\dot{x}_1 \equiv v_1 \equiv 0$. Then, from System (4.5) one obtains

$$\dot{x}_{2,3} = R_\theta v_{2,3}, \tag{4.7a}$$
$$\dot{R}_\theta = \omega_1 R_\theta S_2, \tag{4.7b}$$

and

$$\omega_1 = \dot{\theta}, \tag{4.8a}$$
$$m\dot{v}_{2,3} = -m\omega_1 S_2 v_{2,3} + \overline{F}_{2,3}\ , \tag{4.8b}$$
$$J_{11}\dot{\omega}_1 = \overline{M}_1\ , \tag{4.8c}$$

with

$$S_2 := \begin{pmatrix} 0 & -1 \\ 1 & 0 \end{pmatrix}.$$

The four equations given by (4.8) are the classical equations used to characterize the motions in the vertical plane Π. These equations play a crucial role when analyzing an aircraft in either steady, level flight or climbing or descending in this plane.

4.3 A SURVEY OF AIRCRAFT CONTROL TECHNIQUES

Since 1912, when the first autopilot was designed and tested by the Sperry Gyroscope Company, airplane control techniques have rapidly advanced, and today many fully-autonomous aircraft exist. The purpose of this section is to provide the reader with an introduction to the control of fixed-wing, VTOL, and convertible aircraft (see Chapter 2). Since a thorough review of aircraft control would at least double the size this thesis, it is clearly beyond the scope of the following sections.

4.3.1 FIXED-WING AIRCRAFT

Classically, fixed-wing aircraft dynamics are analyzed by neglecting the body forces $\vec{F}_b$ acting on the body (see Eq. (4.4)) and by using a linearized model for the aircraft motion. More specifically, define (Stevens and Lewis, 2003, p. 118):

- the system's nine-dimensional state vector composed of the *airspeed*, the *side-slip* angle, the *angle of attack*, the *roll, pitch, and yaw* angles, and the *three components of the body frame's angular velocity* expressed in the so-called *stability-axes* frame. This frame is obtained by rotating, through the angle of attack, the body frame about the axis perpendicular to the aircraft's plane of symmetry (i.e. about the vector $\vec{\imath}$ in Figure 4.2);
- The four-dimensional control vector composed of the *thrust intensity* and *three deflection angles* of the elevator, aileron, and rudder.

Then, after neglecting the body forces in Eq.(4.4), the aircraft's nonlinear dynamics is usually linearized around an equilibrium point representing a *steady-state condition* such as *steady wings-level flight*, *steady turning flight*, *steady pull up*, and *steady roll*. A common denominator of these flight conditions is that the body's linear and angular accelerations in the body frame are equal to zero. When the linearization is performed at a steady wing-level flight with zero side-slip angle, the linearized system can be decoupled into the two following *decoupled* dynamics (Stevens and Lewis, 2003, p. 126):

- *The longitudinal dynamics*: the system's state is given by a four-dimensional vector composed of the *angle of attack*, the *pitch rate*, the *airspeed*, and the *pitch angle*, whereas the control vector is given by a two-dimensional vector composed of the *elevator deflection angle* and the *thrust intensity*.
- *The lateral dynamics*: the system's state is given by a four-dimensional vector composed of the *side-slip and roll angles*, and the *stability-axis roll and yaw rates*, whereas the control vector is given by a two-dimensional vector composed of the *aileron and rudder deflection angles*.

Although these dynamics are representative of the real system only in a small flight envelope close to the steady wing-level flight, they provide practical insights about important open-loop aircraft modes. For instance, a study of the longitudinal dynamics points out the existence of two open-loop aircraft oscillating modes at different frequencies , i.e.:

- *Slow oscillations (phugoid)* are characterized by large variations of airspeed, pitch angle, and altitude, but an almost-constant angle of attack. The time period of a phugoid oscillation is in the range of 30–60 seconds.

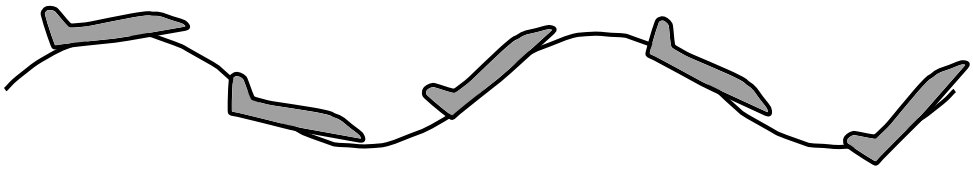

Figure 4.3: A sketch of an aircraft during a phugoid mode.

- *Fast oscillations (short period)* are characterized by large pitch rates, but an almost constant airspeed. The time period of a short period oscillation is about one second.

Analogously, a study of the lateral dynamics and its coupled effects with the longitudinal dynamics points out the existence of other three aircraft modes: *roll*, *spiral*, and *Dutch-roll* mode (Stevens and Lewis, 2003, p. 291) (Stengel, 2004, p. 595).

A well-designed feedback *stability augmentation system* (SAS) *mitigates* the effects of all these modes on the aircraft dynamics, and renders the steady-state condition more stable. Stability augmentation systems are usually designed *ad hoc* for the longitudinal and lateral dynamics by using the aforementioned linear, decoupled approximation of the nonlinear aircraft system. Various augmentation systems have been developed for several purposes such as the *pitch-axis SAS* and the *lateral-directional SAS/yaw damper* (Stevens and Lewis, 2003, p. 291).

High-performance or fighter aircraft need control systems that guarantee stringent properties such as airplane stability at performance limits and the tracking of moving targets. A control system to achieve these requirements is called *control augmentation system* (CAS), which nowadays can give the pilot a selection of *task-tailored control laws*. One can mention the example of the *dogfight control laws*, which aim at maximizing the aircraft maneuverability and agility in air. Various control augmentation systems have been developed for several purposes (Stevens and Lewis, 2003, p. 309), such as the *pitch-rate CAS*, the *normal acceleration CAS*, and the *lateral/directional CAS*.

Beside SAS and CAS, pilot-relief *autopilots* have also been developed to achieve minimal steady-state errors and disturbance rejections (Stevens and Lewis, 2003, p.327).

Conventionally, SAS, CAS, and autopilots are designed through classical control design techniques, the essence of which is the *one-loop-at-a-time* control design and *successive loop closure*. Desired stability characteristics are classically achieved through the use of tools as Bode plots, root locus, pole-placement procedure, etc.

Modern control techniques have also been applied to the control of fixed-wing aircraft and problems addressed with these techniques include: pole-placement/Eigenvector assignment, linear quadratic regulator with output feedback, reference tracking, model following, dynamic inversion (D'Antonio and Monaco, 1995), parabolic flight (D'Antonio and Monaco, 1993), etc. Most of these techniques, however, are based on linearized models for the aircraft's dynamics.

One of the main drawbacks of control design methods based upon linear approximations is that they can only guarantee the *local* stability of the associated nonlinear system. In fact, the linearized dynamics is no longer representative of the real system when the evolution of the real dynamics is far from the desired trajectory. Thus, the global stability of the linearized system does not imply the global stability of the real dynamics. Furthermore, when the linearized system associated with the error dynamics is time-varying – as in the case of a time-varying reference trajectory or disturbance –

ensuring the stability of the origin of this system is far from obvious. In this case, one may try to apply the so-called *gain-scheduling technique* that basically consists of (Kadmiry and Driankov, 2004) *i)* designing a set of local controllers, each of which is associated with a different (constant) reference; *ii)* "scheduling" these local controllers depending on the actual state of the system's evolution. Applications of the gain-scheduling technique to the control of aerial vehicles can be found in (Hyde and Glover, 1993) (Civita et al., 2003) (Kadmiry and Driankov, 2004) (Turner et al., 2002). However, a drawback of this technique is that the stability of the controlled system cannot in general be guaranteed. Also, linearizing an aircraft's dynamics often requires a minimal parametrization of the *rotation matrix* representing the vehicle's orientation. Since minimal parametrization of a rotation matrix are undefined for some attitude configurations, they induce artificial singularities that limit the domain of application of the controlled system. Hence, the larger the domain of its validity, the better the parametrization.

Nonlinear phenomena in aircraft dynamics are particularly important because they can give rise to an aircraft *loss-of-control* (LOC), which remains one of the most important contributors to fatal accidents (Kwatny et al., 2009) (Belcastro and Foster, 2010). A number of different forms of stability loss in longitudinal and lateral/directional motion is related to the *stall phenomena* (Goman et al., 1997, s. 2.2). Among these forms, one can mention a stable flight at high angle of attack without rotation, also called *deep stall* condition. Other forms of loss of stability of aircraft are due to the *roll-* and the *inertia-coupled* problems (Phillips, 1948) (Hacker and Oprisiu, 1974) (Jahnke, 1998).

Many types of aircraft LOCs can be related to the *equilibria pattern* variations of the aircraft dynamics depending on the vehicle control settings. In particular, aircraft dynamics may have more than one equilibrium point associated with a given control setting (Stengel, 2004, p. 728). Consequently, when this setting varies, the equilibrium of the aircraft may *jump* from one stable configuration to another; this may eventually cause abrupt responses of the aircraft motion and an aircraft LOC.

(Carroll and Mehra, 1982) is probably the first work to introduce an approach – called "bifurcation analysis and catastrophe theory methodology" – to understand the qualitative and global behavior of a nonlinear aircraft dynamics in relation to the associated equilibria pattern. For an introduction to bifurcation analysis of aircraft dynamics, the reader is referred to (Cummings, 2004) (Lowenberg, 2002); for a review of some of the subsequent papers, references of interest are (Carroll and Mehra, 1982) (Goman et al., 1997) (Paranjpe et al., 1998) (Sinha, 2001). In essence, the studied nonlinear problem (such as steady wings-level flight at high angle of attack) is usually formulated in the form of a set of ordinary differential equations depending on parameters (Goman et al., 1997), which often represent the control surface deflections. Thus, bifurcation analysis is a tool to investigate the relation between the system's behavior and control deflections variations, but the faster these variations, the worse the prediction of the system's behavior.

Bifurcation control deals with *equilibria* characteristics of a parametrized nonlinear system modified by a designed control input (Chen et al., 2000). Applications of bifurcation control to aircraft dynamics can be found in (Kwatny et al., 1991) (Abed and Lee, 1990). For instance, (Kwatny et al., 1991) focuses on design methods to achieve the local stability of an equilibrium point associated with a *nominal value* of the coefficients that parametrize the nonlinear system. However, the assumption that the system is autonomous clearly impairs the proposed control approach when the error dynamics is time dependent, as in the case of a time-varying reference.

4.3.2 VTOLs

Classically, VTOLs control is addressed by neglecting the aerodynamic reaction forces between the vehicle's shape and the surrounding air. The coupling body force $\vec{F}_b$ (see Eq. (4.4)), instead, requires close attention for some VTOL vehicles. More specifically, this coupling term is usually negligible for quadrotors (Hamel et al., 2002b), (Pounds et al., 2010b), (Bristeau et al., 2009a), but is generally relevant for helicopters because of the swashplate mechanism (Hua, 2009, Ch.1), (Dzul et al., 2002), (Koo and Sastry, 1998), (Mahony et al., 1999), (Olfati-Saber, 2001, Ch. 5), and for ducted-fan tail-sitters because of the rudder system (Pflimlin, 2006, Ch. 3), (Pflimlin et al., 2004). Furthermore, several studies (Hua, 2009, App.A), (Koo and Sastry, 1998), (Pflimlin et al., 2010), (Pounds et al., 2010a) have shown that the body forces can induce unstable zero dynamics depending on the vehicle's configuration. Then, the relevance of the body force in Eq. (4.4), and its implications at the control level, must be discussed in relation to the specific application (Pflimlin et al., 2004) (Pflimlin, 2006, Ch. 3) (Hua et al., 2013).

Over the last decade, modern linear control techniques have also been applied to the control of VTOLs. Among the control problems addressed with these techniques, let us mention optimization based techniques, which may be related to energy efficiency or robustness with respect to model uncertainties and/or aerodynamic disturbances. For example, (Bouabdallah et al., 2004) proposes a Linear-Quadratic-Regulator (LQR) for the rotational dynamics control of a quadrotor helicopter, and compares this controller with a PID. (Castillo et al., 2005) applies an LQR controller to stabilize the lateral position and the roll angle of a quadrotor helicopter, while (Stone, 2004) shows the application of the LQR technique to stabilize the linear and angular velocities of a ducted-fan tail-sitter. A more involved application of a LQ controller is found in (Benallegue et al., 2005), where a sliding mode observer combined with a Linear-Quadratic-Gaussian (LQG) controller is applied to a model of a quadrotor helicopter. To reduce the effects of exogenous disturbances on the control of helicopters, robust control techniques H_2, H_∞ have been widely applied (Civita et al., 2003), (Luo et al., 2003), (Mammar and Duc, 1992), (Prempain and Postlethwaite, 2005), (Takahashi, 1993). However, the main limitation of all above linear control techniques is the local nature of the control design and analysis.

To overcome the limitations of control methods based on linear approximations, over the last decades nonlinear control theory has paved the way for control techniques based upon the system's nonlinear dynamics. These nonlinear methods can yield controllers with a significantly large domain of attraction as well as robustness properties with respect to modeling errors and time-varying perturbations.

Nowadays, a well-known nonlinear control method is the so-called *input-output feedback linearization* technique (Isidori, 1995). When applied to the control of VTOLs, this technique essentially consists in considering the thrust vector $\vec{T}$ as a system state variable, and deriving it until one obtains a system's form allowing one to linearize the translational dynamics. For instance, it has been applied to the control of a planar model of a VTOL (Hauser et al., 1992), and to a 6DOF model of a conventional helicopter (Koo and Sastry, 1998). In particular, (Hauser et al., 1992) points out that a non-zero body force $\vec{F}_b$ may cause an unstable zero dynamics. An approach to address the control problem in the case of unstable zero dynamics consists of neglecting the terms that give rise to these unstable dynamics, and performing the input-output linearization on the approximated system. In

the literature, this approach is known as *approximate feedback linearization approach* and was used in (Hauser et al., 1992) and (Koo and Sastry, 1998). However, the implementation of the control solutions presented in these two papers raises a few important issues. For example, these solutions require the knowledge of the thrust intensity and its first order time derivative, the measurement of which can be problematic in practice. Also, the well-posedeness of these solutions needs to be properly discussed. For example, the solution proposed in (Hauser et al., 1992) is defined only if the thrust intensity is different from zero, and this hypothesis can be violated during *aggressive* maneuvers.

Another nonlinear method for the control of VTOLs is the so-called *backstepping procedure*. For example, under the assumption of no body force, (Frazzoli et al., 2000) and (Mahony et al., 1999) use a dynamic extension of the system and backstepping procedure to prove the boundedness of tracking errors.

In the case of *symmetric* vehicles, a way to take into account body forces consists in stabilizing a specific control point rather than the vehicle's center of mass; this modified control task allows one to mitigate the effects of the body force on the translational dynamics (Pflimlin et al., 2004) (Martin et al., 1996) (Olfati-Saber, 2002).

Nonlinear hierarchical controllers are another type of control technique for VTOLs. This type of controllers, reminiscent of the hierarchical linear controllers, are characterized by a two-stage architecture consisting of: *i*) a "high-level" position controller (Guidance loop), whose role is to determine the *desired* thrust vector $\vec{T}_d$ that stabilizes the vehicle's velocity; *ii*) a "low-level" orientation controller (Control loop), whose role is to stabilize the thrust's direction about the desired direction $\vec{T}_d/|\vec{T}_d|$. Several studies address the "high-level" control problem by expressing the desired thrust vector in terms of a desired rotation matrix (Frazzoli et al., 2000) (Marconi and Naldi, 2007) (Marconi and Naldi, 2008) (Olfati-Saber, 2001, Ch. 5). Then, the desired rotation matrix is considered as a reference tracking value for the stabilization of the vehicle's orientation (low-level control problem), and the stabilization of the rotation matrix to this desired value can be achieved via various techniques (Marconi and Naldi, 2007) (Marconi and Naldi, 2008) (Isidori et al., 2003), (Roberts and Tayebi, 2011), (Tayebi, 2008) (Tayebi and McGilvray, 2006) (Wen and Kreutz-Delgado, 1991) (Frazzoli et al., 2000) (Olfati-Saber, 2001, Ch. 5) (Pounds et al., 2007), etc. Problems addressed with hierarchical controllers are (Hua et al., 2013):

- way-point navigation (Pflimlin et al., 2006);
- visual servoing (Le-Bras et al., 2006);
- control with partial state measurement (Abdessameud and Tayebi, 2010);
- robustness with respect to unmodeled dynamics (Hamel et al., 2002a) (Lee et al., 2009a), aerodynamic disturbances (Hua et al., 2009a) (Pflimlin et al., 2006) (Pflimlin et al., 2004) (Roberts and Tayebi, 2011), parametric uncertainties (Isidori et al., 2003) (Marconi et al., 2002) (Marconi and Naldi, 2007), measurement errors (Plinval et al., 2012);
- actuators saturation (Guerrero-Castellanos et al., 2011) (Marconi and Naldi, 2007) (Marconi and Naldi, 2008) (Sanchez et al., 2008) (Zavala-Rio et al., 2003).

A common denominator of these controllers is the use of Lyapunov theory. In the literature, however, sliding-mode controls (Bouabdallah and Siegwart, 2005) (Bouabdallah and Siegwart, 2005) (Lee et al., 2009b) and predictive controls (Bertrand et al., 2006) (Jadbabaie et al., 1999) (Kim et al., 2002) are also used with the hierarchical scheme.

4.3.3 Convertibles

When controlling a convertible vehicle, one of the main concerns is the control of the transition maneuvers between hovering and high-velocity cruising. From a *systemic* point of view, tilting-thrust convertibles have an additional control input compared to fixed-thrust convertibles since the thrust direction can be modified at will in the former case. In turn, this renders their translational longitudinal dynamics fully actuated since one has a two-dimensional velocity and two control inputs, i.e. thrust's intensity and direction.

In the case of fixed-thrust convertibles, an inherent difficulty is due to the dependency of the aerodynamic effects upon the vehicle's orientation. As a consequence, any variation of the thrust direction modifies aerodynamic effects in most cases. Several studies have been dedicated to the control of transitions maneuvers for fixed-thrust convertibles (Benosman and Lum, 2007) (Frank et al., 2007) (Oishi and Tomlin, 1999) (Desbiens et al., 2010) (Naldi and Marconi, 2011) (Casau et al., 2012), the common denominator of which is a "switching" policy between *hover* and *cruise control* depending on the actual flight state. However, the automatic monitoring of the transitions between stationary flight and cruising modes of fixed-thrust convertibles remains a challenge to these days. One of the major difficulties is ensuring the stability of the closed-loop system along this transition, which is very sensitive to the "switching" policy that must be usually tuned for specific classes of reference trajectories. To our knowledge, a unified approach for the control of the transition maneuvers not relying on a switching policy between several control laws is still missing.

5 Motivations and thesis context

"Never forget your assumptions."

This short chapter presents the main motivations and thesis assumptions.

5.1 Motivations

The reviewed control techniques for aerial vehicles (see Section 4.3) point out that:

- Fixed-wing aircraft control is usually addressed by considering a linearized model for the airplane motion – including aerodynamic effects – and by neglecting the so-called body force. Nonlinear aerodynamic effects, such as stall phenomena, can induce a loss of control authority, which is turn related to the properties of the system's equilibria pattern.
- VTOL control is usually addressed by neglecting aerodynamic effects between the vehicle's shape and its surrounding air. Although the so-called body force can give rise to unstable zero-dynamics, recent techniques show that the effects of this force can be mitigated by controlling another point rather than the body's center of mass.
- Control of convertibles is usually addressed by considering two different dynamics for the aircraft motion: one for hovering and one cruising flight. Control laws are derived for each of these dynamics and the control strategy for large flight envelopes is based on a *switching policy* between these control laws.

This thesis proposes a nonlinear control approach for aerial vehicles subjected to aerodynamic forces. The proposed strategy does not rely on *switching policies* between several controls, so it participates in the development of a unified approach for the control of aerial vehicles. The main assumptions made in this manuscript are summarized next.

5.2 Preliminary assumptions

5.2.1 Forces and moments on the vehicle

Consider the *well-accepted* model of forces and moments acting on the aircraft given by Eqs. (4.4): we assume that the body force $\vec{F}_b$ is negligible with respect to the other forces acting on the vehicle. Therefore, the external forces and moments acting on the

vehicle are assumed to be given by

$$\vec{F} = \vec{F}_a + m\vec{g} + \vec{T}, \tag{5.1a}$$
$$\vec{M} = \vec{M}_a + G\vec{\Theta} \times \vec{T} + \vec{M}_I, \tag{5.1b}$$

with $\vec{g}$ the vector representing the gravity acceleration and $\vec{T}$ the body-fixed thrust force.

The aerodynamic force on the vehicle is assumed to be in the form (3.9) at fixed Reynolds and Mach numbers, namely

$$\vec{F}_a = k_a |\vec{v}_a| \left[C_L(\alpha, \beta) \vec{v}_a^{\perp} - C_D(\alpha, \beta) \vec{v}_a \right]. \tag{5.2}$$

Hence, we assume that the aerodynamic coefficients do not depend on *rotational and unsteady motions* (Stengel, 2004, p. 199). This assumption is better justified when
i) the body's linear acceleration is *small*;
ii) the body's angular velocity and acceleration are *small*;
iii) the wind velocity changes *slowly*.

5.2.2 Vehicle's actuation

By assuming that the vehicle's actuation can generate *any* torque input $\vec{M}_I$ – also referred to as *full-torque actuation* – the expression of the external moments (5.1b) shows that convergence of the angular velocity $\vec{\omega}$ to *any* bounded desired reference value is theoretically possible. To provide the reader with a better comprehension of this fact, let us consider, according to (5.1b), the Euler equation accounting for the rotational dynamics of the vehicle, i.e.

$$J\dot{\omega} = -S(\omega)J\omega + M_a + M_T + M_I,$$

where $\vec{M}_a = (\vec{\imath}, \vec{\jmath}, \vec{k})M_a$, $\vec{M}_I = (\vec{\imath}, \vec{\jmath}, \vec{k})M_a$ and $G\vec{\Theta} \times \vec{T} = (\vec{\imath}, \vec{\jmath}, \vec{k})M_T$. Then, by choosing the torque control input as

$$M_I = J\dot{\omega}_d + S(\omega)J\omega_d - M_a - M_T - k(\omega - \omega_d), \quad k > 0,$$

one obtains exponential stability for any desired angular velocity ω_d. Therefore, under the assumption of full-torque actuation, one may view the angular velocity as an intermediary control input. In practice, this corresponds to the classical decoupled control architecture between inner and outer loops: the inner loop deals with the stabilization of the vehicle's angular velocity based on its direct measurement from an IMU, and the outer control loop deals with the stabilization of the vehicle's velocity based on its direct measurement or estimation and by using the angular velocity set point and thrust intensity as control inputs. This leads to consider the thrust force intensity and the angular velocity as control inputs so that general principles applicable to many aerial vehicles can be worked out.

5.2.3 Vehicle's dynamics

In light of the assumption of full-torque actuation, the control problem is brought back to the control of the following subsystem

$$m\vec{a} = \vec{F}_a + m\vec{g} + \vec{T}, \tag{5.3a}$$
$$\frac{d}{dt}(\vec{\imath}, \vec{\jmath}, \vec{k}) = \vec{\omega} \times (\vec{\imath}, \vec{\jmath}, \vec{k}), \tag{5.3b}$$

with $\vec{a} := \frac{d\vec{v}}{dt}$, $\vec{F}_a$ given by (5.2), and $T := |\vec{T}|$ and $\vec{\omega}$ the system control inputs.

The motion equation (5.3a) points out the role of the aerodynamic force $\vec{F}_a$ in obtaining the body's linear acceleration vector $\vec{a}$. It shows, for instance, that to move with a constant reference velocity the controlled thrust vector $\vec{T}$ must be equal to the resultant external force

$$\vec{F}_{ext} := m\vec{g} + \vec{F}_a.$$

Now, assume that the body's shape is a sphere. Then, under the assumptions discussed in Section 5.2.1, the aerodynamic force does not depend on the body's orientation since it is reduced to its drag component, i.e.

$$\vec{F}_a = -k_a c_0 |\vec{v}_a| \vec{v}_a,$$

with c_0 a positive constant. Consequently, the resultant external force $\vec{F}_{ext}$ does not depend on the vehicle's orientation either. The control strategy then basically consists in aligning the thrust direction $\vec{T}/|\vec{T}|$ with the direction of $\vec{F}_{ext}$ (orientation control with ω) and in opposing the thrust magnitude to the intensity of $\vec{F}_{ext}$ (thrust control with $|\vec{T}|$). The almost-globally stabilizing controllers proposed in (Hua et al., 2009a) illustrate this strategy. However, the production of lift and drag forces that depend on the vehicle's orientation may significantly complexify this strategy. In particular, since the resultant force $\vec{F}_{ext}$ is in general orientation-dependent, the existence and uniqueness of the equilibrium in terms of the vehicle's orientation is no longer systematic, and the stabilization of such an equilibrium can be very sensitive to thrust orientation variations. As a matter of fact, the capacity of calculating the direction and intensity of $\vec{F}_a$ at every time-instant – already a quite demanding requirement – is not sufficient to design a control law capable of performing well in (almost) all situations. Knowing how this force changes when the vehicle's orientation varies is needed, but is still not sufficient. The following shows that orientation dependencies of the aerodynamic force have a fundamental role when attempting to control the dynamics (5.3). An original outcome of the present thesis is to point out the existence of a generic set of aerodynamic models that allow one to recast the control problem into the one of controlling a spherical body – also referred to as *spherical equivalency* – for which strong stability and convergence results can be demonstrated.

Part II

Modeling Analysis and Control of Aerial Vehicles

"Dissect the bat, study it carefully, and on this model construct the machine."

Leonardo da Vinci, Sul volo degli uccelli (1505)

Under the assumptions made in Section 5.2, this part of the thesis is dedicated to the modeling, analysis and control of two-dimensional and three-dimensional motions of aerial vehicles. However, three of the four following chapters are dedicated to two-dimensional motions, also referred to as *aircraft longitudinal dynamics*

Notation

The following notation is used throughout the following three chapters.

• The i_{th} component of a vector x is denoted as x_i.

• For the sake of conciseness, $(x_1\vec{\imath} + x_2\vec{\jmath})$ is written as $(\vec{\imath}, \vec{\jmath})x$.

• $\{e_1, e_2\}$ is the canonical basis in $\mathbb{R}^2$, and I is the (2×2) identity matrix.

• Given a function $f : \mathbb{R} \to \mathbb{R}$, its first and second derivative are denoted as f' and f'', respectively. Given a function f of several variables, the partial derivative of f w.r.t. one of them, say x, is denoted as $\partial_x f = \frac{\partial f}{\partial x}$. If $f \in \overline{\mathbf{C}}^1$, then its derivative is always defined.

• G is the body's center of mass and m is the (constant) mass of the vehicle.

• $\mathcal{I} = \{O; \vec{\imath}_0, \vec{\jmath}_0\}$ is a fixed inertial frame with respect to (w.r.t.) which the vehicle's absolute pose is measured.

• $\mathcal{B} = \{G; \vec{\imath}, \vec{\jmath}\}$ is a frame attached to the body. The vector $\vec{\imath}$ is parallel to the thrust force $\vec{T}$. This leaves two possible and opposite directions for this vector. The direction here chosen, i.e. $\vec{T} = -T\vec{\imath}$, is consistent with the convention used for VTOL vehicles.

• The body's position is denoted by $\vec{p} := \vec{OG} = (\vec{\imath}_0, \vec{\jmath}_0)x$. The body's linear velocity is denoted by $\vec{v} = \frac{d}{dt}\vec{p} = (\vec{\imath}_0, \vec{\jmath}_0)\dot{x} = (\vec{\imath}, \vec{\jmath})v$, and the linear acceleration by $\vec{a} = \frac{d}{dt}\vec{v}$.

• The vehicle's orientation is characterized by the angle θ between $\vec{\imath}_0$ and $\vec{\imath}$. The rotation matrix of the angle θ is $R(\theta)$. The column vectors of R are the vectors of coordinates of $\vec{\imath}, \vec{\jmath}$ expressed in the basis of $\mathcal{I}$. The matrix $S = R(\pi/2)$ is a unitary skew-symmetric matrix. The body's angular velocity is $\omega := \dot{\theta}$.

• The wind's velocity is denoted by $\vec{v}_w$ and its components are defined by $\vec{v}_w = (\vec{\imath}_0, \vec{\jmath}_0)\dot{x}_w = (\vec{\imath}, \vec{\jmath})v_w$. The *airvelocity* $\vec{v}_a = (\vec{\imath}, \vec{\jmath})v_a = (\vec{\imath}_0, \vec{\jmath}_0)\dot{x}_a$ is defined as the difference between the velocity of G and $\vec{v}_w$. Then, $\vec{v}_a = \vec{v} - \vec{v}_w$.

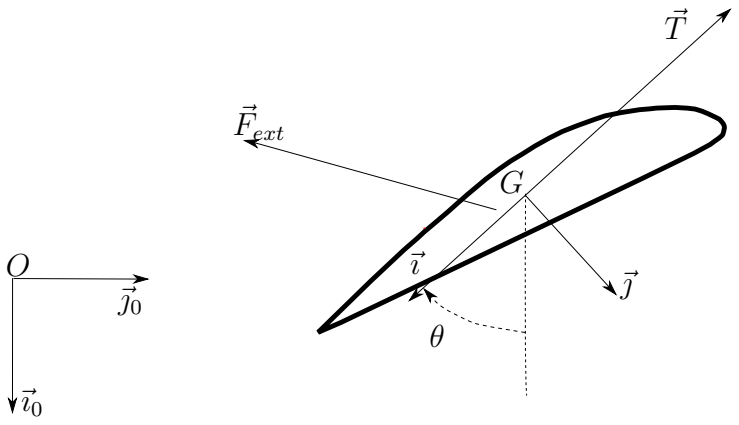

Figure 5.1: Generic body subjected to external reaction forces

6 System modeling

This chapter addresses the modeling of the vehicle's longitudinal dynamics, part of which was discussed in Chapters 3 and 4. In particular, Section 6.1 recalls the vehicle's equations of motion in the vertical plane under the assumptions discussed in Chapter 5. Section 6.2 is dedicated to the modeling of aerodynamic forces, with some emphasis on the aerodynamic properties in the case of *symmetric* body's shapes; in this section, we also present some models for the aerodynamic coefficients of NACA airfoils. Section 6.3 presents the dynamics of the tracking errors when either a reference trajectory or velocity is specified; in this section, we also present some preliminary definitions used throughout Chapters 7 and 8.

6.1 Equations of motion

As discussed in Section 5.2.3, the vehicle's equations of motion are derived by considering two control inputs. The first one is a *thrust* intensity T along the body fixed direction $\vec{\imath}$ whose main role is to produce longitudinal motion; the second control input is the vehicle's angular velocity ω. Also, we recall that the external forces acting on the body are assumed to be composed only of the gravity $m\vec{g}$ and the aerodynamic forces denoted by $\vec{F}_a$. Thus, under the assumption of complete torque actuation (see Section 5.2.2), the vehicle's equations of motion are given by:

$$m\vec{a} = m\vec{g} + \vec{F}_a - T\vec{\imath}, \tag{6.1a}$$

$$\dot{\theta} = \omega, \tag{6.1b}$$

with $\vec{g} = g\vec{\imath}_0$, g the gravity constant, and T and ω the system's control inputs.

6.2 Aerodynamic forces

The aerodynamic forces acting on the vehicle are assumed to be in the form (5.2). Furthermore, since we are interested in the body's longitudinal dynamics, the angle β is considered equal to zero, and thus omitted as argument of the aerodynamic coefficients. Then, the expression used for the aerodynamic force is given by

$$\vec{F}_a = k_a|\vec{v}_a|\left[c_L(\alpha)\vec{v}_a^{\perp} - c_D(\alpha)\vec{v}_a\right], \tag{6.2}$$

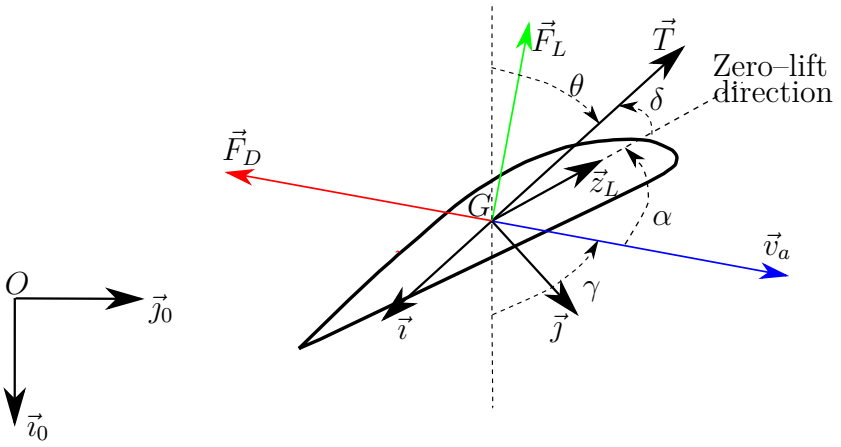

Figure 6.1: Generic body subjected to lift and drag forces.

with $\vec{v}_a^{\perp}$ obtained by rotating anticlockwise the vector $\vec{v}_a = (\vec{i}, \vec{j})v_a$ by 90°, that is

$$\vec{v}_a^{\perp} = v_{a_1}\vec{j} - v_{a_2}\vec{i}.$$

The angle of attack α is here defined as the angle between the body-fixed *zero-lift* direction $\vec{z}_L$, along which the airspeed does not produce lift forces, and the airspeed vector $\vec{v}_a$, i.e.

$$\alpha := \text{angle}(\vec{v}_a, \vec{z}_L). \tag{6.3}$$

By denoting the (constant) angle between the zero-lift direction and the thrust as δ, i.e.

$$\delta := \text{angle}(\vec{z}_L, \vec{T}), \tag{6.4}$$

and also the angle between the vertical direction $\vec{i}_0$ and $\vec{v}_a$ as γ, i.e.

$$\gamma := \text{angle}(\vec{i}_0, \vec{v}_a), \tag{6.5}$$

one has (Figure 6.1)

$$\alpha = \theta - \gamma + (\pi - \delta), \tag{6.6}$$

$$\begin{cases} v_{a_1} = -|\vec{v}_a| \cos(\alpha + \delta), \\ v_{a_2} = \quad |\vec{v}_a| \sin(\alpha + \delta). \end{cases} \tag{6.7}$$

6.2.1 SYMMETRIC SHAPES

Shape symmetries of aerial vehicles are not coincidental. Simplification and cost reduction of the manufacturing process, despite their importance, are clearly not the main incentives accounting for the ubiquitous use of symmetric shapes. In this respect, Nature was first to give the example with most of the animals populating the Earth. On the basis of this observation, one could figure out numerous practical advantages resulting from symmetry properties. However, for flying purposes, not all symmetries are equally interesting. For instance, the sphere, which represents the simplest most perfect symmetric 3D-shape, is not best suited for energy-efficient long-distance flights because it does not allow for the creation of lift forces which can counteract the effects of gravity in the

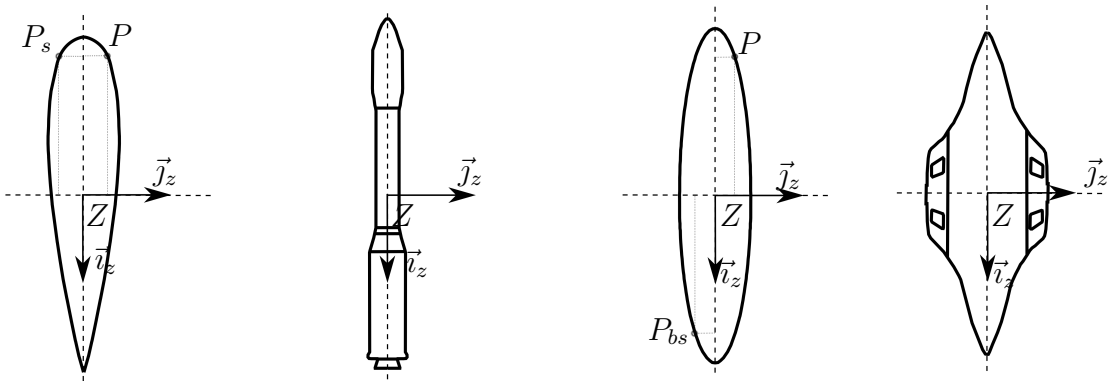

Figure 6.2: Symmetric and bisymmetric bodies satisfying Assumptions 1 and 2.

same way –and almost as well– as wheel-ground contact reaction forces for terrestrial vehicles. We here consider other kinds of symmetries in order to figure out aerodynamic properties induced by them and their practical and theoretical interests. More precisely, we focus on bodies whose surface $\mathcal{S}$ is characterized by the existence of an orthonormal body frame $\mathcal{B}_z = \{Z; \vec{\imath}_z, \vec{\jmath}_z\}$ such that either one of the following assumptions is satisfied.

Assumption 1 (**Symmetry**)**.** Let P be any point of the body surface $\mathcal{S}$ with coordinates (x, y) in $\mathcal{B}_z$. Then, the point P_s with coordinates $(x, -y)$ also belongs to $\mathcal{S}$. In this case, the body's shape is said to be *symmetric*.

Assumption 2 (**Bisymmetry**)**.** Let P be any point of the body surface $\mathcal{S}$ with coordinates (x, y) in $\mathcal{B}_z$. Then, the point P_{bs} with coordinates $(-x, -y)$ also belongs to $\mathcal{S}$. In this case, the body's shape is said to be *bisymmetric*.

Figure 6.2 shows some examples of symmetric and bisymmetric shapes.

When either one of the above assumptions is satisfied, we choose $\vec{z}_L$ parallel to an axis of symmetry so that $c_L(0) = c_L(\pi) = 0$. Note that this choice still leaves two possible and opposite directions for the definition of the vector $\vec{z}_L$, and this in turn reflects in two possible values[1] of the angle δ. Without loss of generality, the direction here chosen is the one that minimizes the angle δ.

Observe that a symmetric shape implies that the aerodynamic characteristics $c_D(\alpha)$ and $c_L(\alpha)$ are even and odd functions, respectively. Hence, for symmetric shapes one has

$$c_D(\alpha) = c_D(-\alpha) \tag{6.8a}$$
$$c_L(\alpha) = -c_L(-\alpha), \tag{6.8b}$$
$$c_L(0) = c_L(\pi) = 0. \tag{6.8c}$$

Bisymmetric shapes have an additional symmetry about the axis $\vec{\jmath}_z$, thus implying the invariance of the aerodynamic forces w.r.t. body rotations of $\pm\pi$. Then, in addition to properties (6.8), a bisymmetric shape implies also that the aerodynamic characteristics are $\pi-$periodic functions versus the angle of attack α, i.e.

$$c_D(\alpha) = c_D(\alpha \pm \pi), \tag{6.9a}$$
$$c_L(\alpha) = c_L(\alpha \pm \pi). \tag{6.9b}$$

[1]Defining the zero-lift-directions parallel to the axis of symmetry yields two values of the angle δ provided that the thrust force is not perpendicular to this axis of symmetry.

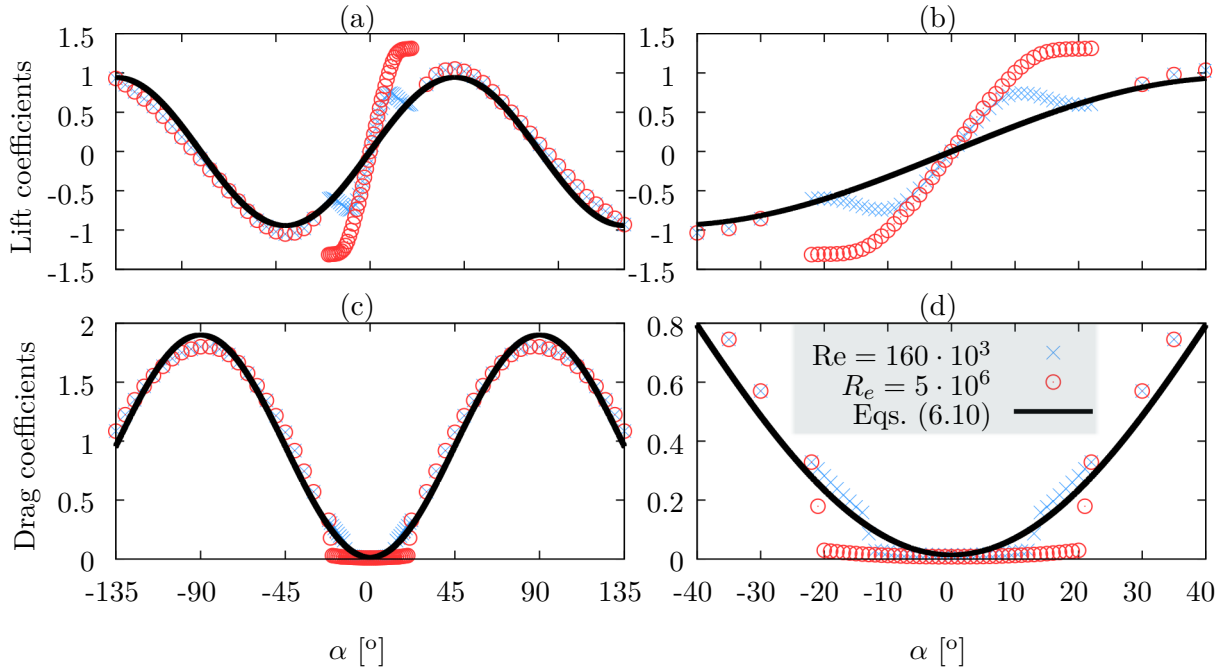

Figure 6.3: Measurements and typical approximations given by the model (6.10).

6.2.2 Models for aerodynamic coefficients of symmetric NACA airfoils

NACA profiles are airfoils widely used in practice and well referenced in the literature. Let us thus focus on the modeling of their aerodynamic coefficients. To do this, we here use three classes of modeling functions that will simplify the control design for System 6.1. The reasons behind the choice of these three classes will be clearer in Chapters 7 and 8, so for the time being we restrict our comments only on the capacities of the chosen functions to approximate the experimental data. The first class of modeling functions is given by

$$\begin{cases} c_L(\alpha) &= c_1 \sin(2\alpha) \\ c_D(\alpha) &= c_0 + 2c_1 \sin^2(\alpha), \end{cases} \tag{6.10}$$

with c_0 and c_1 two positive constants. The process of approximating experimental aerodynamic characteristics with the functions (6.10) is illustrated by the Figure 6.3 where we have used experimental data borrowed from (Davis et al., 2004) for a flat wing of airfoil NACA 0021 with Mach and Reynolds numbers equal to $(R_e, M) \approx (160 \cdot 10^3, 0.3)$. The estimated coefficients $c_0 = 0.0139$ and $c_1 = 0.9430$ minimize the average squared errors between aerodynamic data and the model (6.10). The approximation result, although not perfect, should be sufficient for control design purposes at low Reynolds numbers, which usually yield less pronounced stall phenomena (Section 3.3.1). Observe that increasing the Reynolds number worsens the approximation result only at small angles of attack since the experimental data are mostly independent of the Reynolds number when the angle of attack is beyond the stall angle α_s.

The second class of modeling functions provides better approximations of the experimental data at low angles of attack independently of the Reynolds number; they are

$$\begin{cases} c_L(\alpha) &= \dfrac{0.5c_2^2}{(c_2 - c_3)\cos^2(\alpha) + c_3} \sin(2\alpha) \\ c_D(\alpha) &= c_0 + \dfrac{c_2 c_3}{(c_2 - c_3)\cos^2(\alpha) + c_3} \sin^2(\alpha), \end{cases} \tag{6.11}$$

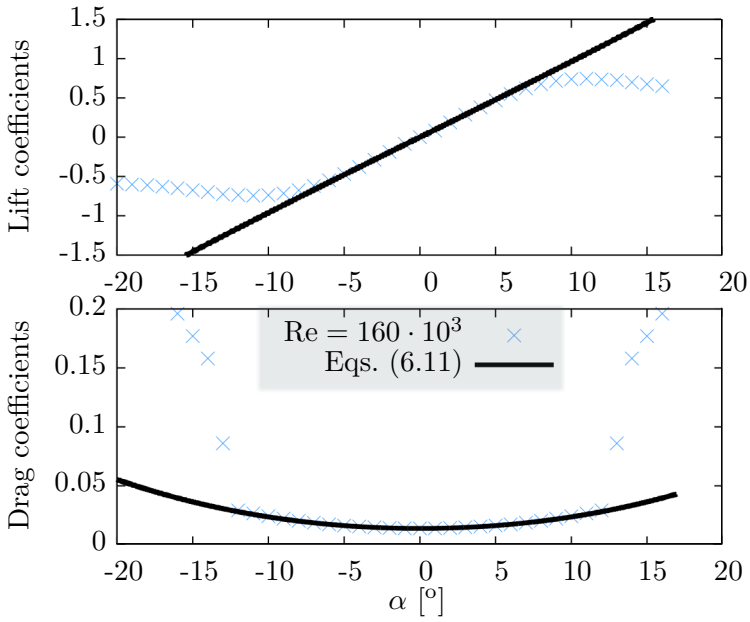

Figure 6.4: Measurements and typical approximations given by the model (6.11).

with c_2 and c_3 two positive constants such that $c_2 > c_3$. These functions are representative of the experimental aerodynamic characteristics at low angles of attack since computing the second order Taylor expansion of (6.11) at $\alpha = 0$ yields

$$\begin{cases} c_L(\alpha) = c_2\alpha \\ c_D(\alpha) = c_0 + c_3\alpha^2, \end{cases}$$

which are the classical modeling functions used to approximate the static aerodynamic characteristics at low angles of attack (Stengel, 2004). Figure 6.4 shows a typical approximation result given by the modeling functions (6.11); clearly, the closer the angle of attack to the stall angle, the worse the approximation result.

The third class of models is obtained by combining the functions (6.10) and (6.11) in only one (pair) of modeling functions, thus building a suitable model to approximate the experimental data over large domains of (R_e, α). In particular, we want that the combined model "smoothly" switches between the models (6.10) and (6.11) when the angle of attack crosses the stall region, and also that it satisfies the symmetric constraints (6.8). Among

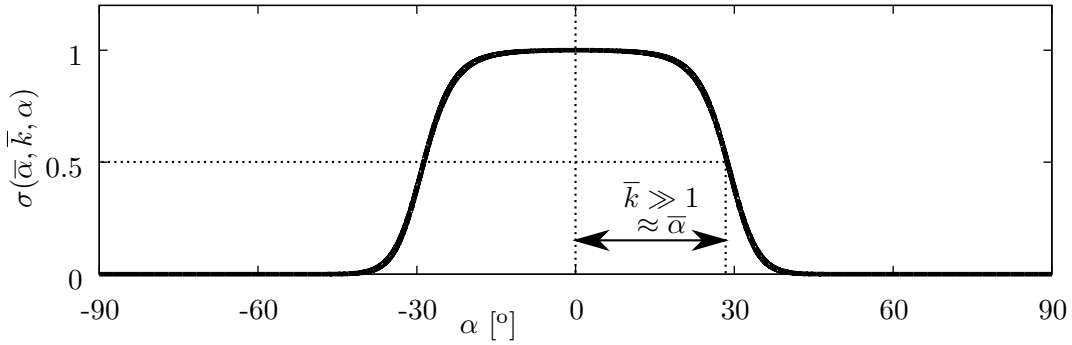

Figure 6.5: Pseudo-sigmoid function $\sigma(\overline{\alpha}, \overline{k}, \alpha)$.

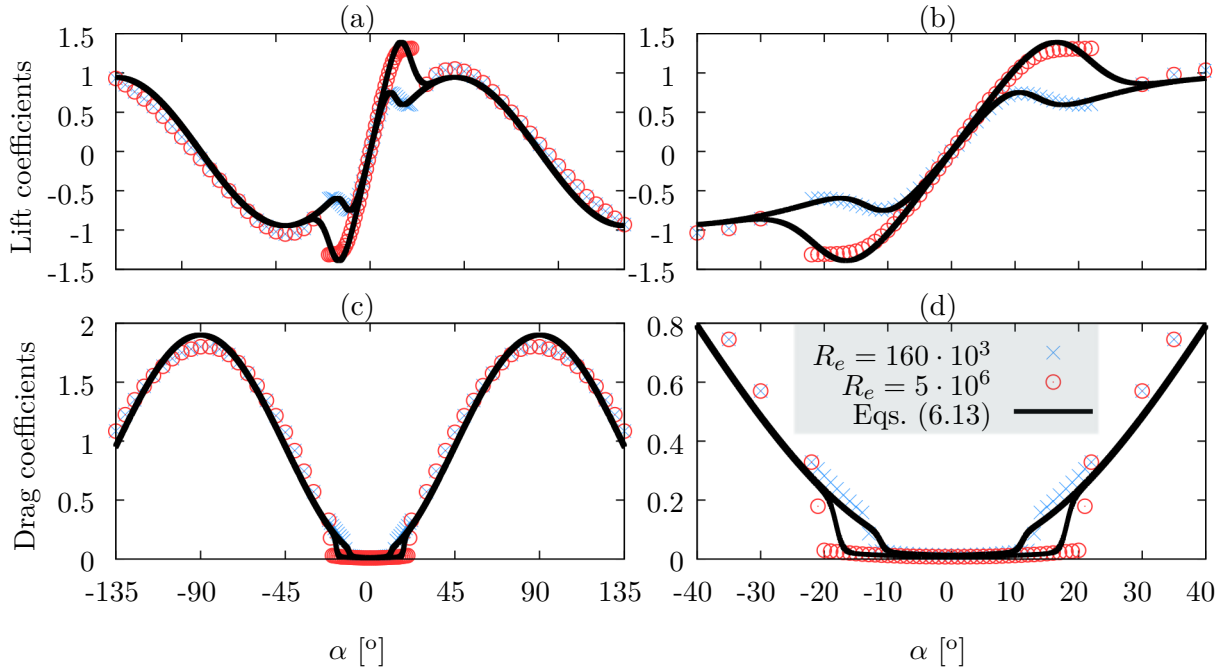

Figure 6.6: Measurements and typical approximations given by the model (6.13).

the infinity of possible ways of doing this combination, we make use of a pseudo-sigmoid function $\sigma(\overline{\alpha}, \overline{k}, \alpha)$ depicted in Figure 6.5 and defined by

$$\sigma(\overline{\alpha}, \overline{k}, \alpha) = \frac{1 + \tanh(\overline{k}\overline{\alpha}^2 - \overline{k}\alpha^2)}{1 + \tanh(\overline{k}\overline{\alpha}^2)}, \quad \alpha \in [-\pi, \pi). \tag{6.12}$$

Now, let (c_{L_L}, c_{D_L}) and (c_{L_S}, c_{D_S}) denote the modeling functions given by Eqs. (6.10) and (6.11), respectively. The aforementioned combined model is thus given by

$$\begin{cases} c_L(\alpha) = c_{L_S}(\alpha)\sigma(\overline{\alpha}, \overline{k}_L, \alpha) + c_{L_L}(\alpha)[1 - \sigma(\overline{\alpha}, \overline{k}_L, \alpha)] \\ c_D(\alpha) = c_{D_S}(\alpha)\sigma(\overline{\alpha}, \overline{k}_D, \alpha) + c_{D_L}(\alpha)[1 - \sigma(\overline{\alpha}, \overline{k}_D, \alpha)]. \end{cases} \tag{6.13}$$

Observe that at small angles of attack one has $\sigma(\cdot) = 1$ so that the model (6.13) coincides with (6.11). At large angles of attack, instead, one has $\sigma(\cdot) = 0$ so that (6.13) coincides with (6.10). Note also that the function $\sigma(\cdot)$ is even versus α, and this means that the models (6.13) satisfy the symmetric constraints (6.8).

Let us comment the role of the parameters $\overline{\alpha}$, $\overline{k}_L$, and $\overline{k}_D$ in Eqs. (6.13). The parameter $\overline{\alpha}$ represents the angle at which the "switch" from the models (c_{L_S}, c_{D_S}) into (c_{L_L}, c_{D_L}) is at the "middle points", while the (positive) parameters $\overline{k}_L$ and $\overline{k}_D$ characterize the domain on which this switch is accomplished. The larger $\overline{k}_L$ and $\overline{k}_D$, the smaller this domain. A first possibility for choosing $\overline{\alpha}$ is

$$\overline{\alpha} = \alpha_s,$$

with α_s the stall angle, while the parameters $\overline{k}_L$ and $\overline{k}_D$ can be chosen so that the slopes of (6.13) are close to those measured experimentally within the stall region. Figure 6.6 shows typical approximations result when considering the model (6.13). The estimated parameters at $R_e = 160 \cdot 10^3$ are $c_0 = 0.0139$, $c_1 = 0.9430$, $c_2 = 5.4641$, $c_3 = 0.3151$, $\overline{\alpha} = \alpha_s = 11°$, $k_L = 28$, and $k_D = 167$; while at $R_e = 5 \cdot 10^6$ they are $c_0 = 0.0078$, $c_1 = 0.9430$, $c_2 = 6.3025$, $c_3 = 0.1378$, $\overline{\alpha} = \alpha_s = 18°$, $k_L = 12$, and $k_D = 86$.

6.3 Dynamics of the tracking errors and preliminary definitions

Let $\vec{v}_r(t)$ denote a differentiable reference velocity, and $\vec{a}_r(t)$ its first time-derivative, i.e. $\vec{a}_r(t) = \dot{\vec{v}}_r(t)$. Define the velocity error as

$$\vec{e}_v := \vec{v} - \vec{v}_r. \tag{6.14}$$

Using System (6.1) one obtains the following error model

$$\dot{\vec{e}}_p = \vec{e}_v, \tag{6.15a}$$
$$m\dot{\vec{e}}_v = \vec{F} - T\vec{\imath}, \tag{6.15b}$$
$$\dot{\theta} = \omega, \tag{6.15c}$$

with $\vec{F}$ the *apparent external force* given by

$$\vec{F} := m\vec{g} + \vec{F}_a - m\vec{a}_r, \tag{6.16}$$
$$\vec{F}_a = k_a|\vec{v}_a|\left[c_L(\alpha)\vec{v}_a^{\perp} - c_D(\alpha)\vec{v}_a\right], \tag{6.17}$$

with $\vec{v}_a^{\perp} = v_{a_1}\vec{\jmath} - v_{a_2}\vec{\imath}$, $\vec{v}_a = \vec{v} - \vec{v}_w$, and either $\vec{e}_p := \int_0^t [\vec{v}(s) - \vec{v}_r(s)]\, ds$, the integral of the velocity error, or $\vec{e}_p := \vec{p} - \vec{p}_r$, the position tracking error when a reference trajectory $\vec{p}_r := (\vec{\imath}_0, \vec{\jmath}_0)x_r$ is specified.

Observe that the aerodynamic force $\vec{F}_a$ explicitly depends upon the angle of attack α. Consequently, $\vec{F}$ depends upon the vehicle orientation θ via Eq. (6.6). Thus, Eq. (6.15b) indicates that the equilibrium condition $(\vec{e}_p, \vec{e}_v) \equiv 0$ implies

$$T\vec{\imath}(\theta) = \vec{F}(\vec{v}_r(t), \theta, t), \qquad \forall t, \tag{6.18}$$

which in turn implies

$$T = \vec{F}(\vec{v}_r(t), \theta, t) \cdot \vec{\imath}(\theta), \tag{6.19a}$$
$$0 \equiv \vec{F}(\vec{v}_r(t), \theta, t) \cdot \vec{\jmath}(\theta) \quad \forall t. \tag{6.19b}$$

In view of Eq. (6.19b), we can then state the following definition.

Definition 6.1. An *equilibrium orientation* $\theta_e(t)$ is a time-valued function such that Eq. (6.19b) is satisfied with $\theta = \theta_e(t)$.

The *existence* of an equilibrium orientation is a necessary condition for the asymptotic stabilization of a reference velocity. Furthermore, observe that there may exist several equilibrium orientations associated with a reference velocity $\vec{v}_r(t)$. In order to classify the number of these equilibrium orientations, define the set $\Theta_{\vec{v}_r}(t)$ as

$$\Theta_{\vec{v}_r}(t) := \left\{\theta_e(t) \in \mathbb{S}^1 : \vec{F}(\vec{v}_r(t), \theta_e(t), t) \cdot \vec{\jmath}(\theta_e(t)) = 0\right\}. \tag{6.20}$$

We can now define a particular case for which there exist only two distinct equilibrium orientations over large domains of the reference velocity $\vec{v}_r$.

Definition 6.2. System (6.15b) is said to have a generically-unique pair of equilibrium orientations if and only if

$$\text{cardinality}(\Theta_{\vec{v}_r}(t)) = 2 \quad \forall t,$$

for any reference velocity $\vec{v}_r(t)$ except for a unique, continuous velocity $\vec{v}_b(t)$ such that

$$\Theta_{\vec{v}_b}(t) = \mathbb{S}^1 \quad \forall t.$$

For the systems having a generically-unique pair of equilibrium orientations, the reference velocity $\vec{v}_r(t)$ *can be performed* with only two vehicle's orientations at any time t, and this holds for any reference velocity except for a unique, *bad* reference velocity $\vec{v}_b(t)$. Therefore, for these classes of systems the problem of investigating the multiplicity of the equilibrium orientations can be totally avoided. In the following chapters, we show that there exist families of aerodynamic forces for which the associated tracking error dynamics (6.15b) has a generically-unique pair of equilibrium orientations.

Remark that given an equilibrium orientation $\theta_e(t)$, the thrust intensity T at the equilibrium configuration is given by Eq. (6.19a) with $\theta = \theta_e(t)$. From a practical point of view, the existence of an equilibrium orientation ensuring a positive thrust is of particular importance, since positive-thrust limitations represent a common constraint when considering aerial vehicles. Now, define

$$\Theta^+_{\vec{v}_r}(t) := \left\{ \theta_e(t) \in \Theta_{\vec{v}_r}(t) : \vec{F}(\vec{v}_r(t), \theta_e(t), t) \cdot \vec{\imath}(\theta_e(t)) \geq 0 \right\}. \tag{6.21}$$

Therefore, the practical cases of particular importance are those in which the cardinality of the set $\Theta^+_{\vec{v}_r}(t)$ is greater than one over large domains of the reference velocities, since they ensure the existence of an equilibrium orientation associated with a positive thrust.

7 Equilibria analysis

This chapter presents an equilibria analysis for System (6.15), where the apparent external force $\vec{F}$ is given by Eq. (6.16). In particular, Section 7.1 discusses the system's equilibria in the simpler case of a spherical shape; this section is also useful to familiarize the reader with the definitions introduced in Section 6.3. Section 7.2 addresses the *existence problem* of the equilibrium orientations in relation to the shape's symmetries. Section 7.3 presents a class of aerodynamic forces for which the system's dynamics (6.15) has a generically-unique pair of equilibrium orientations; for these aerodynamic forces, the considered thrust-propelled vehicle can be seen as another vehicle subjected to an orientation-independent external force only, as in the case of a spherical shape. This equivalency is referred to as *spherical equivalency*. Section 7.4 discusses the multiplicity of the equilibrium orientations and its implications at the control level. Section 7.5 studies the local uniqueness of the equilibrium orientations. Section 7.6 studies the so-called *static stability* of reference velocities. Section 7.7 shows that at fixed vehicle's orientation and thrust intensity there may exist several equilibrium velocities; this analysis is reminiscent of the *deep stall condition* of aircraft.

7.1 The spherical-shape case

If the body's shape is a *sphere*, then the aerodynamic force acting on the body is reduced to its (orientation-independent) drag component, i.e.

$$\vec{F}_a = -k_a c_0 |\vec{v}_a| \vec{v}_a, \tag{7.1}$$

with c_0 a positive constant. Then, the apparent external force given by Eq. (6.16) becomes

$$\vec{F}(\vec{v}, t) = m\vec{g} - k_a c_0 |\vec{v}_a| \vec{v}_a - m\vec{a}_r. \tag{7.2}$$

Therefore, in the case of a spherical shape, the dynamics of the tracking errors are given by Eqs. (6.15) with $\vec{F}$ independent of the vehicle's orientation and given by Eq. (7.2).

Now, since the apparent external force $\vec{F}$ is independent of θ, Eq. (6.15) indicates that the equilibrium condition $(\vec{e}_p, \vec{e}_v) \equiv 0$ implies (recall that $\theta = \text{angle}(\vec{\imath}_0, \vec{\imath})$, see Figure 5.1)

$$\begin{cases} T &= |\vec{F}(\vec{v}_r, t)|, \\ \vec{\imath}(\theta_e) &= \dfrac{\vec{F}(\vec{v}_r, t)}{|\vec{F}(\vec{v}_r, t)|} \Rightarrow \theta_e = \xi(t), \end{cases} \tag{7.3}$$

or

$$\begin{cases} T & = -|\vec{F}(\vec{v}_r, t)|, \\ \vec{\imath}(\theta_e) & = -\dfrac{\vec{F}(\vec{v}_r, t)}{|\vec{F}(\vec{v}_r, t)|} \Rightarrow \theta_e = \xi(t) + \pi, \end{cases} \tag{7.4}$$

where ξ denotes the angle between the vertical direction $\vec{\imath}_0$ and $\vec{F}(\vec{v}_r, t)$, i.e.

$$\xi = \text{angle}(\vec{\imath}_0, \vec{F}(\vec{v}_r, t)).$$

Then, as long as $\vec{F}(\vec{v}_r, t)$ is different from zero, there exist only two equilibrium orientations ensuring $(\vec{e}_p, \vec{e}_v) \equiv 0$. Furthermore, one of these two equilibrium orientations ensures a positive thrust at the equilibrium configuration – see Eq. (7.3). When $|\vec{F}(\vec{v}_r(t), t)| = 0$, any orientation is an equilibrium angle since the equilibrium condition

$$\vec{F}(\vec{v}_r(t), t) - T\vec{\imath}(\theta) = 0$$

holds for any θ with T=0. As a consequence of these facts, one states the following lemma.

Lemma 7.1. System (6.15b) with $\vec{F}$ given by Eq. (7.2) has a generically-unique pair of equilibrium orientations. Furthermore, the cardinality of the set $\Theta^+_{\vec{v}_r}$, as defined by (6.21), is equal to one, i.e.

$$\text{cardinality}(\Theta^+_{\vec{v}_r}(t)) = 1 \quad \forall t,$$

for any reference velocity $\vec{v}_r(t)$ except for a unique, continuous velocity $\vec{v}_b(t)$.

The proof of this lemma is given in Appendix A.1. The above result points out two important facts. First, the dynamics of the velocity errors (6.15b) with $\vec{F}$ given by (7.2) has a generically-unique pair of equilibrium orientations. Therefore, any reference trajectory is associated with only two vehicle's (equilibrium) orientations for many reference velocities. Secondly, the cardinality of the set $\Theta^+_{\vec{v}_r}(t)$ is also equal to one for many reference velocities.

In the next sections, we show that the dependence of the aerodynamic force upon the orientation perturbs the structural properties of the error dynamics (6.15), and that the existence of a vehicle's equilibrium configuration along a reference velocity cannot be guaranteed *a priori*.

7.2 Existence problem of an equilibrium orientation

The asymptotic stabilization of a reference velocity requires the existence of an equilibrium orientation – see Section 6.3. When the aerodynamic force $\vec{F}_a$, and consequently the apparent external force $\vec{F}$, depends upon the vehicle's orientation, ensuring the existence of an equilibrium orientation is far from obvious since any change of the vehicle's attitude affects both vectors $\vec{F}(\vec{v}_r, \theta, t)$ and $\vec{\jmath}(\theta)$ – see the definition of $\Theta_{\vec{v}_r}(t)$ given by (6.20). Nevertheless, we know from experience that airplanes do fly, so the equilibrium orientation must exist in most cases. One may then conjecture that the existence of an equilibrium orientation follows from aerodynamic properties that hold independently of the body's shape, alike the dissipativity of aerodynamic forces due to friction. However, the next lemma points out that the dissipative nature of the aerodynamic force is not in general sufficient to assert the existence of an equilibrium orientation.

Lemma 7.2. The dissipative nature of the aerodynamic force, i.e.

$$\vec{v}_a \cdot \vec{F}_a(\vec{v}_a, \alpha) \leq 0, \quad \forall(\vec{v}_a, \alpha), \tag{7.5}$$

does not always imply the existence of an equilibrium orientation.

The proof is given in Appendix A.2. Another route that we may follow to conclude about the existence of an equilibrium orientation is by considering specific classes of body's shapes. The next theorem addresses the existence problem of the equilibrium orientations by considering symmetric and bisymmetric shapes as defined in Section 6.2.1.

Theorem 7.1. Assume that the aerodynamic characteristics $c_L(\alpha)$ and $c_D(\alpha)$ are continuous functions, and that the reference velocity is differentiable, i.e. $\vec{v}_r(t) \in \overline{\mathbf{C}}^1$. Let $\Theta_{\vec{v}_r}(t)$ and $\Theta^+_{\vec{v}_r}(t)$ be the sets given by (6.20) and (6.21), with $\vec{F}$ given by (6.16).

1) If the body's shape is symmetric and the thrust is parallel to its axis of symmetry, then there exist at least two equilibrium orientations for any reference velocity, i.e.

$$\text{cardinality}(\Theta_{\vec{v}_r}(t)) \geq 2 \quad \forall t, \quad \forall \vec{v}_r(t) \in \overline{\mathbf{C}}^1.$$

2) If the body's shape is bisymmetric, then there exists at least one equilibrium orientation ensuring a positive-semidefinite thrust intensity for any reference velocity, i.e.

$$\text{cardinality}(\Theta^+_{\vec{v}_r}(t)) \geq 1 \quad \forall t, \quad \forall \vec{v}_r(t) \in \overline{\mathbf{C}}^1,$$

whatever the (constant) angle δ between the zero-lift direction and the thrust force.

The proof is given in Appendix A.3. Theorem 7.1 points out that the existence of an equilibrium orientation follows from the symmetry properties of the body's shape, independently of flow regimes or specific families of reference velocities. More specifically, item *1)* asserts that for symmetric body's shapes powered by a thrust force parallel to their axis of symmetry, the existence of (at least) two equilibrium orientations is guaranteed for any reference velocity. By looking at the proof of item 1), remark that the key assumption to prove this existence is

$$c_L(0) = c_L(\pi) = 0, \tag{7.6}$$

which does not depend on the drag coefficient. Hence, drag forces have no role in the existence an equilibrium orientation when considering symmetric shapes powered by a thrust force parallel to their axis of symmetry. When the thrust force is not parallel to the shape's axis of symmetry, one easily shows that the condition (7.6) is no longer sufficient to ensure the existence of an equilibrium orientation for any reference velocity[1].

Item *2)* of Theorem 7.1 states that the bisymmetry of the body's shape implies the existence of an equilibrium orientation independently of the thrust direction with respect to the body's zero-lift direction, namely, independently of the angle δ in Figure 6.1. Of most importance, this item points out that the shape's bisymmetry implies the existence of an equilibrium orientation associated with a positive-semidefinite thrust intensity independently of reference trajectories. Then, an additional sign constraint on the thrust intensity may be satisfied in the case of bisymmetric shapes.

[1]See the proof of Lemma 7.2.

Now, assume that the body's shape is only symmetric and not bisymmetric. If the thrust force is not parallel to the shape's axis of symmetry, the assumptions of Theorem 7.1 are not satisfied and the existence of an equilibrium orientation cannot be asserted, although the common sense makes us think that an equilibrium orientation still exists[2].

By considering symmetric body shapes, the next theorem points out conditions ensuring the existence of an equilibrium orientation independently of reference velocities and thrust directions with respect to the body's zero-lift direction.

Theorem 7.2. Consider a body with a symmetric shape. Assume that the aerodynamic coefficients $c_L(\alpha)$ and $c_D(\alpha)$ are continuous functions, and that $c_D(\pi) > c_D(0)$.
If there exists an angle $\alpha_s \in (0, \pi/2)$ such that $c_L(\alpha_s) > 0$ and

$$\tan(\alpha_s) \leq \frac{c_D(\alpha_s) - c_D(\pi)}{c_L(\alpha_s)}, \tag{7.7}$$

then there exists at least one equilibrium orientation for any reference velocity, i.e.

$$\text{cardinality}(\Theta_{\vec{v}_r}(t)) \geq 1 \quad \forall t, \quad \forall \vec{v}_r(t) \in \overline{\mathbf{C}}^1,$$

whatever the (constant) angle δ between the zero-lift direction and the thrust force.

The proof is given in Appendix A.4. Theorem 7.2 requires some knowledge of the body's aerodynamic coefficients to assert the existence of the equilibrium orientation. More specifically, the key hypothesis in Theorem 7.2 is the existence of an angle α_s such that condition (7.7) is satisfied. Since stall phenomena are rapid, usually important, lift decreases and drag increases, then the likelihood of satisfying the condition (7.7) with α_s belonging to the stall region is very high. As a matter of fact, we verified that Theorem 7.2 applies with α_s belonging to the stall region for the experimental data given in (Davis et al., 2004), which were taken for NACA airfoils 0012, 0015, 0018, and 0021 at $M = 0.3$ and several Reynolds numbers.

7.3 Models yielding a generically-unique pair of equilibrium orientations

Let us recall that when the body's shape is a sphere, the aerodynamic force is reduced to its drag component, i.e. $\vec{F}_a = -k_a c_0 |\vec{v}_a| \vec{v}_a$, and the error dynamics (6.15b) has a generically-unique pair of equilibrium orientations – see Section 7.1. This section shows that there exist other families of aerodynamic forces for which the associated velocity error dynamics has a generically-unique pair of equilibrium orientations. Then, for these families the problem of analyzing the multiplicity of the equilibrium orientations, i.e. the cardinality of the set $\Theta_{\vec{v}_r}(t)$, can be totally avoided.

From the definitions of $\vec{v}_a$ and α given in Section 6.2, one has

$$\begin{aligned} \vec{v}_a &= v_{a_1}\vec{\imath} + v_{a_2}\vec{\jmath}, \\ \vec{v}_a^{\perp} &= v_{a_1}\vec{\jmath} - v_{a_2}\vec{\imath}, \\ \cot(\alpha + \delta) &= -\frac{v_{a_1}}{v_{a_2}}, \end{aligned}$$

[2]Flat wings with a symmetric airfoil and with a thrust force not aligned with their axis of symmetry do fly in the vertical plane.

so that $\vec{F}_a$ given by (6.17) becomes

$$\vec{F}_a = k_a|\vec{v}_a|\left[\bar{c}_L\vec{v}_a^{\perp} - \Big(c_D(\alpha) + [c_L(\alpha) - \bar{c}_L]\cot(\alpha+\delta)\Big)\vec{v}_a\right] - k_a|\vec{v}_a|^2\frac{c_L(\alpha)-\bar{c}_L}{\sin(\alpha+\delta)}\vec{\imath}, \quad (7.8)$$

with $\bar{c}_L \in \mathbb{R}$ not necessarily constant. By using the above relationships, it is a simple matter to establish the following result.

Proposition 7.1. Assume that the aerodynamic forces are given by (6.17) and that the aerodynamic coefficients satisfy the following condition

$$\bar{c}_D = c_D(\alpha) + [c_L(\alpha) - \bar{c}_L]\cot(\alpha+\delta), \quad (7.9)$$

with $\bar{c}_D$ and $\bar{c}_L$ denoting two constant numbers.
Then, the body's dynamic equation (6.1a) can be rewritten as

$$m\vec{a} = m\vec{g} + \vec{f}_p - T_p\vec{\imath}, \quad (7.10)$$

with

$$\vec{f}_p = k_a|\vec{v}_a|\left[\bar{c}_L\vec{v}_a^{\perp} - \bar{c}_D\vec{v}_a\right], \quad (7.11a)$$

$$T_p = T + k_a|\vec{v}_a|^2\frac{c_L-\bar{c}_L}{\sin(\alpha+\delta)}, \quad (7.11b)$$

so that $\vec{f}_p$ is independent of the vehicle's orientation θ. □

When the condition (7.9) is satisfied, the dynamics of the velocity errors (6.15b) become

$$m\dot{\vec{e}}_v = \vec{F}_p - T_p\vec{\imath}, \quad (7.12)$$

with T_p given by (7.11b) and

$$\vec{F}_p := m\vec{g} + \vec{f}_p - m\vec{a}_r \quad (7.13)$$

independent of the vehicle's orientation. From here, one easily shows the following result.

Lemma 7.3. If the aerodynamic coefficients satisfy the condition (7.9) with $\bar{c}_D$ a positive-constant, then System (7.12) has a generically-unique pair of equilibrium orientations.

The proof is given in Appendix A.5. When the condition (7.9) is satisfied, we can see the vehicle with an equivalent shape that provides constant aerodynamic coefficients, but powered by an equivalent thrust force $\vec{T}_p = -T_p\vec{\imath}$. The satisfaction of the condition (7.9) is compatible with an infinite number of functions $c_D(\alpha)$ and $c_L(\alpha)$. Let us point out two particular sets of simple functions already considered in the modeling of aerodynamic coefficients addressed in Section 6.2.2.

Proposition 7.2. Assume that the resultant of the aerodynamic force is given by (6.17).

1) The modeling functions defined by Eq. (6.10), i.e.

$$\begin{cases} c_D(\alpha) = c_0 + 2c_1 \sin^2(\alpha) \\ c_L(\alpha) = c_1 \sin(2\alpha), \end{cases} \tag{7.14}$$

satisfy the condition (7.9) with

$$\begin{cases} \overline{c}_L = -c_1 \sin(2\delta) \\ \overline{c}_D = c_0 + 2c_1 \cos^2(\delta). \end{cases}$$

Then, the equivalent aerodynamic force $\vec{f}_p$ and thrust intensity T_p allowing for the transformation into the dynamics (7.10) with $\vec{f}_p$ independent of θ are given by

$$\vec{f}_p = -k_a|\vec{v}_a|\Big[c_1 \sin(2\delta)\vec{v}_a^{\perp} + (c_0 + 2c_1 \cos^2(\delta))\vec{v}_a\Big], \tag{7.15a}$$

$$T_p = T + 2c_1 k_a |\vec{v}_a|^2 \cos(\alpha - \delta). \tag{7.15b}$$

2) Assume that the thrust force $\vec{T}$ is parallel to the zero-lift direction $\vec{z}_L$ so that $\delta = 0$. The modeling functions defined by Eq. (6.11), i.e.

$$\begin{cases} c_L(\alpha) = \dfrac{0.5c_2^2}{(c_2 - c_3)\cos^2(\alpha) + c_3} \sin(2\alpha) \\ c_D(\alpha) = c_0 + \dfrac{c_2 c_3}{(c_2 - c_3)\cos^2(\alpha) + c_3} \sin^2(\alpha), \end{cases} \tag{7.16}$$

satisfy the condition (7.9) with

$$\begin{cases} \overline{c}_L = 0 \\ \overline{c}_D = c_0 + c_2. \end{cases}$$

Then, the equivalent aerodynamic force $\vec{f}_p$ and thrust intensity T_p allowing for the transformation into the dynamics (7.10) with $\vec{f}_p$ independent of θ are given by

$$\vec{f}_p = -k_a|\vec{v}_a|(c_0 + c_2)\vec{v}_a, \tag{7.17a}$$

$$T_p = T + \frac{c_2^2 k_a |\vec{v}_a|^2 \cos(\alpha)}{(c_2 - c_3)\cos^2(\alpha) + c_3}. \tag{7.17b}$$

□

Concerning the modeling functions (7.14), we can also show the following result.

Lemma 7.4. Assume that the aerodynamic forces are given by (6.17). In case of symmetric body shapes, the model (7.14) is the only family of aerodynamic coefficients for which there exists a vector $\vec{f}_p$ independent of θ such that (7.10) holds true whatever the (constant) angle δ between the zero-lift direction and the thrust force.

The proof of Lemma 7.4 is given in Appendix A.6.

7.3.1 The spherical equivalency

Assume that the thrust force is aligned with the zero-lift-line so that $\delta = 0$. Then, a body whose aerodynamics provides the aerodynamic coefficients given by either (7.14) or (7.16) is equivalent to a sphere subjected to only an equivalent drag force

$$\vec{f}_p = -k_a|\vec{v}_a|\bar{c}_D\vec{v}_a, \tag{7.18}$$

and powered by an equivalent thrust force T_p given by either (7.15b) or (7.17b). Now, consider the physical aerodynamic characteristics of NACA airfoils shown in Figure 6.3, and recall that the lower the Reynolds number, the better the approximation result given by the model (7.14). Therefore, NACA profiles at very-low Reynolds numbers – and with $\delta = 0$ – can be seen as spheres subjected to an equivalent drag and powered by an equivalent thrust. At large Reynolds numbers, this conceptual transformation can be considered valid for either *small* or *large* angles of attack, since the modeling functions (7.14) and (7.16) are representative of the experimental data on these regions – see Figure 6.6.

Now, let us recall that the model (6.13) – obtained by combining the models (7.14) and (7.16) – provides modeling functions that are representative of the experimental data taken for several NACA airfoils – see Section 6.2.2. When we consider this *combined* model for the aerodynamic coefficients, the associated errors dynamics may not have a generically-unique pair of equilibrium orientations, which is however implied by each of the models (7.14) and (7.16) when considered separately. More generically, for the aerodynamic coefficients that do not satisfy the condition (7.9), a reference velocity may be associated with several equilibrium orientations. A study of the multiplicity of the equilibrium orientation is addressed in the next section.

7.4 Equilibria multiplicity and ill-conditioning of the control problem

Given a reference velocity $\vec{v}_r(t)$, the number of possible vehicle's equilibrium orientations along this velocity equals the cardinality of the set $\Theta_{\vec{v}_r}(t)$ defined by Eq. (6.20). Therefore, the problem of determining the *multiplicity* of the equilibrium orientations arises only when the aerodynamic coefficients do not satisfy the condition (7.9) since this condition implies a constant cardinality of $\Theta_{\vec{v}_r}$ over large domains of the reference velocity – see Lemma 7.3.

This section studies the multiplicity of the equilibrium orientations and its control consequences by considering the experimental aerodynamic coefficients shown in Figure 6.6 (symmetric airfoil NACA 0021). For the sake of simplicity, we assume no wind, i.e.

$$|\vec{v}_w| \equiv 0, \tag{7.19}$$

and a thrust force aligned with the body's zero-lift direction, i.e.

$$\delta = 0. \tag{7.20}$$

Remark that since the airfoil NACA 0021 is symmetric, then Theorem 7.1 with $\delta = 0$ ensures the existence of at least one equilibrium orientation along any reference velocity.

Now, from the definition of the set $\Theta_{\vec{v}_r}$ given by (6.20), the cardinality of this set equals the number of solutions θ_e to the following algebraic equation

$$F(\dot{x}_r, \alpha_e)^T R(\theta_e) e_2 = 0, \tag{7.21}$$

where $\dot{x}_r$ is the vector of coordinates of the geometric vector $\vec{v}_r$ expressed in the inertial frame, i.e. $\vec{v}_r{=}(\vec{\imath}_0, \vec{\jmath}_0)\dot{x}_r$, and F is the vector of coordinates of $\vec{F}$, given by (6.16), expressed in the inertial frame, i.e. $\vec{F}{=}(\vec{\imath}_0, \vec{\jmath}_0)F$. Thus, in light of (7.19) and (7.20), one has

$$F(\dot{x}_r, \alpha_e) = mge_1 + k_a|\dot{x}_r|\,[c_L(\alpha_e)S - c_D(\alpha_e)I]\,\dot{x}_r - m\ddot{x}_r, \tag{7.22}$$

with $\alpha_e = \theta_e - \gamma_r + \pi$, and $\gamma_r = \text{angle}(e_1, \dot{x}_r)$ (see Section 6.2). Now, by replacing

$$\theta_e = \alpha_e + \gamma_r - \pi, \tag{7.23}$$

in $R(\cdot)$ in Eq. (7.21), one obtains

$$F(\dot{x}_r, \alpha_e)^T R(\alpha_e + \gamma_r) e_2 = 0. \tag{7.24}$$

Therefore, the problem of seeking for the equilibrium orientations θ_e is *equivalent*[3] to the problem of finding the *equilibrium angles of attack* α_e.

Next sections investigate the multiplicity of the equilibrium angles of attack α_e first for a cruise flight, and then for a generic constant-velocity flight. In addition to this analysis, the following sections provide the reader with some insights into the thrust intensity at the equilibrium configuration by using the equilibrium condition (6.19a). In light of (7.19), (7.20), and (7.23), expressing the equilibrium condition (6.19a) in the inertial frame basis yields

$$T_e = -F(\dot{x}_r, \alpha_e)^T R(\alpha_e + \gamma_r) e_1, \tag{7.25}$$

where $F(\dot{x}_r, \alpha_e)$ is given by Eq. (7.22).

7.4.1 HORIZONTAL FLIGHT

Desired steady-horizontal flight implies that

$$\dot{x}_r = \nu e_2, \tag{7.26}$$

where $\nu \in \mathbb{R}^+$ denotes a constant called *cruise speed*. Then, $\gamma_r = \text{angle}(e_1, \dot{x}_r) = \pi/2$, and the equilibrium condition (7.24) with (7.26) yields

$$[1{-}a_\nu c_L(\alpha_e)]\cos(\alpha_e){-}a_\nu c_D(\alpha_e)\sin(\alpha_e) = 0, \tag{7.27}$$

where a_ν is a *dimensionless number* defined by

$$a_\nu := \frac{k_a \nu^2}{mg}, \tag{7.28}$$

with $k_a = \rho\Sigma/2$. Remark that the dimensionless property of a_ν can be used to determine *dynamic similitude* between different cases. For instance, assume that Eq. (7.27) holds, i.e.

[3]The equivalency holds only if $|\dot{x}_r| > 0$, which implies that γ_r is well defined.

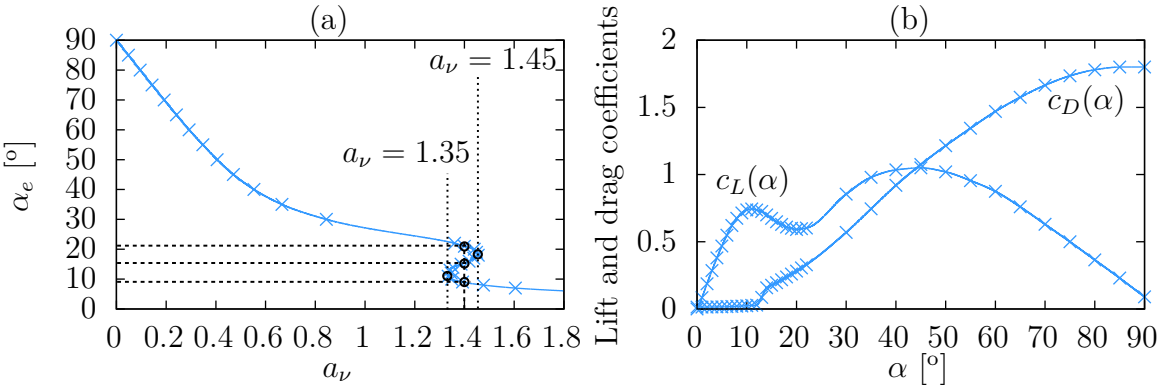

Figure 7.1: (a): pattern of the equilibrium angles α_e; (b): aerodynamic coefficients.

α_e is an equilibrium angle of attack at a given a_ν and for specific aerodynamic coefficients. Then, any aircraft having these aerodynamic coefficients admits α_e as an equilibrium angle of attack at a cruise speed evaluated according to its geometry and weight, i.e.

$$\nu = \sqrt{\frac{mga_\nu}{k_a}}. \tag{7.29}$$

The possibility of finding the explicit expression of the equilibrium angles $\alpha_e = \phi(a_\nu)$ from Eq. (7.27) is intimately related to the model of the aerodynamic coefficients. For instance, when the aerodynamic force is reduced to its drag component, i.e. $c_L(\alpha) \equiv 0$ and $c_D(\alpha) \equiv c_0$, one has

$$\alpha_e = \phi(a_\nu) = \operatorname{atan}\left(\frac{1}{a_\nu c_0}\right).$$

More generically, the existence of the function $\phi(\cdot)$ can be ensured by applying the *implicit function theorem*, although the expression of this function remains in general unknown. Conversely, observe that from Eq. (7.27) we can find the explicit expression of the parameter a_ν in function of the equilibrium angles α_e, i.e.

$$a_\nu(\alpha_e) = \frac{\cot(\alpha_e)}{c_D(\alpha_e) + c_L(\alpha_e)\cot(\alpha_e)}. \tag{7.30}$$

Therefore, a picture of the equilibrium angle α_e as a function of the cruise velocity ν is obtained by plotting Eq. (7.30). Figure 7.1a depicts the function (7.30) evaluated with the experimental aerodynamic characteristics shown in Figure 7.1b (NACA 0021 of $l = 0.91m$, $c = 0.1524m$ and at $R_e = 160 \cdot 10^3$ and $M = 0.3$). From this figure we see that the angle of attack at the equilibrium is unique (on $(0, 90°)$) as long as the parameter $a_\nu < 1.35$. At $a_\nu = 1.35$, the equilibrium angle of attack bifurcates in multiple points. The local bifurcation of α_e is a *saddle-node* kind since a couple of equilibrium angles *collide and annihilate each other* (Chow and Hale, 1996) (Wiggins, 1990) when crossing the bifurcation values $a_\nu = 1.35$ and $a_\nu = 1.45$. When a_ν belongs to a neighborhood of 1.4, one has three equilibrium angles of attack, and this means that a steady-horizontal flight can be performed with (three) different vehicle's orientations.

The bifurcation analysis of the equilibrium orientations is beyond the scope of the present thesis, all the more so because these local phenomena occur principally on the highly nonlinear and chaotic stall region, so they are very sensitive to the modeling of the

aerodynamic coefficients on it. Let us just observe that bifurcations do not occur if $a_\nu(\alpha_e)$ is well-defined and strictly decreasing on $\alpha_e \in (0, 90°)$. On this basis, a simple study of the function $a_\nu(\alpha_e)$ given by (7.30) allows us to state the following lemma.

Lemma 7.5. Consider a steady-horizontal flight with no wind and a thrust force aligned with the zero-lift direction, i.e. $\dot{x}_r = \nu e_2$, $\vec{v}_w = 0$, and $\delta = 0$. Assume that $c_L(\alpha)$ and $c_D(\alpha) > 0$ are continuously differentiable functions such that

$$c_D(\alpha) + c_L(\alpha)\cot(\alpha) > 0 \quad \forall \alpha \in (0, 90°). \tag{7.31}$$

1) If

$$c'_L(\alpha) + c'_D(\alpha)\tan(\alpha) + \frac{c_D(\alpha)}{\cos^2(\alpha)} > 0 \quad \forall \alpha \in (0, 90°), \tag{7.32}$$

then the function $a_\nu(\alpha_e)$ given by (7.30) is strictly decreasing on $\alpha_e \in (0, 90°)$, so no bifurcation occurs on this domain.

2) If there exists one angle $\overline{\alpha}_e$ such that

$$c'_L(\overline{\alpha}_e) + c'_D(\overline{\alpha}_e)\tan(\overline{\alpha}_e) + \frac{c_D(\overline{\alpha}_e)}{\cos^2(\overline{\alpha}_e)} < 0, \quad \overline{\alpha}_e \in (0, 90°), \tag{7.33}$$

then $a'_\nu(\overline{\alpha}_e) > 0$, and there exists $\alpha_b > \overline{\alpha}_e$ such that $a'_\nu(\alpha_b) = 0$ because $a_\nu(90°) = 0$. Consequently, there exists at least a saddle-node bifurcation on $(\overline{\alpha}_e, 90°)$.

Condition (7.31) holds in most cases because the lift coefficient is (usually) positive for small angles of attack and the ratio $c_L(\alpha)/c_D(\alpha)$ is (usually) small for large α. For example, if we consider the aerodynamic characteristics shown in Figure 7.1b, the condition (7.31) is satisfied since $c_L(\alpha) > 0$ $\forall \alpha \in (0, 90°)$. Now, notice that the condition (7.32), which rules out the occurrence of a bifurcation, may be satisfied even when $c'_L(\alpha) < 0$. Hence, the occurrence of the lift stall phenomenon – with $c'_L(\alpha) < 0$ usually when $\alpha \in (0, 45°)$ – is not in general sufficient for α_e to bifurcate. However, by assuming that the drag coefficient is non-decreasing on $\alpha \in (0, 90°)$, a decreasing lift coefficient on $\alpha \in (0, 90°)$ is necessary for the occurrence of a bifurcation; otherwise, the condition (7.32) is satisfied. Stall phenomena induce a bifurcation when, for example, the rate of decrease of the lift coefficient is so large that the condition (7.33) is satisfied.

Let us recall that the aerodynamic coefficients depend also upon the Reynolds and Mach numbers – see Section 3.3 – although these numbers are assumed constant in the aerodynamic modeling in Section 6.2. Recall also that for low-subsonic airflows the aerodynamic coefficients can be considered independent of the Mach number, so the pattern of the equilibrium angles α_e shown in Figure 7.1a principally varies with the Reynolds number R_e and the angle of attack α_e only. To provide the reader with a picture of these variations, Figure 7.2a depicts the function (7.30) evaluated with the experimental aerodynamic characteristics taken at several Reynolds numbers and shown in Figure 7.2b (NACA 0021 of $l = 0.91m$, $c = 0.1524m$ and at $M = 0.3$). Figure 7.2a depicts (in black) also the function $a_\nu(\alpha_e)$ evaluated with the modeling functions (7.14): since these functions yield a generically-unique pair of equilibrium orientations, then no bifurcation occurs. Let us recall that the modeling functions (7.14) better approximate the experimental data of NACA airfoils when the Reynolds numbers is relatively small. Then, we

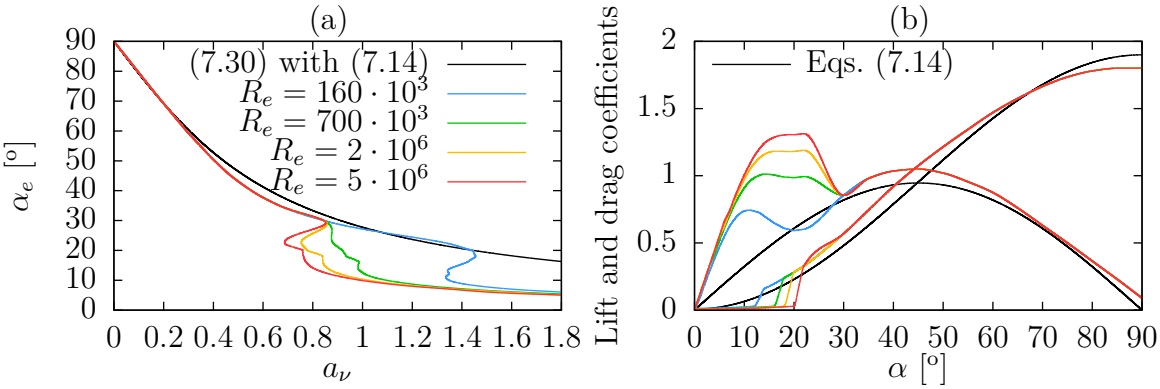

Figure 7.2: $a_\nu(\alpha_e)$ given by (7.30) and the coefficients used to evaluate it.

can claim that the equilibria pattern of NACA airfoils at low Reynolds numbers and in cruise flight never bifurcates. As shown in Figure 7.2a, increasing the Reynolds number principally varies the equilibria pattern only at small angles of attack. This is due to the fact that the experimental data are mostly independent of the Reynolds number when the angle of attack is beyond the stall region. Furthermore, simulations we have performed tend to show that the larger the Reynolds number, the smaller the minimum value of a_ν – and thus of the cruise speed ν – at which multiple equilibria α_e occur independently of the considered NACA airfoil. This phenomenon is due to the shifting of the lift stall region towards higher values of the angles of attack as R_e increases.

A consequence of the existence of several equilibria is that, given a continuous reference velocity profile, the associated equilibrium orientation $\theta_e(t)$ may be discontinuous. In this case, the reference velocity can be *perfectly tracked*, i.e. $(\vec{e}_p, \vec{e}_v) = (0,0)\ \forall t$, only if discontinuities of the vehicle's attitude θ were admissible, and this is clearly impossible in practice. Also, the continuity of the equilibrium orientation $\theta_e(t)$ is a necessary condition for the *well-posedness* of the asymptotic stabilization problem of the equilibrium point $(\vec{e}_p, \vec{e}_v) = (0,0)$ of System (6.15), since the control input ω at the equilibrium, i.e. $\omega = \dot{\theta}_e(t)$, must be defined for any t.

The fact that the continuity of the reference velocity does not in general imply the continuity of the equilibrium orientation $\theta_e(t)$ is visually clear from Figure 7.3 when considering *transition maneuvers* between hovering and high-velocity cruising. For example, consider the transition from hovering to high-velocity cruising with a continuous reference velocity of the form

$$\dot{x}_r(t) = \nu t (0,1)^T, \tag{7.34}$$

with ν a (small) positive number. On the time interval $t \in (0, t_1)$ (see Figure 7.3a), one has $\alpha_e \approx 90°$ because the horizontal reference velocity is of low intensity (the thrust opposes the weight). As time goes by, the intensity of the reference velocity increases, and this in turn implies smaller values of the angle of attack at the equilibrium configuration. At $t = \bar{t}$, the equilibrium attitude $\alpha_e(t)$ instantaneously goes from 19° to 12°, thus making the equilibrium orientations $\theta_e(t)$ discontinuous. Such discontinuities destroy the *well-posedness* of the asymptotic stabilization problem related to the transition maneuver given by (7.34). Consequently, this reference velocity cannot be perfectly tracked by any aircraft whose aerodynamic characteristics are similar to those shown in Figure 7.1b.

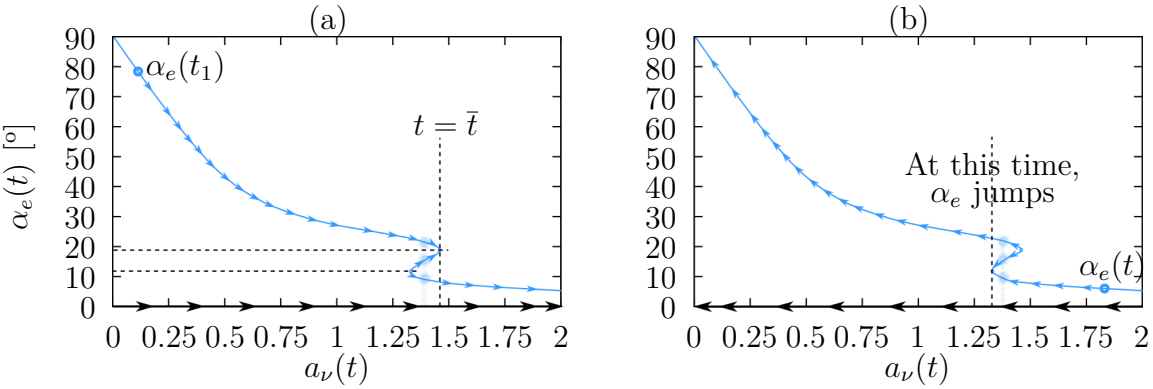

Figure 7.3: Equilibria pattern for: (a) $\dot{x}_r{=}(0, \nu t)^T$; (b) $\dot{x}_r{=}(0, \nu_0{-}\nu t)^T$, $\nu_0{\gg}1$, $0{<}\nu{\ll}1$.

7.4.2 Other flight directions

Assume that the reference velocity $\dot{x}_r$ is constant and different from zero so that it can be written as

$$\dot{x}_r = \nu\Big(\cos(\gamma_r),\ \sin(\gamma_r)\Big)^T, \tag{7.35}$$

with $\nu \in \mathbb{R}_+$ and $\gamma_r \in \mathbb{S}^1$ two constant values. Then, the equilibrium condition (7.24) combined with (7.35) yields

$$\begin{aligned} &a_\nu\Big[c_D(\alpha_e)\sin(\gamma_r) - c_L(\alpha_e)\cos(\gamma_r)\Big]\cos(\alpha_e+\gamma_r) + \\ &\Big[1 - a_\nu(c_L(\alpha_e)\sin(\gamma_r) + c_D(\alpha_e)\cos(\gamma_r))\Big]\sin(\alpha_e+\gamma_r) = 0, \end{aligned} \tag{7.36}$$

where the dimensionless positive constant a_ν is still given by Eq. (7.28) (i.e. $a_\nu = \frac{k_a \nu^2}{mg}$).

By analogy with the case of steady-horizontal flight, from Eq. (7.36) we derive the expression of $a_\nu = a_\nu(\alpha_e, \gamma_r)$ to obtain a picture of the equilibrium angles α_e, i.e.

$$a_\nu(\alpha_e, \gamma_r) = \frac{\sin(\gamma_r)\cot(\alpha_e) + \cos(\gamma_r)}{\overline{c}(\alpha_e)}, \tag{7.37}$$

with $\overline{c}(\alpha_e)$ given by

$$\overline{c}(\alpha_e) = c_D(\alpha_e) + c_L(\alpha_e)\cot(\alpha_e). \tag{7.38}$$

To depict also a picture of the thrust intensity at the equilibrium point $\dot{x} \equiv \dot{x}_r$, from Eq. (7.25) we derive the *thrust-to-weight ratio* T_W at the reference velocity, i.e.

$$T_W := \frac{T_e}{mg} = a_\nu[c_D(\alpha_e)\cos(\alpha_e) - c_L(\alpha_e)\sin(\alpha_e)] - \cos(\alpha_e+\gamma_r).$$

Since a_ν at the equilibrium $\dot{x} \equiv \dot{x}_r$ satisfies Eq. (7.37), substituting (7.37) in the above expression of T_W yields

$$T_W(\alpha_e, \gamma_r) = \frac{c_D(\alpha_e)\sin(\gamma_r) - c_L(\alpha_e)\cos(\gamma_r)}{\sin(\alpha_e)\overline{c}(\alpha_e)}. \tag{7.39}$$

By using the experimental aerodynamic characteristics shown in Figures 7.1b, Figure 7.4 depicts the curves $a_\nu(\alpha_e, \gamma_r)$ and $T_W(\alpha_e, \gamma_r)$ for different values of the reference angle γ_r.

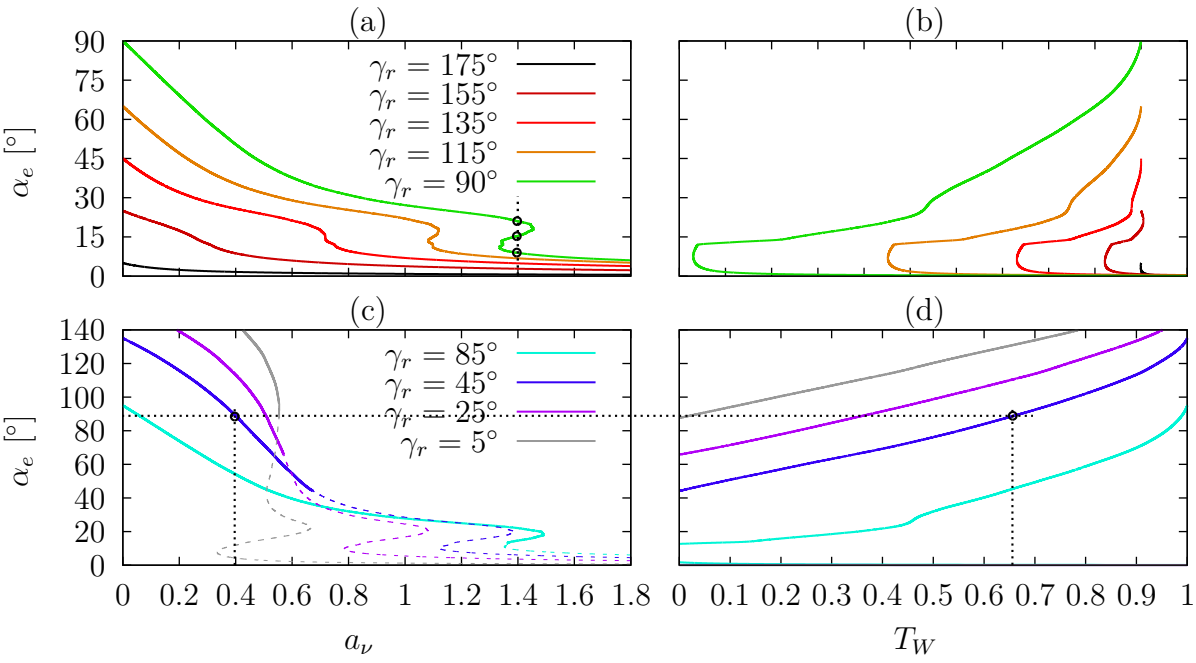

Figure 7.4: $a_\nu(\alpha_e, \gamma_r)$ (left) and $T_w(\alpha_e, \gamma_r)$ (right) with $c_L(\alpha)$ and $c_D(\alpha)$ as Figure 7.1b.

To illustrate how we can use Figure 7.4, focus on the case $\gamma_r = 45°$ and fix the parameter $a_\nu = 0.4$ (Figure 7.4c). Now, follow the vertical, dotted line drawn at $a_\nu = 0.4$. Then, the equilibrium angle α_e is given by the intersection between this vertical line and the blue curve (i.e. the curve corresponding to $\gamma_r = 45°$), namely $\alpha_e \approx 89°$. In turn, the vehicle's orientation at the equilibrium is given by Eq. (7.23), i.e.

$$\theta_e = \alpha_e + \gamma_r - \pi \approx -46°.$$

To derive also the thrust-to-weight ratio at this equilibrium, follow the dotted, horizontal line drawn at $\alpha_{e_1} \approx 89°$. Then, the thrust-to-weight ratio at the equilibrium is given by the intersection between this horizontal line and the blue curve in Figure 7.4d, namely $T_{W_1} \approx 0.66°$. The dashed (colored) lines in Figure 7.4c represent the equilibrium configurations requiring a negative thrust.

Observe that bifurcations of the equilibrium angle α_e occur not only in horizontal flight ($\gamma_r = 90°$), but also for other flight directions. Note for example the case of $\gamma_r = 5°$, which is associated with multiple equilibria even at relatively small velocities ($a_\nu \approx 0.45$). As a consequence, there may exist discontinuous equilibrium orientations associated with generic continuous reference velocities.

Let us finally observe that when the aerodynamic coefficients are given by either (7.14) or (7.16), the coefficient $\bar{c}$ in Eq. (7.38) is constant and given by either $\bar{c} = c_0 + 2c_1$ or $\bar{c} = c_0 + c_2$, respectively – see Proposition 7.2 with $\delta = 0$. This allows us to calculate the equilibrium angle of attacks on the domains where the models (7.14) and (7.16) are representative of the experimental data, i.e. on large and small angles of attack, respectively. More specifically, assume that $\bar{c}$ is constant. Then, Eq. (7.37) points out that the equilibrium angle α_e is given by

$$\alpha_e = \operatorname{atan}\left(\frac{\sin(\gamma_r)}{a_\nu \bar{c} - \cos(\gamma_r)}\right). \tag{7.40}$$

Now, assume that the aerodynamic coefficients are given by (7.16) – recall this model is representative of the experimental data on *small* angles of attack – so that $\overline{c} = c_0 + c_2$. Therefore, if α_e resulting from Eq. (7.40) is *small*, it is an estimate of the *real* angle of attack at the equilibrium configuration.

7.5 Local uniqueness of equilibrium orientations

An equilibrium orientation is locally unique, or isolated, when there are no other equilibria in its (infinitesimally small) neighborhood. For instance, let us focus on Figure 7.4a and assume that $a_\nu = 1.4$ and $\gamma_r = 90°$. Then, each of the three equilibria is isolated. The local uniqueness of an equilibrium orientation is intimately related to the equilibrium equation (6.19b), which writes in terms of vectors of coordinates in the inertial frame:

$$e_2^T R^T(\theta) F(\dot{x}_r(t), \theta, t)\Big|_{\theta=\theta_e(t)} = 0, \tag{7.41}$$

where $F = mge_1 + F_a - m\ddot{x}_r$. Assume that F is continuously differentiable. If

$$\partial_\theta \Big[e_2^T R^T(\theta) F(\dot{x}_r(t), \theta, t)\Big]\Big|_{\theta=\theta_e(t)} \neq 0, \tag{7.42}$$

then the *implicit function theorem* ensures the existence of a unique differentiable function $\theta = \phi(\overline{t})$ satisfying (7.41) when $\overline{t}$ belongs to a neighborhood $\mathcal{I}_t$ of t and such that $\theta_e(t) = \phi(t)$, i.e.

$$e_2^T R^T(\phi(\overline{t})) F(\dot{x}_r(\overline{t}), \phi(\overline{t})) = 0, \quad \forall \overline{t} \in \mathcal{I}_t,\ \theta_e(t) = \phi(t). \tag{7.43}$$

Hence, the condition (7.42) ensures that the equilibrium orientation $\theta_e(t)$ is isolated and differentiable at the time instant t.

The possibility of satisfying the condition (7.42) is intimately related to the dependencies of the aerodynamic force F_a upon the orientation θ via the angle of attack α – see Eq. (6.6). For example, assume that the aerodynamic force is reduced to its drag component, – i.e. spherical shape $c_L(\alpha) \equiv 0$ and $c_D(\alpha) \equiv c_0$ – so that the apparent external force F does not depend on the vehicle's orientation θ. Then, one easily verifies that the condition (7.42) is satisfied if and only if the apparent external force along the reference velocity is different from zero at the time t, namely

$$|F(\dot{x}_r(t), t)| > 0.$$

When $|F(\dot{x}_r(t), t)| = 0$, the equilibrium orientation is not locally isolated since any orientation of the vehicle satisfies Eq. (7.41) (see Section 7.1 for more details on the equilibria analysis in the case of a spherical shape). However, as soon as we consider the dependencies of the aerodynamic force upon the vehicle's orientation, the apparent external force F being different from zero is no longer sufficient for $\theta_e(t)$ to be isolated[4]. Let us consider another example. When the aerodynamic force depends upon θ but satisfies the condition (7.9) (see Proposition 7.1), then the condition (7.42) becomes

$$\partial_\theta \Big[e_2^T R^T(\theta) F_p(\dot{x}_r(t), t)\Big]\Big|_{\theta=\theta_e(t)} \neq 0,$$

[4]For example, assume that $F = Re_1$. Then, $|F| = 1$ (nonzero external force), but the equilibrium orientation is not isolated since any orientation satisfies (7.41).

with $\vec{F}_p = (\vec{\imath}_0, \vec{\jmath}_0)F_p$ given by (7.13) and independent of θ. Hence, the vector F_p plays the same role of the external apparent force F in the spherical case, namely, the vector F_p being different from zero ensures that the equilibrium orientation is isolated and differentiable at the time instant t. However, when the aerodynamic force does not satisfy the condition (7.9), the condition $F_p(\dot{x}_r, t) \neq 0$ no longer ensures these proprieties of $\theta_e(t)$.

The next theorem shows that there exists a change of the thrust control input $T \to T_p$ such that the dynamics of the velocity errors can be written as

$$m\dot{\vec{e}}_v = \vec{F}_p - T_p\vec{\imath}, \tag{7.44}$$

and such that the strict positivity of $|\vec{F}_p|$ at the equilibrium point, i.e.

$$|\vec{F}_p(\vec{v}_r(t), \theta_e(t), t)| > \overline{\delta}, \quad \overline{\delta} \in \mathbb{R}^+, \tag{7.45}$$

implies that the equilibrium orientation $\theta_e(t)$ is isolated and differentiable at the time t. Furthermore, other properties of the vector $\vec{F}_p$ are pointed out in the next result.

Theorem 7.3. Assume that the resultant of the aerodynamic force is given by (6.17) and that the aerodynamic coefficients are twice-differentiable functions.
The body's dynamic equation (6.1a) may be rewritten as

$$m\vec{a} = m\vec{g} + \vec{f}_p - T_p\vec{\imath}, \tag{7.46}$$

where the equivalent aerodynamic force $\vec{f}_p$ and thrust intensity T_p are given by:

$$\vec{f}_p = k_a|\vec{v}_a|\left[c_{Lp}(\alpha)\vec{v}_a^{\perp} - c_{Dp}(\alpha)\vec{v}_a\right], \tag{7.47a}$$

$$T_p = T + k_a|\vec{v}_a|^2[c'_L(\alpha)\cos(\alpha+\delta) + c'_D(\alpha)\sin(\alpha+\delta)], \tag{7.47b}$$

with

$$\begin{cases} c_{Lp}(\alpha) = c_L(\alpha) - [c'_L(\alpha)\cos(\alpha+\delta) + c'_D(\alpha)\sin(\alpha+\delta)]\sin(\alpha+\delta) \\ c_{Dp}(\alpha) = c_D(\alpha) + [c'_L(\alpha)\cos(\alpha+\delta) + c'_D(\alpha)\sin(\alpha+\delta)]\cos(\alpha+\delta). \end{cases} \tag{7.48}$$

Then, the dynamics of the velocity error is given by Eqs. (7.44) with

$$\vec{F}_p := m\vec{g} + k_a|\vec{v}_a|\left[c_{Lp}(\alpha)\vec{v}_a^{\perp} - c_{Dp}(\alpha)\vec{v}_a\right] - m\vec{a}_r, \tag{7.49}$$

and the following results hold.

1) If the condition (7.45) is satisfied, then the equilibrium orientation $\theta_e(t)$ is isolated and differentiable at the time t.

2) If the condition (7.45) is satisfied, then the direction of the vector $\vec{F}_p$ is *almost constant* w.r.t. θ close to the equilibrium configuration, i.e.

$$\partial_\theta \left[\frac{\vec{F}_p}{|\vec{F}_p|}\right]\Bigg|_{(\vec{e}_v,\theta)=(0,\theta_e)} = 0. \tag{7.50}$$

3) If the aerodynamic coefficients satisfy the condition (7.9), then $\vec{f}_p$ given by (7.47a) is independent of θ and coincides with the vector given by (7.11a).

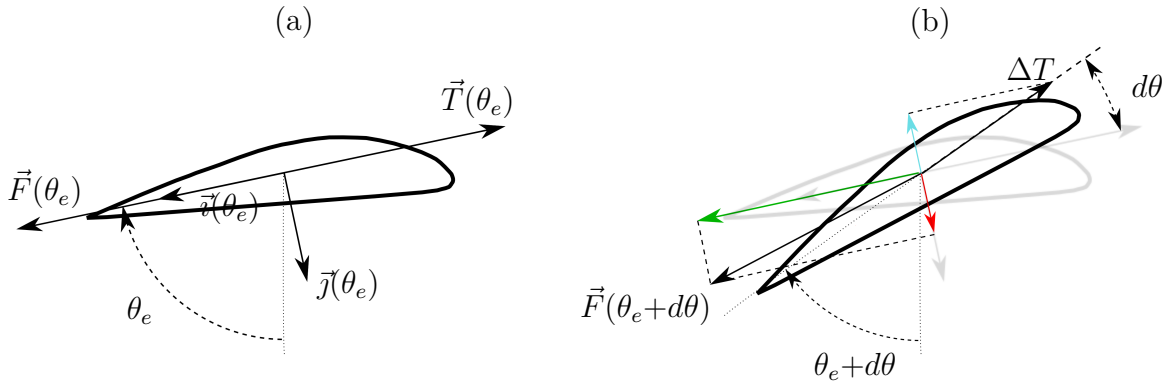

Figure 7.5: An aircraft under small perturbations from an equilibrium configuration.

The proof is given in Appendix A.7. The above theorem points out that if the vector $\vec{F}_p$ is different from zero at the equilibrium configuration, then the associated equilibrium orientation is isolated and differentiable at the time t, independently from the aerodynamic force acting on the vehicle. Hence, the vector $\vec{F}_p$ plays the same role of the external apparent force $\vec{F}$ in the spherical case. Another result pointed out in Theorem 7.3 is that in a neighborhood of the equilibrium point $(\vec{e}_v, \theta) = (0, \theta_e)$, the direction of the vector $\vec{F}_p$ is *almost* constant w.r.t. the vehicle's orientation. In fact, the variable change T_p in Theorem 7.3 has its origin in the process of imposing this property of $\vec{F}_p$, which will allow us to find local stabilizers for System (7.44) in the next chapter.

To provide the reader with an insight into the genesis of the variable change T_p, focus on Figure 7.5. Figure 7.5a shows the body at an equilibrium configuration, so the thrust force $\vec{T}$ opposes the apparent external force $\vec{F}$. Since this force depends upon θ, any perturbation $d\theta$ of the thrust direction modifies the apparent external force $\vec{F}$. Now, the perturbed force $\vec{F}(\theta_e + d\theta)$ shown in Figure 7.5b is not aligned with the thrust direction since the vehicle is not in an equilibrium configuration. Then, $\vec{F}(\theta_e + d\theta)$ can be decomposed into two components (see Figure 7.5b): a force along the thrust direction at the equilibrium configuration, i.e. the green vector, and a force along $\vec{\jmath}(\theta_e)$, i.e. the red vector. Since we can modify the thrust intensity at will, we can compensate for the red vector by adding to the thrust intensity the term ΔT shown in Figure 7.5b. Consequently, the vector resulting from

$$\vec{F}(\theta_e + d\theta) - \Delta T \vec{\imath}(\theta_e + d\theta)$$

is along the direction of $\vec{F}(\theta_e)$. One can verify that ΔT corresponds to the second term on the right hand side of Eq. (7.47b).

Finally, note that Theorem 7.3 includes Proposition 7.1 since the vector $\vec{f}_p$ given by (7.47a) is independent of the vehicle's orientation when the aerodynamic coefficients satisfy the condition (7.9).

7.6 Static stability of a reference velocity

Suppose that an aircraft is flying at a constant reference velocity and a small gust, which rapidly vanishes, perturbs the equilibrium of the system. If the aircraft's velocity tends to return to the original value with the control inputs kept at the equilibrium values, then that configuration is called *statically* stable. In our case, the control inputs are the thrust intensity and the angular velocity, so keeping the inputs at the equilibrium values means fixing the vehicle's thrust and orientation. The stability characteristics of the perturbed velocities can be deduced by analyzing the linearization of System (6.15b), i.e.

$$m\dot{\vec{e}}_v = \vec{F} - T\vec{\imath} \tag{7.51}$$

at the equilibrium point $\vec{e}_v = 0$ with $(T, \theta) \equiv (T_e(t), \theta_e(t))$. Although the practical interest of this analysis is arguable[5], it is interesting as it highlights some consequences of the *stall phenomena* at the control level. The next lemma states a static stability criterion in the case of no wind and constant reference velocity.

Lemma 7.6. Assume no wind and a constant reference velocity $\dot{x}_r = \nu(\cos(\gamma_r), \sin(\gamma_r))^T$, with $\nu \in \mathbb{R}^+$ and $\gamma_r \in \mathbb{S}^1$. Let α_e be an equilibrium angle of attack at the reference velocity and assume that the vehicle's orientation is kept at $\theta_e = \alpha_e + \gamma_r + \delta - \pi$. Define:

$$p(\alpha) := 3c_D + c_L', \tag{7.52a}$$
$$q(\alpha) := c_D^2 + c_L^2 + c_D c_L' - c_D' c_L. \tag{7.52b}$$

1) If either one of the following two conditions is satisfied

$$p(\alpha_e)q(\alpha_e) < 0, \tag{7.53a}$$
$$p(\alpha_e) < 0 \quad \text{and} \quad q(\alpha_e) < 0, \tag{7.53b}$$

then the reference velocity $\dot{x}_r$ is locally unstable.

2) If both $p(\cdot)$ and $q(\cdot)$ are positive at the equilibrium angle α_e, i.e.

$$p(\alpha_e) > 0 \quad \text{and} \quad q(\alpha_e) > 0, \tag{7.54}$$

then the reference velocity $\dot{x}_r$ is locally asymptotically stable.

The proof is given in Appendix A.8. Prior to applying this lemma, we need to determine the equilibrium angle(s) of attack α_e at the reference velocity $\dot{x}_r$. To this purpose, we can either calculate numerical solutions to the equilibrium equation (7.24) or use diagrams alike Figure 7.6 for which $\delta = 0$. For example, if we choose a reference velocity $\dot{x}_r$ such that $(a_\nu, \gamma_r) = (1.4, 90^\circ)$ (recall that $a_\nu = \frac{k_a|\dot{x}_r|^2}{mg}$), then Figure 7.6a points out that the system has three equilibrium angles of attack: $\alpha_{e_1} = 8.8^\circ$, $\alpha_{e_2} = 15.4^\circ$ and $\alpha_{e_3} = 20.6^\circ$. By applying[6] Lemma 7.6 with these angles, we deduce that if the vehicle's orientation is kept at

$$\theta_{e_2} = \alpha_{e_2} + \gamma_r - \pi = -74.6^\circ,$$

[5]The static stability of a vehicle is strongly related to its *angular dynamics*, here neglected.

[6]We apply Lemma 7.6 by using the aerodynamic coefficients shown in Figure 7.1b, which are those used to depict the Figures 7.6.

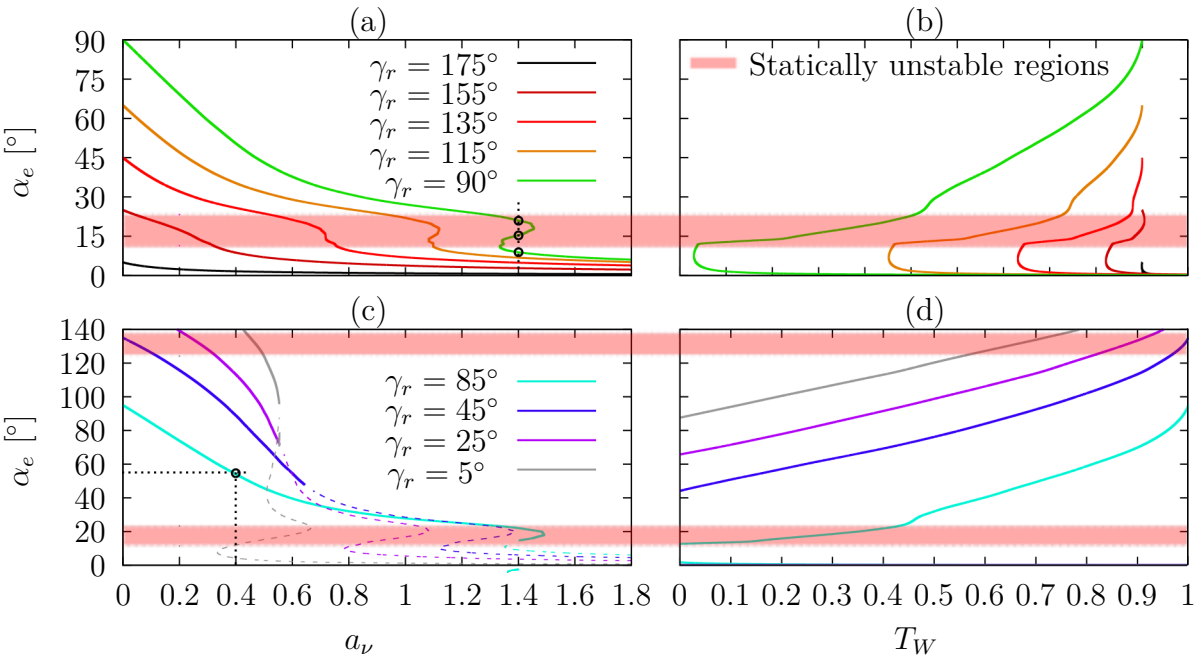

Figure 7.6: Static unstable regions of NACA airfoil 0021 with $(R_e, M) \approx (160 \cdot 10^3, 0.3)$.

then the reference velocity is unstable. However, this result was expected. In fact, the likelihood of satisfying the condition (7.53) – which implies the instability of the associated reference velocity – increases when α_e belongs to the stall region because $c_L > 0$, $c'_L \ll 0$ and $c'_D \gg 0$ in this domain. In contrast, for either small or large equilibrium angles of attack (on $[0, 90°]$), the condition (7.54) holds in most cases because: *i*) the lift coefficient is positive for small (positive) angles of attack; *ii*) $c_L(\alpha)/c_D(\alpha)$ is small for large α; *iii*) the aerodynamic characteristics are *smooth* in these two domains. Therefore, in most practical cases, the reference velocity is statically unstable when the associated equilibrium angle of attack belongs to the stall region, and statically stable otherwise. As a matter of fact, one verifies that the modeling functions given by either (7.16) or (7.14) – which are representative of the experimental aerodynamic characteristics of several NACA profiles for *small* and *large* angles of attack – satisfy the condition (7.54) for many values of the coefficients (c_0, c_1, c_2, c_3).

Applying Lemma 7.6 with the aerodynamic characteristics shown in Figure 7.1b yields the statically unstable/stable regions depicted in Figure 7.6. The statically asymptotically stable reference velocities are those such that the equilibrium angles α_e belong to the white regions, as in the case of Figure 7.4c with $(a_\nu, \gamma_r) = (0.4, 85°)$. Let us remark that on the borders between the white and red regions, Lemma 7.6 fails to determine the stability characteristics of $\dot{x}_e$ because the matrix associated with the linearization of System (7.51) at $\vec{e}_v = 0$ has an eigenvalue with zero real part. The analysis of these cases – e.g. via the application of the *Center Manifold Theorem* (Khalil, 2003, p. 303) – is beyond the scope of the present thesis, all the more so because it is very sensitive to the modelling of the aerodynamic coefficients in the chaotic stall region.

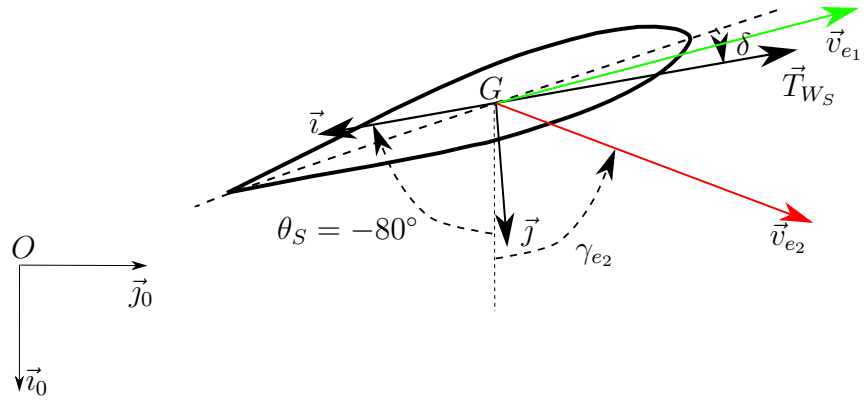

Figure 7.7: An airfoil at given (T_{W_S}, θ_S) having two equilibrium velocities $\vec{v}_{e_1}$, $\vec{v}_{e_2}$.

7.7 EQUILIBRIUM VELOCITIES FOR FIXED THRUST INTENSITY AND ORIENTATION

So far, given a reference velocity $\vec{v}_r$, much effort was put to characterize the vehicle's orientation and thrust intensity at the equilibrium configuration $\vec{v} \equiv \vec{v}_r$. In this section, instead, given a thrust intensity and a vehicle's orientation, we analyze the equilibrium velocities $\vec{v}_e$. Although this analysis is reminiscent of the one performed in the previous sections, it provides practical insights and consequences of the stall phenomena. For instance, consider a cruising airliner subjected, at some point, to a wind gust that perturbs the equilibrium of the system and makes the aircraft *stall* (i.e. the angle of attack grows beyond the stall angle). Then, in most practical cases the airplane starts losing altitude because of the reduced lift force. Among the *stall recovery* procedures aimed at recovering altitude, the pilot may choose to stabilize the airplane's orientation about a fixed value – the same as for take-off, for example – and increase the thrust intensity up to a large value. Let θ_S and T_{W_S} denote the vehicle's orientation and thrust-to-weight ratio chosen and stabilized by the pilot. If there exists a stable equilibrium velocity causing loss of altitude – such as $\vec{v}_{e_2}$ in Figure 7.7 – then this stall recovery procedure is ineffective if the aircraft's velocity belongs to region of attraction of the stable equilibrium velocity, and the pilot keeps the same vehicle's orientation and thrust intensity. We show below that these stable velocities occur for relatively large values of the thrust-to-weight ratio.

For the sake of simplicity, assume that no wind is blowing. Let the equilibrium velocity $\vec{v}_e = (\vec{\imath}_0, \vec{\jmath}_0)\dot{x}_e$ be in the form

$$\dot{x}_e = \nu_e(\cos(\gamma_e), \sin(\gamma_e))^T,$$

so that, when $-90° \leq \gamma_e < 90°$, the equilibrium velocity yields a loss-of-altitude.

By evaluating the equilibrium conditions (6.19) at $(T, \theta, \vec{v}_r, \vec{a}_r, \vec{v}_w) \equiv (mgT_{W_S}, \theta_S, \vec{v}_e, 0, 0)$ and by expressing them in the inertial frame basis, one can verify that

$$T_{W_S} = \frac{c_L(\alpha_S)\cos(\gamma_e) - c_D(\alpha_S)\sin(\gamma_e)}{c_D(\alpha_S)\sin(\theta_S - \gamma_e) + c_L(\alpha_S)\cos(\theta_S - \gamma_e)}, \tag{7.55a}$$

$$a_{\nu e} = \frac{\sin(\theta_S)}{c_D(\alpha_S)\sin(\theta_S - \gamma_e) + c_L(\alpha_S)\cos(\theta_S - \gamma_e)}, \tag{7.55b}$$

where

$$\alpha_S = \alpha_S(\gamma_e) = \theta_S - \gamma_e + (\pi - \delta),$$

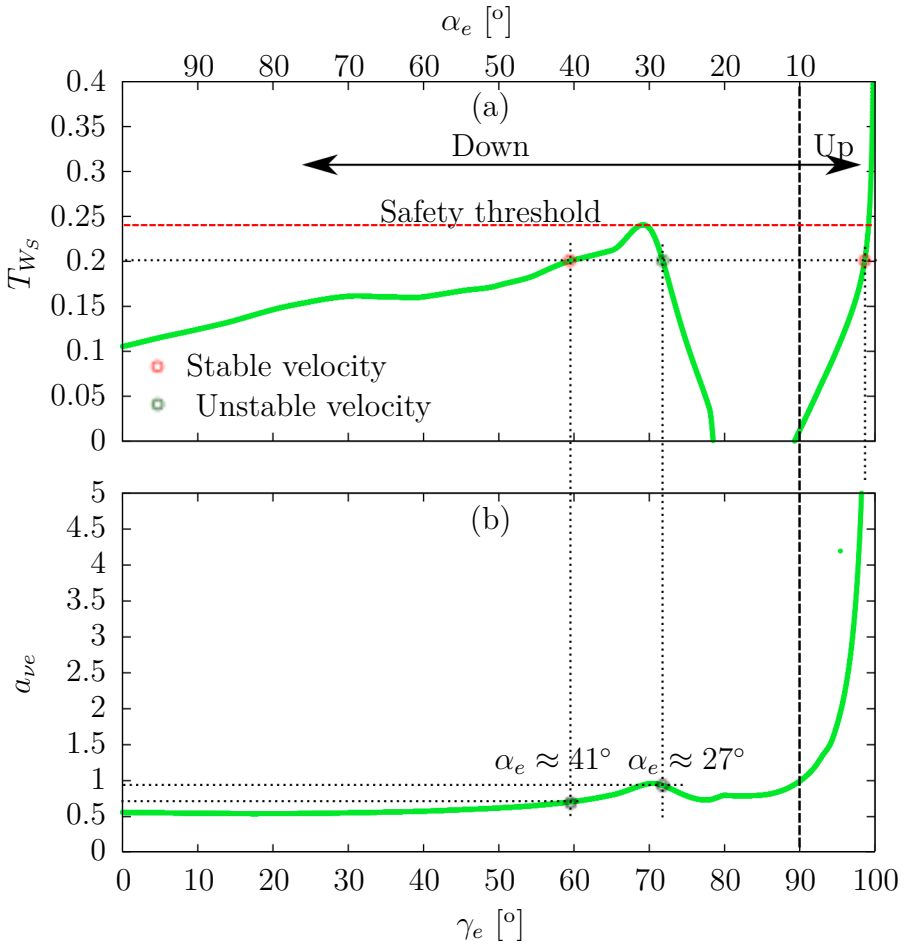

Figure 7.8: Plot of the functions T_{W_S} and $a_{\nu e}$ at fixed $(\theta_S, \delta) = (-80°, 0°)$.

and the dimensionless parameter $a_{\nu e}$ given by

$$a_{\nu e} = \frac{k_a \nu_e^2}{mg},$$

so that the *equilibrium velocity magnitude* ν_e is given by

$$\nu_e = \sqrt{\frac{mga_{\nu e}}{k_a}}. \tag{7.56}$$

By using the experimental aerodynamic characteristics shown in red in Figure 7.2b, Figure 7.8 depicts the functions T_{W_S} and a_{ν_e} versus γ_e with the vehicle's orientation $\theta_S = -80°$, and with $\delta = 0°$. To illustrate how we can use these curves, let us focus on Figure 7.8a and fix $T_{W_S} = 0.2$ (the pilot sets a thrust corresponding to the 20% of the vehicle's weight), and let us draw a horizontal line at this value. Then, the directions of the equilibrium velocity are given by the intersections between this virtual line and the green curve, namely $\gamma_{e_1} \approx 59°$, $\gamma_{e_2} \approx 71°$ and $\gamma_{e_3} \approx 98°$. By projecting the angles γ_e vertically until Figure 7.8b, we also find out the value $a_{\nu e}$ corresponding to each γ_e, and thus the magnitude of the equilibrium velocity ν_e via Eq. (7.56). Hence, any airplane whose aerodynamic coefficients are similar to those shown in Figure 7.2b (red curves) has three equilibrium velocities when the thrust-to-weight ratio is set at $T_{W_S} = 0.2$, and the

vehicle's orientation is kept at $\theta_S = -80°$. Observe that if the aircraft's velocity is close to the equilibrium velocities $\gamma_{e_1} \approx 59°$ or $\gamma_{e_2} \approx 71°$, the vehicle's altitude decreases.

The stability characteristics of the equilibrium velocities at given vehicle's thrust and orientation can be deduced by applying Lemma 7.6 with the reference velocity $\dot{x}_r$ replaced by the equilibrium velocity $\dot{x}_e$ and with

$$\alpha_e = \theta_S - \gamma_e + (\pi - \delta). \tag{7.57}$$

For example, the aforementioned case $(T_{W_S}, \theta_S, \delta)$=$(0.2, -80°, 0°)$ yields three equilibrium velocity directions γ_e, each of which is associated with a different equilibrium angle of attack, given by (7.57), to be used in Lemma 7.6. However, once the portrait of the function T_{W_S} is drawn, we can immediately identify the unstable equilibrium velocities. In fact, by direct calculations one verifies that

$$\text{sign}(q(\alpha_e)) = \text{sign}(\partial_{\gamma_e} T_{W_S}), \quad \theta_S \in (-180°, 0), \tag{7.58}$$

where $q(\alpha)$ and T_{W_S} are given by Eqs (7.52b) and (7.55a), respectively.

Now, by drawing the function T_{W_S} versus γ_e at fixed $\theta_S \in (-180°, 0)$, the domain(s) of γ_e in which T_{W_S} is strictly decreasing represent the unstable equilibrium velocities – see Lemma 7.6 and Eq. (7.58). For example, from Figure 7.8a we see that whatever the value of

$$T_{W_S} \in [0, 0.24],$$

the equilibrium velocity directions

$$\gamma_e \in (68°, 79°)$$

are locally unstable since T_{W_S} decreases in this domain. In contrast, the domain(s) in which T_{W_S} is strictly increasing versus γ_e imply a positive q . Consequently, in view of Lemma 7.6, these domain(s) represent stable equilibrium velocities if

$$p(\alpha_e) = 3c_D(\alpha_e) + c'_L(\alpha_e) > 0.$$

Let us remark that in most practical cases, $p(\alpha_e)$ is positive everywhere except in the stall region, where the function T_{W_S} is usually decreasing. Hence, a rough estimation of the stable equilibrium velocities is given by the domain(s) on which the function T_{W_S}, with $\theta_S \in (-180°, 0)$, is strictly increasing. Figure 7.8a shows that when the pilot sets a thrust-to-weight ratio greater than

$$T_{W_{safety}} = 0.24,$$

there exists a unique (usually stable) equilibrium velocity associated with a climbing phase ($\gamma_e > 90°$). Then, there exists a threshold of the thrust intensity above which the vehicle's altitude is expected to increase. However, because of thrust limitations, this safety threshold may not be reached. The safety threshold gets larger when the angle δ is negative (see Figure 7.9), as in the case of most airliners where small, negative values of δ allow the airplane's fuselage in cruise flight to be (almost) horizontal.

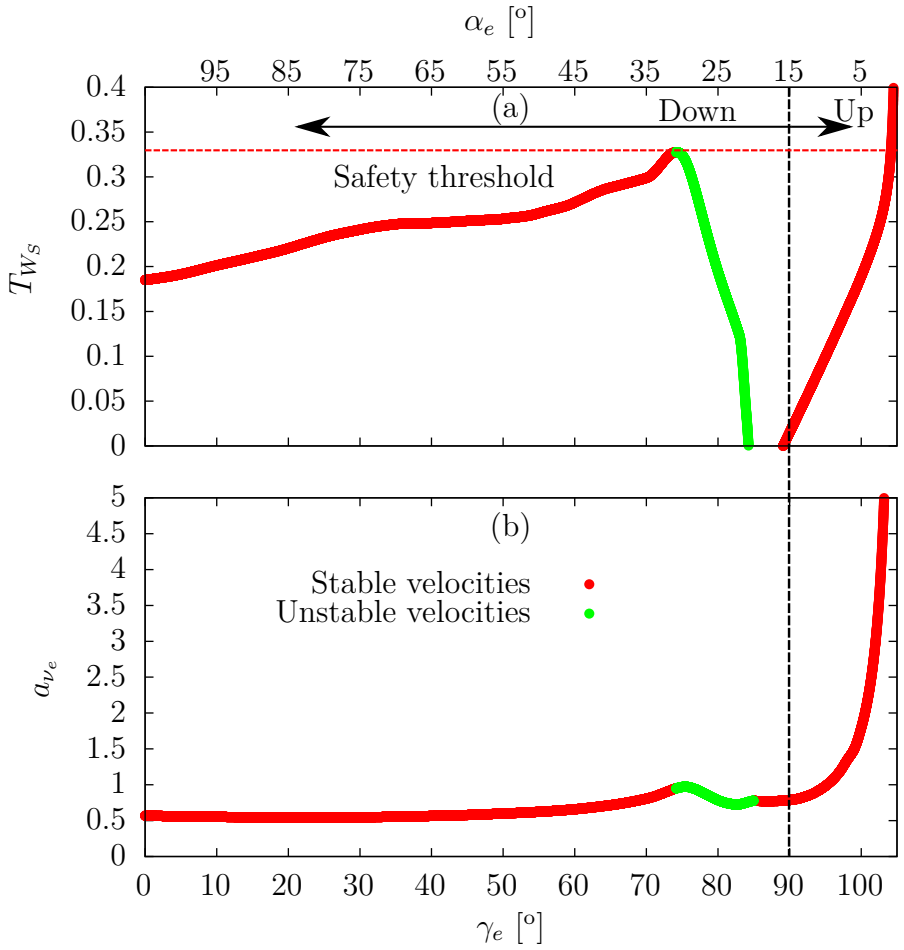

Figure 7.9: Plot of the functions T_{W_S} and $a_{\nu e}$ at fixed $(\theta_S, \delta) = (-80°, -5°)$.

8 Control design

In this chapter, we design and validate a Lyapunov-based control approach for the asymptotic stabilization of either reference positions $\vec{p}_r$ or reference velocities $\vec{v}_r$. This approach is based on the equilibria analysis presented in Chapter 7, especially Section 7.5. The chapter is composed of five sections. Section 8.1 discusses the control problem, the main assumptions made in this chapter, and the key idea behind the proposed solutions. Sections 8.2 and 8.3 present the velocity and position controls, respectively. Since these controls make use of terms that may be undefined in some regions of the state space, Section 8.4 presents control expressions that are defined everywhere. Section 8.5 presents simulations results.

8.1 Main assumptions and problem statement

The dynamics of the tracking errors associated with the asymptotic stabilization problem are given by Eqs. (6.15), namely

$$\dot{\vec{e}}_p = \vec{e}_v, \tag{8.1a}$$
$$m\dot{\vec{e}}_v = \vec{F} - T\vec{\imath}, \tag{8.1b}$$
$$\dot{\theta} = \omega, \tag{8.1c}$$

with

$$\vec{F} = m\vec{g} + \vec{F}_a - m\vec{a}_r, \tag{8.2a}$$
$$\vec{F}_a = k_a|\vec{v}_a|\left[c_L(\alpha)\vec{v}_a^{\perp} - c_D(\alpha)\vec{v}_a\right], \tag{8.2b}$$

$\vec{v}_a^{\perp} = v_{a_1}\vec{\jmath} - v_{a_2}\vec{\imath}$, and either $\vec{e}_p := \int_0^t [\vec{v}(s) - \vec{v}_r(s)]\, ds$, the integral of the velocity error, or $\vec{e}_p := \vec{p} - \vec{p}_r$, the position tracking error when a reference trajectory is specified. Recall that the vector $\vec{e}_v$ is the velocity error defined by $\vec{e}_v := \vec{v} - \vec{v}_r$.

Equation (8.1b) points out the role of the external apparent force $\vec{F}$ in obtaining the dynamics of the velocity error $\vec{e}_v$. It shows, for instance, that the controlled thrust vector $T\vec{\imath}$ must oppose the apparent external force $\vec{F}$ at the equilibrium point $\vec{e}_v \equiv 0$. When the aerodynamic force $\vec{F}_a$ does not depend on the vehicle's orientation – as in the case of spherical shapes, see Section 7.1 – neither does the apparent external force $\vec{F}$. The control strategy then basically consists in aligning the thrust direction $\vec{\imath}$ with the direction of $\vec{F}$ (orientation control via ω) and in opposing the thrust magnitude to the intensity of $\vec{F}$ (thrust control via T). However, lift and drag forces that depend on the vehicle orientation

may significantly complexify this strategy. As discussed in Chapter 7, the dependencies of the apparent external force $\vec{F}$ upon the orientation make the existence, the uniqueness and the continuity of the vehicle's equilibrium no longer guaranteed a priori, and the stabilization of such an equilibrium can be very sensitive to thrust orientation variations. Hence, the way of aligning the thrust $\vec{T}$ and the apparent external force $\vec{F}$ is far from obvious when this force depends upon the vehicle's orientation.

Now, Theorem 7.3 (Section 7.5) points out the existence of a change of thrust control $T \to T_p$ yielding the tracking errors dynamics in the form

$$\dot{\vec{e}}_p = \vec{e}_v, \tag{8.3a}$$
$$m\dot{\vec{e}}_v = \vec{F}_p - T_p\vec{\imath}, \tag{8.3b}$$
$$\dot{\theta} = \omega, \tag{8.3c}$$

where the direction of $\vec{F}_p$ is *almost constant* close to the vehicle's equilibrium configuration $(\vec{e}_v, \theta) = (0, \theta_e)$. A local control strategy then basically consists in aligning the thrust direction $\vec{\imath}$ with the direction of $\vec{F}_p$ (orientation control via ω) and in opposing the magnitude T_p to the intensity of $\vec{F}_p$ (thrust control via T). Based on this idea, this chapter proposes nonlinear control laws to achieve asymptotic stabilizations of either reference positions or reference velocities. To avoid non essential complications, we make the following assumptions on the vehicle's shape and thrust.

Assumption 3.

a) The vehicle's shape is symmetric – see Section 6.2.1.
b) The thrust force $\vec{T}$ is parallel to the zero-lift direction $\vec{z}_L$ so that $\delta = 0$.
c) The aerodynamic coefficients $c_L(\alpha)$ and $c_D(\alpha)$ are twice differentiable functions, and their derivatives are bounded $\forall \alpha \in \mathbb{S}^1$.

From Theorem 7.3 with Assumption 3b, one verifies that the vector $\vec{F}_p$ and the thrust intensity T_p yielding the tracking errors dynamics in the form (8.3) are given by:

$$\vec{F}_p = m\vec{g} + \vec{f}_p - m\vec{a}_r, \tag{8.4}$$
$$T_p = T + k_a|\vec{v}_a|^2 \left[\overline{c}'(\alpha)\sin(\alpha) + \frac{c_L(\alpha)}{\sin(\alpha)}\right], \tag{8.5}$$

with

$$\vec{f}_p = k_a|\vec{v}_a|\left[c_{Lp}(\alpha)\vec{v}_a^{\perp} - c_{Dp}(\alpha)\vec{v}_a\right], \tag{8.6}$$

$$\begin{cases} c_{Lp}(\alpha) = -\overline{c}'(\alpha)\sin^2(\alpha), \\ c_{Dp}(\alpha) = \overline{c}(\alpha) + 0.5\overline{c}'\sin(2\alpha), \end{cases} \tag{8.7}$$

$$\overline{c}(\alpha) = c_D(\alpha) + c_L(\alpha)\cot(\alpha). \tag{8.8}$$

Let us now remark an important fact. In light of Eq. (8.7) and according[1] to Proposition 7.1, if the aerodynamic coefficients satisfy the following condition

$$\overline{c} = c_D(\alpha) + c_L(\alpha)\cot(\alpha), \tag{8.9}$$

[1]When $\delta = 0$, the constant $\overline{c}_L$ in the condition (7.9) is zero; in the contrary case, the equivalent drag $\overline{c}_D$ would not be defined at $\alpha = 0$ since $c_L(\alpha) = 0$.

with $\bar{c}$ a constant number, then $\vec{F}_p$ in (8.3b) is independent of the vehicle's orientation θ. For instance (see Propositions 7.1 and 7.2 with $\delta = 0$), the aerodynamic coefficients given by either (7.14), i.e.

$$\begin{cases} c_D(\alpha) = c_0 + 2c_1 \sin^2(\alpha) \\ c_L(\alpha) = c_1 \sin(2\alpha), \end{cases} \tag{8.10}$$

or (7.16), i.e.

$$\begin{cases} c_L(\alpha) = \dfrac{0.5c_2^2}{(c_2 - c_3)\cos^2(\alpha) + c_3} \sin(2\alpha) \\ c_D(\alpha) = c_0 + \dfrac{c_2 c_3}{(c_2 - c_3)\cos^2(\alpha) + c_3} \sin^2(\alpha), \end{cases} \tag{8.11}$$

satisfy (8.9) with a constant $\bar{c}$, and the corresponding coefficients c_{Lp} and c_{Dp} are given by either

$$\begin{cases} c_{Lp} \equiv 0 \\ c_{Dp} \equiv \bar{c} = c_0 + 2c_1, \end{cases} \tag{8.12}$$

or

$$\begin{cases} c_{Lp} \equiv 0 \\ c_{Dp} \equiv \bar{c} = c_0 + c_2, \end{cases} \tag{8.13}$$

respectively. Once the error dynamics (8.1b) is transformed into the form (8.3b) with $\vec{F}_p$ independent of the vehicle's orientation, the control design can be addressed by adapting the methods developed for the class of systems subjected to an orientation-independent external force. For example, the control solution presented in (Hua et al., 2009a) provides globally stabilizing controllers for either a reference velocity $\vec{v}_r$ or a reference trajectory $\vec{p}_r$. However, when the aerodynamic coefficients do not yield a constant $\bar{c}$, the control of system (8.3) is no longer systematic. The following sections basically extend and encompass the control approach (Hua et al., 2009a) by loosening the assumption that *the apparent external force does not depend on the vehicle's orientation.*

8.1.1 Equilibria of interest

The transformed system dynamics (8.3b) points out that $\vec{e}_v \equiv 0$ implies

$$T_p = \vec{F}_p(\vec{v}_r, \theta_e, t) \cdot \vec{\imath}(\theta_e), \tag{8.14a}$$

$$0 \equiv \vec{F}_p(\vec{v}_r, \theta_e, t) \cdot \vec{\jmath}(\theta_e), \quad \forall t. \tag{8.14b}$$

Let $\widetilde{\theta} \in (-\pi, \pi]$ denote the angle between $\vec{\imath}$ and $\vec{F}_p$. The control objective is then equivalent to the asymptotic stabilization of either $\widetilde{\theta}$=0 or $\widetilde{\theta} = \pi$, depending on the equilibrium orientation θ_e. These two equilibria correspond to either T_p=$|\vec{F}_p|$ or T_p=$-|\vec{F}_p|$, respectively. However, we derive control laws stabilizing $(T_p, \widetilde{\theta}) = (|\vec{F}_p|, 0)$ only. Let us justify this choice. First, in view of (8.8), observe that the term between square braces in the right hand side of Eq. (8.5) can be written as

$$\bar{c}'(\alpha)\sin(\alpha) + \frac{c_L(\alpha)}{\sin(\alpha)} = c_L'(\alpha)\cos(\alpha) + c_D'(\alpha)\sin(\alpha),$$

which is usually positive on either *small* or *large* angles of attack. Then, in most practical cases (see Eq. (8.5)), one has a positive T_p and $\widetilde{\theta} = 0$ along reference trajectories requiring

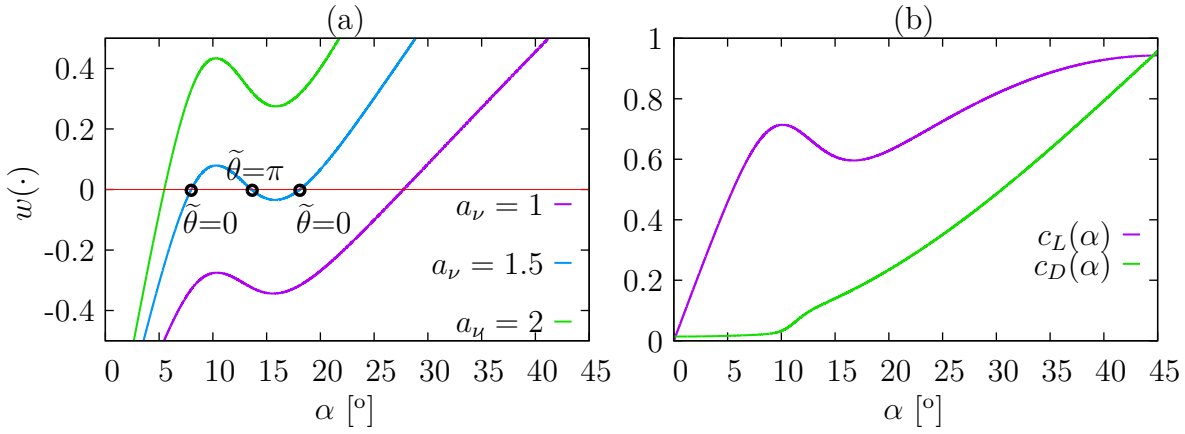

Figure 8.1: Function $w(\cdot)$ in steady-horizontal flight and aerodynamic characteristics.

either *small* or *large* angles of attack and a positive thrust intensity. Besides, one can verify that the aerodynamic coefficients given by either (8.10) or (8.11) yield a positive T_p when $T > 0$ and $\alpha \in (-90°, 90°)$. Nevertheless, to provide the reader with a better comprehension of the reasons behind the choice of stabilizing $(T_p, \widetilde{\theta}) = (|\vec{F}_p|, 0)$ only, let us analyze the properties of the equilibrium orientations yielding $(T_p, \widetilde{\theta}) = (-|\vec{F}_p|, \pi)$.

First, note that since Eqs. (8.1b) and (8.3b) coincide, then the vector $\vec{F}_p$ and $\vec{F}$ satisfy

$$\vec{F}_p \cdot \vec{\jmath} \equiv \vec{F} \cdot \vec{\jmath}.$$

Consequently, seeking for the equilibrium orientations such that (8.14b) holds is equivalent to searching for the zeros of the following function

$$w(\theta) := -\frac{1}{mg} F^T(\dot{x}_r(t), \theta, t) R(\theta) e_2, \tag{8.15}$$

where $\vec{F} = (\vec{\imath}_0, \vec{\jmath}_0)F$, and $\vec{v}_r = (\vec{\imath}_0, \vec{\jmath}_0)\dot{x}_r$. Now, from Eqs. (8.2a), (8.5), and (8.15), one verifies that at the equilibrium point $\vec{e}_v = (\vec{\imath}_0, \vec{\jmath}_0)\dot{\tilde{x}} = (\vec{\imath}_0, \vec{\jmath}_0)(\dot{x} - \dot{x}_r) \equiv 0$ one has

$$T_p|_{\vec{e}_v \equiv 0} = mg\partial_\theta w(\theta_e). \tag{8.16}$$

Therefore, $\widetilde{\theta} = 0$ and $\widetilde{\theta} = \pi$ correspond to the derivative of the function $w(\cdot)$ being either positive or negative at the equilibrium orientation θ_e, i.e. $w(\theta_e) = 0$.

Figure 8.1a depicts typical trends of the function $w(\cdot)$ for steady-horizontal flight, i.e. $\dot{x}_r = \nu(0, 1)^T$ and $|\dot{x}_w| \equiv 0$, where we have used the aerodynamic characteristics shown in Figure 8.1b – recall that $a_\nu = \frac{k_a \nu^2}{mg}$. From Figure 8.1a it is visually evident that the equilibrium angles at which the function $w(\cdot)$ crosses zero are associated with a positive derivative w.r.t. θ (recall that $\partial_\theta w = \partial_\alpha w$) except for the equilibria occurring in a neighborhood of the stall region. Then, for the case shown in Figure 8.1, stabilizing $\widetilde{\theta} = 0$ ensures that the equilibrium angle of attack does *not belong to the stall region*.

However, simulations that we have performed point out that large-constant reference velocities representing a descending phase may be associated with $\partial_\theta w > 0$, and consequently $\widetilde{\theta} = 0$, but a negative thrust intensity. Hence, to comply with the additional constraint $T > 0$, one must stabilize $\widetilde{\theta} = \pi$ in these cases. Although this kind of reference velocities are not frequently used in practice, we remark that the choice of stabilizing either $\widetilde{\theta} = 0$ or $\widetilde{\theta} = \pi$ requires in general close attention, since stabilizing the former equilibrium does not always ensure a positive thrust at the equilibrium configuration $\vec{e}_v \equiv 0$.

8.1.2 Well-posedeness of the control problem

Let us now make the following complementary assumption.

Assumption 4. The reference velocity $\vec{v}_r(t)$ ensures the existence of a continuous equilibrium orientation $\theta_e(t)$ such that

$$|\vec{F}_p(\vec{v}_r(t), \theta_e(t), t)| > \overline{\eta}, \quad \forall t \in \mathbb{R}_+, \quad \overline{\eta} \in \mathbb{R}_+. \tag{8.17}$$

Under the Assumptions 3 and 4, the asymptotic stabilization problem associated with the dynamics (8.1) is *well-posed*. In particular, because of Theorem 7.1, Assumption 3 ensures the existence of an equilibrium orientation for any reference velocity. Assumption 4 supposes that the reference trajectory is associated with a continuous equilibrium orientation (see Section 7.4.1) so that no jump of the equilibrium can occur; in addition, since the condition (8.17) holds, it also ensures that the equilibrium orientation is differentiable (see Section 7.5), so the angular velocity along the reference velocity is defined for any time t. To avoid non-essential complications, we make the following assumption.

Assumption 5. The wind velocity $\vec{v}_w$ and the reference velocity $\vec{v}_r$ are bounded in norm on $\mathbb{R}^+$, and their first and second order derivatives are defined and bounded on this set.

8.2 Velocity control

This section proposes a solution to the asymptotic stabilization of a reference velocity $\vec{v}_r = (\vec{\imath}_0, \vec{\jmath}_0)\dot{x}_r$. The control result is stated next.

Proposition 8.1. Assume that Assumptions 3, 4, and 5 are satisfied. Let $k_i > 0$, $i = \{1, 2, 3\}$ and apply the control

$$T = \overline{F}_1 + k_1 |F_p| \widetilde{v}_1, \tag{8.18a}$$

$$\omega = k \left[k_2 |F_p| \widetilde{v}_2 + \frac{k_3 |F_p| \overline{F}_{p_2}}{(|F_p| + \overline{F}_{p_1})^2} - \frac{\overline{F}_p^T S R^T F_\delta}{|F_p|^2} \right], \tag{8.18b}$$

to System (8.1b)-(8.1c) with $\overline{F}_p = R^T F_p$, $\overline{F} = R^T F$,

$$F = mge_1 + F_a - m\ddot{x}_r, \tag{8.19a}$$

$$F_p = mge_1 + f_p - m\ddot{x}_r, \tag{8.19b}$$

$$F_\delta := \partial_{\dot{x}_a} f_p \ddot{x}_a - \partial_\alpha f_p \dot{\gamma} - m\dddot{x}_r(t), \tag{8.19c}$$

$$F_a(\dot{x}_a, \alpha) = k_a |\dot{x}_a| [c_L(\alpha) S - c_D(\alpha) I] \dot{x}_a, \tag{8.20a}$$

$$f_p(\dot{x}_a, \alpha) = k_a |\dot{x}_a| [c_{L_p}(\alpha) S + c_{D_p}(\alpha)] \dot{x}_a, \tag{8.20b}$$

and k given by:

$$k = k(\dot{x}_a, \theta) := \left(1 + k_a |\dot{x}_a|^2 \overline{F}_2 \frac{\sin(\alpha)\overline{c}'' + 2\cos(\alpha)\overline{c}'}{|F_p|^2} \right)^{-1}. \tag{8.21}$$

with $\overline{c}$ as (8.8). Then,

1) the control laws (8.18) are well defined in a neighborhood of the reference velocity;

2) $(\vec{e}_v, \widetilde{\theta})$=$(0, 0)$ is a locally asymptotically stable equilibrium point of (8.1b)-(8.1c).

The proof of this result is given in Appendix A.9. Let us remark an important fact. As mentioned before, the expressions (8.7) point out that if $\bar{c}$ is constant, then the vector $\vec{F}_p$ in (8.3) does not depend on the vehicle's orientation. In this case, the control design for System (8.3) can be addressed by adapting the method developed for the class of systems subjected to an orientation-independent external force. For example, (Hua et al., 2009a) proposes globally stabilizing controllers for this system. One can then verify that the velocity control derived by the application of (Hua et al., 2009a) to System (8.3) – with a constant $\bar{c}$ – coincides with that given by (8.18) with $k \equiv 1$ and $\bar{c}$ a constant number. Then, the control laws (8.18) yield a large domain of attraction for the class of modeling functions for which $\bar{c}$ is a constant. These facts are stated in the following proposition.

Proposition 8.2. If the aerodynamic coefficients satisfy the following condition

$$\bar{c} = c_D(\alpha) + c_L(\alpha)\cot(\alpha), \tag{8.22}$$

with $\bar{c}$ a constant number, then the control laws (8.18) coincide with the velocity control proposed by (Hua et al., 2009a) when applied to system (8.1b)-(8.1c). Consequently, if

$$|F_p| > \bar{\delta} \quad \forall t, \quad \bar{\delta} > 0, \tag{8.23}$$

and Assumptions 3, 4, and 5 hold, then the application of the controls (8.18) to System (8.1b)-(8.1c) renders $(\vec{e}_v, \widetilde{\theta})=(0,0)$ an asymptotically stable equilibrium point with domain of attraction equal to $\mathbb{R}^2 \times (-\pi, \pi)$.

A consequence of the above proposition is that when the aerodynamic characteristics are given by either (8.10) or (8.11) any reference velocity is semi-globally asymptotically stable provided that the condition (8.23) is satisfied. This latter condition characterizes the set of reference velocities for which the control is not defined. For example, among constant reference velocities and no wind, one can verify that the unique reference velocity implying $|F_p| = 0$ corresponds to a vertical fall at $\sqrt{mg/k_a\bar{c}}$ $[m/s]$, a situation rarely met in practice. The condition (8.23) is thus satisfied in most cases.

Now, if we assume that the aerodynamic characteristics are given by the model (6.13) – i.e. a combination of the models (8.10) and (8.11), see Section 6.2 – then $\bar{c}$ is constant and $k \equiv 1$ for either *small* or *large* angles of attack. In this case, the control laws (8.18) are well-defined in these two regions independently of the *closeness* of the system's trajectory to the equilibrium point provided that $|F_p| \neq 0$ only.

Observe that the control laws (8.18) ensure the local asymptotic stability of any equilibrium orientation θ_e yielding $\widetilde{\theta} = 0$. If several equilibrium orientations exist associated with $\widetilde{\theta} = 0$, then the control (8.18) stabilizes each of these equilibria (Section 8.5.2).

In practice, the control law (8.18) must be complemented with integral correction terms in order to deal with almost constant unmodeled additive perturbations. Define

$$I_v := \int_0^t \dot{\widetilde{x}}(s)\, ds, \tag{8.24}$$

and $\dot{\widetilde{x}} := R\widetilde{v}$, the velocity error expressed in the inertial frame. Let h denote a smooth bounded strictly positive function defined on $[0, +\infty)$ satisfying the following properties for some positive constant numbers η, μ,

$$\forall s \in \mathbb{R}, \quad |h(s^2)s| < \eta, \qquad \text{and} \qquad 0 < \frac{\partial}{\partial s}(h(s^2)s) < \mu. \tag{8.25}$$

An example of such a function is,

$$h: \quad s \to h(s) = \frac{\eta}{\sqrt{1+s}},$$

with $\eta > 0$. Then, a control result taking integral terms into account is stated next.

Proposition 8.3. Assume that Assumptions 3, 4, and 5 are satisfied. Apply the control law (8.18) to System (8.1) with

$$F = mge_1 + F_a - m\ddot{x}_r + h(|I_v|^2)I_v, \tag{8.26a}$$
$$F_p = mge_1 + f_p - m\ddot{x}_r + h(|I_v|^2)I_v, \tag{8.26b}$$
$$F_\delta := \partial_{\dot{x}_a} f_p \ddot{x}_a - \partial_\alpha f_p \dot{\gamma} - m\dddot{x}_r(t) + \tfrac{d}{dt}[h(|I_v|^2)I_v], \tag{8.26c}$$

Then, $(I_v, \vec{e}_v, \widetilde{\theta}) = (0,0,0)$ is a locally asymptotically stable equilibrium point of System (8.1b)-(8.1c) augmented with the equation $\dot{I}_v = R\widetilde{v}$.

The proof is given in Appendix A.10. Analogously to the result presented in Proposition 8.2, one can show that the domain of attraction of the equilibrium point $(I_v, \vec{e}_v, \widetilde{\theta}) = (0,0,0)$ becomes $\mathbb{R}^2 \times \mathbb{R}^2 \times (-\pi, \pi)$ when the aerodynamic coefficients and the vector F_p given by (8.26b) satisfy conditions (8.22) and (8.23), respectively.

Observe that the properties (8.25) limit the influence of the term I_v in the control actions. Then, the size of the constant η has to be chosen in relation to the size of the modeling errors and of the unmodeled perturbation acting on the vehicle. On the other hand, a small value for η may reduce the risk of driving $|F_p|$ close to zero. Therefore, a trade off has to be found depending on the considered case.

8.3 Position control

The control objective is now the combined stabilization of the position error $\vec{e}_p$ and the velocity error $\vec{e}_v$ to zero. A solution to this problem is already given by Proposition 8.3 when setting $I_0 = x(0) - x_r(0)$ in Eq. (8.24) so that $I_v = \widetilde{x}$. However, this solution would not take into account position integral correction terms, so we complement the control action with terms of this kind. Let us recall that the classical integrator (*i.e.* $\dot{z} = \widetilde{x}$) presents several drawbacks. For instance, the integral term may grow very large and this, in turn, would cause overshoots of the position tracking errors. To avoid this problem, and also cope with actuator limitations, one must saturate the integral terms. The solution presented here relies, in the first place, on the nonlinear integrator presented in (Hua et al., 2009a, Sec. III.D), which prevents the so-called desaturation problem to occur and the system's time response to overly increase. More precisely, the nonlinear "bounded integral" of the position error used to compensate for almost constant unmodeled additive perturbations is defined as the solution to the following second-order system:

$$\ddot{z} = -2k_z\dot{z} - k_z^2[z - \mathrm{sat}_\Delta(z)] + k_z h_z(|\widetilde{x}|^2)\widetilde{x}, \tag{8.27}$$
$$k_z > 0, \; z(0) = 0, \; \dot{z}(0) = 0,$$

where h_z is a smooth bounded strictly positive function defined on $[0, +\infty)$ satisfying (8.25) for some positive constant numbers η_z, β_z, and sat_Δ is the classical *saturation*

function, i.e. $\text{sat}_\Delta(z) = z\min(1, \Delta/|z|)$. Let

$$y := \widetilde{x} + z, \tag{8.28a}$$
$$\overline{v} := \widetilde{v} + R^T(\theta)\dot{z}, \tag{8.28b}$$

with h a smooth bounded positive function satisfying (8.25) for some positive constant numbers η, β. Then, the control result is stated next.

Proposition 8.4. Assume that Assumptions 3, 4, and 5 are satisfied. Let $k_i > 0$, $i = \{1, 2, 3\}$ and apply the control

$$T = \overline{F}_1 + k_1|F_p|\overline{v}_1, \tag{8.29a}$$
$$\omega = k\left[k_2|F_p|\overline{v}_2 + \frac{k_3|F_p|\overline{F}_{p_2}}{(|F_p| + \overline{F}_{p_1})^2} - \frac{\overline{F}_p^T S R^T F_\delta}{|F_p|^2}\right], \tag{8.29b}$$

to System (8.1) with $\overline{F}_p{=}R^T F_p$, $\overline{F} = R^T F$,

$$F = mge_1 + F_a - m\ddot{x}_r + h(|y|^2)y + \ddot{z}, \tag{8.30a}$$
$$F_p = mge_1 + f_p - m\ddot{x}_r + h(|y|^2)y + \ddot{z}, \tag{8.30b}$$
$$F_\delta = \partial_{\dot{x}_a} f_p \ddot{x}_a - \partial_\alpha f_p \dot{\gamma} - m\dddot{x}_r(t) + \dddot{z} + \tfrac{d}{dt}[h(|y|^2)y], \tag{8.30c}$$

F_a and f_p given by (8.20), and k by:

$$k = k(\dot{x}_a, \theta) := \left[1 + k_a|\dot{x}_a|^2\overline{F}_2\frac{\sin(\alpha)\overline{c}'' + 2\cos(\alpha)\overline{c}'}{|F_p|^2}\right]^{-1}. \tag{8.31}$$

Then,

1) the control laws (8.29) are well defined in a neighborhood of the reference trajectory,

2) $(z, \dot{z}, \vec{e}_p, \vec{e}_v, \widetilde{\theta}) = (0, 0, 0, 0, 0)$ is a locally asymptotically stable equilibrium point of System (8.1) complemented with System (8.27).

The proof is given in Appendix A.10. Analogously to the result in Proposition 8.2, one can show that the domain of attraction of the equilibrium point $(z, \dot{z}, \vec{e}_p, \vec{e}_v, \widetilde{\theta}) = 0$ becomes $\mathbb{R}^2 \times \mathbb{R}^2 \times (-\pi, \pi)$ when the conditions (8.22) and (8.23) are satisfied with F_p given by (8.30b).

We remark that property (8.25) of the function h limit to the influence of the position error in the control, and reduces the risk of saturating the actuators. Concerning the constant k_z in Eq. (8.27), it influences the *desaturation rate* of the variable z (via the dynamics of $\ddot{z}$). Also, note that this parameter is proportional to the upper-bound of $|\ddot{z}|$, so a large value of k_z increases the range interval of F_p and, subsequently, modifies the set in which F_p gets close to zero. Hence, the tuning of k_z depends on the situation and a trade off must be found.

8.4 Control robustification

The control laws presented so far use terms that involve singularities for specific situations. To obtain control laws that are well-defined everywhere, we first set the nonlinear coefficient $k \equiv 1$ so that we do not destroy the local stability property of the above control laws ($k \approx 1$ near the reference trajectory since $\overline{F}_2 \approx 0$). Secondly, we multiply the terms $1/(|F_p| + \overline{F}_{p_1})^2$ and $1/|F_p|^2$ by the function $\mu_\tau \in \mathbb{C}^1 : [0, +\infty) \to [0, 1]$ defined by:

$$\mu_\tau(s) = \begin{cases} \sin\left(\frac{\pi s^2}{2\tau^2}\right), & \text{if } s \leq \tau \\ 1, & \text{otherwise} \end{cases} \tag{8.32}$$

with $\tau > 0$. This yields the well-defined control expression given by

$$T = k_1|F_p|\widetilde{v}_1 + \overline{F}_1, \tag{8.33a}$$

$$\omega = k_2|F_p|\widetilde{v}_2 + \mu_\tau(|F_p| + \overline{F}_{p_1})\frac{k_3|F_p|\overline{F}_{p_2}}{(|F_p|+\overline{F}_{p_1})^2} - \mu_\tau(|F_p|)\frac{\overline{F}_p^T S R^T F_\delta}{|F_p|^2}. \tag{8.33b}$$

The property:

$$\lim_{s\to 0} \frac{\mu_\tau(s)}{s^2} = \lim_{s\to 0} \sin\left(\frac{\pi s^2}{2\tau^2}\right) s^{-2} = \frac{\pi}{2\tau^2},$$

implies that the modified control is well-defined everywhere.

Remark 8.1. *The control laws* (8.18) *and* (8.29) *make use of the feedforward term* $\ddot{x}_a$, $\dot{\gamma}$ *that is not always available in practice. Simulations with wing models, however, have shown that neglecting this term when its actual value is not too large does not much affect the control performance, in the sense that ultimate tracking errors remain small.*

8.5 Simulations

In this section, we illustrate through simulations the performance and robustness of the proposed approach for the symmetric NACA 0021 airfoil model with the thrust force parallel to the zero-lift-line, e.g. $\delta = 0$. The system's equations of motion are defined by Eqs. (8.1) and the aerodynamic coefficients, shown in Figure 8.1b, are given by

$$\begin{cases} c_L(\alpha) = c_{L_S}(\alpha)\sigma(\overline{\alpha}, \overline{k}_L, \alpha) + c_{L_L}(\alpha)[1 - \sigma(\overline{\alpha}, \overline{k}_L, \alpha)], \\ c_D(\alpha) = c_{D_S}(\alpha)\sigma(\overline{\alpha}, \overline{k}_D, \alpha) + c_{D_L}(\alpha)[1 - \sigma(\overline{\alpha}, \overline{k}_D, \alpha)]. \end{cases} \tag{8.34a}$$

with

$$\sigma(\overline{\alpha}, \overline{k}, \alpha) = \frac{1 + \tanh(\overline{k}\overline{\alpha}^2 - \overline{k}\alpha^2)}{1 + \tanh(\overline{k}\overline{\alpha}^2)}, \quad \alpha \in [-\pi, \pi),$$

$$\begin{cases} \overline{\alpha} = 11^\circ, \\ k_L = 14, \\ k_D = 41.8, \end{cases}$$

$$\begin{cases} c_{L_L}(\alpha) = c_1 \sin(2\alpha), \\ c_{D_L}(\alpha) = c_0 + 2c_1 \sin^2(\alpha), \end{cases}$$

$$\begin{cases} c_{L_S}(\alpha) = \dfrac{0.5c_2^2}{(c_2 - c_3)\cos^2(\alpha) + c_3}\sin(2\alpha), \\ c_{D_S}(\alpha) = c_0 + \dfrac{c_2 c_3}{(c_2 - c_3)\cos^2(\alpha) + c_3}\sin^2(\alpha), \end{cases}$$

$$\begin{cases} c_0 = 0.0139, \\ c_1 = 0.9430, \\ c_2 = 5.4641, \\ c_3 = 0.3151. \end{cases}$$

The other physical parameters are:

$$\begin{aligned} m &= 10\ [Kg], \\ \rho &= 1.292\ \left[Kg/m^3\right], \\ \Sigma &= 1\ [m^2]. \\ k_a &= \frac{\rho\Sigma}{2} = 0.6460\ \left[Kg/m\right]. \end{aligned}$$

We here assume that the control objective is the asymptotic stabilization of a reference velocity and we apply the control laws given by (8.18) in the modified form (8.33).

Other values are used for the calculation of the control laws in order to test the robustness w.r.t. parametric errors. They are chosen as follows:

$$\begin{aligned} \widehat{m} &= 9\ [Kg], \\ \widehat{k}_a &= 0.51\ \left[Kg/m\right], \end{aligned}$$

The term $\ddot{x}_a$ in Eq. (8.19c) is kept equal to zero, thus providing another element to test the robustness of the controller. The parameters of the control laws are $k_1 = 0.1529$, $k_2 = 0.0234$, $k_3 = 6$, $\tau = 80$.

8.5.1 FROM HOVERING TO CRUISING FLIGHT WITH AN UNFEASIBLE TRAJECTORY

The first chosen reference velocity represents a transition maneuver from hovering to cruising flight in the form (7.34), so perfect tracking would involve jumps of the equilibrium orientation. With a reference velocity of this kind we test our control approach when the Assumption 4 is not satisfied. In particular, the reference velocity is given by:

$$\dot{x}_r(t) = \begin{cases} (0, 2t)^T & 0 \le t < 10, \\ (0, 20)^T & t \ge 10. \end{cases} \tag{8.35}$$

It is then composed of: i) an horizontal velocity ramp on the time interval $[0, 10)$ $[sec]$; ii) cruising with constant horizontal velocity of 20 $[m/sec]$ for $t \ge 10$ $[sec]$. The initial velocity and attitude are $\dot{x}(0) = [0, 0]$, and $\theta(0) = 0$, respectively.

From top to bottom, Figure 8.2 depicts the evolution of the desired reference velocity, the velocity errors, the angle of attack, the desired angular velocity, the thrust-to-weight ratio, and the vehicle's orientation. No wind is assumed.

At $t = 0$, the vehicle's attitude is zero (vertical configuration), and the thrust tends to oppose the body's weight. However, because of modeling errors and a nonzero reference

acceleration, the thrust-to-weight ratio is different from one. In the interval $(0, 10)$ $[sec]$, the horizontal velocity of the vehicle increases, the angle of attack decreases, and the vehicle's orientation converges towards $-90°$ (horizontal configuration). At $t = 8$, the equilibria pattern of the system is approximately the one shown in Figure 7.3a with $\bar{t} = 8$. Hence, the equilibrium orientation is close to the discontinuity point. When $t > 8$ the equilibrium orientation jumps from one value to another one, thus creating abrupt variations of the thrust intensity and of the (desired) angular velocity. Let us remark that the control value just after the jump depends sensitively upon the constant τ. In fact, if $\tau = 0$ were chosen, the desired angular velocity would tend to infinity when the vehicle's orientation is close to both the discontinuity and the equilibrium orientation in the stall region ($\widetilde{\theta} \approx \pi \Rightarrow |F_p| + \overline{F}_{p1} \approx 0$). The jump of the equilibrium orientation forbids perfect tracking of the reference velocity, and one can observe that the velocity errors significantly increase right after the discontinuity occurrence.

8.5.2 Stabilization of different orientations depending on initial conditions

Recall that the aerodynamic coefficients used to simulate the airfoil's aerodynamics are shown in Figure 8.1b. Figure 8.1a points out that a steady-horizontal flight at $a_\nu = 1.5$ can be performed with three different equilibrium orientations corresponding to

$$\alpha_{e_1} = 7.5°, \quad \alpha_{e_2} = 13°, \quad \alpha_{e_3} = 18°.$$

Under the control laws (8.18), the equilibrium orientations associated with $\widetilde{\theta} = 0$, namely

$$\alpha_{e_1} = 7.5°, \quad \alpha_{e_3} = 18°,$$

are both locally asymptotically stable. Then, we expect that the equilibrium angle of attack converges to either one of these two equilibria depending on its initial condition. To show this, we assume that no wind is blowing, and that the reference velocity is of the form $\dot{x}_r = \nu(0, 1)$ with $\nu = 15.0926$ [m/sec] so that $a_\nu = 1.5$. Figure 8.3 depicts the results of two simulations performed with two different initial vehicle's orientations corresponding to $\alpha(0) = 9°$ and $\alpha(0) = 15°$ with $\dot{x}(0) = [0, \nu]$. The fact that the system's trajectories converge to the closest equilibrium illustrates the possibility of ending up with two different equilibrium angles of attack depending on its initial condition.

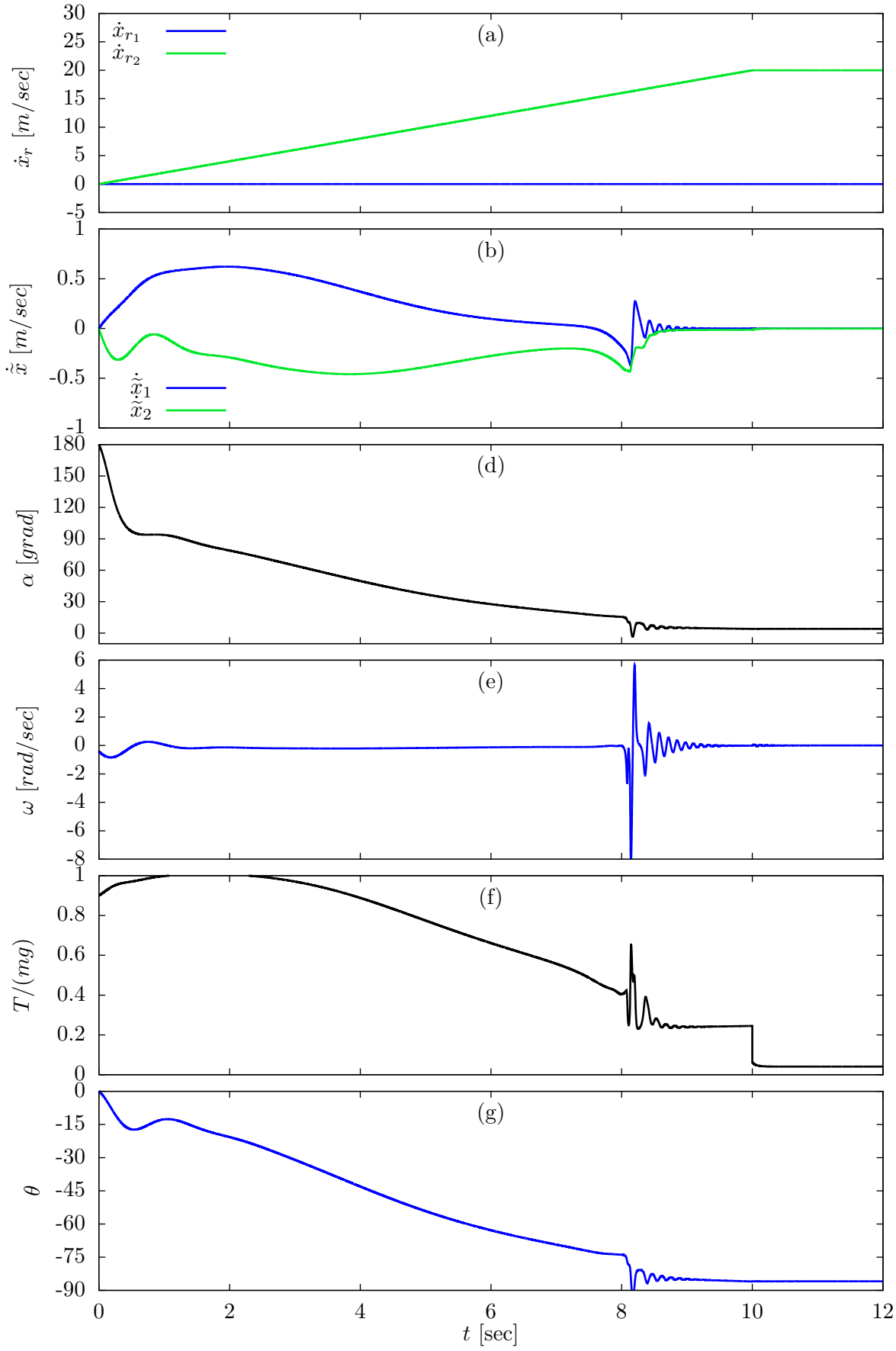

Figure 8.2: Simulation 1 of a NACA 0021 profile.

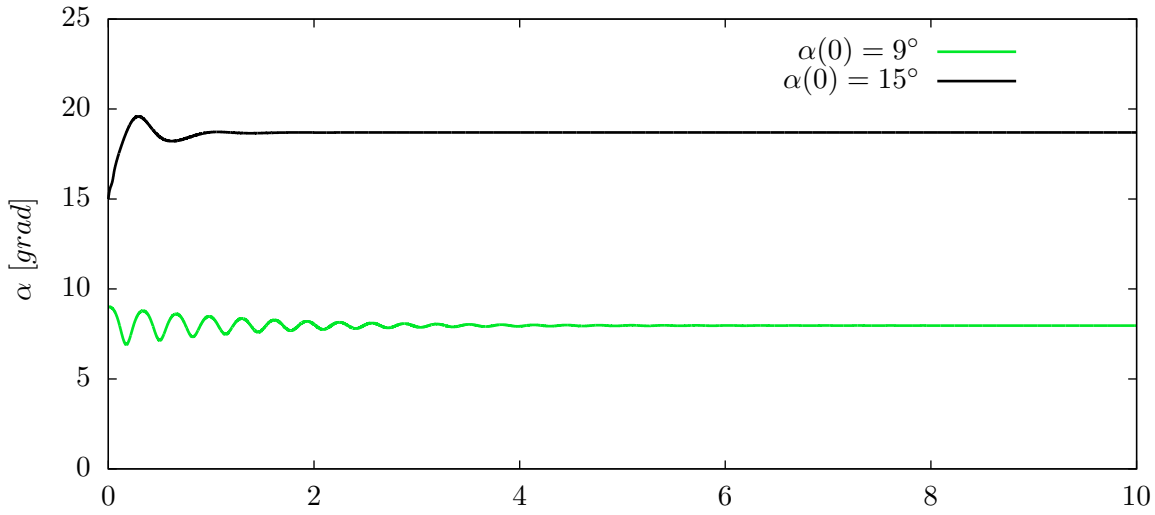

Figure 8.3: Simulation 2 of a NACA 0021 profile.

9 Extension to 3-D symmetric aircraft

"Treat nature in terms of the cylinder, the sphere, the cone, all in perspective[1]*."*

This chapter is dedicated to the modeling and control of symmetric aerial vehicles flying in three-dimensional space.

After recalling some notation, the chapter is decided into four sections. Section 9.1 is dedicated to the system modeling of aerial vehicles flying in three-dimensional space. Original results concerning the modeling of aerodynamic forces acting on symmetric bodies and the characterization of a family of models that allow one to recast the control problem into the simpler case of a spherical body – i.e. the *spherical equivalency* – are reported in section 9.2. Members of this family are singled out and tuned by using experimental data borrowed from (Keyes, 1965) and (Saffel et al., 1971) for elliptic-shaped and missile-like bodies. To illustrate the usefulness of these results at the control design level, Section 9.3 gives the adapted version of the velocity and position control schemes proposed in (Hua et al., 2009a). Section 9.4 repeats a few simulation results.

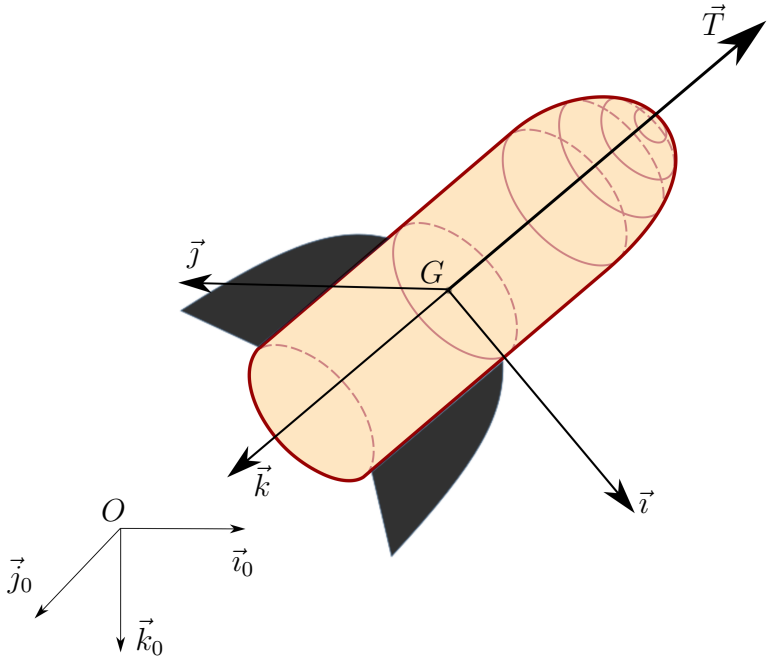

Figure 9.1: Generic three-dimensional flying body with a thrust force parallel to $\vec{k}$

[1] Paul Cézanne (1890)

The following notation is used throughout this chapter.

- The i_{th} component of a vector x is denoted as x_i.
- For the sake of conciseness, $(x_1\vec{\imath} + x_2\vec{\jmath} + x_3\vec{k})$ is written as $(\vec{\imath}, \vec{\jmath}, \vec{k})x$.
- $S(\cdot)$ is the skew-symmetric matrix-valued operator associated with the cross product in $\mathbb{R}^3$, i.e. such that $S(x)y = x \times y$, $\forall (x, y) \in \mathbb{R}^3 \times \mathbb{R}^3$.
- $\{e_1, e_2, e_3\}$ is the canonical basis in $\mathbb{R}^3$.
- m is the mass of the vehicle, assumed to be constant, and G_m is the body's center of mass.
- $\mathcal{I} = \{O; \vec{\imath}_0, \vec{\jmath}_0, \vec{k}_0\}$ is a fixed inertial frame with respect to (w.r.t.) which the vehicle's absolute pose is measured, and $\mathcal{B} = \{G; \vec{\imath}, \vec{\jmath}, \vec{k}\}$ is a frame attached to the body. Observe that G and G_m may not coincide.
- The body's linear velocity is denoted by $\vec{v} = \frac{d}{dt}\vec{OG}_m = (\vec{\imath}_0, \vec{\jmath}_0, \vec{k}_0)\dot{x} = (\vec{\imath}, \vec{\jmath}, \vec{k})v$.
- The linear acceleration vector is $\vec{a} = \frac{d}{dt}\vec{v}$.
- The body's angular velocity is $\vec{\omega} = (\vec{\imath}, \vec{\jmath}, \vec{k})\omega$.
- The vehicle's orientation w.r.t. the inertial frame is represented by the rotation matrix R. The column vectors of R are the vectors of coordinates of $\vec{\imath}, \vec{\jmath}, \vec{k}$ expressed in the basis of $\mathcal{I}$.
- The wind's velocity vector $\vec{v}_w$ is assumed to be the same at all points in a domain surrounding the vehicle, and its components are defined by $\vec{v}_w = (\vec{\imath}, \vec{\jmath}, \vec{k})v_w$. The *airvelocity* $\vec{v}_a = (\vec{\imath}, \vec{\jmath}, \vec{k})v_a = (\vec{\imath}_0, \vec{\jmath}_0, \vec{k}_0)\dot{x}_a$ is defined as the difference between $\vec{v}$ and $\vec{v}_w$. Thus, $v_a = v - v_w$.

9.1 System modeling

9.1.1 Vehicle's dynamics

As discussed in Section 5.2.1, the external forces acting on the body are assumed to be composed only of the weight vector $m\vec{g}$ and the sum of aerodynamic forces denoted by $\vec{F}_a$. Now, let us make the following assumption concerning the thrust direction.

Assumption 6. The thrust force $\vec{T}$ is parallel to the vector $\vec{k}$, i.e. $\vec{T} = -T\vec{k}$ with T denoting the thrust intensity.

In view of Assumption 6 and the assumption of complete torque actuation (see Section 5.2.2), the vehicle's equations of motion considered in this chapter are given by:

$$m\vec{a} = m\vec{g} + \vec{F}_a - T\vec{k}, \tag{9.1a}$$

$$\frac{d}{dt}(\vec{\imath}, \vec{\jmath}, \vec{k}) = \vec{\omega} \times (\vec{\imath}, \vec{\jmath}, \vec{k}), \tag{9.1b}$$

with T and $\vec{\omega}$ the system's control inputs.

9.1.2 Aerodynamic forces

As mentioned in Chapter 3, working out a functional model of aerodynamic forces from celebrated *Navier–Stokes nonlinear partial differential equations* is a very complex task.

Notwithstanding the delicate and complex issues associated with turbulent flows –a side effect of which is the well known *stall* phenomenon– for which no general complete theory exists to our knowledge. We thus propose to take here a different route by combining the well-accepted general expression of the aerodynamic forces given by the Buckingham pi theorem (see Section 3.2) with geometric considerations based on the body's symmetry properties. To be more precise, in view of the assumptions discussed in Section 5.2.1, the aerodynamic force is assumed to be in the form

$$\vec{F}_a := k_a|\vec{v}_a|\left[C_L(\alpha,\beta)\vec{v}_a^{\perp} - C_D(\alpha,\beta)\vec{v}_a\right], \tag{9.2a}$$

$$k_a := \frac{\rho\Sigma}{2}, \tag{9.2b}$$

with $\vec{v}_a^{\perp}$ a perpendicular to the airvelocity, (α,β) (any) pair of angles characterizing the orientation of $\vec{v}_a$ w. r. t. the body frame, ρ the *free stream* air density, Σ an area germane to the given body shape, and $C_D(\cdot)$ $(\in \mathbb{R}^+)$ and $C_L(\cdot)$ the aerodynamic coefficients. To characterize the vector $\vec{v}_a^{\perp}$, we make use of a unit vector-valued function $\vec{r}(\cdot)$ such that

$$\vec{v}_a := \vec{r}(\alpha,\beta) \times \vec{v}_a, \tag{9.3a}$$

$$\vec{r}(\alpha,\beta) \cdot \vec{v}_a = 0. \tag{9.3b}$$

Then, the expression (9.2a) becomes

$$\vec{F}_a = k_a|\vec{v}_a|\left[C_L(\alpha,\beta)\vec{r}(\alpha,\beta) \times \vec{v}_a - C_D(\alpha,\beta)\vec{v}_a\right]. \tag{9.4}$$

Observe that the constraint (9.3b) implies that $|\vec{F}_a| = k_a|\vec{v}_a|^2\sqrt{C_L^2 + C_D^2}$, as in the two-dimensional case treated previously.

9.2 AERODYNAMIC MODELS FOR SYMMETRIC BODIES

The expression (9.4) of the aerodynamic forces holds independently of the body's shape, since it is derived without any assumption upon this shape. We consider here two kinds of body symmetries in order to point out aerodynamic properties induced by them and their practical interest. More specifically, we focus on vehicles whose external surface $\mathcal{S}$ is characterized by the existence of an orthonormal body frame $\mathcal{B} = \{G; \vec{\imath}, \vec{\jmath}, \vec{k}\}$ – with $\vec{k}$ denoting the thrust direction according to Assumption 6 – that satisfies either one of the following assumptions.

Assumption 7 (**Symmetry**)**.** Any point $P \in \mathcal{S}$ transformed by the rotation of an angle θ about the axis $G\vec{k}$, i.e. by the operator defined by

$$g_\theta(\cdot) = \mathrm{rot}_{G\vec{k}}(\theta)(\cdot),$$

also belongs to $\mathcal{S}$, i.e. $g_\theta(P) \in \mathcal{S}$.

Assumption 8 (**Bisymmetry**)**.** Any point $P \in \mathcal{S}$ transformed by the composition of two rotations of angles θ and π about the axes $G\vec{k}$ and $G\vec{\jmath}$, i.e. by the operator defined by

$$g_\theta(\cdot) := (\mathrm{rot}_{G\vec{k}}(\theta) \circ \mathrm{rot}_{G\vec{\jmath}}(\pi))(\cdot),$$

also belongs to $\mathcal{S}$, i.e. $g_\theta(P) \in \mathcal{S}$.

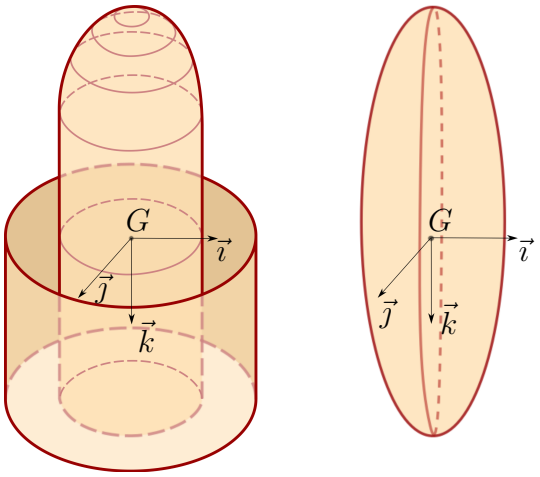

Figure 9.2: Symmetric and bisymmetric body shapes.

The operator $\text{rot}_{O\vec{v}}(\xi)(P)$ stands for the rotation about the axis $O\vec{v}$ by the angle ξ of the point P. Examples of "symmetric" and "bisymmetric" shapes satisfying these assumptions are shown in Figure 9.2.

For symmetric shapes, i.e. such that Assumption 7 holds true, one can define $\alpha \in [0, \pi]$ as the *angle of attack*[2] between $-\vec{k}$ and $\vec{v}_a$, and $\beta \in (-\pi, \pi]$ as the angle between the unit frame vector $\vec{\imath}$ and the projection of $\vec{v}_a$ on the plane $\{G; \vec{\imath}, \vec{\jmath}\}$ (see Figure 9.3). Observe that this assumption also implies that:

P1 : the aerodynamic force $\vec{F}_a$ does not change when the body rotates about its axis of symmetry $G\vec{k}$;

P2 : the aerodynamic force $\vec{F}_a$ belongs to the plane created by the vectors $\vec{k}$ and $\vec{v}_a$, i.e. $\vec{F}_a \in \text{span}\{\vec{k}, \vec{v}_a\}$.

Property P1 in turn implies that the aerodynamic characteristics do not depend on β, whereas Property P2 implies that *i)* $\vec{r}$ is orthogonal to $\vec{k}$, *ii)* $\vec{r}$ is independent of α, and *iii)* the lift coefficient is equal to zero when $\alpha = \{0, \pi\}$. Subsequently, the expression (9.4) of aerodynamic force specializes to

$$\vec{F}_a = k_a |\vec{v}_a| \Big[C_L(\alpha, \beta) \vec{r}(\beta) \times \vec{v}_a - C_D(\alpha, \beta) \vec{v}_a \Big], \tag{9.5a}$$

$$\vec{r}(\beta) = \cos(\beta)\vec{\jmath} - \sin(\beta)\vec{\imath}. \tag{9.5b}$$

Under the stronger Assumption 8, i.e. when the body's shape is also π-symmetric w.r.t. the $G\vec{\jmath}$ axis, the aerodynamic characteristics C_L and C_D must be $\pi-$periodic w.r.t. α.

The aforementioned choice of (α, β) implies that

$$\alpha = \cos^{-1}\left(-\frac{v_{a_3}}{|\vec{v}_a|}\right), \tag{9.6a}$$

$$\beta = \text{atan2}(v_{a_2}, v_{a_1}), \tag{9.6b}$$

and

[2]The angle of attack α so defined does not coincide with the one used for airplanes equipped with flat wings which break the body's rotational symmetry about $G\vec{k}$ (Stengel, 2004, p. 53).

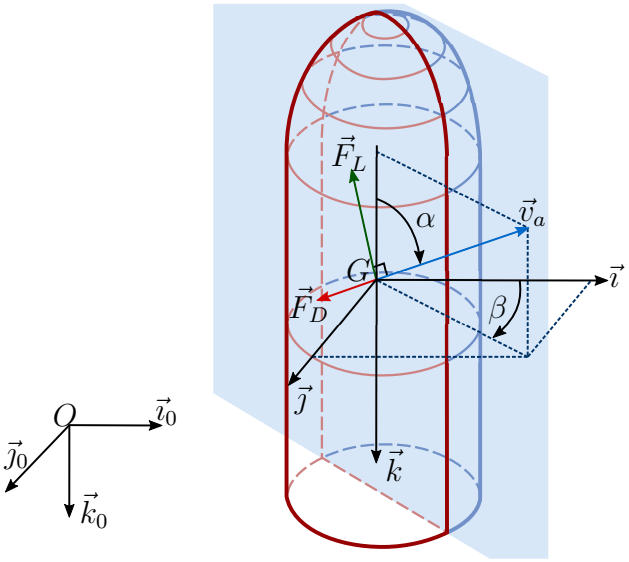

Figure 9.3: Aerodynamic forces and (α, β) angles.

$$\begin{cases} v_{a_1} = |\vec{v}_a| \sin(\alpha)\cos(\beta), \\ v_{a_2} = |\vec{v}_a| \sin(\alpha)\sin(\beta), \\ v_{a_3} = -|\vec{v}_a| \cos(\alpha). \end{cases} \tag{9.7}$$

From the definitions of α and $\vec{r}(\beta)$, one then verifies that

$$\vec{r}(\beta) \times \vec{v}_a = -\cot(\alpha)\vec{v}_a - \frac{|\vec{v}_a|}{\sin(\alpha)}\vec{k},$$

so that the aerodynamic force $\vec{F}_a$ becomes

$$\vec{F}_a = -k_a|\vec{v}_a|\Big(C_D(\alpha) + C_L(\alpha)\cot(\alpha)\Big)\vec{v}_a - k_a|\vec{v}_a|^2\frac{C_L(\alpha)}{\sin(\alpha)}\vec{k}.$$

9.2.1 AERODYNAMIC MODELS YIELDING SPHERICAL EQUIVALENCY

By using the above relationship, it is a simple matter to establish the following result.

Proposition 9.1. Consider a symmetric thrust-propelled vehicle. Assume that the aerodynamic forces are given by (9.5) and that the aerodynamic coefficients satisfy the following relationship

$$C_D(\alpha) + C_L(\alpha)\cot(\alpha) = \overline{C}_D, \tag{9.8}$$

with $\overline{C}_D$ denoting a constant number. Then the body's dynamic equation (9.1a) may also be written as

$$m\vec{a} = m\vec{g} + \vec{f}_p - T_p\vec{k}, \tag{9.9}$$

with

$$T_p = T + k_a|\vec{v}_a|^2\frac{C_L(\alpha)}{\sin(\alpha)}, \tag{9.10a}$$

$$\vec{f}_p = -k_a\overline{C}_D|\vec{v}_a|\vec{v}_a, \tag{9.10b}$$

so that $\vec{f}_p$ is independent of the vehicle's orientation.

The important result is the non-dependence of $\vec{f_p}$ upon the angle of attack α, and thus upon the vehicle's orientation. The interest of this proposition is to point out the possibility of seeing a symmetric body subjected to both drag and lift forces as a sphere subjected to an equivalent drag force $\vec{f_p}$ and powered by an equivalent thrust force $\vec{T_p} = -T_p\vec{k}$. The main condition is that the relation (9.8) must be satisfied. Obviously, this condition is compatible with an infinite number of functions C_D and C_L. Let us point out a particular set of simple functions, already considered in the 2-D case (see Section 7.3), which also satisfy the π-periodicity property w.r.t. the angle of attack α associated with bisymmetric shapes.

Proposition 9.2. The functions C_D and C_L defined by

$$\begin{cases} C_D(\alpha) = c_0 + 2c_1 \sin^2(\alpha) \\ C_L(\alpha) = c_1 \sin(2\alpha), \end{cases} \tag{9.11}$$

with c_0 and c_1 two real numbers, satisfy the condition (9.8) with $\overline{C}_D = c_0 + 2c_1$. The equivalent drag force and thrust intensity are then given by

$$\vec{f_p} = -k_a(c_0 + 2c_1)|\vec{v}_a|\vec{v}_a, \tag{9.12a}$$

$$T_p = T + 2c_1 k_a |\vec{v}_a|^2 \cos(\alpha). \tag{9.12b}$$

A particular bisymmetric body is the sphere whose aerodynamic characteristics (zero lift and constant drag) are obtained by setting $c_1 = 0$ in (9.11). Elliptic-shaped bodies are also symmetric but, in contrast with the sphere, they do generate lift in addition to drag. The process of approximating measured aerodynamic characteristics with functions given by (9.11) is illustrated by the Figure 9.4. The left column of this figure shows the experimental aerodynamic coefficients borrowed from (Keyes, 1965, p.19) for an elliptic-shaped body with Mach and Reynolds numbers equal to $M = 6$ and $R_e = 7.96 \cdot 10^6$ respectively. For this example, the estimated coefficients were calculated in order to minimize the average squared errors between aerodynamic data and the model (9.11), i.e. $c_0 = 0.43$ and $c_1 = 0.462$. Since missile-like devices are "almost" bisymmetric, approximating their aerodynamic coefficients with such functions can also be attempted. For instance, the approximation shown in the right column of Figure 9.4 was obtained by using experimental data taken from (Saffel et al., 1971, p.54) for a missile moving at $M = 0.7$. In this case, the identified coefficients that minimize the average squared errors between aerodynamic data and the model (9.11) are $c_0 = 0.1$ and $c_1 = 11.55$. In both cases shown in Figure 9.4, the match between experimental data and the approximating functions, although not perfect, should be sufficient for feedback control purposes.

As for the 2-D case, other functions satisfying the condition (9.8) may also be of interest to model the aerodynamic characteristics of other bodies. For instance, by considering annular wings, functions of the form

$$C_D(\alpha) = \overline{c}_0, \quad C_L(\alpha) = \overline{c}_1 \tan(\alpha),$$

with $\overline{c}_0$ and $\overline{c}_1$ denoting two real numbers, can be used to model classical linearly increasing lift and quasi-constant drag at small angles of attack, i.e. before the stall region is reached. These functions can also be combined with functions (9.11) that are more representative of the physics for angles beyond the stall region.

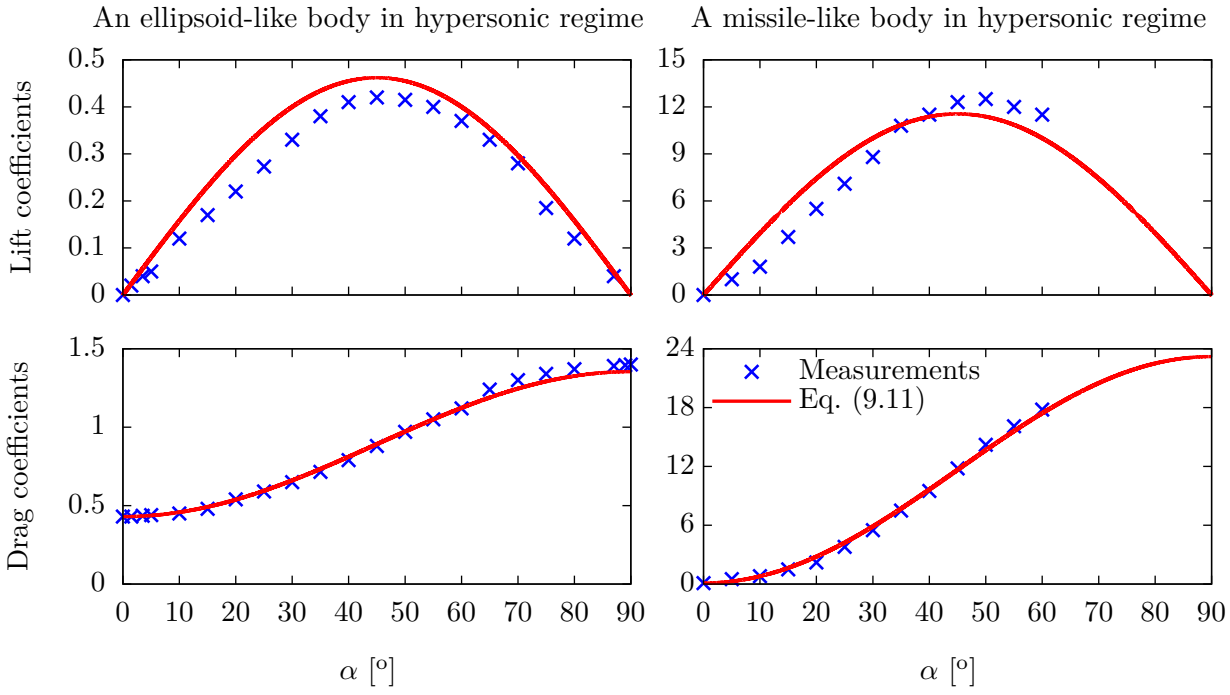

Figure 9.4: Aerodynamic coefficients of elliptic (left) and missile (right) like bodies.

9.3 Control design

Once the system's dynamics (9.1a) is transformed into the form (9.9) with $\vec{F}_p$ independent of the vehicle's orientation, the control design can be addressed by adapting the method developed for the class of systems subjected to an orientation-independent external force. We illustrate in this section the application of the control solutions (Hua et al., 2009a) to stabilize either a reference velocity $\vec{v}_r$ or a reference trajectory $\vec{p}_r$.

9.3.1 Velocity control

The control objective is the asymptotic stabilization of a reference velocity $\vec{v}_r = (\vec{\imath}_0, \vec{\jmath}_0, \vec{k}_0)\dot{x}_r = (\vec{\imath}, \vec{\jmath}, \vec{k})v_r$. The application of the control solution proposed in (Hua et al., 2009a, Sec. III.D) to System (9.1), with $(\vec{F}_a, T)$ replaced by the equivalent drag force and thrust intensity $(\vec{f}_p, T_p)$ defined in Proposition 9.1, yields the following control expressions

$$T = \overline{F}_3 + k_1|F_p|\widetilde{v}_3, \tag{9.13a}$$

$$\omega_1 = -k_2|F_p|\widetilde{v}_2 - \frac{k_3|F_p|\overline{F}_{p_2}}{(|F_p| + \overline{F}_{p_3})^2} - \frac{\overline{F}_p^T S(e_1) R^T \dot{F}_p}{|F_p|^2}, \tag{9.13b}$$

$$\omega_2 = k_2|F_p|\widetilde{v}_1 + \frac{k_3|F_p|\overline{F}_{p_1}}{(|F_p| + \overline{F}_{p_3})^2} - \frac{\overline{F}_p^T S(e_2) R^T \dot{F}_p}{|F_p|^2}, \tag{9.13c}$$

with $\widetilde{v} := v - v_r$, $\vec{a}_r := \frac{d}{dt}\vec{v}_r = (\vec{\imath}_0, \vec{\jmath}_0, \vec{k}_0)\ddot{x}_r$,

$$\vec{F} = (\vec{\imath}_0, \vec{\jmath}_0, \vec{k}_0)F = (\vec{\imath}, \vec{\jmath}, \vec{k})\overline{F} := m\vec{g} + \vec{F}_a - m\vec{a}_r, \tag{9.14a}$$

$$\vec{F}_p = (\vec{\imath}_0, \vec{\jmath}_0, \vec{k}_0)F_p = (\vec{\imath}, \vec{\jmath}, \vec{k})\overline{F}_p := m\vec{g} + \vec{f}_p - m\vec{a}_r, \tag{9.14b}$$

and $k_{1,2,3}$ three positive real numbers. Note that, using (9.10b), the vector f_p of coordinates of $\vec{f_p}$ expressed in the fixed frame $\mathcal{I}$ is

$$f_p = -k_a \overline{C}_D |\dot{x}_a| \dot{x}_a, \tag{9.15}$$

so that the vector of coordinates of the geometric vector $\vec{F}_p$ in the inertial frame becomes

$$F_p = mge_3 - k_a \overline{C}_D |\dot{x}_a| \dot{x}_a - m\ddot{x}_r, \tag{9.16}$$

which is independent of the vehicle's orientation. Therefore, its time-derivative does not depend on the angular velocity vector ω and the above expressions of the first two components of this vector are well defined. The interest of the invoked transformation, combined with (9.8), lies precisely there.

As for the last component ω_3, since it does not influence the vehicle's longitudinal motion due to the symmetry about the axis $G\vec{k}$, it does not have to be defined at this point. This free degree of freedom can be used for complementary purposes involving, for instance, the angle β.

Let $\widetilde{\theta} \in (-\pi, \pi]$ denote the angle between e_3 and F_p. In (Hua et al., 2009a), stability and convergence properties associated with the feedback control (9.13) are established by using the Lyapunov function candidate

$$V = \frac{|\widetilde{v}|^2}{2} + \frac{1}{k_2 m}\big[1 - \cos(\widetilde{\theta})\big],$$

whose time-derivative along any trajectory of the controlled system is

$$\dot{V} = -k_1 |F_p| \widetilde{v}_3^2 - \frac{k_3}{k_2} \tan^2\left(\widetilde{\theta}/2\right).$$

Assuming that $\vec{v}_w$ and $\vec{v}_r$ are bounded in norm up to their second time-derivatives, and provided that $\exists\, \delta > 0$ such that $|F_p| > \delta$, $\forall t \in \mathbb{R}^+$, one shows that the equilibrium $(\widetilde{v}, \widetilde{\theta}) = (0, 0)$ of the controlled system is asymptotically stable, with the domain of attraction equal to $\mathbb{R}^3 \times (-\pi, \pi)$.

In practice, the control law must be complemented with integral correction terms to compensate for almost constant unmodeled additive perturbations. The solution proposed in (Hua et al., 2009a) involves $\vec{I_v} = (\vec{\imath}_0, \vec{\jmath}_0, \vec{k}_0) I_v$ with

$$I_v := \int_0^t \dot{\widetilde{x}}(s)\, ds,$$

and $\dot{\widetilde{x}} := R\widetilde{v}$ the longitudinal velocity error expressed in the inertial frame. Let h denote a smooth bounded strictly positive function defined on $[0, +\infty)$ satisfying the following properties (Hua et al., 2009a, Sec. III.C) for some positive constant numbers η, μ,

$$\forall s \in \mathbb{R}, \quad |h(s^2)s| < \eta, \quad \text{and} \quad 0 < \frac{\partial}{\partial s}(h(s^2)s) < \mu \tag{9.17}$$

An example of such function is,

$$h: \quad s \to h(s) = \frac{\eta}{\sqrt{1+s}},$$

with $\eta > 0$. It then suffices to replace the definitions (9.14) of $\vec{F}$ and $\vec{F}_p$ by

$$\vec{F} := m\vec{g} + \vec{F}_a - m\vec{a}_r + h(|I_v|^2)\vec{I}_v \tag{9.18a}$$

$$\vec{F}_p := m\vec{g} + \vec{f}_p - m\vec{a}_r + h(|I_v|^2)\vec{I}_v \tag{9.18b}$$

in (9.13) to obtain a control which incorporates an integral correction action and for which strong stability and convergence properties can also be proven (Hua et al., 2009a).

9.3.2 Position control

The control objective is now the asymptotic stabilization of a reference trajectory $\vec{p}_r := (\vec{\imath}_0, \vec{\jmath}_0)x_r$. Let us first (re)introduce the nonlinear "bounded integral" of the position error used to compensate for almost constant unmodeled additive perturbations. Define z as the solution of the following second-order system:

$$\ddot{z} = -2k_z\dot{z} - k_z^2[z - \mathrm{sat}_\Delta(z)] + k_z h_z(|\widetilde{x}|^2)\widetilde{x}, \qquad k_z > 0,\ z(0) = 0,\ \dot{z}(0) = 0, \tag{9.19}$$

where h_z is a smooth bounded strictly positive function defined on $[0, +\infty)$ satisfying (9.17) for some positive constant numbers η_z, β_z, and sat_Δ the classical *saturation function*, i.e. $\mathrm{sat}_\Delta(z) = z\min(1, \Delta/|z|)$. Let

$$y := \widetilde{x} + z, \tag{9.20a}$$

$$\overline{v} := \widetilde{v} + R^T(\theta)\dot{z}, \tag{9.20b}$$

with h a smooth bounded positive function satisfying (9.17) for some positive constant numbers η, β. The application of the control solution proposed in (Hua et al., 2009a, Sec. III.D) to System (9.1), with $(\vec{F}_a, T)$ replaced by the equivalent drag force and thrust intensity $(\vec{f}_p, T_p)$ defined in Proposition 9.1, yields the following control expressions

$$T = \overline{F}_3 + k_1|F_p|\overline{v}_3, \tag{9.21a}$$

$$\omega_1 = -k_2|F_p|\overline{v}_2 - \frac{k_3|F_p|\overline{F}_{p_2}}{(|F_p| + \overline{F}_{p_3})^2} - \frac{\overline{F}_p^T S(e_1)R^T\dot{F}_p}{|F_p|^2}, \tag{9.21b}$$

$$\omega_2 = k_2|F_p|\overline{v}_1 + \frac{k_3|F_p|\overline{F}_{p_1}}{(|F_p| + \overline{F}_{p_3})^2} - \frac{\overline{F}_p^T S(e_2)R^T\dot{F}_p}{|F_p|^2}, \tag{9.21c}$$

with $k_{1,2,3}$ three positive real numbers, $\overline{F} := R^T F$, $\overline{F}_p := R^T F_p$,

$$F := mge_3 + F_a - m\ddot{x}_r + h(|y|^2)y + \ddot{z}, \tag{9.22a}$$

$$F_p := mge_3 + f_p - m\ddot{x}_r + h(|y|^2)y + \ddot{z}, \tag{9.22b}$$

F_a is the vector of coordinates of the aerodynamic force expressed in the inertial frame, and f_p is the vector of coordinates given by (9.15).

Let $\widetilde{\theta} \in (-\pi, \pi]$ denote the angle between e_3 and F_p. In (Hua et al., 2009a), stability and convergence properties associated with the feedback control (9.21) are established by using the Lyapunov function candidate

$$V = \frac{|\overline{v}|^2}{2} + \frac{1}{k_2 m}\big[1 - \cos(\widetilde{\theta})\big] + \int_0^{|y|} h(s^2)s\,ds,$$

whose time-derivative along any trajectory of the controlled system is

$$\dot{V} = -k_1|F_p|\overline{v}_1^2 - \frac{k_3}{k_2}\tan^2\left(\widetilde{\theta}/2\right).$$

Assuming that $\vec{v}_w$ and $\vec{v}_r$ are bounded in norm up to their second time-derivatives, and provided that $\exists\,\delta > 0$ such that $|F_p| > \delta$, $\forall t \in \mathbb{R}^+$, one shows that the equilibrium $(\widetilde{x}, \widetilde{v}, \widetilde{\theta}) = (0, 0, 0)$ of the controlled system is asymptotically stable, with the domain of attraction equal to $\mathbb{R}^3 \times \mathbb{R}^3 \times (-\pi, \pi)$.

9.3.3 Control robustification

The control laws presented so far use terms that may introduce singularities far from the reference trajectory. We here carry out modifications for the control law (9.21), but they are also valid for the other control laws via straightforward transpositions. Let us multiply the terms $1/(|F_p| + \overline{F}_{p_3})^2$ and $1/|F_p|^2$ by the function $\mu_\tau \in \mathbb{C}^1 : [0, +\infty) \to [0, 1]$ defined by:

$$\mu_\tau(s) = \begin{cases} \sin\left(\frac{\pi s^2}{2\tau^2}\right), & \text{if } s \leq \tau \\ 1, & \text{otherwise} \end{cases} \tag{9.23}$$

with $\tau > 0$. This yields the well-defined control expression

$$T = \overline{F}_3 + k_1|F_p|\overline{v}_3, \tag{9.24a}$$

$$\omega_1 = -k_2|F_p|\overline{v}_2 - \mu_\tau(|F_p| + \overline{F}_{p_3})\frac{k_3|F_p|\overline{F}_{p_2}}{(|F_p| + \overline{F}_{p_3})^2} - \mu_\tau(|F_p|)\frac{\overline{F}_p^T S(e_1) R^T \dot{F}_p}{|F_p|^2}, \tag{9.24b}$$

$$\omega_2 = k_2|F_p|\overline{v}_1 + \mu_\tau(|F_p| + \overline{F}_{p_3})\frac{k_3|F_p|\overline{F}_{p_1}}{(|F_p| + \overline{F}_{p_3})^2} - \mu_\tau(|F_p|)\frac{\overline{F}_p^T S(e_2) R^T \dot{F}_p}{|F_p|^2}, \tag{9.24c}$$

The property:

$$\lim_{s\to 0} \frac{\mu_\tau(s)}{s^2} = \lim_{s\to 0} \sin\left(\frac{\pi s^2}{2\tau^2}\right) s^{-2} = \frac{\pi}{2\tau^2},$$

implies that the modified control is well-defined everywhere.

Remark 9.1. *The control laws* (9.24)*,* (9.21) *and* (9.13) *make use of the feedforward term* $\ddot{x}_a$ *(via* $\dot{F}_p$*) that is not always available in practice. Simulations with wing models, however, have shown that neglecting this term when its actual value is not too large does not much affect the control performance, in the sense that ultimate tracking errors remain small.*

9.4 Simulations in sub-sonic airflow

In this section, we illustrate through simulations the performance and robustness of the proposed control strategy for a model of a missile-like body in sub-sonic airflow. The shape of the body roughly corresponds to the one shown in Figure 9.3. The system's equations of motion used for simulations are given by Eqs. (9.1) with $\vec{F}_a$ given by (9.5) and the aerodynamic coefficients by (9.11) with

$$c_0 = 0.1, \quad c_1 = 11.55.$$

The aerodynamic coefficients are depicted in red in the right column of Figure 9.4. They are representative of the experimental data measured for a missile-like body moving with $M = 0.7$. We consider a body's shape alike the one shown in Figure 9.3, with the radius r of the semi-sphere at the top of the body equal to the base radius. Let $\overline{h}$ denote the height of the body; the body's and environment's physical parameters are given by:

$$
\begin{aligned}
m &= 500\ [Kg],\\
\overline{h} &= 7.5\ [m],\\
r &= 0.75\ [m],\\
\Sigma &= \frac{1}{2}(\pi-4)r^2 + 2hr \approx 11\ [m^2],\\
\rho &= 1.225\ \left[Kg/m^3\right],\\
k_a &= \frac{\rho\Sigma}{2} \approx 6.7\,[Kg/m]\,.
\end{aligned}
$$

We assume that the control objective is the asymptotic stabilization of a reference trajectory, and we apply the control solution proposed in Section 9.3.2. Other values are used for the calculation of the control laws (9.21) in order to test the robustness w.r.t. parametric errors; they are chosen as follows:

$$\widehat{m} = 425\ [Kg], \tag{9.25}$$
$$\widehat{k}_a = 4.58\ \ [Kg/m]\,, \tag{9.26}$$
$$\widehat{c}_0 = 0.08, \tag{9.27}$$
$$\widehat{c}_1 = 9.2, \tag{9.28}$$

The term $\dot{F}_p$ in the expression of the control laws (9.21) is kept equal to zero, thus providing another element to test the robustness of the controller. The values for the other control parameters are:

- $k_1 = 0.3058$, $k_2 = 0.1247$, $k_3 = 16$;
- $h(s) = \beta \Big/ \sqrt{1 + \frac{\beta^2}{\eta^2} s}$ with $\beta = 2$ and $\eta = 15$;
- $k_z = 1$, $h_z(s) = \beta_z \Big/ \sqrt{1 + \frac{\beta_z^2}{\eta_z^2} s}$ with $\beta_z = 1$ and $\eta_z = 1$;
- $\mathrm{sat}_\Delta(z) = z \min\left(1, \frac{\Delta}{|z|}\right)$ with $\Delta = 100$.

The gains k_1, k_2, k_3, k_z, $h(0)$ and $h_z(0)$ are determined via a pole placement procedure performed on the linear approximation of the tracking errors dynamics – together with (9.19) – in hovering flight (see (Hua et al., 2008) for details). Let us recall that the constants η and η_z limit the influence of the integral I_v and $\dot{z}$ in the control action (see Eqs. (9.14) (9.17) (9.18) and (9.19)). Hence, they should not be chosen too small if large modeling errors have to be compensated. On the other hand, taking them small reduces the risk of F_p evolving close to zero and of saturating the actuators.

9.4.1 Simulation 1: from hovering to cruising flight

We show below a simulation of a transition maneuver from hovering to cruising flight. The reference trajectory used to simulate the transition is given by:

$$\dot{x}_r(t) = \begin{cases} 10\,[1,1,-1]^T & 0 \le t < 30,\\ 0.97(t-30)\,[1,0,0]^T & 30 \le t < 55,\\ 24.25\,[1,0,0]^T & t \ge 55. \end{cases} \tag{9.29}$$

with $x_r(0) = (0, 0, 0)^T$. Therefore, it consists of: i) a stationary point on the time interval $[0, 30)$ $[s]$; ii) an horizontal velocity ramp on the time interval $[30, 55)$ $[s]$; iii) cruising with constant speed of 24.25 $[m/s]$ for $t \geq 55$ $[s]$. The initial position and velocity are $x(0) = [0, 0, 0]$, $\dot{x}(0) = [0, 0, 0]$ respectively; the initial vehicle's orientation[3] is characterized by $\phi(0) = 0$, $\theta(0) = 0$, $\psi(0) = 0$.

From top to bottom, Figure 9.5 depicts the evolution of the reference velocity, the velocity errors, the position errors, the angle of attack, the angular velocity, the thrust-to-weight ratio, the vehicle's attitude, and the wind velocity. Wing gusts are simulated only along the vertical direction $\vec{k}_0$. On the interval $[0, 30)$ $[s]$, the vehicle's attitude converges towards zero (vertical configuration), and the thrust tends to oppose the body's weight. When $t > 30$ $[sec]$, the horizontal velocity of the vehicle increases, so the angle of attack and the pitch angle start decreasing . At the time instant $t = 55$ $[sec]$, the reference acceleration $\ddot{x}_r$ becomes instantaneously zero. This makes the thrust force discontinuous. Observe also that the vehicle's is flying almost horizontally at this time instant ($\theta \approx -90°, |\dot{\tilde{x}}| \approx 0$). On the time interval $[62, 70]$ $[sec]$ a constant wind gust "pushing the body down" ($\dot{x}_{w_3} > 0$) is simulated; as a consequence, the control law requires the pitch angle and the thrust force to increase in order to maintain small tracking errors. Conversely, a constant wind gust "pushing the body up" ($\dot{x}_{w_3} < 0$) is simulated on the time interval $[74, 82]$ $[sec]$. In this case the control law requires greater values for the pitch angle and the thrust force than those required with no wind. On the time interval $[82, 90]$ $[sec]$, a non-constant wind gust perturbs the vehicle, and this requires non-constant control inputs to maintain the tracking errors small.

9.4.2 SIMULATION 2: HELICOIDAL HORIZONTAL FLIGHT WITH LIMITED THRUST

The control objective is to track the following reference trajectory

$$\dot{x}_r(t) = \begin{cases} [0.97t, -4\sin(0.2t), 4\cos(0.2t)]^T & 0 \leq t < 25, \\ [24.25, -4\sin(0.2t), 4\cos(0.2t)]^T & t \geq 25. \end{cases} \tag{9.30}$$

with $x_r(0) = (0, 0, 0)^T$. The initial position and velocity are $x(0) = [0, 0, 0]$, $\dot{x}(0) = [0, 0, 0]$ respectively; the initial vehicle's orientation is characterized by $\phi(0) = \theta(0) = \psi(0) = 0$. Limitations on the thrust force are taken into account by imposing the following constraint

$$0 < T < 2mg.$$

From top to bottom, Figure 9.6 depicts the evolution of the reference velocity, the velocity errors, the position errors, the angle of attack, the angular velocity, the thrust-to-weight ratio, and the vehicle's attitude; no wind is blowing. On the time interval $[0, 27)$ $[sec]$, the control requires a positive thrust intensity, and both velocity and position errors converge to zero. On the time intervals where the thrust force saturates, the tracking errors increase before tending to zero again.

[3]Standard roll ϕ, pitch θ and yaw ψ angles are used to parametrize the rotation matrix R; see (Stengel, 2004, p. 47) for details.

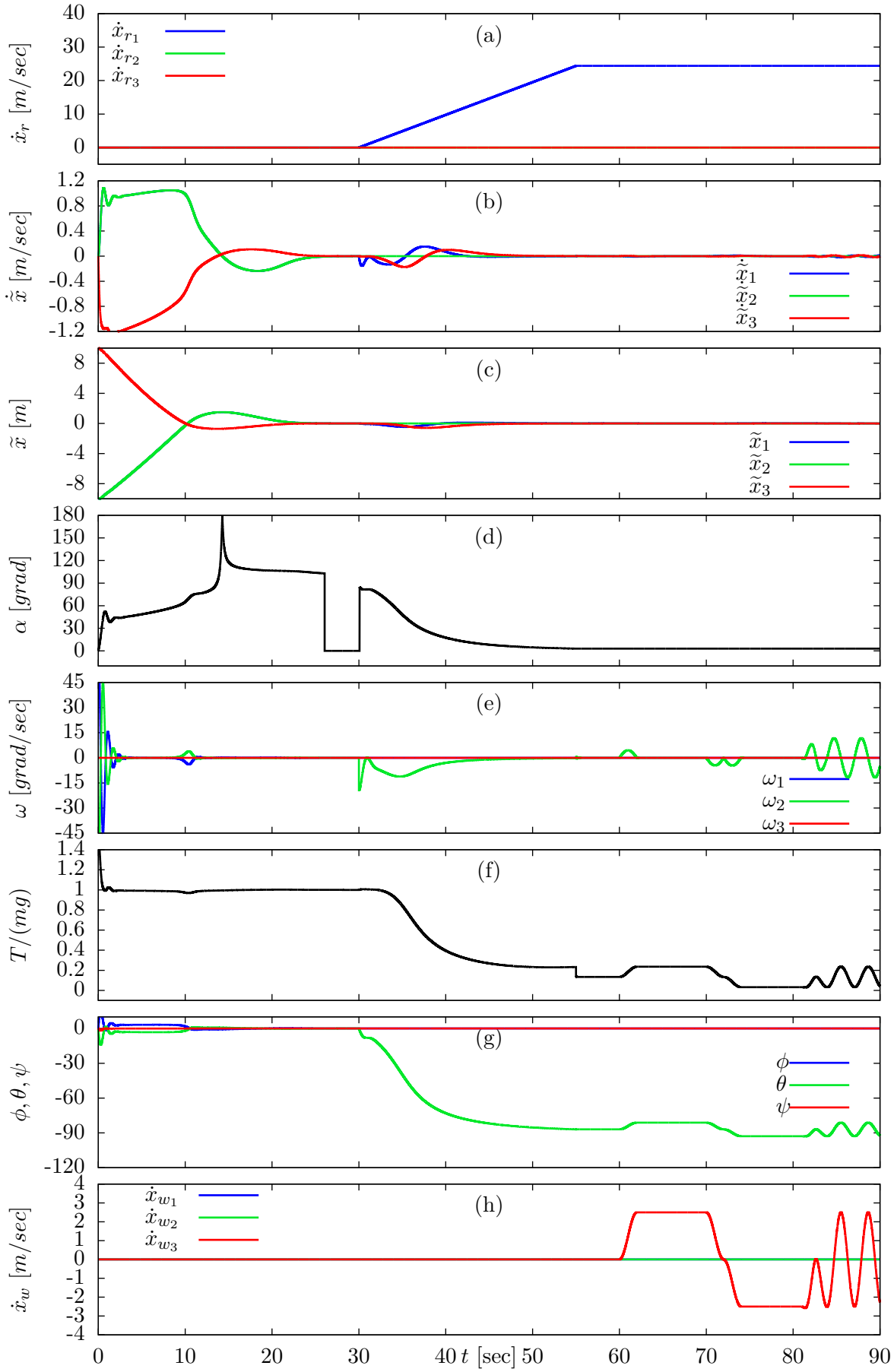

Figure 9.5: Simulation 1 of a missile-like body.

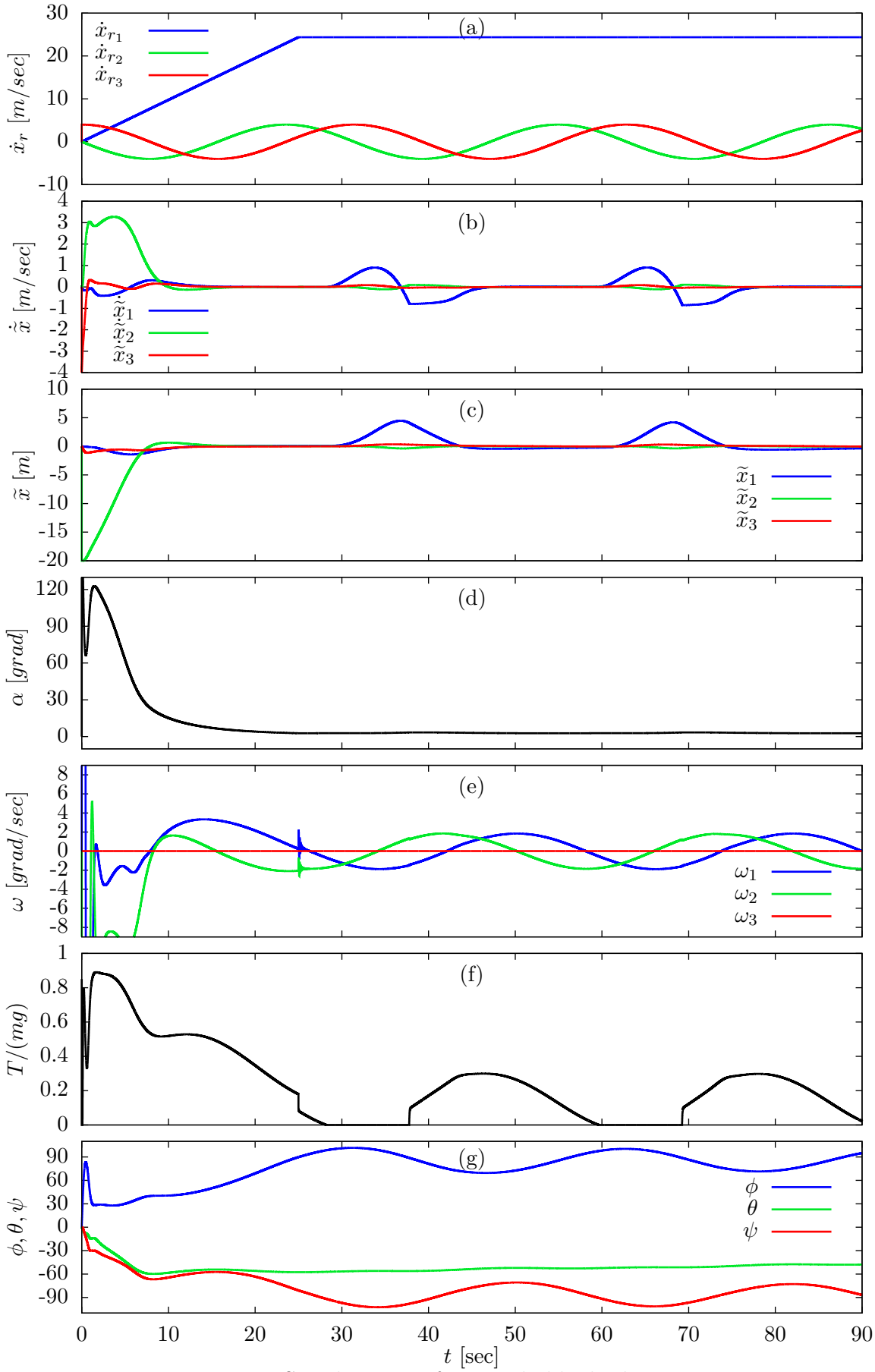

Figure 9.6: Simulation 2 of a missile-like body.

Epilogue in Italian

Questa tesi è dedicata alla *modellizzazione*, *analisi* e *controllo* dei veicoli aerei sottoposti a forze di reazione aerodinamica. Essa ambisce a gettare le basi di un approccio unificato per il controllo dei veicoli volanti in modo tale da proporre una metodologia per i cosiddetti *veicoli ibridi*, i quali possono sia decollare verticalmente che volare orizzontalmente ad alte velocità.

La prima parte di questa tesi fornisce le basi di aerodinamica e dinamica del volo, ed inoltre si focalizza su una parte della letterattura esistente. Questo processo ha fatto emergere che il controllo dei veicoli arei è di norma risolto progettando diverse strategie di comando in relazione a diverse classi di veicoli volanti, come esemplificato da elicotteri ed aerei di linea. Un approccio unificato che prendesse in conto le forze aereodinamiche nel controllo era ancora mancante. Tuttavia, un'attenta analisi delle equaizioni che regolano il moto mostra che progettare una metodologia di comando che sia indipendente dall'attuazione e dalle forze aerodinamiche sul veicolo è impraticabile. Questa conclusione ci ha condotto a delle ipotesi semplificatrici.

E' stato ipotizzato che l'attuazione è composta da una forza di propulsione solidale al veicolo e da un controllo in coppia per il controllo del suo orientamento. Di conseguenza, il problema del controllo è stato disaccoppiato nella (classica) architettura a due stadi composta da: un loop interno che è responsabile del controllo dell'orientamento (pilot loop); un loop esterno che si occupa della stabilizzazione della velocità del veicolo (guidance loop). Questa tesi si occupa di quest'ultimo loop e la determinazione di come regolare la propulsione ai fini di compensare per le forze esterne agenti sul veicolo, che dipendono dal suo orientamento, è stato uno degli obiettivi principali. Nel linguaggio dell'Automatica, questa è una classica ipotesi di "backstepping". Riguardo le forze esterne agenti sul veicolo, è stato assunto che esse dipendano minimamente dai cosiddetti "efffetti aerodinamici non stazionari". Questa ipotesi ha a sua volta implicato che la forza aerodinamica non dipenda dalla velocità angolare del veicolo.

Sotto queste ipotesi, la seconda parte di questa tesi si focalizza sulla modellizzazione, analisi e controllo della dinamica longitudinale degli aerei – ossia moti planari – e poi estende alcuni di queste analisi a moti tridimensionali di veicoli simmetrici, come la fusoliera di un aeroplano o di un missile. Un risultato originale della seconda parte di questa tesi è definire delle condizioni per le quali si può riscrivere il problema del controllo come quello associato ad un veicolo con superficie sferica. Tale trasformazione viene chiamata *equivalenza sferica*, ed una volta eseguita permette di applicare le metodologie di controllo sviluppate per un corpo sferico ad un veicolo non sferico.

Più precisamente, il capitolo dedicato alla modellizzazione della dinamica longitudinale presenta le equazioni che descrivono i moti planari, e si focalizza sulle forze aerodinamiche agenti sui profili simmetrici NACA in regime subsonico. Modelli che descrivono i *coefficienti aerodinamici* di questi profili, anche nella regione di stallo, vengono presentati.

L'*analisi* della dinamica longitudinale si focalizza su questioni fondamentali come l'*esistenza* e la *multiplicità* della configuarzione di equilibrio dell'aereo – in termini di

intensità di propulsione e orientamento del veicolo – lungo la traiettoria di riferimento. Un risultato originale di questa analisi è mostrare che esiste una configuarzione di equilibrio per ogni velocità di riferimento e del vento quando la forma del veicolo è *simmetrica*. Tuttavia, in accordo con la letteratura esistente, l'unicità di tale configuarzione di equilibrio non può essere garantita a priori. Infatti, uno studio della multiplicità della configuarzione di equilibrio mostra che i fenomeni di stallo aerodinamico possono dar vita a diverse orientamenti di equilibrio associati ad una velocità di riferimento. Come conseguenza, si mostra che alcune velocità di riferimento possono essere seguite perfettamente solo se fossero possibili variazioni discontinue dell'orientamento del veicolo. L'analisi della dinamica longitudinale mostra anche che possono esistere diverese velocità di equilibrio ad una fissata intensità di propulsione e orientamento del veicolo. Tale fatto è simile alla condizione di "deep stall" per gli aerei.

Il controllo della dinamica longitudianle viene risolto usando l'analisi di Lyapunov, la quale fornice controllori locali che stabilizzano sia velocità che posizioni di riferimento. Quando la forza aerodinamica soddisfa le condizioni che permettono di applicare l'equivalenza sferica, grandi domini di stabilità possono essere dimostrati.

Alcuni dei risultati trovati per i moti bidimensionali vengono poi estesi al caso di un veicolo che vola nello spazio tridimensionale assumendo che la forma del corpo sia simmetrica rispetto l'asse di propulsione. In particolare, risultati interessanti riguardano la modellizzazione delle forze aerodinamiche su corpi simmetrici e la caratterizzazione di una famiglia di modelli che permettono di applicare la menzionata equivalenza sferica. Membri di tale famiglia sono rappresentativi della forza aerodinamica che agisce su missili in regime subsonico ed ipe3rsonico. Per illustrare l'utilità di questi risultati di modellizzazione al livello di controllo, un metodo sviluppato per corpi sferici viene applicato al sistema sferico equivalente in modo tale da fornire leggi di controllo che stabilizzano velocità e posizioni desiderate. Video di simulazioni possono essere trovate al seguente link

http://goo.gl/HKQtz

Numerosi estensioni di questo studio sui corpi simmetrici possono essere menzionate. Esse riguardano aeroplani ed altri veicoli dotati di superfici non simmetriche rispetto l'asse di propulsione.

A questo punto, il paradigma di unificazione presentato in questa tesi è ancora concettuale. Sebbene la validazione tramite simulazione è incoraggiante, le leggi di controllo qui proposte chiamano per una moltitudine di estensioni prima che possano essere applicate in un sistema fisico. Ad esempio, la misura e la stima di variabili fisiche come la velocità del veicolo relativa al vento merità studi complementari.

Epilogue in French

Cette thèse est consacrée à la modélisation, à l'analyse et au contrôle des véhicules aériens à propulsion sujet à des forces aérodynamiques. Elle propose une approche unifiée qui prend en compte les forces aérodynamiques dans la conception des commandes et propose une méthodologie pour le contrôle de véhicules aériens avec un vaste domaine de vol comme les véhicules convertibles, aussi appelés véhicules hybrides.

La première partie de ce manuscrit fournit au lecteur les bases de l'aérodynamique et de la dynamique du vol et se focalise sur certaines parties de la littérature existante concernant les techniques de contrôle des avions. Ce dernier point souligne le fait que la commande des véhicules aériens est habituellement réalisée en utilisant des stratégies différentes selon le type d'appareil, comme le montre le cas des avions et des hélicoptères. A notre connaissance, une approche unifiée qui prend en compte les forces aérodynamiques non-linéaires dans la conception des lois de commande était manquante. Cependant en regardant de plus près les équations du mouvement d'un aéronef, on peut constater que développer une approche unifiée pour l'asservissement, indépendante du type d'actionneur de l'avion et des effets aérodynamique sur l'ensemble de la structure, est irréaliste et techniquement infaisable. Ceci nous conduit à simplifier le problème de commande.

Les moyens de contrôler l'avion sont ici une force de propulsion fixe par rapport à la structure de l'avion, permettant la translation et un couple pour le contrôle de l'attitude. Le problème de la commande est alors découplé en une architecture (classique) à deux étages consistant en une boucle intérieure pour le contrôle d'attitude (boucle de pilotage) et une boucle extérieure pour le contrôle de la vitesse (boucle de guidage). Cette thèse se focalise sur ce dernier point et déterminer comment réguler la force de propulsion pour compenser les forces extérieures dépendantes de l'orientation a été l'un des principaux objectifs. En Automatique, cette architecture découplée reflète une hypothèse typique de "backstepping" et la manière de produire le mouvement angulaire désiré peut être effectué via des méthodes de contrôle non-linéaire classique. Pour ce qui est des forces environnementales sur le véhicule, on considère que la force aérodynamique dépend faiblement d'effets aérodynamiques instationnaires. Ceci conduit à négliger la dépendance de la force aérodynamique par rapport à la vitesse angulaire du véhicule.

Sous ces hypothèses, la seconde partie de la thèse se focalise en premier lieu sur la modélisation, l'analyse et le contrôle de la dynamique longitudinale de l'avion - c'est à dire le mouvement à deux dimensions – et ensuite étend certaines de ces études au cas du mouvement en trois dimensions d'un véhicule symétrique, comme le fuselage d'un avion ou le corps d'un missile. Un résultat original de de cette partie du manuscrit est de donner les conditions sur la force aérodynamique qui nous permettent de reformuler le problème sous la forme de celui du contrôle d'un corps sphérique, aussi appelé équivalence sphérique, pour laquelle des résultats puissants sur la stabilité peuvent être démontrés. Les lois de commande non-linéaires proposées incorporent des termes de corrections intégrales et anti-wind-up pour gérer les incertitudes du modèle. Plus précisément, la modélisation de la dynamique longitudinale de l'avion présente les équations gouvernant le mouvement plan et se focalise sur les forces aérodynamiques agissant sur des profils symétriques NACA

dans des flux d'air subsoniques. La conception des fonctions qui sont représentatives des coefficients aérodynamiques de ces profils, incluant les phénomènes de décrochage sont présentées.

L'analyse de la dynamique longitudinale du véhicule se concentre sur des problèmes de commande basiques mais importants comme l'existence et la multiplicité des configurations de l'avion, en terme d'intensité de poussée et d'orientation de l'appareil, le long de la trajectoire. Un résultat original de cette analyse est de montrer qu'il existe une configuration d'équilibre pour chaque vitesse de référence et vitesse de vent quand la forme du corps est symétrique, indépendamment du régime d'écoulement. Selon la littérature existante, cependant, une analyse de la multiplicité des configurations de l'avion souligne que le phénomène de décrochage peut induire plusieurs orientations du véhicule pour une vitesse donnée. Comme conséquence, un suivi parfait d'une vitesse continue de référence peut requérir une configuration discontinue, ce qui n'est pas faisable en pratique. Ceci appelle une multitude de remarque quant au choix d'une vitesse de référence représentant les manœuvres de transitions entre le vol stationnaire et le vol de croisière à haute vitesse puisque le suivi parfait de cette transition peut être infaisable en pratique. L'analyse de la dynamique longitudinale montre aussi que pour une poussée et une orientation données, il peut exister plusieurs vitesses d'équilibre associées avec de larges angles d'attaque et des pertes d'altitude. Cette analyse est réminiscente de la situation de deep stall.

Le contrôle du mouvement plan est réalisé en utilisant l'analyse de Lyapunov, qui fournit des contrôleur locaux qui stabilisent la vitesse de référence ou la position. Quand la force aérodynamique nous permet d'appliquer l'équivalence sphérique évoquée plus haut, de large domaines de stabilité sont obtenus. La lois de commande qui en dérivent ne s'appuient pas sur un changement de lois de commandes en fonction du domaine de vol mais représentent une approche unifiée pour des véhicules se déplaçant dans le plan vertical et sujets à des forces aérodynamique non linéaires.

Certains des résultats obtenus dans le cas du mouvement plan sont étendus à celui d'un avion volant en trois dimensions en supposant la symétrie de rotation de la forme du véhicule autour de l'axe d'action de la poussée. En particulier, les résultats originaux concernent la modélisation des forces aérodynamiques agissant sur des corps symétriques et la caractérisation d'une famille de modèles qui permettent d'appliquer l'équivalence sphérique précitée. Les membres de cette famille sont les représentants de la force aérodynamique agissant sur

des corps elliptique et de forme comparable à des missiles dans des flux d'air subsonique et hypersoniques. Pour illustrer l'utilité de ces résultats dans la phase de conception des commandes, des contrôleurs développés pour le cas sphérique sont appliqués pour donner au lecteur les lois qui stabilisent la vitesse de référence ou la trajectoire de référence. Des vidéos et des simulations avec différentes trajectoires de référence sont disponibles ici :

http://goo.gl/HKQtz

Des extensions possibles de cette étude sur les appareils symétriques en 3 dimensions sont nombreuses. Elles concernent les avions et autres véhicules dont les propriétés de portance reposent principalement sur de grandes surfaces plates qui coupent la symétrie du corps sur l'axe d'action de la poussée.

A ce niveau, le paradigme d'unification présenté dans cette thèse est encore principalement conceptuel. Bien que la validation par les simulations soit encourageante, les solutions proposées pour la commande appellent à une multitude d'extensions complémentaires et d'adaptations avant qu'elles ne soient implémentées sur des appareils réels.

On peut mentionner la production du mouvement angulaire désiré et la détermination de la boucle d'asservissement bas biveau correspondante qui prend en compte les limites des actionneurs – en relation, par exemple, avec la commande dépendante de la vitesse de l'air. La mesure et l'estimation de variables physiques variées intervenant dans le calcul de la lois de commande impliquent une combinaison de problèmes matériels et logiciels dont il est important de tenir compte.

Epilogue in English

This thesis is devoted to the modeling, analysis and control of thrust-propelled aerial vehicles subjected to aerodynamic reaction effects. It attempts to lay down a unified approach that takes into account aerodynamic forces in the control design, and proposes a control methodology for aircraft with large flight envelopes such as *convertible* vehicles, also called *hybrid* aircraft.

The first part of this manuscript provides the reader with basic aerodynamic and flight dynamics background, and focuses on part of the existing literature on aircraft control techniques. This latter process pointed out that the control of aerial vehicles is usually addressed by designing different control strategies in relation to different kinds of aircraft, as exemplified by airliners and helicopters. A unified approach that takes into account nonlinear aerodynamic forces in the control design was missing to the best of our knowledge. However, a closer look at the vehicle's equations of motion points out that developing a unified control approach independently of the vehicle's actuation and of the aerodynamic effects acting on the body is unrealistic and technically impracticable. This, in turn, led to simplifying assumptions.

The vehicle's means of actuation are assumed to consist of a body-fixed thrust force for translational motion, and a control torque for attitude monitoring. The control problem is then decoupled into the (classical) two stage architecture consisting of: an inner loop dealing with attitude control (pilot loop); an outer loop dealing with velocity control (guidance loop). This thesis focuses on the latter, and determining how to regulate the thrust force to compensate for the orientation-dependent external forces has been one of the main objectives. In the language of Automatic Control Theory, this decoupled architecture reflects a typical "backstepping" assumption, and the way of producing the determined *desired angular motion* can be achieved via classical nonlinear control techniques. Concerning the environmental force on the vehicle, it is assumed that the aerodynamic force depends minimally on the *unsteady-aerodynamic* effects. This led to neglecting the dependencies of the aerodynamic force on the vehicle's angular velocity.

Under these assumptions, the second part of this thesis focuses, in the first place, on the *modeling*, *analysis*, and *control* of the *longitudinal aircraft dynamics* – i.e. two-dimensional motions – and then extends some of these studies for three-dimensional motions of *symmetric* aircraft, such as the fuselage of an airliner or a missile-like body. An original outcome of this part of the manuscript is to point out conditions on the aerodynamic force that allow us to recast the control problem into the one of controlling a *spherical* body – referred to as *spherical equivalency* – for which strong stability results can be demonstrated. The proposed nonlinear control laws incorporate integral and anti-wind up correction terms to deal with model uncertainties.

More precisely, the *modeling* of the longitudinal dynamics presents the equations governing planar motions, and focuses on the aerodynamic forces acting on symmetric NACA airfoils in subsonic flows. Modeling functions that are representative of the *aerodynamic coefficients* of these airfoils over large domains of the angle of attack are presented.

The *analysis* of the vehicle's longitudinal dynamics focuses on basic but important control issues such as the *existence* and the *multiplicity* of the aircraft's configurations – in terms of thrust intensity and vehicle's orientation – along a reference trajectory. An original outcome of this analysis is to show that there exists an *equilibrium* aircraft's configuration for any reference and wind velocities when the body's shape is *symmetric* independently of fluid regimes. However, according to the existing literature, the uniqueness of this equilibrium configuration cannot be in general guaranteed. In fact, an analysis of the *multiplicity* of the aircraft's configurations points out that *stall phenomena* can induce several vehicle's orientations at a given reference velocity. As a consequence, perfect tracking of a continuous reference velocity may require a discontinuous aircraft configuration, which is not feasible in practice. This calls for a multitude of remarks when choosing a reference velocity representing the transition maneuvers between hovering and high velocity cruising since the perfect tracking of this transition may be unfeasible in practice. The analysis of the vehicle's longitudinal dynamics shows also that at a fixed vehicle's thrust intensity and orientation there may exist several equilibrium velocities associated with large angles of attack and loss-of-altitude. This analysis is reminiscent of the *deep stall* situation.

The *control* of planar motions is addressed using Lyapunov analysis, which yields local controllers that stabilize either reference velocities or positions. When the aerodynamic force allows us to apply the aforementioned *spherical equivalency*, large domains of stability are obtained. The derived control laws do not rely on switching policies between several controls, so they represent a unified control approach for vehicles moving in the vertical plane and subjected to nonlinear aerodynamic forces.

Some of the results found for two-dimensional body motions are then extended to aircraft flying in three-dimensional space assuming a rotational symmetry of the vehicle's shape about the thrust force axis. In particular, original results concern the modeling of aerodynamic forces acting on symmetric bodies and the characterization of a family of models that allow one to apply the aforementioned *spherical-equivalency*. Members of this family are representative of the aerodynamic force acting on elliptic-shaped and missile-like bodies in subsonic and hypersonic flows. To illustrate the usefulness of these results at the control design level, prior control controllers are applied to provide the reader with laws that stabilize either a reference velocity or a reference trajectory. Videos of simulations with several reference trajectories can be found at

http://goo.gl/HKQtz

Possible extensions of this study on three-dimensional symmetric aircraft are numerous. They concern airplanes and other vehicles whose lift properties mostly rely on the use of large flat surfaces (wings) which break the body symmetries about the thrust force axis.

At this stage, the unification paradigm presented in this thesis is still mostly conceptual. Although validation by simulations is encouraging, the proposed control solutions call for a multitude of complementary extensions and adaptations before they are implemented on a physical device. One can mention the production of the *desired angular motion* and the determination of corresponding low level control loops that take actuators' limitations into account – in relation, for instance, to the airspeed dependent control authority associated with the use of flaps and rudders. Measurement and estimation of various physical variables involved in the calculation of the control law also involve a combination of hardware and software issues which are instrumental to implementation.

Bibliography

Abdessameud, A. and Tayebi, A. (2010). Global trajectory tracking control of VTOL-UAVs without linear velocity measurements. *Automatica*, 46(6):1053–1059.

Abed, E. H. and Lee, H. C. (1990). Nonlinear stabilization of high angle-of-attack flight dynamics using bifurcation control. In *American Control Conference*, pages 2235 – 2238.

Anderson, J. (1997). *A History of Aerodynamics: And Its Impact on Flying Machines*. Cambridge Aerospace Series.

Anderson, J. (2010). *Fundamentals of Aerodynamics*. McGraw Hill Series in Aeronautical and Aerospace Engineering, 5nd ed edition.

Belcastro, C. M. and Foster, J. V. (2010). Aircraft loss-of-control accident analysis. *Control*, (August):1–41.

Benallegue, A., Belaidi, A., and Mokhtari, A. (2005). Polynomial linear quadratic gaussian and sliding mode observer for a quadrotor unmanned aerial vehicle. *Journal of Robotics and Mechatronics*, 17(4):483–495.

Benosman, M. and Lum, K. (2007). Output trajectory tracking for a switched nonlinear non-minimum phase system: The vstol aircraft. In *IEEE Intl. Conf. on Control Applications*, pages 262 –269.

Bertin, J. J. and Smith, M. L. (2008). *Aerodynamics for engineers*. Pearson Education International.

Bertrand, S., Hamel, T., and Piet-Lahanier, H. (2006). Performance improvement of an adaptive controller using model predictive control : Application to an UAV model. In *4th IFAC Symposium on Mechatronic Systems*.

Boncagni, L., Pucci, D., Piesco, F., Zarfati, E., Mazzitelli, G., and Monaco, S. (2012a). A control approach for gas injection in tokamak machines. In *Fusion Technology 27th (SOFT)*.

Boncagni, L., Pucci, D., Piesco, F., Zarfati, E., Mazzitelli, G., and Monaco, S. (2012b). A control approach for gas injection in tokamak machines. *Tokamak Machines Fusion Engineering and Design*.

Boncagni, L., Sadeghi, Y., Carnevale, D., Geronimo, A., Varano, G., Vitelli, R., Galperti, C., Zafarati, E., and Pucci, D. (2012c). Marte at ftu: The new feedback control. *Fusion Engeneering and Design*, 87(12):1917 – 1920.

Boncagni, L., Sadeghi, Y., Carnevale, D., Mazzitelli, G., Neto, A., Pucci, D., Sartori, F., Piesco, F., Sinibaldi, S., Vitale, V., Vitelli, R., Zaccarian, L., and Monaco, S. (2011). First steps in the ftu migration towards a modular and distributed real-time control architecture. *IEEE Transactions on Nuclear Science*, 58(4):1778 – 1783.

Bouabdallah, S., Noth, A., and Siegwart, R. (2004). PID vs LQ control techniques applied to an indoor micro quadrotor. In *Intelligent Robots and Systems*, pages 2451–2456.

Bouabdallah, S. and Siegwart, R. (2005). Backstepping and sliding-mode techniques applied to an indoor micro quadrotor. In *IEEE International Conference on Robotics and Automation*.

Bridgman, P. W. (1969). Dimensional analysis. *Encyclopedia Britannica (Wm. Haley, Editor-in-Chief)*, 7:439–449.

Bristeau, P., Martin, P., and Salaun, E. (2009a). The role of propeller aerodynamics in the model of a quadrotor uav. In *European Control Conference*, pages 683 – 688.

Bristeau, P., Martin, P., and Salaun, E. (2009b). The role of propeller aerodynamics in the model of a quadrotor UAV. In *European Control Conference*, pages 683–688.

Buckingham, E. (1914). On physically similar systems; illustrations of the use of dimensional equation. *Physical Review*, 4:345–376.

Campbell, P. J. (1962). *Vertical Takeoff and Landing Aircraft*. New York: The MacMillan Company.

Carroll, J. V. and Mehra, R. K. (1982). Bifurcation analysis of nonlinear aircraft dynamics. *Journal of Guidance, Control, and Dynamics*, 5(5):529– 536.

Casau, P., Cabecinhas, D., and Silvestre, C. (2012). Hybrid control strategy for the autonomous transition flight of a fixed-wing aircraft. *IEEE Transactions on control systems technology*, PP:1–18.

Castillo, P., Lozano, R., and Dzul, A. (2005). Stabilization of a mini rotorcraft with four rotors. *IEEE Control Systems Magazine*, pages 45–55.

Chen, G., Moiola, J. L., and Wang, H. O. (2000). Bifurcation control: theories, methods, and applications. *International Journal of Bifurcation and Chaos*, 10(3):511–548.

Chow, S.-N. and Hale, J. K. (1996). *Methods of Bifurcation Theory*. Springer Verlag.

Civita, M. L., Papageorgiou, G., Messner, W. C., and Kanade, T. (2003). Design and flight testing of a gain-scheduled H_∞ loop shaping controller for wide-envelope flight of a robotic helicopter. In *American Control Conference*, pages 4195–4200.

Constantin, P. (2001). Some open problems and research directions in the mathematical study of fluid dynamics. In *Mathematics Unlimited-2001 and Beyond, Springer Verlag*, pages 353–360.

Critzos, C. C. and Heyson, H. H. (1955). Aerodynamic characteristics of naca 0012 airfoil section at angles of attack from 0 to 180. Technical report, NASA.

Cummings, P. A. (2004). Continuation methods for qualitative analysis of aircraft dynamics. Technical Report CR-2004-213035, NASA.

D'Antonio, L. and Monaco, S. (1993). A nonlinear controller for parabolic flight. In *IEEE Conf. on Decision and Control*, pages 1513–1518.

D'Antonio, L. and Monaco, S. (1995). Microgravity conditions under nonlinear inversion techniques. *Microgravity Quarterly*, 4:137–145.

Davis, K., Kirke, B., and Lazauskas, L. (2004). Material related to the aerodynamics of airfoils and lifting surfaces. `http://www.cyberiad.net/foildata.htm`. Retrieved April 8, 2013.

Desbiens, A. L., Asbeck, A., and Cutkosky, M. (2010). Hybrid aerial and scansorial robotics. In *IEEE Conf. on Robotics and Automation*, pages 1–6.

Dzul, A., Hamel, T., and Lozano, R. (2002). Modeling and nonlinear control for a coaxial helicopter. In *IEEE Conf. on Systems, Man and Cybernetics*, volume 6.

Fabiani, P., Fuertes, V., Piquereau, A., Mampey, R., and Teichteil-Konigsbuch, F. (2007). Autonomous flight and navigation of vtol uavs: from autonomy demonstrations to out-of-sights flights. *Aerospace Science and Technology*, 11:183–193.

Fefferman, C. L. (2000). Existence and smoothness of the Navier-Stokes equation. The ClayMathematics Institute, Official Problem Description.

Fossen, T. I. (1994). *Guidance and control of ocean vehicles*. John Wiley and Sons.

Frank, A., McGrew, J. S., Valenti, M., Levine, D., and How, J. P. (2007). Hover, transition, and level flight control design for a single-propeller indoor airplane. In *Guidance, Navigation and Control Conference and Exhibit (AIAA)*, pages 6318–6336.

Frazzoli, E., Dahleh, M. A., and Feron, E. (2000). Trajectory tracking control design for autonomous helicopters using a backstepping algorithm. In *American Control Conference*, pages 4102–4107.

Goman, M., Zagainov, G., and Khramtsovsky, A. (1997). Application of bifurcation methods to nonlinear flight dynamics problems. *Progress in Aerospace Sciences*, 33:539–586.

Guerrero-Castellanos, J., Marchand, N., Hably, A., Lesecq, S., and J.Delamare (2011). Bounded attitude control of rigid bodies: Real-time experimentation to a quadrotor mini-helicopter. *Control Engineering Practice*, 19:790–797.

Hacker, T. and Oprisiu, C. (1974). A discussion of the roll-coupling problem. *Progress in Aerospace Sciences*, 15(5):151–180.

Hamel, T., Mahony, R., Lozano, R., and Ostrowski, J. (2002a). Dynamic modelling and configuration stabilisation for an x4-flyer. In *IFAC World Congress*, pages 200–212.

Hamel, T., Mahony, R., Lozano, R., and Ostrowski, J. (2002b). Dynamic modelling and configuration stabilization for an X4-flyer. In *IFAC World Congress*, pages 200–212.

Hansen, J. R. (2003). *The Wind and Beyond. A Documentary Journey into the History of Aerodynamics in America*, volume 1. NASA Hystory office.

Hauser, J., Sastry, S., and Meyer, G. (1992). Nonlinear control design for slightly non-minimum phase systems: Application to V/STOL. *Automatica*, 28:651–670.

Hua, M., Hamel, T., Morin, P., and Samson, C. (2009a). A control approach for thrust-propelled underactuated vehicles and its application to vtol drones. *IEEE Transactions on Automatic Control*, 54:1837–1853.

Hua, M.-D. (2009). *Contributions to the Automatic Control of Aerial Vehicles*. PhD thesis, Université de Nice-Sophia Antipolis. Available at http://hal.archives-ouvertes.fr/tel-00460801/.

Hua, M. D., Hamel, T., Morin, P., and Samson, C. (2008). Control of thrust propelled underactuated vehicles. Technical Report 6453, INRIA.

Hua, M.-D., Hamel, T., Morin, P., and Samson, C. (2009b). A control approach for thrust-propelled underactuated vehicles and its application to VTOL drones. *IEEE Trans. on Automatic Control*, 54(8):1837–1853.

Hua, M. D., Hamel, T., Morin, P., and Samson, C. (2013). Introduction to feedback control of underactuated vtol vehicles. *IEEE Control Systems Magazine*, 33:61–75.

Huang, H., Hoffmann, G. M., Waslander, S. L., and Tomlin, C. J. (2009). Aerodynamics and Control of Autonomous Quadrotor Helicopters in Aggressive Maneuvering. In *IEEE Conf. on Robotics and Automation*, pages 3277–3282.

Hyde, R. A. and Glover, K. (1993). The application of scheduled controllers to a vstol aircraft. *IEEE Trans. on Automatic Control*, 38(7):1021–1039.

Isidori, A. (1995). *Nonlinear Control Systems*. Springer Verlag, third edition.

Isidori, A., Marconi, L., and Serrani, A. (2003). Robust nonlinear motion control of a helicopter. *IEEE Trans. on Automatic Control*, 48(3):413–426.

Jadbabaie, A., Yu, J., and Hauser, J. (1999). Receding horizon control of the caltech ducted fan : A control lyapunov function approach. In *IEEE Conference on Control Applications*, pages 51–56.

Jahnke, C. C. (1998). On the roll-coupling instabilities of high-performance aircraft. *Philosophical Transactions of the Royal Society of London*, 356(1745):2223–2239. Serie A.

Johnson, E. N. and Kannan, S. K. (2005). Adaptive trajectory control for autonomous helicopters. *AIAA Journal of Guidance, Control, and Dynamics*, 28:524–538.

Johnson, E. N. and Turbe, M. A. (2005). Modeling, control, and flight testing of a small ducted fun aircraft. In *AIAA Guidance, Navigation, and Control Conference and Exhibit*, pages 6281 – 6633.

Johnson, E. N. and Turbe, M. A. (2006). Modeling, control, and flight testing of a small ducted fan aircraft. *Journal of Guidance, Control, and Dynamics*, 29(4):769–779.

Kadmiry, B. and Driankov, D. (2004). A fuzzy gain-scheduler for the attitude control of an unmanned helicopter. *IEEE Transactions on Fuzzy Systems*, 12(4):502–515.

Keyes, J. W. (1965). Aerodynamic characteristics of lenticular and elliptic shaped configurations at a mach number of 6. Technical Report NASA-TN-D-2606, NASA.

Khalil, H. K. (2003). *Nonlinear Systems*. Prentice Hall, Upper Saddle River, New Jersey, 3rd ed edition.

Kim, H. J., Shim, D. H., and Sastry, S. (2002). Nonlinear model predictive tracking control for rotorcraft-based unmanned aerial vehicles. In *American Control Conference*, pages 3576–3581.

Ko, A., Ohanian, O. J., and Gelhausen, P. (2007). Ducted fan UAV modeling and simulation in preliminary design. In *AIAA Modeling and Simulation Technologies Conference and Exhibit*, number 2007–6375.

Koo, T. J. and Sastry, S. (1998). Output tracking control design for a helicopter model based on approximate linearization. In *IEEE Conf. on Decision and Control*, pages 3635–3640.

Kwatny, H., Dongmo, J.-E., Chang, B.-C., Bajpai, G., Belcastro, C., and Yasar, M. (2009). Aircraft accident prevention: Loss-of-control analysis. In *AIAA Guidance, Navigation, and Control Conference and Exhibit*.

Kwatny, H. G., Bennett, W. H., and Berg, J. (1991). Regulation of relaxed static stability aircraft. *IEEE Trans. on Automatic Control*, 36(11):1315 – 1323.

Le-Bras, F., Mahony, R., Hamel, T., and Binetti, P. (2006). Adaptive filtering and image based visual servo control of a ducted fan flying robot. In *IEEE Conference on Decision and Control (CDC)*, pages 1751– 1757.

Lee, D., Burg, T. C., Dawson, D. M., Shu, D., Xian, B., and Tatlicioglu, E. (2009a). Robust tracking control of an underactuated quadrotor aerial-robot based on a parametric uncertain model. In *Conference on System, Man, and Cybernetics*, pages 3187–3192.

Lee, D., Kim, H. J., and Sastry, S. (2009b). Feedback linearization vs. adaptive sliding mode control for a quadrotor helicopter. *International Journal of Control, Automation, and Systems*, 7(3):419–428.

Lipera, L., Colbourne, J., Tischler, M., Mansur, M., Rotkowitz, M., and Patangui, P. (2001). The micro craft istar micro-air vehicle: Control system design and testing. *Annual Frum of the American Helicopter Society*, pages 1–11.

Lowenberg, M. (2002). Bifurcation and continuation method. *Advanced Techniques for Clearance of Flight Control Laws, Selier*, (6):88–106.

Luo, C.-C., Liu, R.-F., Yang, C.-D., and Chang, Y.-H. (2003). Helicopter H_∞ control design with robust flying quality. *Aerospace Science and Technology*, 7(2):159–169.

Macagno, E. O. (1971). Historico-critical review of dimensional analysisdimensional analysis. *Journal of the Frnaklin Institute*, 292:391–402.

Mahony, R., Hamel, T., and Dzul, A. (1999). Hover control via an approximate lyapunov control for a model helicopter. In *IEEE Conf. on Decision and Control*, pages 3490–3495.

Mammar, S. and Duc, G. (1992). Loop shaping H_∞ design applied to the robust stabilization of an helicopter. In *IEEE Conference on Control Applications*, pages 806–811.

Marconi, L., Isidori, A., and Serrani, A. (2002). Autonomous vertical landing on an oscillating platform: an internal-model based approach. *Automatica*, 38:21–32.

Marconi, L. and Naldi, R. (2007). Robust full degree-of-freedom tracking control of a helicopter. *Automatica*, 43:1909–1920.

Marconi, L. and Naldi, R. (2008). Aggressive control of helicopters in presence of parametric and dynamical uncertainties. *Mechatronics*, 18:381–389.

Markman, S. and Holder, B. (1962). *Straight Up: A History of Vertical Flight*. New York: The MacMillan Company.

Martin, P., Devasia, S., and Paden, B. (1996). A different look at output tracking : Control of a VTOL aircraft. *Automatica*, 32, No 1:101–107.

McMasters, J. H. and Henderson, M. L. (1979). Low-speed single-element airfoil synthesis. *NASA/SSA Third International Symposium on the Science and Technology of Low-Speed and Motorless Right*, 4.

Naldi, R. (2008a). *Prototypin, Modeling and control of a Class of VTOL Aerial Robots*. PhD thesis, University of Bologna.

Naldi, R. (2008b). *Prototyping, Modeling and Control of a Class of VTOL Aerial Robots*. PhD thesis, University of Bologna.

Naldi, R. and Marconi, L. (2011). Optimal transition maneuvers for a class of v/stol aircraft. *Automatica*, 47(5):870–879.

Oishi, M. and Tomlin, C. (1999). Switched nonlinear control of a vstol aircraft. In *IEEE Conf. on Decision and Control (CDC)*, pages 2685 –2690.

Olfati-Saber, R. (2001). *Nonlinear Control of Underactuated Mechanical Systems with Application to Robotics and Aerospace vehicles*. PhD thesis, Massachusetts Institute of Technology.

Olfati-Saber, R. (2002). Global configuration stabilization for the VTOL aircraft with strong input coupling. *IEEE Trans. on Automatic Control*, 47:1949–1952.

Paranjpe, A., Sinha, N., and Ananthkrishnan, N. (1998). Use of bifurcation and continuation methods for aircraft trim and stability analysis - a state of the art. *Journal of Aerospace Sciences and Technologies, Aeronautical Society of India*, 60(2):85–100.

Peddle, I. K., Jones, T., and Treurnicht, J. (2009). Practical near hover flight control of a ducted fun (slade). *IFAC Control Engineering Practice*, 17:48–58.

Pfimlin, J. (2006). *Commande d'un minidrone a helice carenee: de la stabilisation dans le vent a la navigation autonome (In French)*. PhD thesis, Ecole Doctorale Systeme de Toulouse.

Pflimlin, J.-M. (2006). *Commande d'un minidrone à hélice carénée: de la stabilisation dans le vent à la navigation autonome (in French)*. PhD thesis, Ecole Doctorale Systèmes de Toulouse.

Pflimlin, J.-M., Binetti, P., Souères, P., Hamel, T., and Trouchet, D. (2010). Modeling and attitude control analysis of a ducted-fan micro aerial vehicle. *Control Engineering Practice*, pages 209–218.

Pflimlin, J.-M., Hamel, T., Souères, P., and Mahony, R. (2006). A hierarchical control strategy for the autonomous navigation of a ducted fan flying robot. In *IEEE Conf. on Robotics and Automation*, pages 2491– 2496.

Pflimlin, J.-M., Souères, P., and Hamel, T. (2004). Hovering flight stabilization in wind gusts for ducted fan UAV. In *IEEE Conf. on Decision and Control*, pages 3491–3496.

Phillips, W. (1948). Effect of steady rolling on longitudinal and directional stability. Technical Report 1627, NACA.

Plinval, H., Morin, P., and Mouyon, P. (2012). Nonlinear control of underactuated vehicles with uncertain position measurements and application to visual servoing. In *American Control Conference*, pages 3253–3259.

Pounds, P., Hamel, T., and Mahony, R. (2007). Attitude control of rigid body dynamics from biased IMU measurements. In *IEEE Conf. on Decision and Control*, pages 4620–4625.

Pounds, P., Mahony, R., and Corke, P. (2010a). Modelling and control of a large quadrotor robot. *Control Engineering Practice*, pages 691–699.

Pounds, P., Mahony, R., and Corke, P. (2010b). Modelling and control of a large quadrotor robot. *Control Engineering Practice*, 48(7):691–699.

Prempain, E. and Postlethwaite, I. (2005). Static H_∞ loop shaping control of a fly-by-wire helicopter. *Automatica*, 41:1517–1528.

Prouty, R. (2005). *Helicopter Performance, Stability, and Control*. Krieger.

Pucci, D. (2012). Flight dynamics and control in relation to stall. In *IEEE American Control Conf. (ACC)*, pages 118–124.

Pucci, D., Hamel, T., Morin, P., and Samson, C. (2011). Nonlinear Control of PVTOL Vehicles subjected to Drag and Lift. In *IEEE Conf. on Decision and Control*, pages 6177–6183.

Pucci, D., Hamel, T., Morin, P., and Samson, C. (2012). Modeling for control of symmetric aerial vehicles subjected to aerodynamic forces. *arXiv*, 41.

Pucci, D., Hamel, T., Morin, P., and Samson, C. (2013). Modeling for control of symmetric aerial vehicles subjected to aerodynamic forces. *Submitting to Journal Guidance, Control and Dynamics*.

Roberts, A. and Tayebi, A. (2011). Adaptive position tracking of vtol uavs. *IEEE Trans. on Robotics*, 27(1):129–142.

Saffel, B. F., Howard, M. L., and Brooks, E. N. (1971). A method for predicting the static aerodynamic characteristics of typical missile configurations for angles of attack to 180 degrees. Technical Report AD0729009, Department of the navy naval ship research and development center.

Sanchez, A., Garcia, P., Castillo, P., and Lozano, R. (2008). Simple real-time stabilization of a VTOL aircraft with bounded signals. *Journal of Guidance, Control, and Dynamics, AIAA*, 31(4).

Saripalli, S., Montgomery, J. F., and Sukhatme, G. S. (2002). Vision based autonomous landing of an unmanned aerial vehicle. In *IEEE Conference on Robotics and automation*, pages 2799–2804.

Scott, J. A. (2002). Overview of the basic parts and control surfaces of a typical aircraft. `http://www.aerospaceweb.org/question/design/q0101.shtml`. Retrieved April 8, 2013.

Shyy, W., Lian, Y., and Tang, J. (2008). *Aerodynamics of Low Reynolds Number Flyers*. Cambridge University Press.

Sinha, N. (2001). Application of bifurcation methods to nonlinear aircraft dynamics. *Journal of the Aeronautical Society of India*, 53(4):253–270.

Sonin, A. A. (2001). Dimensional analysis. Technical report, Massachusetts Institute of Technology.

Stengel, R. F. (2004). *Flight Dynamics*. Princeton University Press.

Stevens, B. L. and Lewis, F. L. (2003). *Aircraft Control and Simulation*. Wiley-Interscience, 2nd ed edition.

Stone, R. H. (2004). Control architecture for a tail-sitter unmanned air vehicle. In *5th Asian Control Conference*, pages 736–744.

Takahashi, M. D. (1993). Systhesis and evaluation of an H_2 control law for a hovering helicopter. *Journal of Guidance, Control, and Dynamics*, 16(3):579–584.

Talay, T. A. (2005). Introduction to the aerodyanmics of flight. `http://history.nasa.gov/SP-367/cover367.htm`. Retrieved April 8, 2013.

Tayebi, A. (2008). Unit quaternion-based output feedback for the attitude tracking problem. *IEEE Trans. on Automatic Control*, 53(6):1516–1520.

Tayebi, A. and McGilvray, S. (2006). Attitude stabilization of a VTOL quadrotor aircraft. *IEEE Trans. on Control Systems Technology*, 14(3):562–571.

Turner, M., Aouf, N., Bates, D., Postlethwaite, I., and Boulet, B. (2002). A switching scheme for the full-envelope control of a v/stol aircraft using lq bumpless transfer. In *IEEE International Conference on Control Applications*.

Vilchis, J. C. A., Brogliato, B., Dzul, A., and Lozano, R. (2003). Nonlinear modelling and control of helicopters. *Automatica*, 39:1583–1596.

Vissiere, D., Briteau, P.-J., Martin, A., and Petit, N. (2008). Experimental autonomous flight of a small-scaled helicopter using accurate dynamics model and low-cost sensors. In *IFAC World Congress*, pages 14642–14650.

von Kármán, T. (1967). *The Wind and Beyond*. Little Brown.

Wen, J. T.-Y. and Kreutz-Delgado, K. (1991). The attitude control problem. *IEEE Trans. on Automatic Control*, 36(10):1148–1162.

Wiggins, S. (1990). *Introduction to Applied Nonlinear Dynamical Systems and Chaos*. Springer Verlag.

Zavala-Rio, A., Fantoni, I., and Lozano, R. (2003). Global stabilization of a PVTOL aircraft model with bounded inputs. *International Journal of Control*, 76(18):1833–1844.

Zhou, Alam, M., Yang, Guo, and Wood (2011). Fluid forces on a very low Reynolds number airfoil and their prediction. *Internation Journal of Heat and Fluid Flow*, 21:329–339.

A Appendix

A.1 Proof of Lemma 7.1

By using the same arguments as those in Section 7.1, one has that

$$\text{cardinality}(\Theta_{\vec{v}_r}(t)) = 2, \quad \text{cardinality}(\Theta^+_{\vec{v}_r}(t)) = 1,$$

if $|\vec{F}(\vec{v}_r(t), t)| \neq 0$, and

$$\Theta_{\vec{v}_r}(t) = \Theta^+_{\vec{v}_r}(t) = \mathbb{S}^1,$$

if $|\vec{F}(\vec{v}_r(t), t)| = 0$. Then System (6.15b) with $\vec{F}$ given by Eq. (7.2) has a generically-unique pair of equilibrium orientations (see Definition 6.2) if and only if there exists a unique, continuous *bad* reference velocity $\vec{v}_b(t)$ such that

$$|\vec{F}(\vec{v}_b(t), t)| = 0 \quad \forall t.$$

Now, from Eq. (7.2) observe that $\vec{F}(\vec{v}_b, t) = 0 \; \forall t \iff$

$$\ddot{x}_b = f(\dot{x}_b, t), \tag{A.1}$$

with

$$f(\dot{x}_b, t) := ge_1 - \overline{c}|\dot{x}_b - \dot{x}_w|(\dot{x}_b - \dot{x}_w),$$

$\overline{c} = k_a c_0/m$, $\vec{v}_w = (\vec{\imath}_0, \vec{\jmath}_0)\dot{x}_w$, $\vec{v}_b = (\vec{\imath}_0, \vec{\jmath}_0)\dot{x}_b$, and $\vec{a}_b = (\vec{\imath}_0, \vec{\jmath}_0)\ddot{x}_b$. Thus, the problem is to ensure the existence of a unique, continuous solution $\dot{x}_b(t)$ to the differential system (A.1). Without loss of generality, assume that the wind velocity and its derivative are bounded, i.e. $\exists c \in \mathbb{R}^+ : |\ddot{x}_w| < c, |\dot{x}_w| < c$. Then, one verifies that $f(\dot{x}_b, t)$ is uniformly, locally Lipschitz (Khalil, 2003, p. 90 Lemma 3.2) on any compact, convex $D_c \subset \mathbb{R}^2$ since $\exists \delta \in \mathbb{R}^+ : |\partial_{\dot{x}_b} f| < \delta, \forall \dot{x}_b \in D_c$. Consequently, there exists a unique, continuous solution $\dot{x}_b(t)$ to the differential system (A.1) in D_c. However, we cannot claim that the solution $\dot{x}_b$ is unique in $\mathbb{R}^2$ since this solution may leave any compact set – it may tend to infinity in finite time (Khalil, 2003, p. 93 Example 3.3). By considering the derivative of the positive-definite function given by

$$V = \frac{1}{2}|\dot{x}_b - \dot{x}_w|^2,$$

one shows that the solutions to the differential system (A.1) are bounded, so there exists a convex, compact D_c that contains any solution starting at $\dot{x}_b(0) \in \mathbb{R}^2$. Therefore, we deduce that there exists a unique, continuous solution to System (A.1) $\forall \dot{x}_b(0) \in \mathbb{R}^2$ and, consequently, to $F(\vec{v}_b, t) = 0 \; \forall t$.

A.2 Proof of Lemma 7.2

First, in view of $\vec{F} = (\vec{\imath}_0, \vec{\jmath}_0)F$, $\vec{F}_a = (\vec{\imath}_0, \vec{\jmath}_0)F_a$, $\vec{g} = (\vec{\imath}_0, \vec{\jmath}_0)ge_1$, $\vec{\jmath} = (\vec{\imath}_0, \vec{\jmath}_0)Re_2$, $\vec{v}_w = (\vec{\imath}_0, \vec{\jmath}_0)\dot{x}_w$, $\vec{v}_r = (\vec{\imath}_0, \vec{\jmath}_0)\dot{x}_r$, $\vec{a}_r = (\vec{\imath}_0, \vec{\jmath}_0)\ddot{x}_r$, and $\vec{v}_a = (\vec{\imath}_0, \vec{\jmath}_0)\dot{x}_a$, the existence of an equilibrium orientation such that (6.19b) holds is equivalent to the existence, at any fixed time t, of one zero of the following function

$$f_t(\theta) := F^T(\dot{x}_r(t), \theta, t)R(\theta)e_2, \tag{A.2}$$

where

$$\begin{aligned} F(\dot{x}, \theta, t) &= F_{gr}(t) + F_a(\dot{x}_a, \alpha(\dot{x}_a, \theta)), && \text{(A.3a)}\\ F_{gr} &:= mge_1 - m\ddot{x}_r, && \text{(A.3b)}\\ F_a &= k_a|\dot{x}_a|[c_L(\alpha)S - c_D(\alpha)I]\dot{x}_a, && \text{(A.3c)}\\ \dot{x}_a &= \dot{x} - \dot{x}_w, && \text{(A.3d)}\\ \alpha &= \theta - \gamma + (\pi - \delta) && \text{(A.3e)}\\ \gamma &= \operatorname{atan2}(\dot{x}_{a_2}, \dot{x}_{a_1}). && \text{(A.3f)} \end{aligned}$$

In terms of vectors of coordinates, the dissipativity of the aerodynamic force (7.5) writes

$$\dot{x}_a^T F_a \leq 0 \quad \forall(\dot{x}_a, \alpha). \tag{A.4}$$

To show that (A.4) does not in general imply the existence of an equilibrium orientation, it suffices to find an aerodynamic force satisfying (A.4) and such that the function given by (A.2) never crosses zero for some reference and wind velocities at a some fixed time instant. To show this, assume

$$\begin{cases} c_L(\alpha) = \sin(\alpha) \\ c_D(\alpha) = c_0 + 1 - \cos(\alpha), \end{cases} \tag{A.5}$$

with $c_0 > 0$. It is then straightforward to verify that the aerodynamic force given by (A.3c) with the coefficients (A.5) satisfies (A.4); in addition, note also that

$$c_L(0) = c_L(\pi) = 0.$$

Now, since the vector F in the right hand side of Eq. (A.2) is evaluated at the reference velocity, we have to evaluate the quantities (A.3) at $\dot{x}_r$. Let us assume that
A1 : the thrust force is perpendicular to the zero-lift direction, e.g. $\delta = \pi/2$;
A2 : there exists a time $\bar{t}$ such that

i the reference and wind velocities imply $\gamma(\dot{x}_r(\bar{t}) - \dot{x}_w(\bar{t})) = \pi/2$ and $k_a|\dot{x}_r(\bar{t}) - \dot{x}_w(\bar{t})|^2 = 1$;

ii the reference acceleration $\ddot{x}_r(\bar{t})$ implies $F_{gr_1}(\bar{t}) = 0$ and $F_{gr_2}(\bar{t}) = c_0 + 1$.

By evaluating the angle of attack (A.3e) at the reference velocity with the assumptions **A1** and **A2***i*, one verifies that $\alpha(\bar{t}) = \theta$. Then, (A.2) at $t = \bar{t}$ becomes

$$f_{\bar{t}}(\theta) = [F_{gr_2}(\bar{t}) - c_D(\theta)]\cos(\theta) + [c_L(\theta) - F_{gr_1}(\bar{t})]\sin(\theta). \tag{A.6}$$

In view of the aerodynamic coefficients (A.5) and the assumption **A2***ii*, one has

$$f_{\bar{t}}(\theta) \equiv 1 \neq 0.$$

Hence, there exists an aerodynamic force that satisfies (A.4) but for which there does not exist an equilibrium orientation for some reference and wind velocities at a fixed time instant. Then, (A.4) does not in general imply the existence of an equilibrium orientation.

A.3 Proof of Theorem 7.1

Recall that the existence of an equilibrium orientation such that (6.19b) holds is equivalent to the existence, at any fixed time t, of one zero of the function $f_t(\theta)$ given by (A.2).

A.3.1 Proof of the Item 1

Assume that the thrust force is parallel to the zero-lift-line so that $\delta = 0$; the existence of the equilibrium orientation in the case $\delta = \pi$ can be proven using the same arguments as those below. Now, in view of Eqs. (6.7), namely

$$\begin{cases} v_{a_1} = -|\dot{x}_a| \cos(\alpha + \delta) \\ v_{a_2} = \quad |\dot{x}_a| \sin(\alpha + \delta), \end{cases} \tag{A.7}$$

$\dot{x}_a = R(\theta)v_a$, $S = R^T(\theta)SR(\theta)$, and of $\delta = 0$, one verifies that the function $f_t(\theta)$ given by (A.2) becomes

$$f_t(\theta) = F_{gr}^T(t)R(\theta)e_2 - k_a|\dot{x}_{rw}(t)|^2[c_L(\alpha_r)\cos(\alpha_r) + c_D(\alpha_r)\sin(\alpha_r)], \tag{A.8}$$

where $F_{gr}(t)$ is given by (A.3b) and

$$\alpha_r(\theta, t) = \theta - \gamma_r(t) + \pi, \tag{A.9a}$$
$$\gamma_r(t) = \text{atan2}(\dot{x}_{rw_2}, \dot{x}_{rw_1}), \tag{A.9b}$$
$$\dot{x}_{rw}(t) := \dot{x}_r(t) - \dot{x}_w(t). \tag{A.9c}$$

It follows from (A.9a) that at any time t there exists an orientation $\theta_0(t)$ such that $\theta = \theta_0(t)$ yields $\alpha_r(t) = 0$, namely

$$\theta = \theta_0(t) = \gamma_r(t) - \pi \quad \Rightarrow \quad \alpha_r(t) = 0.$$

Consequently, $\theta = \theta_0(t) + \pi$ yields $\alpha_r(t) = \pi$ and $\theta = \theta_0(t) - \pi$ yields $\alpha_r(t) = -\pi$. Now, the assumption that the body's shape is symmetric implies (see Section 6.2.1)

$$c_L(0) = c_L(\pi) = c_L(-\pi) = 0.$$

Thus, from Eq. (A.8) one obtains

$$f_t(\theta_0(t) + \pi) = f_t(\theta_0(t) - \pi) = -f_t(\theta_0(t)) \tag{A.10}$$

since $e_2^T R^T(\theta_0 + \pi)F_{gr}(t) = e_2^T R^T(\theta_0 - \pi)F_{gr}(t) = -e_2^T R^T(\theta_0)F_{gr}(t)$. In view of (A.10), the proof of the existence of (at least) two zeros of the function $f_t(\theta)$ at any fixed time t, and thus of two equilibrium orientations, is then a direct application of the *intermediate value theorem* since, by assumption, $f_t(\theta)$ is continuous versus θ (c_L and c_D are continuous) and defined $\forall t$ ($\dot{x}_r$ is differentiable). These two zeros, denoted by $\theta_{e_1}(t)$ and $\theta_{e_2}(t)$, belong to $\theta_{e_1}(t) \in [\theta_0(t) - \pi, \theta_0(t)]$ and $\theta_{e_2}(t) \in [\theta_0(t), \theta_0(t) + \pi]$.

A.3.2 PROOF OF THE ITEM 2

Under the assumption that the body's shape is bisymmetric one has (see Section 6.2.1).

$$c_D(\alpha) = c_D(\alpha \pm \pi)\ \forall \alpha,$$
$$c_L(\alpha) = c_L(\alpha \pm \pi)\ \forall \alpha.$$

In view of F_a given by (A.3c), the above property of the aerodynamic coefficients imply

$$F_a(\dot{x}_a, \alpha) = F_a(\dot{x}_a, \alpha \pm \pi).$$

Then, using this property of the aerodynamic force and the expression of the angle of attack in (A.3e), one verifies that the apparent external force given by (A.3a) satisfies

$$F(\dot{x}, \theta, t) = F(\dot{x}, \theta \pm \pi, t) \quad \forall (\dot{x}, \theta, t). \tag{A.11}$$

In turn, it is straightforward to verify that the function $f_t(\theta)$ given by (A.2) satisfies, at any fixed time t, the following property

$$f_t(\theta + \pi) = f_t(\theta - \pi) = -f_t(\theta) \quad \forall \theta. \tag{A.12}$$

Then, analogously to the proof of the Item 1), the existence of at least two equilibrium orientations $\theta_{e_1}(t)$ and $\theta_{e_2}(t)$ such that

$$f_t(\theta_{e_1}(t)) = f_t(\theta_{e_2}(t)) = 0$$

can be shown by applying the *intermediate value theorem*.

Observe that Eqs. (A.12) imply that if $\theta_{e_1}(t)$ is an equilibrium orientation, i.e.

$$f_t(\theta_{e_1}(t)) = 0 \quad \forall t,$$

then another equilibrium orientation is given by $\theta_{e_2}(t) = \theta_{e_1}(t) + \pi$. Now, to show that there always exists an equilibrium orientation ensuring a positive-semi definite thrust intensity, from Eq (6.19a) observe that the thrust intensity at the equilibrium point is given by

$$T_e = F^T(\dot{x}_r(t), \theta_e(t), t) R(\theta_e(t)) e_1.$$

Then, it follows from (A.11) that if the thrust intensity is negative-semi definite at t along an equilibrium orientation, i.e.

$$T_e(\dot{x}_r(t), \theta_{e_1}(t), t) \leq 0,$$

then it is positive-semi definite at the the equilibrium orientation given by $\theta_{e_2}(t)$=$\theta_{e_1}(t)$+π, i.e.

$$T_e(\dot{x}_r(t), \theta_{e_1}(t) + \pi, t) \geq 0.$$

Hence, on can always build up an equilibrium orientation $\theta_e(t)$ associated with a positive-semi definite thrust intensity. Clearly, the continuity of such an equilibrium cannot be guaranteed a priori.

A.4 Proof of Theorem 7.2

First, observe that if $\sin(\delta) = 0$, then the existence of the equilibrium orientation follows from Theorem 7.1 since the thrust force is parallel to the zero-lift-direction in this case. Hence assume that

$$\sin(\delta) \neq 0. \tag{A.13}$$

Recall that the existence of an equilibrium orientation such that (6.19b) holds is equivalent to the existence, at any fixed time t, of one zero of the function $f_t(\theta)$ given by (A.2). In view of (A.7), $\dot{x}_a = R(\theta)v_a$, and of $S = R^T(\theta)SR(\theta)$, one can verify that (A.2) becomes

$$f_t(\theta) = F_{gr}^T(t)R(\theta)e_2 - k_a|\dot{x}_{rw}(t)|^2[c_L(\alpha_r)\cos(\alpha_r + \delta) + c_D(\alpha_r)\sin(\alpha_r + \delta)], \tag{A.14}$$

where F_{gr} is given by (A.3b),

$$\alpha_r = \alpha_r(\theta, t) = \theta - \gamma_r(t) + \pi - \delta, \tag{A.15}$$

γ_r by (A.9b), and $\dot{x}_{rw}$ by (A.9c).

From Eq. (A.14) note that if $|\dot{x}_{rw}(t)| = 0$, then there exist two zeros for the function $f_t(\theta)$, i.e. two equilibrium orientations at the time t. Thus, let us now focus when

$$|\dot{x}_{rw}(t)| \neq 0. \tag{A.16}$$

It follows from (A.15) that at any fixed time t, there exists an orientation

$$\theta_0(t) = \gamma_r(t) - \pi + \delta$$

such that $\theta = \theta_0(t)$ yields $\alpha_r = 0$, so $\theta = \theta_0(t) + \pi$ yields $\alpha_r = \pi$. Now, if

$$f_t(\theta_0(t))f_t(\theta_0(t) + \pi) \leq 0,$$

then there exists a zero for the function $f_t(\theta)$, and this zero belongs to the domain $[\theta_0(t), \theta_0(t) + \pi]$. This is due to the fact that the function $f_t(\theta)$ changes sign on this domain and is continuous versus θ. We are thus interested in the case when the above inequality is not satisfied. Therefore, assume also that

$$f_t(\theta_0(t))f_t(\theta_0(t) + \pi) > 0. \tag{A.17}$$

Given the assumption that the body's shape is symmetric, one has $c_L(0) = c_L(\pi) = 0$. So, in view of (A.14), imposing (A.17) divided by $k_a^2|\dot{x}_{rw}(t)|^4\sin(\delta)^2$, which we recall is assumed to be different from zero, yields

$$[a_t - c_D(0)][c_D(\pi) - a_t] > 0, \tag{A.18}$$

where

$$a_t := \frac{F_{gr}^T(t)R(\theta_0(t))e_2}{k_a\sin(\delta)|\dot{x}_{rw}(t)|^2}. \tag{A.19}$$

Under the assumption that $c_D(0) < c_D(\pi)$, the inequality (A.18) implies that

$$c_D(0) < a_t < c_D(\pi). \tag{A.20}$$

When the constraint (A.20) is satisfied, the inequality (A.17) holds and we cannot (yet) claim the existence of an equilibrium orientation at the time instant t. The following shows that when the inequality (A.20) is satisfied, the existence of an equilibrium orientation at the time instant t follows from the symmetry of the body's shape provided that the conditions of Theorem 7.2 hold true. Recall that when the inequality (A.20) is not satisfied, the existence of an equilibrium orientation at the time t follows from the arguments used in the beginning of this proof.

Now, under the assumption that the body's shape is symmetric one has

$$c_D(\alpha) = c_D(-\alpha), \tag{A.21a}$$

$$c_L(\alpha) = -c_L(-\alpha). \tag{A.21b}$$

Let $\overline{\alpha} \in \mathbb{R}^+$; then, by using (A.14) and the above properties of the aerodynamic coefficients, one verifies that (recall that $\theta = \theta_0(t) \Rightarrow \alpha_r(t) = 0$, so $\theta = \theta_0(t) \pm \overline{\alpha} \Rightarrow \alpha_r(t) = \pm\overline{\alpha}$)

$$f_t(\theta_0(t) - \overline{\alpha}) f_t(\theta_0(t) + \overline{\alpha}) = [\Delta_a \sin(\delta) + \Lambda_b][\Delta_a \sin(\delta) - \Lambda_b] = \Delta_a^2 \sin^2(\delta) - \Lambda_b^2, \tag{A.22}$$

with

$$\begin{aligned} \Delta_a = \Delta_a(\overline{\alpha}) &:= [a_t - c_D(\overline{\alpha})]\cos(\overline{\alpha}) + c_L(\overline{\alpha})\sin(\overline{\alpha}), \\ \Lambda_b = \Lambda_b(\overline{\alpha}) &:= [b_t + c_D(\overline{\alpha})\cos(\delta)]\sin(\overline{\alpha}) + c_L(\overline{\alpha})\cos(\overline{\alpha})\cos(\delta), \\ b_t &:= \frac{F_{gr}^T(t) R(\theta_0(t)) e_1}{k_a |\dot{x}_{rw}(t)|^2}. \end{aligned} \tag{A.23}$$

It follows from Eq. (A.22) that if

$$\forall a_t \ : \ c_D(0) < a_t < c_D(\pi), \quad \exists \overline{\alpha}_a \in \mathbb{R} \ : \ \Delta_a(\overline{\alpha}_a) = 0, \tag{A.24}$$

then there exists a zero for the function $f_t(\theta)$, and this zero belongs to the domain given by $[\theta_0(t) - \overline{\alpha}_a, \theta_0(t) + \overline{\alpha}_a]$ (the function $f_t(\theta)$ would change sign in this domain). The existence of a value $\overline{\alpha}_a$, such that (A.24) holds, can be deduced by imposing that

$$\forall a_t \ : \ c_D(0) < a_t < c_D(\pi), \quad \exists \alpha_0, \alpha_s \in \mathbb{R}, \ : \ \Delta_a(\alpha_0)\Delta_a(\alpha_s) \leq 0, \tag{A.25}$$

which implies (A.24) with $\overline{\alpha}_a \in [\alpha_0, \alpha_s]$ since $\Delta_a(\overline{\alpha})$ is continuous versus $\overline{\alpha}$. Now, in view of (A.23) note that $\forall a_t : c_D(0) < a_t < c_D(\pi)$ one has

$$\Delta_a(0) > 0. \tag{A.26}$$

In addition, still from (A.23) note that $\forall a_t \ : \ c_D(0) < a_t < c_D(\pi)$ one has

$$\Delta_a(\overline{\alpha}) \leq c_D(\pi)|\cos(\overline{\alpha})| - c_D(\overline{\alpha})\cos(\overline{\alpha}) + c_L(\overline{\alpha})\sin(\overline{\alpha}).$$

Therefore, if there exists an angle $\alpha_s \in (0, 90^\circ)$ such that $c_L(\alpha_s) > 0$ and

$$c_L(\alpha_s)\sin(\alpha_s) - [c_D(\alpha_s) - c_D(\pi)]\cos(\alpha_s) \leq 0 \iff \tan(\alpha_s) \leq \frac{c_D(\alpha_s) - c_D(\pi)}{c_L(\alpha_s)},$$

then $\Delta_a(\alpha_s) \leq 0$ and (A.25) holds with $\alpha_0 = 0$. Consequently, there exists an angle $\overline{\alpha}_a$ such that (A.24) is satisfied and, subsequently, an equilibrium orientation $\theta_e(t)$ such that $f_t(\theta_e(t)) = 0$.

A.5 Proof of Lemma 7.3

Once the velocity errors dynamics are transformed into the form (7.12), i.e.

$$m\dot{\vec{e}}_v = \vec{F}_p - T_p\vec{\imath},$$

with $\vec{F}_p$ independent of θ, one verifies that $\vec{e}_v \equiv 0$ implies (recall that $\theta = \text{angle}(\vec{\imath}_0, \vec{\imath})$)

$$\begin{cases} T_p &= |\vec{F}_p(\vec{v}_r, t)|, \\ \vec{\imath}(\theta_e) &= \dfrac{\vec{F}_p(\vec{v}_r, t)}{|\vec{F}_p(\vec{v}_r, t)|} \Rightarrow \theta_e = \xi_p(t), \end{cases} \tag{A.27}$$

and

$$\begin{cases} T_p &= -|\vec{F}_p(\vec{v}_r, t)|, \\ \vec{\imath}(\theta_e) &= -\dfrac{\vec{F}_p(\vec{v}_r, t)}{|\vec{F}_p(\vec{v}_r, t)|} \Rightarrow \theta_e = \xi_p(t) + \pi, \end{cases} \tag{A.28}$$

where ξ_p denotes the angle between the vertical direction $\vec{\imath}_0$ and $\vec{F}_p(\vec{v}_r, t)$, i.e.

$$\xi_p = \text{angle}(\vec{\imath}_0, \vec{F}_p(\vec{v}_r, t)).$$

Consequently, at the time instant t one has

$$\text{cardinality}(\Theta_{\vec{v}_r}(t)) = 2,$$

if $|\vec{F}_p(\vec{v}_r(t), t)| \neq 0$ and

$$\Theta_{\vec{v}_r}(t) = \mathbb{S}^1,$$

if $|\vec{F}_p(\vec{v}_r(t), t)| = 0$. Then, system (6.15b) has a generically-unique pair of equilibrium orientations (see the Definition 6.2) if and only if there exists a unique, continuous *bad* reference velocity $\vec{v}_b(t)$ such that

$$|\vec{F}_p(\vec{v}_b(t), t)| = 0 \ \forall t.$$

From here, the proof proceeds as the proof of Lemma A.1.

A.6 Proof of Lemma 7.4

The aerodynamic force in the form (7.8) points out that we can transform the system's dynamics (6.1a) into (7.10) with $\vec{f}_p$ independent of θ if and only if $\overline{c}_D$, i.e.

$$\overline{c}_D = c_D(\alpha) + [c_L(\alpha) - \overline{c}_L]\cot(\alpha + \delta),$$

and $\overline{c}_L$ are independent of θ. Now, if $\overline{c}_D$ is independent of θ, then its derivative w.r.t. θ (which equals its derivative w.r.t. α) is equal to zero everywhere, i.e.

$$\begin{aligned} \overline{c}'_D = c'_D(\alpha) + [c'_L(\alpha) - \overline{c}'_L]\cot(\alpha + \delta) - \frac{c_L(\alpha) - \overline{c}_L}{\sin(\alpha + \delta)^2} \equiv 0 \iff \\ c'_D(\alpha)\sin(\alpha + \delta)^2 + [c'_L(\alpha) - \overline{c}'_L]\cos(\alpha + \delta)\sin(\alpha + \delta) - c_L(\alpha) + \overline{c}_L \equiv 0. \end{aligned} \tag{A.29}$$

If there exists an orientation-independent $\bar{c}_L$ such that the above equation is satisfied, then differentiating Eq. (A.29) w.r.t. θ yields

$$(c_D'' - 2c_L')\sin(\alpha+\delta) + (c_L'' + 2c_D')\cos(\alpha+\delta) \equiv 0.$$

Since the aerodynamic coefficients are independent of the angle δ, i.e. the angle between the thrust force and the zero-lift direction, the above differential equation is satisfied for any value of δ only if

$$\begin{cases} c_D'' - 2c_L' = 0 \quad \forall\alpha, \\ c_L'' + 2c_D' = 0 \quad \forall\alpha. \end{cases} \tag{A.30}$$

The general solution to the linear differential system (A.30) is:

$$\begin{cases} c_D(\alpha) = b_0 + b_1\sin(2\alpha) - b_2\cos(2\alpha), \\ c_L(\alpha) = b_3 + b_1\cos(2\alpha) + b_2\sin(2\alpha), \end{cases}$$

with b_j denoting constants numbers. When the shape of the body is symmetric, the above functions must also satisfy the conditions (6.8). This implies that b_1 and b_3 are equal to zero. Using the fact that $\cos(2\alpha) = 1 - 2\sin^2(\alpha)$, one obtains (7.14) with $c_0 = b_0 - b_2$ and $b_2 = c_1$.

A.7 Proof of Theorem 7.3

By using (A.7) and $\dot{x}_a = Rv_a$, one verifies that

$$F_a - TRe_1 \equiv f_p - T_pRe_1, \tag{A.31}$$

where F_a and f_p are the vectors of coordinates of the geometric vectors $\vec{F}_a$ and $\vec{f}_p$, given by (6.2) and (7.47a) expressed in the inertial frame basis, i.e.

$$f_p = k_a|\dot{x}_a|\,[c_{Lp}(\alpha)S - c_{Dp}(\alpha)I]\,\dot{x}_a, \tag{A.32a}$$
$$F_a = k_a|\dot{x}_a|\,[c_L(\alpha)S - c_D(\alpha)I]\,\dot{x}_a, \tag{A.32b}$$

with $c_{Lp}(\alpha)$ and $c_{Dp}(\alpha)$ given by (7.48) and T_p by (7.47b), i.e.

$$\begin{cases} c_{Lp}(\alpha) = c_L(\alpha) - [c_L'(\alpha)\cos(\alpha+\delta) + c_D'(\alpha)\sin(\alpha+\delta)]\sin(\alpha+\delta), \\ c_{Dp}(\alpha) = c_D(\alpha) + [c_L'(\alpha)\cos(\alpha+\delta) + c_D'(\alpha)\sin(\alpha+\delta)]\cos(\alpha+\delta), \end{cases} \tag{A.33}$$

and

$$T_p = T + k_a|\vec{v}_a|^2[c_L'(\alpha)\cos(\alpha+\delta) + c_D'(\alpha)\sin(\alpha+\delta)]. \tag{A.34}$$

Then, the possibility of writing the body's dynamic equation (6.1a) as (7.46) follows from (A.31). Observe that (A.31) also implies that

$$e_1^TR^T(F_a - f_p) \equiv -k_a|\vec{v}_a|^2[c_L'(\alpha)\cos(\alpha+\delta) + c_D'(\alpha)\sin(\alpha+\delta)], \tag{A.35a}$$
$$e_2^TR^T(F_a - f_p) \equiv 0. \tag{A.35b}$$

A.7.1 Proof of the Item 1

Recall that a sufficient condition for $\theta_e(t)$ to be isolated and differentiable at the time t is (see Section 7.5)

$$\partial_\theta e_2^T R^T F\Big|_{(\dot{x},\theta)\equiv(\dot{x}_r(t),\theta_e(t))} \neq 0, \tag{A.36}$$

where F is the vector of coordinates of the apparent external force $\vec{F}$ in the inertial frame, i.e.

$$F = mge_1 + F_a - m\ddot{x}_r. \tag{A.37}$$

By using the relationships (A.7), $\partial_\theta F = \partial_\theta F_a = \partial_\alpha F_a$, and Eq. (A.35a), one has

$$\partial_\theta e_2^T R^T F = -e_2^T S R^T F + e_2^T R^T \partial_\alpha F_a = -e_1^T R^T F + e_1^T R^T (F_a - f_p). \tag{A.38}$$

Let F_p denote the vector of coordinates of the geometric vector given by (7.49) expressed in the inertial frame basis, i.e.

$$F_p = mge_1 + f_p - m\ddot{x}_r, \tag{A.39}$$

with f_p given by (A.32a). Then, it follows from (A.37), (A.38), and (A.39) that

$$\partial_\theta e_2^T R^T F = -e_1^T R^T F_p. \tag{A.40}$$

Now, from (A.35b), (A.37), and (A.39), it is a simple matter to verify that

$$e_2^T R^T F \equiv e_2^T R^T F_p. \tag{A.41}$$

Also, recall that at the equilibrium one has

$$e_2^T R^T F\Big|_{(\dot{x},\theta)\equiv(\dot{x}_r,\theta_e)} \equiv 0,$$

therefore, in view of (A.41), at the equilibrium one has

$$e_2^T R^T F_p\Big|_{(\dot{x},\theta)\equiv(\dot{x}_r,\theta_e)} \equiv 0, \tag{A.42}$$

i.e. the second component of the vector $R^T F_p$ is equal to zero at the equilibrium point. Now, in view of

$$|F_p| = |R^T F_p|,$$

and of the assumption that the vector F_p is different from zero at the equilibrium point, one has that the first component of the vector $R^T F_p$ is necessarily different from zero at the equilibrium point, i.e.

$$e_1^T R^T F_p\Big|_{(\dot{x},\theta)\equiv(\dot{x}_r,\theta_e)} \neq 0.$$

This in turn implies, via (A.40), that the condition (A.36) is satisfied. Consequently, the equilibrium orientation $\theta_e(t)$ is isolated and differentiable at the time instant t.

A.7.2 PROOF OF THE ITEM 2

To show that the direction of the vector $\vec{F}_p$ is *almost constant* w.r.t. the orientation close to the equilibrium configuration, i.e.

$$\partial_\theta \left[\frac{\vec{F}_p}{|\vec{F}_p|}\right]\Bigg|_{(\vec{e}_v,\theta)=(0,\theta_e(t))} = 0,$$

we equivalently show that

$$\partial_\theta \xi_p\Big|_{(\vec{e}_v,\theta)=(0,\theta_e(t))} = 0, \tag{A.43}$$

where

$$\xi_p := \text{angle}(\vec{\imath}_0, \vec{F}_p) = \text{atan2}(F_{p_2}, F_{p_1}), \tag{A.44}$$

with F_p given by (A.39). By using the above equation and the fact that

$$\partial_\theta F_p = \partial_\theta f_p = \partial_\alpha f_p,$$

one verifies that

$$\partial_\theta \xi_p = -\frac{F_p^T S \partial_\theta F_p}{|F_p|^2} = -\frac{F_p^T R S R^T \partial_\alpha f_p}{|F_p|^2}, \tag{A.45}$$

where f_p is given by (A.32a). Now, in view of f_p as given by (A.32a), $\dot{x}_a = Rv_a$, and (A.7), one verifies that the second component of the vector $R^T \partial_\theta f_p$ is equal to zero everywhere, i.e.

$$e_2^T R^T \partial_\alpha f_p \equiv 0. \tag{A.46}$$

Then from Eq. (A.45) one obtains

$$\partial_\theta \xi_p = -\frac{e_1^T R^T \partial_\alpha f_p}{|F_p|^2} e_2^T R^T F_p. \tag{A.47}$$

Therefore, because of (A.42) and (7.45), one shows (A.43).

A.7.3 PROOF OF THE ITEM 3

It is straightforward to verify that the coefficients $c_{Lp}(\alpha)$ and $c_{Dp}(\alpha)$ given by (A.33) can be rewritten as

$$\begin{cases} c_{Lp}(\alpha) = \overline{c}_L - \overline{c}'_D \sin(\alpha+\delta)^2, \\ c_{Dp}(\alpha) = \overline{c}_D + \overline{c}'_D \sin(\alpha+\delta)\cos(\alpha+\delta), \end{cases}$$

with

$$\overline{c}_D = \overline{c}_D(\alpha) = c_D(\alpha) + [c_L(\alpha) - \overline{c}_L]\cot(\alpha+\delta),$$

and $\overline{c}_L$ a constant number. If the condition (7.9) is satisfied, i.e. $\overline{c}_D$ is constant, then

$$\begin{cases} c_{Lp} = \overline{c}_L, \\ c_{Dp} = \overline{c}_D, \end{cases}$$

and $\vec{f}_p$ given by (7.47a) coincides with the vector given by (7.11a).

A.8 Proof of Lemma 7.6

By decomposing the velocity error $\vec{e}_v$ w.r.t. the inertial frame, i.e. $\vec{e}_v = (\vec{\imath}_0, \vec{\jmath}_0)\dot{\tilde{x}}$, the dynamics (6.15b) with no wind and constant reference velocity writes

$$m\ddot{\tilde{x}} = mge_1 + k_a H(\alpha(\dot{x}, \theta))\dot{x}|\dot{x}| - TR(\theta)e_1, \tag{A.48}$$

where

$$H(\alpha) := \begin{pmatrix} -c_D(\alpha) & -c_L(\alpha) \\ c_L(\alpha) & -c_D(\alpha) \end{pmatrix}, \tag{A.49a}$$

$$\alpha_r(\dot{x}, \theta) = \theta - \gamma(\dot{x}) + \pi - \delta, \tag{A.49b}$$

$$\gamma(\dot{x}) = \operatorname{atan2}(\dot{x}_2, \dot{x}_1). \tag{A.49c}$$

To study the static stability of a reference velocity in the form

$$\dot{x}_r = \nu(\cos(\gamma_r), \sin(\gamma_r))^T, \quad \nu > 0, \tag{A.50}$$

fix the thrust intensity and vehicle's orientation at their (constant) equilibrium values, i.e.

$$T \equiv T_e, \tag{A.51a}$$

$$\theta \equiv \theta_e. \tag{A.51b}$$

Then $TR(\theta)e_1$ in Eq. (A.48) is a constant vector. Consequently, the linearization of the dynamics (A.48) at the equilibrium point $\dot{\tilde{x}} = 0$ is given by

$$m\ddot{\tilde{x}} = k_a \, \partial_{\dot{x}}\Big[H(\alpha(\dot{x}, \theta_e))\dot{x}|\dot{x}|\Big]\Big|_{\dot{x}=\dot{x}_r} \dot{\tilde{x}}. \tag{A.52}$$

The stability characteristics of system (A.52) can be then deduced by analyzing the characteristic polynomial of the matrix

$$\partial_{\dot{x}}\Big[H(\alpha(\dot{x}, \theta_e))\dot{x}|\dot{x}|\Big]\Big|_{\dot{x}=\dot{x}_r}.$$

Now, by direct calculations one can verify that

$$\partial_{\dot{x}}\Big[H(\alpha(\dot{x}, \theta_e))\dot{x}|\dot{x}|\Big] = [(\partial_{\dot{x}_1} H)\dot{x}|\dot{x}|, (\partial_{\dot{x}_2} H)\dot{x}|\dot{x}|] + H(\alpha)\partial_{\dot{x}}(\dot{x}|\dot{x}|), \tag{A.53a}$$

$$\partial_{\dot{x}_1} H = \partial_\alpha H \partial_{\dot{x}_1}\alpha = H' \frac{\dot{x}_2}{|\dot{x}|^2}, \tag{A.53b}$$

$$\partial_{\dot{x}_2} H = \partial_\alpha H \partial_{\dot{x}_2}\alpha = -H' \frac{\dot{x}_1}{|\dot{x}|^2}, \tag{A.53c}$$

$$\partial_{\dot{x}}(\dot{x}|\dot{x}|) = \frac{\dot{x}\dot{x}^T}{|\dot{x}|} + |\dot{x}|I. \tag{A.53d}$$

Therefore, in view of (A.50) and (A.53), one has

$$\begin{aligned} \frac{1}{\nu}\partial_{\dot{x}}\Big[H(\alpha(\dot{x}, \theta_e))\dot{x}|\dot{x}|\Big]\Big|_{\dot{x}=\dot{x}_r} = {} & H'(\alpha_e)\left[\begin{pmatrix}\cos(\gamma_r)\\ \sin(\gamma_r)\end{pmatrix}\sin(\gamma_r), -\begin{pmatrix}\cos(\gamma_r)\\ \sin(\gamma_r)\end{pmatrix}\cos(\gamma_r)\right] + \\ & H(\alpha_e)\left[\begin{pmatrix}\cos(\gamma_r)\\ \sin(\gamma_r)\end{pmatrix}\begin{pmatrix}\cos(\gamma_r) & \sin(\gamma_r)\end{pmatrix} + I\right], \end{aligned} \tag{A.54}$$

where α_e is the angle of attack at the equilibrium $\dot{x} \equiv \dot{x}_r$, i.e.

$$\alpha_e = \theta_e - \gamma_r + \pi - \delta.$$

Since $H(\alpha) = c_L(\alpha)S - c_D(\alpha)I$, observe that this matrix satisfies

$$H = R(\cdot)HR^T(\cdot), \tag{A.55a}$$
$$H' = R(\cdot)H'R^T(\cdot). \tag{A.55b}$$

Then, (A.54) becomes

$$\begin{aligned}
\frac{1}{\nu}\partial_{\dot{x}}\Big[H(\alpha(\dot{x},\theta_e))\dot{x}|\dot{x}|\Big]\Big|_{\dot{x}=\dot{x}_r} &= R(\gamma_r)H'R^T(\gamma_r)\left[\begin{pmatrix}\cos(\gamma_r)\\ \sin(\gamma_r)\end{pmatrix}\sin(\gamma_r), -\begin{pmatrix}\cos(\gamma_r)\\ \sin(\gamma_r)\end{pmatrix}\cos(\gamma_r)\right] \\
&\quad + R(\gamma_r)HR^T(\gamma_r)\left[\begin{pmatrix}\cos(\gamma_r)\\ \sin(\gamma_r)\end{pmatrix}\begin{pmatrix}\cos(\gamma_r) & \sin(\gamma_r)\end{pmatrix} + I\right] \\
&= R(\gamma_r)H'\left[R^T(\gamma_r)\begin{pmatrix}\cos(\gamma_r)\\ \sin(\gamma_r)\end{pmatrix}\sin(\gamma_r), -R^T(\gamma_r)\begin{pmatrix}\cos(\gamma_r)\\ \sin(\gamma_r)\end{pmatrix}\cos(\gamma_r)\right] \\
&\quad + R(\gamma_r)H\left[R^T(\gamma_r)\begin{pmatrix}\cos(\gamma_r)\\ \sin(\gamma_r)\end{pmatrix}\begin{pmatrix}\cos(\gamma_r) & \sin(\gamma_r)\end{pmatrix}R(\gamma_r) + I\right]R^T(\gamma_r) \\
&= R(\gamma_r)\begin{pmatrix}-2c_D(\alpha_e) & c_D'(\alpha_e) - c_L(\alpha_e)\\ 2c_L(\alpha_e) & -c_L'(\alpha_e) - c_D(\alpha_e)\end{pmatrix}R^T(\gamma_r).
\end{aligned} \tag{A.56}$$

The expression (A.56) points out that the real parts of the eigenvalues of

$$\partial_{\dot{x}}\Big[H(\alpha(\dot{x},\theta_e))\dot{x}|\dot{x}|\Big]\Big|_{\dot{x}=\dot{x}_r}$$

have the same signs of those of

$$\begin{pmatrix}-2c_D(\alpha_e) & c_D'(\alpha_e) - c_L(\alpha_e)\\ 2c_L(\alpha_e) & -c_L'(\alpha_e) - c_D(\alpha_e)\end{pmatrix},$$

the characteristics polynomial of which results

$$\lambda^2 + p(\alpha_e)\lambda + 2q(\alpha_e) = 0.$$

An application of the Routh–Hurwitz stability criterion to the above equation leads to the statement in Lemma 7.6.

A.9 Proof of Proposition 8.1

By decomposing the velocity errors in the body frame basis, i.e. $\vec{e}_v = (\vec{\imath}, \vec{\jmath})\widetilde{v}$, from System (8.3b)-(8.3c) one obtains

$$m\dot{\widetilde{v}} = -m\omega S\widetilde{v} - T_p e_1 + \overline{F}_p, \tag{A.57a}$$
$$\dot{\theta} = \omega, \tag{A.57b}$$

with $\overline{F}_p = R^T F_p$, F_p given by (A.39), and f_p by (A.32a). Recall that $\widetilde{\theta} \in (-\pi, \pi]$ denotes the angle between the two vectors e_1 and $\overline{F}_p$ so that $|F_p|\cos(\widetilde{\theta}) = \overline{F}_{p_1}$, and that the

control objective is the asymptotic stabilization of $\widetilde{\theta}$ to zero. Now, consider the candidate Lyapunov function V defined by:

$$V = \frac{m}{2}|\widetilde{v}|^2 + \frac{1}{k_2}\left(1 - \frac{\overline{F}_{p_1}}{|F_p|}\right). \tag{A.58}$$

Via direct calculations one can verify that

$$\frac{d}{dt}\left(1 - \frac{\overline{F}_{p_1}}{|F_p|}\right) = -\frac{\overline{F}_{p_2}}{k_2|F_p|}\left(\omega + \frac{F_p^T S \dot{F}_p}{|F_p|^2}\right). \tag{A.59}$$

In view of (A.39), $f_p(\dot{x}_a, \alpha)$ as (A.32a), F_δ as (8.19c), and $\alpha = \theta - \gamma + \pi - \delta$, the term $\dot{F}_p$ in the right hand side of the above equation becomes

$$\dot{F}_p = \partial_{\dot{x}_a} f_p \; \ddot{x}_a + \partial_\alpha f_p \; \dot{\alpha} - m\dddot{x}_r = \partial_{\dot{x}_a} f_p \; \ddot{x}_a - \partial_\alpha f_p \; \dot{\gamma} + \partial_\alpha f_p \; \omega - m\dddot{x}_r = F_\delta + \partial_\alpha f_p \; \omega.$$

In light of (A.59) and of the above relationship, the function $\dot{V}$ along the solutions of System (A.57) becomes

$$\dot{V} = \widetilde{v}_1(\overline{F}_{p_1} - T_p) - \frac{\overline{F}_{p_2}}{k_2|F_p|}\left[\left(1 + \frac{F_p^T S \partial_\alpha f_p}{|F_p|^2}\right)\omega + \frac{F_p^T S F_\delta}{|F_p|^2} - k_2|F_p|\widetilde{v}_2\right]. \tag{A.60}$$

Given $S = RSR^T$, (A.46), $f_p(\dot{x}_a, \alpha)$ as (A.32a), $\dot{x}_a = Rv_a$, (A.7), (A.41), $\delta = 0$, and

$$\overline{c} = c_D(\alpha) + c_L(\alpha)\cot(\alpha),$$

the term multiplying ω in (A.60) becomes:

$$1 + \frac{F_p^T S \partial_\alpha f_p}{|F_p|^2} = 1 + \overline{F}_{p_2}\frac{e_1^T R^T \partial_\alpha f_p}{|F_p|^2} = 1 + k_a \overline{F}_2 |\dot{x}_a|^2 \frac{\sin(\alpha)\overline{c}'' + 2\cos(\alpha)\overline{c}'}{|F_p|^2}, \tag{A.61}$$

which is equal to one, and thus different from zero, close to the equilibrium point[1]. Now, given T_p in (A.34), the property (A.35b), F in (A.37), and F_p in (A.39), one verifies that

$$\overline{F}_{p_1} - T_p \equiv \overline{F}_1 - T.$$

Then, by using (A.61) and the above relationship, the expression $\dot{V}$ in (A.60) becomes

$$\dot{V} = \widetilde{v}_1(\overline{F}_1 - T) - \frac{\overline{F}_{p_2}}{k_2|F_p|}\left[\left(1 + k_a \overline{F}_2 |\dot{x}_a|^2 \frac{\sin(\alpha)\overline{c}'' + 2\cos(\alpha)\overline{c}'}{|F_p|^2}\right)\omega + \frac{F_p^T S F_\delta}{|F_p|^2} - k_2|F_p|\widetilde{v}_2\right].$$

The application of the control laws (T, ω) given by (8.18) thus yields

$$\dot{V} = -k_1|F_p|\widetilde{v}_1^2 - \frac{k_3 \overline{F}_{p_2}^2}{k_2(|F_p| + \overline{F}_{p_1})^2} = -k_1|F_p|\widetilde{v}_1^2 - \frac{k_3}{k_2}\tan^2\left(\frac{\widetilde{\theta}}{2}\right), \tag{A.62}$$

because

$$\tan^2(\widetilde{\theta}/2) = \frac{\overline{F}_{p_2}^2}{(|F_p| + \overline{F}_{p_1})^2}.$$

[1]From Eq. (A.57a) note that close at the equilibrium point, i.e. $\widetilde{v} \equiv 0$, one has $\overline{F}_{p_2} \equiv 0$.

Since $\dot{V}$ is negative semi-definite, the velocity error term $\widetilde{v}$ is bounded. The next step of the proof consists in showing the uniform continuity of $\dot{V}$ along every system's solution and, using Barbalat's lemma, one deduces the convergence of $\widetilde{v}$ and $\widetilde{\theta}$ to zero. This part of the proof is similar to the proof developed in (Hua et al., 2009a, Appendix C) (Hua, 2009, p. 80), which is recalled here for the sake of completeness.

In order to prove the mentioned uniform continuity of $\dot{V}$, it suffices to show that $\ddot{V}$ is bounded. Note that in view of Assumption 4, the vector F_p is different from zero in an open neighborhood of $(\widetilde{v}, \widetilde{\theta}) = (0, 0)$. Consequently, it is a simple matter to verify that there exists an open neighborhood of $(\widetilde{v}, \widetilde{\theta}) = (0, 0)$ in which $\ddot{V}$ is bounded. As a consequence, in view of (A.62), there exists an open neighborhood of $(\widetilde{v}, \widetilde{\theta}) = (0, 0)$ such that for any initial condition in it, $\widetilde{v}_1$ and $\widetilde{\theta}$ converge to zero. Now, in order to show that $\widetilde{v}_2$ tends to zero, observe that

$$\frac{d}{dt}\frac{\overline{F}_{p_2}}{|F_p|} = -k_2 \overline{F}_{p_1} \widetilde{v}_2 + k_3 \frac{\overline{F}_{p_1} \overline{F}_{p_2}}{(|F_p| + \overline{F}_{p_1})^2}, \tag{A.63}$$

where the control inputs (T, ω) were chosen as (8.18). By applying Barbalat's Lemma, one verifies the uniform continuity of (A.63) in a neighborhood of $(\widetilde{v}, \widetilde{\theta}) = (0, 0)$. Then, the right hand side of (A.63) tends to zero. Since

$$\overline{F}_{p_2} \to 0, \quad (|F_p| + \overline{F}_{p_1})^2 > 0, \quad \overline{F}_{p_1} \to |F_p| > 0$$

in a neighborhood of $(\widetilde{v}, \widetilde{\theta}) = (0, 0)$, then there exists an open neighborhood of $(\widetilde{v}, \widetilde{\theta}) = (0, 0)$ such that for any initial condition in it, $\widetilde{v}_2$ necessarily tends to zero. As for the stability of the equilibrium $(\widetilde{v}, \widetilde{\theta}) = (0, 0)$, it is a consequence of relations (A.58) and (A.62).

A.10 Proof of Proposition 8.3

The proof of this proposition is similar to the proof of the velocity control given by (Hua et al., 2009a, Appendix D) (Hua, 2009, p. 82) by setting, in these proofs, the so-called modeling errors c equal to zero. Let us briefly recall that the proof relies on rewriting the dynamics $\dot{\widetilde{v}}$ as

$$m\dot{\widetilde{v}} = -m\omega S\widetilde{v} - T_p e_1 + R^T F_p - R^T h(|I_v|^2) I_v, \tag{A.64}$$

and on the candidate Lyapunov function

$$V = \frac{m}{2}|\widetilde{v}|^2 + \frac{1}{k_2}\left(1 - \frac{\overline{F}_{p_1}}{|F_p|}\right) + \int_0^{|I_v|} f(s)\, ds \tag{A.65}$$

with $f : s \to h(s^2)s$, which satisfies properties (8.25). In view of the statement in Proposition 8.3, differentiating the above relation w.r.t. t points out that $\dot{V}$ satisfies equality (A.62) in a neighborhood of the equilibrium point. Then the convergence of $(I_v, \widetilde{v}, \widetilde{\theta})$ to $(0, 0, 0)$ proceeds like the proof of Proposition 8.1.

A.11 Proof of Proposition 8.4

The proof of this proposition is similar to the proof of the position control presented in (Hua et al., 2009a, Appendix E) (Hua, 2009, p. 83) by setting, in these proofs, the so-called modeling errors c equal to zero. Let us briefly recall that the proof relies on the dynamics of $\overline{v}$, i.e.

$$m\dot{\overline{v}} = -m\omega S\overline{v} - T_p e_1 + R^T F_p - R^T h(|I_v|^2) I_v, \tag{A.66}$$

with $f : s \to h(s^2)s$, , which satisfies properties (8.25), and on the candidate Lyapunov function defined by

$$V = \frac{m}{2}|\overline{v}|^2 + \frac{1}{k_2}\left(1 - \frac{\overline{F}_{p_1}}{|F_p|}\right) + \int_0^{|y|} f(s)\, ds. \tag{A.67}$$

By differentiating the above function, one verifies that $\dot{V}$ satisfies

$$\dot{V} = -k_1|F_p|\overline{v}_1^2 - \frac{k_3\overline{F}_{p_2}^2}{k_2(|F_p| + \overline{F}_{p_1})^2}. \tag{A.68}$$

Then, the convergence of $(y, \overline{v}, \widetilde{\theta})$ to $(0, 0, 0)$ and the stability of the associated subsystem can be proven by using the same arguments as in the proof of Proposition 8.3. Now, the convergence of $(z, \dot{z})$ to zero can be shown as follows. First, rewrite System (8.27) as

$$\dot{Z} = F(Z) + G(y, Z), \tag{A.69}$$

with $Z = (z, \dot{z})$, $F(Z) = (\dot{z}, -2k_z\dot{z} - k_z^2 z + k_z^2 \mathrm{sat}_\Delta(z) - k_z h_z(|z|^2)z)^T$, and $G(y, Z) = k_z(0, h_z(|y - z|^2)(y - z) + h_z(|z|^2)z)^T$; observe that $G(y, Z)$ is bounded and vanishes ultimately (one can verify from system (8.27) that z and $\dot{z}$ are bounded, see (Hua, 2009, p. 89) for details). Then, the convergence of $(z, \dot{z})$ to zero can be shown by verifying that $Z = 0$ is a globally exponentially stable point of the system $\dot{Z} = F(Z)$. To this purpose, consider the Lyapunov function defined by

$$U = \frac{1}{2}|z|^2 + \frac{1}{k_2}\left(1 - \frac{\overline{F}_{p_1}}{|F_p|}\right) + \frac{1}{2k_z}\int_0^{|z|^2} h_z(s)\, ds + \frac{1}{2}\left|z + \frac{\dot{z}}{k_z}\right|^2. \tag{A.70}$$

Then, the derivative of the above function w.r.t. t can be shown to satisfy

$$\dot{U} \leq -\alpha_u U, \tag{A.71}$$

with α_u some positive constant. So, the the convergence of $(z, \dot{z})$ to zero follows from (A.69). Then, since $G(\cdot)$ is a continuous function, one shows that the equilibrium point $(z, \dot{z}, \widetilde{x}, \widetilde{v}, \widetilde{\theta})$ $= (0, 0, 0, 0, 0)$ is an asymptotically stable equilibrium point of the controlled System (8.1) complemented with System (8.27).